INVESTIGATION INTO THE MECHANISMS OF STEVENS-JOHNSON SYNDROME AND TOXIC EPIDERMAL NECROLYSIS

Thesis submitted in accordance with the requirements of the

University of Liverpool for the degree of Doctor in Philosophy

By

Gospel Baridakara Nwikue

September 2019

UNIVERSITY OF LIVERPOOL

Declaration

I declare that this thesis is the outcome of my own work. The material contained in this thesis has not been presented, nor is currently being presented in part or in whole for any other degree or qualification.

Gospel Baridakara Nwikue

Acknowledgements

My profound gratitude goes to God Almighty whose strength I relied on throughout the trying times of this PhD. I would like to appreciate my primary supervisor Prof Sir Munir Pirmohamed for all his numerous generous financial supports including bench fee waiver and for giving me the opportunity to perform this project. To Dr Daniel Carr, my secondary supervisor, I want to say thank you for your contribution. My heartfelt appreciation goes to Prof Andrea Varro and the Institute of Translational Medicine (University of Liverpool) senior management committee members including Prof David MacEwan for awarding me tuition fees bursary (£16, 807.40 per annum) for two years! Also, I would like to thank Dr Nicholas Harper, for his expertise and guidance on molecular gene cloning. I want to appreciate Prof Kevin Park and Prof Dean Naisbitt for their audience in my time of need. My heart-felt appreciation goes to Dr Benedicta Iyinbor for her encouragement and support during the trying times. I am grateful to my Dad and Mum, Mr and Mrs Friday Nwikue for their support and prayers at critical times. Thank you to Valerie Tilston for her contribution. My appreciation goes to Biobank at IdiPAZ (Spain) for the management of the Spanish samples. Thank you to my younger siblings Eva-Mary Nwikue and Destiny Nwikue for their encouragements.

Furthermore, I would like to thank the following persons for their encouragement/ support and friendship: Olga Vasieva (Dr), Oluebube Promise Nwikue, Alexander Penrose (Dr), Ana Alfirevic (Prof), Govinda Yavadu, Stephanie French, Tony Okocha, Steve Chukwu, Steve Harry, Fola Olaoye, Noble Pepple, Godwin Poi, Emmanuel Fanor, Barinaadaa Ntorbe, Niraj Shah (Dr), Gurpreet Ghattaoraya (Dr), Samantha Moss, Celestine Esume (Dr), Soban Sadiq (Dr), Reyadh Al-Mosawi (Dr), Shankar

Varadarajan (Dr), Arun Tailor (Dr), Phillip Omogbai (Dr), Bright Enyindah, Nengi Benstowe, Ebuka Okeke, Ala Atiegoba, Ledornu Diigbo, Esther Nwanodi, Samuel Baribiea, Monday Ogese (Dr), Lawrence McEvoy, Eunice Zhang (Dr), Augustine Omokhoa and Audrey Hamachila. Finally, I would like to thank all those who at different times gave an encouraging word in the course of my PhD.

Contents page

Publications, conferences and posters

Published paper

Carr DF, Wang CW, Bellon T, Ressel L, **Nwikue G**, Shrivastava V, Bergfeld W, Jorgensen AL, Chung WH, Pirmohamed M (2019)

Serum and blister-fluid elevation and decreased epidermal content of high-mobility group box 1 protein in drug-induced Stevens-Johnson syndrome/toxic epidermal necrolysis. British Journal of Dermatology.

Conference papers/posters

Nwikue G, Carr DF, Antoine D, Pirmohamed M

The role of HMGB1 in drug-induced Stevens-Johnson syndrome/toxic epidermal necrolysis. 7th International symposium HMGB1/DAMPS. 10-12th September 2015, Bonn, Germany.

Nwikue GB, Carr DF, Lea J, Harper N, Jenkins R, Antoine DJ, Pirmohamed M

HMGB1 as a prognostic biomarker of SJS/TEN and its putative role in the pathogenesis due to keratinocyte cell death. British Pharmacological Society (BPS) Annual Conference, 13-15TH December 2016, London, UK

Nwikue G, Carr DF, Jenkins R, Antoine DJ, Pirmohamed M

Investigating the role of HMGB1 in drug-induced Stevens-Johnson syndrome/toxic epidermal necrolysis. Institute of Translational Medicine (ITM) research Day, 7TH July, 2016. Liverpool, UK.

Abbreviations

Acronym	Meaning
4HB	Four-helix bundle
aa	Amino acid
ADR	Adverse drug reaction
AIF	Apoptosis inducing factor
Akt	Rac-a serine/threonine-protein kinase
Apaf-1	Apoptosis protease activating factor-1
APC	Antigen presenting cell
ART	Antiretroviral therapy
ATP	Adenosine triphosphate
AV/PI	Annexin V-Propidium Iodide
BH	Bcl-2 homology domain
bp	Base pair
cADRs	Cutaneous adverse drug reactions
CARD	Caspase recruitment domain
CCR	C-C chemokine receptor
CD	Cluster of differentiation
cIAP	Cellular inhibitor of apoptosis protein
CRISPR	Clustered Regularly Interspaced Short Palindromic Repeats
C-terminus	Carboxyl-terminus
CXCR	C-X-C chemokine receptor
Da	Dalton
DAMP	Damage-associated molecular pattern
DC	Dendritic cell
DD	Death domain

DED	Death effector domain
DISC	Death inducing signalling complex
DMEM	Dulbecco Modified Eagle's Medium-high glucose
DMSO	Dimethyl sulfoxide
DNA	Deoxy-ribonucleic acid
DRESS	Drug rash with eosinophilia and systemic symptoms
EDTA	Ethylenediamine tetraacetic acid
ELISA	Enzyme-linked immunosorbent assay
ER	Endoplasmic reticulum
EtBr	Ethidium bromide
EU	European Union
FADD	Fas-associated death domain containing protein
FasL	Fas ligand
FBS	Fetal Bovine Serum
Fc	Fragment crystallisable
FDA	United States (US) Food and Drug Administration
FFPE	Formalin-fixed paraffin-embedded
FLIP	FLICE-like inhibitory protein
g	grams
g	Force of gravity
GSK'872	N-5-Benzothiazolyl-6-[(1-methylethyl)sulfonyl]-4-quinolinamine
h	Hour
HBSS	Hank's Balanced Salt Solution
HIV	Human immunodeficiency virus
HRP	Horse radish peroxidase
HLA	Human leukocyte antigen

HMGB1	High mobility group box-1
IAP	Inhibitor of apoptosis protein
IFN-γ	Interferon-gamma
Ig	Immunoglobulin
IHC	Immunohistochemistry
IL	Interleukin
IKK	IκB kinase
JNK	JUN N-terminal kinase
k	kilo
KAR	Killer activating receptor
KD	Kinase Domain
kDa	Kilo Dalton
KIR	Killer inhibitory receptor
LTT	Lymphocyte transformation test
LUBAC	Linear ubiquitin chain assembly complex
M	Molar
MAPK	Mitogen activated protein kinase
MAC	Monoclonal antibody clone
MeSH	Medical Subject Headings
mg	Milli grams
MHC	Major histocompatibility complex
ml	Milli litre
MLKL	Mixed lineage kinase domain-like
min	Minute
mmol	Milli mole
MOMP	Mitochondrial outer membrane permeabilization

MPE	Maculopapular exanthema
MTT	3-(4,5-dimethythiazol-2-yl)-2,5-diphenyl tetrazolium bromide
NCBI	National Center for Biotechnology Information
Nec-1	Necrostatin-1
NEMO	Nuclear factor Kb essential modulator
NF-Kb	Nuclear factor-Kb
ng	Nano grams
NK	Natural killer
NKT	Natural killer T
NLS	Nuclear localization signal
NO	Nitric oxide
NOC-18	DETA/NO, 2-2'-(Hydroxynitrosohydrazino) *bis*-ethanamine,DETA NONoate
NSA	Necrosulfonamide
NSAID	Nonsteroidal anti-inflammatory drug
N-terminus	Amino-terminus
PAMP	Pathogen–associated molecular pattern
PBMCs	Peripheral blood mononuclear cells
PBS	Phosphate buffered saline
PCR	Polymerase chain reaction
PLAD	Pre-ligand assembly domain
PI	Protease inhibitor
P-I	Pharmacological interaction
PI3K	Phosphoinositide-3-kinase
PIP	Phosphatidylinositol phosphate
PsKD	Pseudokinase domain

RAGE	Receptor for advanced glycation end products
RIPK1	Receptor interacting protein kinase 1
RIPK3	Receptor interacting protein kinase 3
RNA	Ribonucleic acid
ROS	Reactive oxygen species
rpm	Revolutions per minute
SCAR	Severe cutaneous adverse drug reaction
SDS	Sodium dodecyl sulphate
sFasL	Soluble Fas ligand
SJS	Stevens-Johnson syndrome
SNP	Single Nucleotide Polymorphism
TAB	MAP3K7 binding protein
TAE	Tris-Acetate-EDTA
TAK	TGFβ-activated kinase
TBS	Tris Buffered Saline
TCR	T cell receptor
TEN	Toxic epidermal necrolysis
T_H	T helper cell
TLR	Toll-like receptor
Tm	Transmembrane
TNF	Tumour necrosis factor
TNF-α	Tumour necrosis factor-alpha
TNFR	Tumour necrosis factor receptor
TRADD	TNFR-associated death domain protein
TRAF	TNFR-associated factor
TRAIL	TNF-related apoptosis inducing ligand

UK	United Kingdom
USD	United States $
WHO	World Health Organisation
µl	Micro litre
µM	Micro molar
zVAD	Benzyloxycarbonyl-Val-Ala-Asp (O-Me) fluoromethyl ketone

Abstract

Stevens-Johnson syndrome and toxic epidermal necrolysis (SJS/TEN) are life-threatening immune-mediated blistering cutaneous reactions with mortality rates ranging from 10-30%. The pathophysiological mechanisms of SJS/TEN are complex and not fully understood. However, fulminant keratinocyte death and inflammation have been suggested as the major players in the mechanisms of disease.

To further understand the mechanisms of SJS/TEN, we utilised both clinical samples and *in vitro* human immortalised keratinocyte cell line (HaCaT) cell death models to investigate mediators and putative biomarkers of SJS/TEN. HaCaT cells are phenotypically similar to primary keratinocytes and represent a suitable *in vitro* model for dermatologic studies.

A previous study had suggested that serum profiles of high mobility group box-1 (HMGB1) protein, a known of marker of cell death and inflammation distinguished SJS/TEN from other cutaneous phenotypes (drug rash with eosinophilia and systemic symptoms, DRESS and maculopapular exanthema, MPE). To further elucidate the putative role of HMGB1 in SJS/TEN, serum, blister-fluid and skin biopsy samples from SJS/TEN were analysed for HMGB1 profile and expression. HMGB1 levels in serum were elevated compared to tolerant controls with even higher levels detected in blister-fluid compared to serum from a Spanish SJS/TEN cohort ($p<0.001$, $n=12$). In addition, HMGB1 skin epidermal expression was diminished in SJS/TEN compared to both MPE and healthy control.

Nitric oxide (NO) is implicated in the destruction of the epidermis in SJS/TEN. The mechanisms of NO mediated keratinocyte death and its effect on extracellular HMGB1 levels was investigated using a NO-donating compound (NOC-18). NOC-18 treated HaCaT cells were killed via both apoptosis and necrosis and extracellular HMGB1 release was higher ($p<0.05$, $n=3$) in comparison to untreated control.

Apoptosis is regulated by caspases while necroptosis is regulated by receptor interacting protein kinase-1 (RIPK1), RIPK3 and mixed lineage kinase domain-like (MLKL) protein. Tumour necrosis factor-α (TNF-α) is implicated in SJS/TEN pathology. To determine the mechanisms of TNF-α induced HaCaT keratinocyte death and assess their impact on extracellular HMGB1 profiles, HaCaT cells were treated with TNF-α. This showed that TNF-α caused keratinocyte necroptosis and apoptosis, and that necroptosis contributed significantly ($p<0.05$) more to HMGB1 levels.

RIPK3 is thought to play a role in SJS/TEN pathology. Triggering necroptosis in cells is problematic and generally results in a mixture of apoptosis and necroptosis. Constructs of wild-type human RIPK3, MLKL and Bak were made and stable HaCaT cell lines generated. Interestingly, RIPK3 activated both caspase-dependent apoptosis and MLKL-dependent necroptosis. Also, MLKL-induced extracellular HMGB1 levels were significantly higher than both Bak and RIPK3.

Together, these results suggest that TNF-α, RIPK3 and HMGB1 might be involved in the mechanisms of SJS/TEN and could potentially be used as putative biomarkers of SJS/TEN. Further preclinical and clinical studies are needed to confirm the mechanistic roles of these proteins in the pathogenesis of SJS/TEN.

CHAPTER 1

GENERAL INTRODUCTION

Contents

1.1 Adverse drug reactions

1.1.1 Definitions of adverse drug reaction

The term adverse drug reaction has multiple definitions. According to the World Health Organisation (WHO, accessed February 2018), an adverse drug reaction (ADR) is "a response to a drug which is noxious and unintended and which occurs at doses normally used in man for the prophylaxis, diagnosis or therapy of disease, or for the modification of physiological function" (WHO, 1972). In 2000, Edwards and Aronson defined an ADR as "an appreciably harmful or unpleasant reaction, resulting from an intervention related to the use of a medicinal product, which predicts hazard from future administration and warrants prevention or specific treatment, or alteration of the dosage regimen, or withdrawal of the product" (Edwards and Aronson, 2000). The European Parliament and Council of the European Union made a proposal in 2010 to amend the definition of ADRs "to accommodate the coverage of "noxious and unintended effects resulting not only from the authorised use of a medicinal product at therapeutic doses, but to also include medication errors and uses outside the terms of the marketing authorisation, including the misuse and abuse of the medicinal product" (EU, 2010). Whilst all definitions define an ADR, however, the second and third definitions encapsulate to a larger extent some serious and life-threatening reactions.

1.1.2 Incidence and health cost of adverse drug reactions

Adverse drug reactions (ADRs) represent a significant problem to patients and health care providers in terms of mortality, morbidity and cost. A study conducted on 18,820 patient hospital admissions over a 6 month period in the United Kingdom showed that ADRs accounted for 6.5% of total admission with a projected annual cost of £466m on the United Kingdom National Health Service (Pirmohamed et al., 2004).

1.1.3 Classifications of adverse drug reactions

Adverse drug reactions were originally grouped using a binomial system into dose-dependent (type A) and dose-independent (type B) reactions (Rawlings and Thompson, 1977) (Table 1.1):

Type A reactions are the most common type of ADRs (Pirmohamed et al., 1998). They are generally based on the known pharmacological function of the drug and therefore can be predicted (Pirmohamed and Park, 2001). Although they are usually mild, they can sometimes become very severe but the morbidity and mortality rates are usually low (Edwards and Aronson, 2000) (Pirmohamed et al., 2004). A number of factors such as age, gender, drug-drug interactions, health status, polypharmacy, changes in pharmacokinetic and pharmacodynamic parameters as well as environmental stimulants may increase the chance of developing this type of ADR (Alomar, 2014). An example of type A reaction is the bleeding risk associated with warfarin (an anticoagulant) use. Type A reactions are the most prevalent and account for approximately 80% of all adverse drug reactions (Duran-Figueroa et al., 2015).

Type B reactions are witnessed by a relatively small number of susceptible individuals and cannot be predicted from the known pharmacological function of the drug (Pirmohamed et al., 1998). They generally tend to cause more serious reactions and are a leading cause of drug attrition during drug-development (Waring et al., 2015). Type B reactions are sometimes referred to as idiosyncratic drug reactions (Pirmohamed et al., 2004) (Uetrecht and Naisbitt, 2013) and they represent approximately 20% of all adverse drug reactions (Duran-Figueroa et al., 2015).

Several decades later, ADRs classification was expanded to account for reactions not covered by the above classification and as a result, four additional types (type C-F) were added (Edwards and Aronson, 2000). A few years later, a new classification was proposed to take into account Dose-dependency, Timing/and, individual Susceptibility (DoTS) (Aronson and Ferner, 2003).

Table 1.1: Characteristics of type A and type B adverse drug reactions. (Adapted from Pirmohamed and Park, 2001).

Characteristics of ADR	**Type A**	**Type B (Idiosyncratic)**
Dose-dependency	Yes, good relationship	No simple relationship
Predictable from known pharmacology	Yes	Not usually
Frequency	Common	Uncommon
Severity	Variable, mostly mild	Variable, usually more severe
Clinical burden	High morbidity and low mortality	High morbidity and mortality

1.1.4 Characteristics and classification of idiosyncratic adverse drug reactions

Idiosyncratic reactions have complex manifestations that do not follow a simple dose-response relationship and are characterised by a variable onset of symptoms which can vary from a few minutes to several hours and many days following drug exposure in susceptible individuals. Reactions are usually very rapid if patients who have previously had idiosyncratic adverse drug reactions are re-exposed to the same culprit drug (Uetrecht, 2007).

Idiosyncratic reactions can be subdivided into two main groups namely immune-mediated and non-immune-mediated (Thien, 2006). Idiosyncratic reactions with an immune aetiology are known as drug hypersensitivity reactions or drug allergy. Drug allergy may be limited in context as it refers to a specific immune response to a drug which may be acting as an allergen while drug hypersensitivity has a wider context and can be used to describe immune simulations and resulting clinical symptoms as a result of drug binding to immune receptors or T-cell receptors (TCRs) (Pichler and Hausmann, 2016).

1.2 Drug hypersensitivity reactions

Drug hypersensitivity reactions are a form of serious adverse drug reactions with an immune-mediated aetiology that can affect a range of organs with the skin being the most common target (Duran-Figueroa et al., 2015). Drug hypersensitivity reactions are clinically and functionally heterogeneous in nature (Pichler and Hausmann, 2016).

According to Coombs and Gell classification, drug hypersensitivity is subdivided into four groups (type I-IV) on the basis of the underlying immune mechanism linked to certain clinical phenotypes (Coombs and Gell, 1976) (Figure 1.1). Based on this classification system, type I to III include antibody mediated reactions while type IV reactions (also known as delayed hypersensitivity reactions) are T-cell mediated (Posadas and Pichler, 2007). Cutaneous manifestations of type IV drug hypersensitivity reactions can range from mild maculopapular exanthema (MPE), to more severe drug rash with eosinophilia and systemic symptoms (DRESS) and blistering Stevens-Johnson syndrome (SJS) and toxic epidermal necrolysis (TEN) (Böhm and Cascorbi, 2016).

Not long ago, because of the heterogeneity of T-cell subpopulations, type IV reactions were further subdivided into four groups A-D (Pichler, 2003) (Figure 1.1). However, this classification oversimplifies the complex immune developments and the multiplicity of reactions that can sometimes occur simultaneously in drug hypersensitivity (Pichler et al., 2010) (Pichler, 2019). A huge number of demographic and clinical factors including age, gender, disease comorbidities, co-medication and genetic polymorphisms are predisposing factors for ADRs (Becquemont, 2009).

	Type I IgE-mediated	Type II Cytotoxic (IgM or IgG)	Type III Immune complexes	Type IV Delayed (T-cell mediated)
Clinical manifestation	Urticaria Anaphylaxis	Haemolytic anaemia Neutropenia	Vasculitis Rash, fever.	Maculopapular rash DRESS, SJS/TEN.
Time to onset of reactions following drug exposure	Few minutes to 1 hour	Within hours (less than 24 hours)	Within hours	48 hours to several days or weeks
Cell type	B cells	B cells	B cells	T cells
Type of immune response	Drug IgE complex, inflammatory mediators	Specific IgM or IgG antibodies plus Fc receptor interaction	Drug IgG complexes plus complement activation or Fc receptor interaction	MHC presentation to T cells A. T helper 1 B. T helper 2 C. Cytotoxic T cells D. T cells
Pathological mechanism	Mast cell degranulation	Fc receptor dependent cell killing	Immunological complex deposition	A. Monocyte activation B. Eosinophilic recruitment C. CD4+ or CD8+ T cells D. Neutrophil recruitment/activation

Figure 1.1: Sub-classification of drug hypersensitivity. Drug hypersensitivity classification by Coombs and Gell is presented coupled with additional division of type IV reaction into A-D by Pichler. DRESS; drug rash with eosinophilia and systemic symptoms, SJS/TEN; Stevens-Johnson syndrome/toxic epidermal necrolysis, Ig; immunoglobulin, Fc; fragment crystallisable, MHC; major histocompatibility complex. (Adapted from Pichler 2003; Thien 2006; Pirmohamed *et al* 2004; Coombs and Gell, 1976; Posadas and Pichler 2007; Pichler 2019).

1.2.1 Mechanism leading to T cell activation in drug hypersensitivity reactions

Drug hypersensitivity reactions are the result of immune reactions to low molecular weight drugs. The mechanisms through which delayed-type drug hypersensitivity reactions can elicit an immune reaction have been the focus of much research. However, it is not completely understood how T cells are activated by drugs in this type of hypersensitivity reactions. Conventionally, T cells through the TCRs recognise peptides presented on major histocompatibility complex (MHC) by antigen presenting cells (APCs) (Adam et al., 2011) (Yun et al., 2016). This MHC/TCR interaction promotes an antigen-specific immune response. A number of pathways or models that can lead to T-cell activation have been proposed and will be discussed briefly below.

1.2.2 The major histocompatibility complex

The major histocompatibility complex represents a set of cell surface proteins that bind peptides derived from pathogens and endogenous sources and display them for recognition by specific T cells. In humans, the MHC is located on chromosome 6 and contains over 200 genes collectively known as human leukocyte antigen (HLA) which function in both innate and adaptive immunity (Janeway et al., 2001). There are two defining properties of MHC molecules. First, the MHC molecule is polygenic indicating that it contains several different MHC class I and II genes that can give an individual a distinct set of MHC molecules with different ranges of peptide binding specificities. Second, the MHC molecule is highly polymorphic indicating multiple variants of each gene within a population (Janeway et al., 2001). The expression of all MHC genes is co-dominant and is displayed on the cell surface. In humans, there

are three class I α-chain genes called HLA-A, -B and –C while there are also three pairs of MHC class IIα- and β-chain genes called HLA-DR, -DP and –DQ (Wieczorek et al., 2017). HLA class I receptors are expressed on almost all nucleated cell types whereas MHC class II molecules are exclusively expressed by APCs which include dendritic cells, B cells and macrophages (Bharadwaj et al., 2012). The HLA class I genes code for a heavy α chain comprising of three extracellular domains which are non-covalently linked to β2-microglobulin (β2M) light chain proximal to the membrane (Wieczorek et al., 2017) (Figure 1.2). By contrast, the HLA class II genes code for two polymorphic chains (α and β) comprising of two extracellular α1 and β1 domains which fold to provide the peptide binding groove and two transmembrane immunoglobulin-like α2 and β2 domains (Bharadwaj et al., 2012) (Figure 1.2).

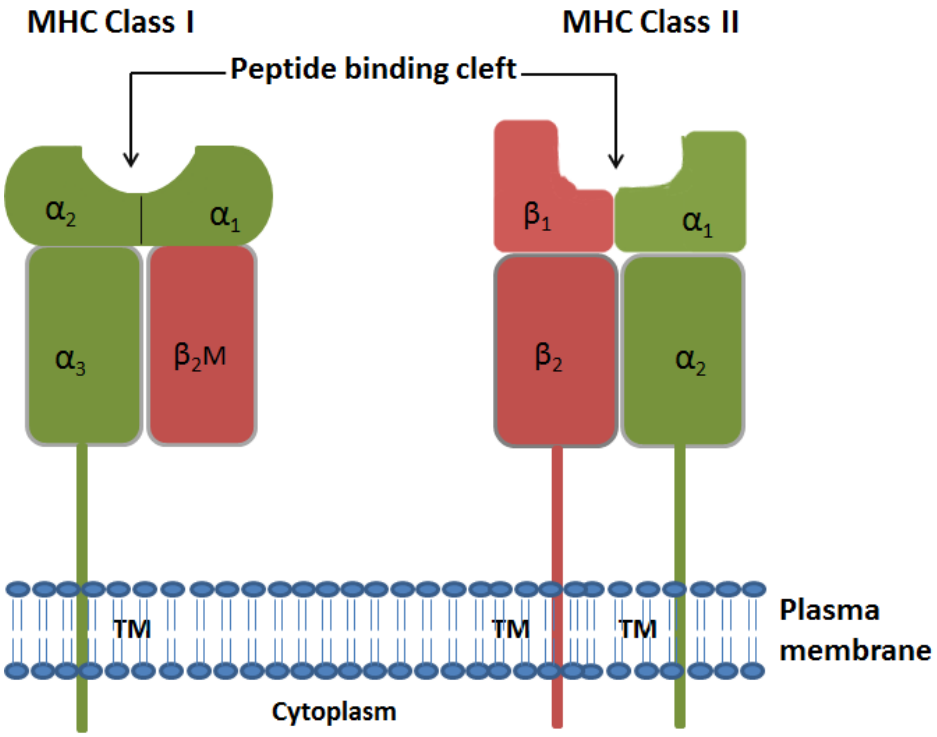

Figure 1.2: Structure of the MHC class I and II antigens. MHC class I consists of a transmembrane (TM) heavy α-chain that is non-covalently linked to β2-immunoglobulin (β2M) which is the light chain. The N-terminal α1 and α2 domains fold to form the peptide binding cleft of MHC class I antigens. The α3 domain of the heavy chain has a similar structural homology to immunoglobulin constant region domain. MHC class II consists of two immunoglobulin-like transmembrane (α2 and β2) domains. The N-terminal α1 and β2 of each domain fold to form the peptide binding groove of the MHC class II. Both the MHC class I and II have cytoplasmic tails

1.2.3 Antigen presentation and T cell interaction

In the cytosol, proteins are degraded through the process of proteolysis by the proteasome machinery of the cell and the resulting peptides are either broken down directly into individual amino acids or transported into the endoplasmic reticulum (ER) as intact peptides. In the ER, peptides bind to MHC class I without the need of exogenous proteins and the resultant MHC/peptide complex is then conveyed via vesicles to the cell surface. By contrast, antigen binding to MHC class II

requires the presence of exogenous trafficking proteins like vesicles. Endocytosed vesicles conveying packaged peptides fuse with endosomes forming the MHC class II compartment whereby peptides obtained from exogenous proteins are deposited into the peptide binding cleft of MHC class II (Blum et al., 2013). Peptide bound MHC class II is then carried to the cell surface for recognition by CD4+ T cells. In general, MHC class I and MHC class II pathways bind intracellular and extracellular proteins respectively; however, a phenomenon referred to as cross-presentation by specific subsets of dendritic cells can permit class I molecules to be deposited with exogenous peptides internalised through phagocytosis (Joffre et al., 2012). Similarly, the fusion of auto-phagosomes with MHC class II compartments leads to the deposition of intracellular antigens on MHC class II molecules (Munz, 2012).

MHC class I peptide binding groove is in a closed conformation and this is adapted for the binding of shorter peptides (8-9 amino acids in length) compared to MHC class II open-ended groove configuration which is adapted for longer peptides (12-25 amino acids). Antigen specificity demonstrated by the selectivity of antigens that can bind to a particular MHC allele is determined by a small number of amino acid residues that interact with the pockets within the peptide binding cleft. The interaction between the MHC/peptide complex and the TCR of T cells occurs at the cell surface. Generally, most mature T cells express either CD4 or CD8 co-receptor, giving rise to CD4+ and CD8+ T cell subtypes. CD8+ T cells recognize peptides of protein origin bound to MHC class I molecules whereas CD4+ T cells recognize peptides in association with MHC class II molecules (Blum et al., 2013). T cells can also recognize molecules not associated with MHC molecules as a subset of T cells that recognize lipid antigens associated with CDI molecules has also been

discovered and described (Cohen et al., 2009). Each mature T cell expresses a distinct type of αβ TCR (αβTCR) which enhances its selective ability to bind to specific peptides presented on MHC molecules (Birnbaum et al., 2014). TCR binds to the groove containing bound peptide, making direct contact with the peptide and the groove (peptide binding groove) of MHC molecules. CD4 and CD8 co-receptors on the other hand engage MHC molecules at sites allosteric to the peptide binding groove (Hennecke and Wiley, 2001). This interaction of TCR with the MHC/peptide complex (TCR/peptide/MHC complex) triggers antigen-specific proliferation and differentiation of the engaged T cell. As a consequence, CD4+ and CD8+ T cells differentiate into T helper cells and cytotoxic T cells respectively (Taniuchi, 2018) (Bedoui et al., 2016).

Currently, three established hypotheses exist to explain how T cells may be activated by peptides derived from drugs or other antigens (including self and non-self). They include the hapten/pro-hapten hypothesis, the Pharmacological interaction (P-I) hypothesis, and the altered peptide repertoire hypothesis. Although there is a fourth hypothesis called the danger hypothesis but this is considered to be an additive to the hapten hypothesis (Pirmohamed et al., 2002). Nevertheless, the danger hypothesis and the role it is thought to play in the pathogenesis of drug hypersensitivity reactions will be discussed in this thesis. Experimental systems such as in-vitro and in-vivo models represent vital tools in the generation and validation of hypotheses. Notably, only the hapten concept has been reportedly validated using *in vivo* models including in man at the moment (Castrejon et al., 2010) (Elsheikh et al., 2010). The others have only been tested via

in-vitro models where drug-antigen interaction may likely vary from actual occurrence in hypersensitive patients (Duran-Figueroa et al., 2015).

Hapten and pro-hapten hypothesis

The hapten hypothesis was developed based on the observation made by Landsteiner and Jacobs that reactive low-molecular weight compounds bind to proteins covalently to cause hypersensitivity reactions in guinea pigs (Landsteiner and Jacobs, 1935) (Yun et al., 2016). Haptens are chemically reactive small molecules that are able to covalently bind to larger endogenous proteins or peptides and modify the side chain of the bound residue. Drugs that are chemically reactive and can readily form drug-protein adducts are regarded as haptens (Whitaker et al., 2011). Most drugs are generally chemically inert but can be converted into reactive products upon metabolism and this describes the pro-hapten concept (Naisbitt et al., 2000) (Pichler et al., 2010).

A number of drugs implicated in drug hypersensitivity have been reported to form drug-protein conjugates. They include β-lactam antibiotics, carbamazepine, abacavir, nevirapine and sulfamethoxazole amongst others (Duran-Figueroa et al., 2015). Although how drug-protein binding precisely relates to the initiation of drug hypersensitivity is not fully understood. For small molecules or drugs as well as their reactive metabolites to stimulate T cell dependent immune response, they must be able to bind covalently to endogenous proteins and then form drug-protein conjugates. These drug-protein adducts are taken into the cell by endocytosis and thereafter undergo processing by APCs. Drug-modified peptides are displayed by APCs using the MHC molecules. The recognition of drug-modified peptide/MHC

complex by the appropriate TCR stimulates naïve T helper cells differentiation into T helper cell 1 (T_H1) and T helper cell 2 (T_H2) effector cells via a process known as signal 1 (Pirmohamed et al., 2002). T_H1 and T_H2 effector cells promote a phagocyte-dependent inflammation through the activation of both macrophages and cytotoxic T cells including in some instances stimulation of B cell dependent antibody production.

The danger hypothesis

The danger hypothesis first proposed by Matzinger in 1994, provides an alternative viewpoint to the self-nonself hypothesis. It states that the presence of endogenously released danger signals as a consequence of cellular damage but not the nature of the antigen itself (self and non-self) is important for the immune system activation (Matzinger, 1994). The danger hypothesis attracted criticism and controversy among immunologists because it contradicted conventional immunological dogmas (Pradeu and Cooper, 2012). Danger signals are a diverse class of molecules released in response to cellular injury or death (apoptosis, necrosis and necroptosis), oxidative stress and inflammation. They include cytokines (example tumour necrosis factor-α; TNF-α), reactive oxygen intermediates and damaged-associated molecular patterns; high mobility group box-1 (HMGB1) (Hu et al., 2015) amongst others (Yun et al., 2016) (Heil and Land, 2014). Most of these so-called danger signals are ligands for toll-like receptors (TLRs) providing an alternative signal to pathogen-associated molecular patterns (PAMPs) for the activation of APCs.

The activation of APCs by danger signals leads to increased expression and upregulation of co-stimulatory molecules particularly B7 on APCs (Hathcock et al., 1994). The interaction between B7 and CD28 co-stimulatory receptor on naïve (CD4+ and CD8+) T cell membrane then leads to the activation of both cytotoxic T cell and B-cell dependent adaptive immune response (Chen and Flies, 2013). In a nutshell, the danger hypothesis argues that the stimulation of an immune response by drug-protein conjugates (signal 1) requires the participation of co-stimulatory molecules (signal 2) and cytokines (signal 3) (Li and Uetrecht, 2010) (Pirmohamed et al., 2002) (Matzinger, 1994) and that the absence of this co-stimulatory signal results in immune tolerance in spite of the presence of signal 1 represented by MHC/TCR interaction.

The postulated involvement of the danger signal in co-stimulation of T-cell immune response lacks convincing clinical evidence as it is difficult to define the nature of the danger signal at the time of reaction in drug hypersensitivity reactions. However, the frequency of drug hypersensitivity reactions is increased in human immunodeficiency virus (HIV) positive patients (Pirmohamed et al., 2002) (Zhang et al., 2011). In addition, it has been demonstrated experimentally that the administration of parent drugs or their reactive metabolites induces increased expression of danger signal molecules (Duran-Figueroa et al., 2015). Importantly, the role of danger signals in the pathogenesis of drug hypersensitivity is yet to be fully elucidated.

Pharmacological interaction (P-I) hypothesis

The pharmacological interactions of drugs with immune receptors shortened as P-I concept was developed by Pichler's group over two decades ago to explain an observation where a drug binds reversibly and non-covalently to immune cell receptors particularly TCR and/or HLA directly (Pichler, 2002) (Pichler, 2008). The P-I hypothesis implies that the direct reversible and non-covalent interaction between drugs and TCR receptors and/or HLA is sufficient to induce activation of drug-specific memory T-cells (Pichler, 2008). This process could be linked to receptor-ligand interaction facilitated by Van der Waals forces and hydrogen bonds. The key postulates of the P-I concepts are (i) the drug interacts with TCR and/or HLA and that both TCR and HLA are required for T-cell activation; (ii) the drug-receptor binding occurs independently of processing and metabolism; (iii) drug binding is reversible as drug is removed by washing drug-pulsed APCs; (iv) Activation of drug reactive T-cells is quicker in the presence of the drug (Pichler, 2003) (Yun et al., 2016). An exception to postulate iii of the P-I concept is abacavir which bind to HLA-B*57:01 in the ER.

The P-I concept can be subdivided into P-I TCR and P-I HLA (Pichler et al., 2015). In P-I TCR, a drug binds preferentially to TCR and can activate T cells by reinforcing its interaction with peptide-HLA (pHLA) complex. While in P-I HLA, a drug binds predominantly to peptide-MHC (pMHC) complex. A number of drugs strongly associated with severe cutaneous adverse reaction (SCAR); Stevens-Johnson syndrome and toxic epidermal necrolysis which include carbamazepine, allopurinol, abacavir, lamotrigine and phenytoin activate T cells through the P-I mechanism

(Pichler et al., 2006). Effectors and memory T-cells in the P-I concept have a substantially reduced threshold for activation than naïve T-cells.

Altered HLA-peptide repertoire hypothesis

An association was shown between HLA-B*57:01 and abacavir-induced hypersensitivity using a candidate gene approach (Mallal et al., 2002). Previous theories were unable to fully explain the mechanism of T-cell activation seen in abacavir hypersensitive patients after Chessman et al reported that abacavir activated CD8+ T-cells in an HLA-B*57:01 restricted fashion (Chessman et al., 2008). A few years later, three independent studies demonstrated that abacavir binds non-covalently to the F-pocket within the peptide binding cleft of endogenous HLA-B*57:01 and that this interaction consequently alters the repertoire of self-peptides that interact and are presented to T cells (Illing et al., 2012) (Ostrov et al., 2012) (Norcross et al., 2012). This discovery led to the postulation of the altered HLA-peptide repertoire hypothesis.

The use of advanced techniques such as mass spectrometric analysis, X-ray crystallography and docking studies have revealed that drugs interact non-covalently with serine-116 found exclusively in the F-pocket of HLA-B*57:01 but not in other closely related alleles (HLA-B*57:02, HLA-B*57:03, HLA-B*57:11, or HLA-B*58:01) (Ostrov et al., 2012) (Illing et al., 2012) (Duran-Figueroa et al., 2015). Furthermore, the presence of abacavir can result in 25% shift in the repertoire of peptides recognised by APC to T cells. Notably, about 45% of patients with HLA-B*57:01 did not develop hypersensitivity to abacavir suggesting that other factors such as metabolism, the clone of TCR, and the type of disease present may

contribute further to susceptibility (Ostrov et al., 2012). Importantly, with abacavir, two differing mechanisms of T-cell activation namely P-I and altered HLA-peptide repertoire have been documented (Meng et al., 2018) (Pichler et al., 2015) (Bell et al., 2013).

1.2.4 Drug induced severe blistering cutaneous hypersensitivity reactions

Severe blistering cutaneous hypersensitivity reactions can be life-threatening and include Stevens-Johnson syndrome (SJS) and toxic epidermal necrolysis (TEN; also called Lyell syndrome). Drugs are the leading causes of SJS and TEN (Guillaume et al., 1987) (Roujeau et al., 1995). However, a few cases of SJS and TEN can be attributed to viral infections especially the human herpes simplex virus and *Mycoplasma pneumoniae* (Hu et al., 2015) (Tay et al., 1996). The focus of this thesis will be drug-induced SJS/TEN.

1.2.5 Definition, incidence and health burden of SJS and TEN

SJS and TEN are serious drug hypersensitivity reactions to the skin and mucous membranes which typically manifest as detachment of the epidermis from the dermis at the dermal-epidermal junction including mucosal sloughing. SJS and TEN are characterised by widespread keratinocyte death.

SJS and TEN are rare and have an estimated incidence between 1 to 6 and 0.4 to 1.2 per million person-years, respectively (Rzany et al., 1996) (Roujeau et al., 1995). Recently, a study has reported a higher incidence of SJS/TEN in the UK estimated at 5.76 cases per million person-years (Frey et al., 2017). Although rare, the mortality rates of SJS/TEN are high ranging from 10% to 30% and represent a substantial

burden to both health care providers and patients. According to a study conducted in the US in 2007 on 21 SJS patients and 94 TEN patients by the American Burn Association National Burn Repository, it was discovered that the cost of hospitalisation per person was approximately 20, 962 USD for SJS and 59, 073 USD for TEN (Kagan et al., 2007). Although SJS and TEN affect all age groups, from young infants to the elderly, SJS in particular, is common in children and adolescents (Pereira et al., 2007) while TEN is more common in women than in men (French, 2006).

1.2.6 Defining the clinical spectrum of SJS and TEN from erythema multiforme

SJS and TEN, including erythema multiforme major are diseases belonging to the same clinical spectrum of severe cutaneous adverse drug reactions (SCARs) which affect the skin and mucous membranes. Defining the clinical spectrum of SJS and TEN is very important for the purpose of applying a prognostic test as well as diagnosis. For over three decades, SJS and TEN were viewed by clinicians as different diseases and there was little consistency not only in setting clear diagnostic criteria for erythema multiforme major and SJS but also in differentiating SJS from TEN. However, the International SJS/TEN Study under the leadership of Roujeau defined the precise diagnostic criteria for SJS and TEN including erythema multiforme (Bastuji-Garin et al., 1993). Based on that study, erythema multiforme was differentiated from SJS and TEN and even led to the understanding that SJS and TEN were variants of the same clinical syndrome with varying degrees of severity of mucocutaneous surface detachment involved (Figure 1.3). This is now the

consensus view that SJS and TEN are variants of the same disease with a common aetiology and pathology.

Erythema multiforme major differs in its clinical pattern from SJS and TEN in terms of aetiology, pathology and prognosis. Unlike SJS and TEN that is predominantly caused by drugs, the herpes simplex virus is the most common cause of erythema multiforme. Clinically, erythema multiforme is defined as detachment below 10% of the total body surface area plus localised “typical or atypical raised targets” with only two zones and a poorly defined border. These raised spots are mostly present on the limbs but can sometimes be found on the face and trunk particularly in children. The affected body surface area in erythema multiforme is usually between 1-2% (Mockenhaupt, 2011). Differential diagnosis for SJS/TEN is presented below (Table 1.2).

For SJS, body surface area detachment is less than 10% plus widespread purpuric macules or flat atypical targets; for SJS/TEN overlap of detachment is between 10-30% of the body surface area plus widespread purpuric macules or flat atypical targets; for TEN with spots, detachment greater than 30% of the body surface area is present plus widespread purpuric macules or flat atypical targets; TEN without spots, detachment above 10% of body surface area with large epidermal sheets but lacking purpuric macules or targets.

In addition to mucosal and body surface area and nature of physical spots, histologically analysed biopsy samples demonstrating full thickness necrosis of the epidermis and keratinocyte apoptosis with minimal underlying dermal filtration must be incorporated to fully diagnose SJS and TEN. Diagnostic criteria for SJS/TEN

will be elaborated upon in Chapter 2. This thesis will define SJS/TEN as any degree of epidermal skin and mucosal surface detachment ranging between 0 to 100% and will hereafter use the term as SJS/TEN.

Table 1.2: Differential diagnosis of Stevens-Johnson syndrome and toxic epidermal necrolysis. Data obtained from multiple sources. (Adapted from Schwartz *et al* 2013c; Kohanim *et al*, 2016; Creamer *et al* 2016).

Disease	**Mucositis**	**Morphology**	**Onset**
Erythema multiforme major	present	Raised atypical targets or purpuric macules	Acute
Linear IgA bullous dermatosis	Rare	Tense, sub-epidermal bullae like pemphigoid	Acute
Acute generalised exanthematous pustulosis (AGEP)	Rare	Superficial pustules (resembles pustular psoriasis)	Acute
Staphylococcal scalded skin syndrome (SSSS)	Absent	Erythema, skin, tenderness, perioral crusting	Acute
Pemphigus vulgaris	Rare	Flaccid bullae, erosion of oral mucosa	Gradual
Paraneoplastic pemphigus	Present	Polymorphous skin lesions, flaccid bullae	Gradual
Bullous pemphigoid	Rare	Crops of large tense fluid-filled blisters	Acute
Mucous membrane pemphigoid	Present	Multi-site mucosal lesions and erosions	Gradual
Bullous lupus erythematosus	Present	Tense vesicles and bullae sometimes haemorrhagic	Gradual
Bullous acute graft-versus-host disease	Present	Morbilliform rash, bullae, and erosions	Acute
Generalised bullous fixed drug eruption	Usually absent	Red-brown patches, with overlying bullae	Acute

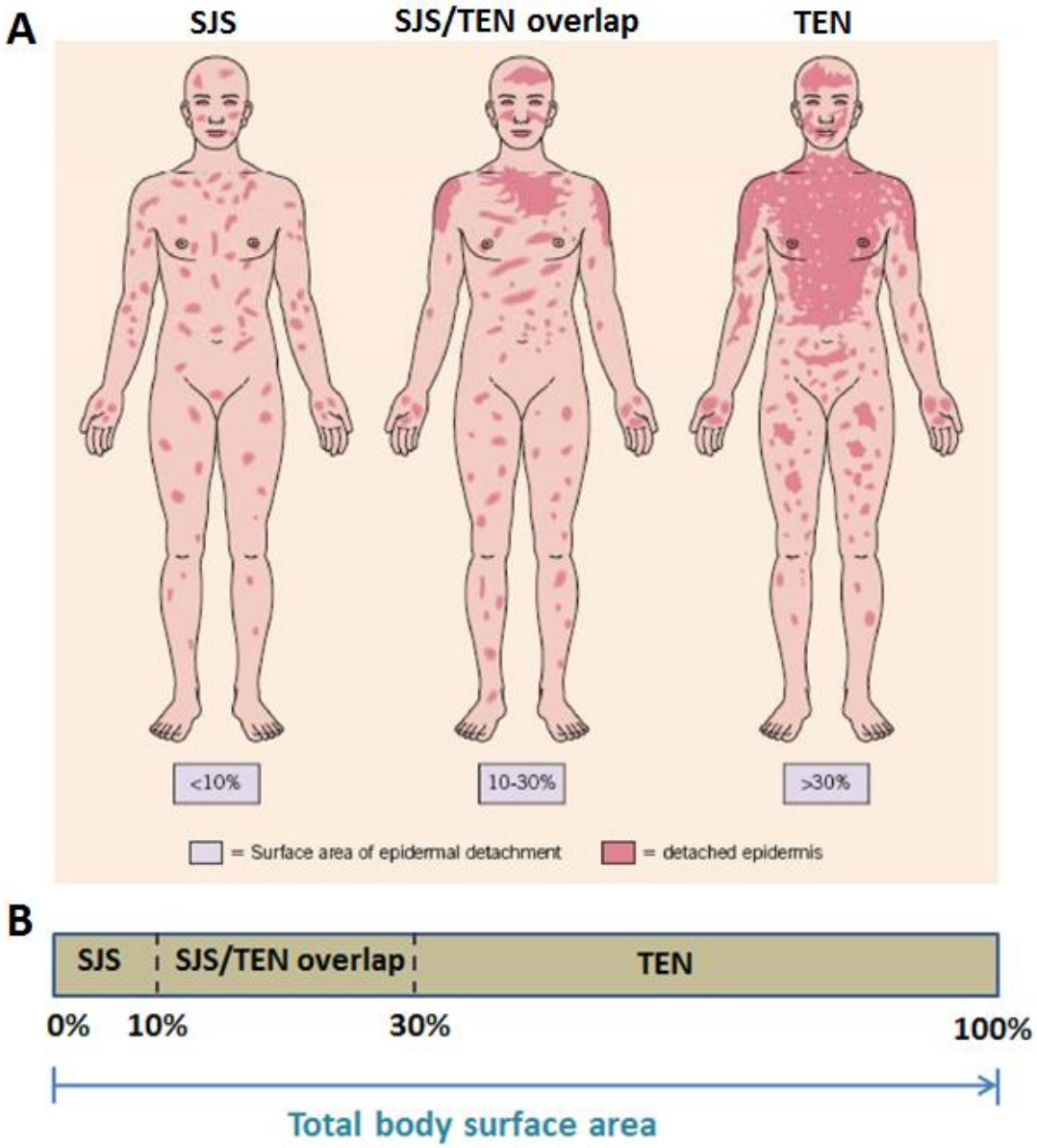

Figure 1.3: **Classification of Stevens-Johnson syndrome and toxic epidermal necrolysis according to affected body surface area**. A) Body map schematic representation of skin involvement in SJS/TEN showing the surface of epidermal sloughing adapted from Harr and French, 2010 B) Schematic representation of total body surface area for classifying SJS, SJS/TEN overlap and TEN. Both pictures show the clinical criterion for differentiating SJS from TEN including SJS/TEN overlap.

1.2.7 Drugs commonly associated with SJS/TEN

A number of drugs have been reported to have associations with SJS/TEN. In fact, about 259 low molecular weight drugs and biologics have US Food and Drug Administration (FDA) warnings for risk of SJS/TEN (Hur et al., 2015). Some of the drugs shown to have frequent associations with SJS/TEN include anti-epileptics (carbamazepine, phenytoin, lamotrigine, phenobarbital), anti-retrovirals (abacavir, nevirapine) anti-gout (allopurinol), Sulphonamide and beta-lactam class of antibiotics, and Oxicam class of the nonsteroidal anti-inflammatory drugs (NSAIDs) (Schwartz et al., 2013b) (Schwartz et al., 2013c) (Creamer et al., 2016) (Table 1.3).

Drug causality in SJS/TEN can be defined by various causality assessment tools. An algorithm specific for SJS/TEN called ALDEN (ALgorithm of Drug causality in Epidermal Necrolysis) (Sassolas et al., 2010) has also been developed. ALDEN is a specialised tool for the retrospective assessment of drug culpability in SJS/TEN and is not viable for use in the acute phase of illness. However, in clinical practice, the key parameters described in ALDEN can be incorporated into clinical frameworks used to determine drug culpability (Creamer et al., 2016).

Table 1.3: List of commonly prescribed drugs most frequently associated with Stevens-Johnson syndrome and toxic epidermal necrolysis. (Adapted from Schwartz et al, 2013a; Schwartz et al 2013c; Creamer et al, 2016).

Drug	**Indication**
Carbamazepine	Anti-epileptics
Phenytoin	
Lamotrigine	
Phenobarbital	
Abacavir	Anti-retrovirals
Nevirapine	
Allopurinol	Anti-gout drug
Meloxicam	Oxicam class of nonsteroidal ant-inflammatory drugs (NSAIDs)
Piroxicam	
Tenoxicam	
Trimethoprim-sulfamethoxazole	Antibiotic
Fluoroquinolones	
Minocycline	Tetracycline antibiotic
Cephalosporins	Beta-lactam antibiotics
Carbapenems	
penicillins	
Sulfasalazine	Sulphonamide class of antibiotics
Sulfadiazine	
Sulfadoxine	
Sulfafurazole	
Sertraline	Antidepressant
Chlormezanone	anxiolytic

There are other appropriate tests to identify or confirm the causal drug in SJS/TEN. They include patch testing and in-vitro assays such as drug-induced T-cell proliferation (lymphocyte transformation test, LTT) and drug-induced lymphocyte cytokine production (lymphocyte function test) (Porebski, 2017). Patch testing has variable sensitivity and specificity in different reactions with different drugs which limits its applicability as a diagnostic in drug culpability (Wolkenstein et al., 1996). In LTT, lymphocyte proliferation is assessed by uptake of 3H-thymidine into dividing cells. However, it might be difficult to comparatively interpret results from different sources partly due to variations in standard methodology as well as low amount of reports in which LTT has been used to characterise and confirm drug causality in SJS/TEN (Creamer et al., 2016). Unfortunately, LTT has a very low sensitivity in SJS/TEN even when the test is performed within one week after disease onset (Kano et al., 2007) (Porebski et al., 2013). Lymphocyte production of cytokines and other mediators can be measured by techniques such as enzyme-linked immunosorbent assay and enzyme-linked immunospot. In addition, CD69 upregulation on T lymphocytes two days after lymphocyte stimulation *in vitro* has been explored for its utility (Beeler et al., 2008) but has not come into widespread use.

1.2.8 Clinical presentation of SJS/TEN

The pattern of preceding symptoms at the onset of SJS/TEN differs from patient to patient, but overall, it most often consists of a prodrome of malaise, cough, anorexia, lethargy, fever, rhinorrhoea, pharyngitis and multisite mucositis affecting the oral and genital mucosa. Ocular inflammation and ulceration may also develop

prior to the appearance of any skin signs and eruption by several days. These are then accompanied by painful generalised erythema and massive bullae formation (Revuz et al., 1987). Very early lesions presenting as atypical targets and/or purpuric macules appear usually on the upper trunk, proximal limbs and face. Subsequently, lesions spread to cover the rest of the trunk and distal limbs (Creamer et al., 2016). SJS/TEN lesional skin usually appears tender when palpated and the application of minimal shearing forces causes the epidermis to peel away from the dermis (Harr and French, 2010).

The fragility of SJS/TEN lesional skin is indicated by a positive Nikolsky sign in which lateral pressure aids the detachable epidermis to slide over the dermis (Creamer et al., 2016). Although Nikolsky's sign is not specific for SJS/TEN given that it is also positive in pemphigus, it provides a good indicator of the extent of epidermal necrolysis (Harr and French, 2010) (Shah et al., 2018). Widespread necrolysis gives rise to sloughing of sheets of epidermis thereby leaving the dermis exposed. Denuded dermis exudes serum and becomes prone to secondary infection and bleeding.

1.2.9 Evaluation of severity and mortality of toxic epidermal necrolysis

Serious cases of SJS/TEN are usually accompanied by acute systemic sequelae which can lead to multi-organ failure and death (Creamer et al., 2016). Investigators in the field of SJS/TEN were interested to find potential prognostic clinical and pathological markers that can predict the risk of mortality from TEN: this resulted in the identification of several predictive factors including delayed transfer to a specialist unit, increasing patient age, thrombocytopenia, leukopenia and treatment

with antibiotics or corticosteroids before hospital admission. Bastuji-Garin et al proposed a scoring system known as SCORTEN (SCORe of TEN) in 2000 as a mathematical model to predict death from TEN (Bastuji-Garin et al., 2000).

The SCORTEN uses 7 independent risk factors including age, tachycardia, skin detachment of 10% or more and other laboratory parameters for computation (Mockenhaupt, 2011) (Table 1.4). Each parameter is assigned a score value of 1 leading to a total value between 0 and 7, with increasing overall score value indicating poorer prognosis. The SCORTEN data are to be completed within 24 hours of admission and repeated on day 3 or 4 after admission (Kohanim et al., 2016) (Creamer et al., 2016). Thus SCORTEN has been used to accurately predict mortality from SJS/TEN (Trent et al., 2004).

Table 1.4: Severity of illness score (SCORTEN) calculation for toxic epidermal necrolysis. (Adapted from Mockenhaupt 2011).

SCORTEN Parameter	Score	Weight/Score value
Age	≥ 40 years	1
Malignancy	Yes	1
Body surface area detached on day 1	≥ 10%	1
Heart rate	≥ 120 beats per min	1
Serum urea	≥ 10 mmol/l	1
Serum glucose	≥ 14 mmol/l	1
Serum bicarbonate	< 20 mmol/l	1
	Possible score	0-7

1.2.10 Pathogenesis of SJS/TEN

The pathophysiological mechanisms of SJS/TEN are complicated and controversial. However, available evidence suggests that a combination of genetic and innate immune mechanisms ultimately lead to keratinocyte cell death by primary apoptosis which later degenerates into secondary epidermal necrosis (Su and Chung, 2013). A review performed by Nickoloff in 2008 summarised other possible mechanisms including altered drug metabolism resulting in drug specific T cells, immune-mediated mechanisms and activation of downstream death receptors expressed on keratinocytes (Nickoloff, 2008).

1.2.11 Immuno-genetic associations in SJS/TEN

Until recently, little was known about the predisposing factors for SJS/TEN. Advances in pharmacogenetic research have led to the identification of several immuno-genetic markers as predictors of SJS/TEN risk but they are not sensitive predictors of risk (Table 1.5). Genetic risk factors are drug-specific and vary among populations (Usui and Naisbitt, 2017). Allopurinol-induced SJS/TEN was strongly associated with HLA-B*58:01 in patients of Han Chinese descent. Interestingly, in Asian populations including Han Chinese, Thais and Malays, HLA-B*15:02 allele has been detected in SJS/TEN cases caused by carbamazepine (Yip et al., 2012). However, no genetic correlation was found with HLA-B*15:02 in Europeans (Alfirevic et al., 2006) or Japanese patients (Kaniwa et al., 2008). Later studies have shown an association of carbamazepine-induced SJS/TEN with HLA-A*31:01 in Caucasian patients (McCormack et al., 2011) (Genin et al., 2014). An association

between HLA-C*04:01 and nevirapine-induced SCARs including SJS/TEN was detected in HIV-positive Malawian patients (Carr et al., 2013).

Other HLA loci seem to increase the risk of SJS/TEN. In fact, a study reported high incidence of HLA-B12 in TEN survivors (Roujeau et al., 1987). Another study identified HLA-DQB1*06:01 and linked it to an increased risk of SJS/TEN (Power et al., 1996). In addition, single nucleotide polymorphism analyses using candidate genes involved in innate immunity and apoptosis have revealed polymorphisms in TLR3 (Ueta et al., 2007) and interferon-gamma (Charli-Joseph et al., 2013) genes in Japanese and Mexican population respectively with SJS/TEN. Importantly, prospective HLA genetic testing has been implemented into clinical practice to reduce the risk of developing carbamazepine-induced SJS/TEN (Ferrell and McLeod, 2008) (Pirmohamed et al., 2015). In fact, screening of HLA-B*57:01 (Ma et al., 2010) and HLA-B*15:02 in Asians (Amstutz et al., 2014) is recommended for patients being considered to be placed on abacavir and carbamazepine therapy respectively by the FDA. Patients testing positive for these risk alleles are not prescribed the drug to which risk is associated. Importantly, all of these associations are drug specific and the two available genome-wide association (GWA) studies on SJS/TEN have not yielded any significant clinically utilisable genetic associations (Ueta et al., 2017) (Genin et al., 2011). Remarkably, the same HLA allelotypes can yield different skin phenotypes (SJS/TEN versus MPE) but what predisposes some individuals to blistering skin reactions is poorly understood.

Table 1.5: Genetic associations of HLA alleles in SJS/TEN. (Adapted from Su and Chung 2013; Usui and Naisbitt 2017).

Drug	HLA allele	Ethnic population	Reference
Allopurinol	B*58:01	Han Chinese, Thai, Japanese, European	(Hung et al., 2005) (Tassaneeyakul et al., 2009) (Kaniwa et al., 2008)
Carbamazepine	B*15:02	Han Chinese, Thai, Indian	(Chung et al., 2004) (Locharernkul et al., 2008) (Mehta et al., 2009)
	B*15:11, B*59:01	Japanese	(Kaniwa et al., 2010) (Ikeda et al., 2010)
	A*31:01	Han Chinese, Japanese, European	(Hung et al., 2006) (McCormack et al., 2011)
Lamotrigine	B*15:02, B*38	Han Chinese	(Lonjou et al., 2008) (Hung et al., 2010)
	B*58:01, A*68:01, Cw*07:18, DQB1*06:09, DRB1*13:01	European	(Hung et al., 2010) (Kazeem et al., 2009)
Methazolamide	B*59:01, Cw*01:02	Korean, Japanese	(Kim et al., 2010) (Yang et al., 2016)
Oxicam NSAIDs	B*73, A*3, B*12	European	(Lonjou et al., 2008) (Kazeem et al., 2009)
Oxcarbazepine	B*15:02	Han Chinese	(Hung et al., 2010)
Phenytoin	B*15:02	Han Chinese, Thai	(Hung et al., 2010) (Locharernkul et al., 2008)
Sulfamethoxazole	B*38	European	(Lonjou et al., 2008)

1.2.12 Immunological pathophysiological mechanism of acute SJS/TEN

The precise immuno-pathogenesis of SJS/TEN is not fully understood. In general, acute SJS/TEN is considered a T-cell mediated type IV hypersensitivity reaction that can be viewed as an “immunologic burn” (White et al., 2015). Re-exposure of SJS/TEN recovered patients to the causative drug results in a more severe reaction. Components of the type II and III reactions are rarely seen in SJS/TEN. To this end, only C3 and IgG have been detected at the dermal-epidermal junction and around blood cells but they are thought to arise from non-specific exudation (Paquet et al., 1994).

There is strong evidence indicating a role for T lymphocytes, particularly CD8+ T lymphocytes as the main effectors in the pathogenesis of SJS/TEN especially in the acute stages of the syndrome (Nassif et al., 2002) (Nassif et al., 2004a). CD8+ T lymphocytes are present in high concentrations in blister fluid and also in the epidermis whereas CD4+ T lymphocytes are concentrated to the dermal layers in the early stages of TEN (Correia et al., 1993). CD8+ T lymphocyte presence in blister fluid at the early stage of SJS/TEN, most probably suggests that antigen presentation occurs via MHC class I-restricted drug presentation leading to the clonal expansion of CD8+ cytotoxic T lymphocytes (Harr and French, 2010) (White et al., 2015) (Ko et al., 2011).

At the later stages of the disease, however, there is a relative decrease in the number of lymphocytes and an increase in activated monocytes (Abe, 2015) (Chung et al., 2008). In addition, soluble IL-2 receptor, a marker for activated T cells is present at elevated levels in blister fluid and serum of TEN patients and at levels

that correlate with disease severity (Correia et al., 2002b). A number of studies have demonstrated a rise in the amount of activated T lymphocytes expressing the skin-homing receptor, cutaneous lymphocyte-associated antigen (CLA) in the early development of cutaneous reactions (Villada et al., 1992) (Correia et al., 1993) (Leyva et al., 2000).

Chung and colleagues demonstrated the presence of several immune cells including T lymphocytes, natural killer (NK) cells and natural killer T (NKT) cells in blister fluid from SJS/TEN patients and that these cells demonstrate target killing *in vitro* (Chung et al., 2008). CD8+ T cells isolated from peripheral blood mononuclear cells (PBMCs) of patients with SJS/TEN caused by carbamazepine were shown to release the cytotoxic mediator granulysin *in vitro* when stimulated with drug (Ko et al., 2011). In addition, characterisation of CD8+ T cells isolated from both the epidermis and TEN blister fluid samples revealed that majority of isolated immune cells express different surface markers normally present on natural killer cells. For instance, CD8+ T cells in the epidermis express both the killer inhibitory receptor (KIR) and the killer activating receptor (KAR) while CD8+ T cells from blister fluid express CD56 neural cell adhesion molecule (Le Cleach et al., 2000).

Apart from T cells and natural killer cells, other cell types of the immune system have been shown in SJS/TEN. Skin biopsy data analysed via immunohistochemistry have shown a predominance of cells belonging to the monocyte-macrophage origin. Also, cytokines like tumour necrosis factor-alpha and potentially IFN-gamma are thought to play a role in SJS/TEN (Paquet et al., 1994). One study also found a dominant expression of monoclonal antibody clone (MAC) 387+ macrophages and

factor XIIIa+ dendritic cells (dermal dendrocytes) in the epidermis and dermis respectively of TEN patients (Paquet et al., 2000). MAC 387 is a monoclonal antibody clone that is used to detect cytoplasmic antigen expressed on the surfaces of monocytes and macrophages in inflammatory skin diseases (Kirkham et al., 1990). Factor XIIIa+ dendritic cells are major players in phagocytosis and antigen presentation (Paquet et al., 2003).

Further implicating immune-mediated pathogenesis in SJS/TEN, a myriad of cytokines/chemokines with roles in trafficking, proliferation and activation of T cells and other immune cells have been found at high levels in the skin lesions, blister fluids, blister cells, PBMCs, or plasma of SJS/TEN patients (Su and Chung, 2013). These include IL-2, IL-5, IL-10, IL-12, IL-13, C-C chemokine receptor type 3 (CCR3), CCR10, C-X-C chemokine receptor 3 (CXCR3), and CXCR4.

1.2.13 Mechanistic biomarkers involved in the mechanisms of cell death in SJS/TEN

The hallmark of SJS/TEN pathology is fulminant death of keratinocytes. Cellular death was initially described to involve two major pathways namely necrosis and apoptosis. T lymphocytes are generally believed to induce cell death via apoptosis by activating intracellular caspases within target cells which results in minimal inflammation. There is a general consensus that keratinocyte cell death in SJS/TEN occurs mainly through apoptosis (Paul et al., 1996). Early evidence in support of this was drawn from light and electron microscopy imaging of SJS/TEN epidermis which show characteristic physical changes typical of apoptosis. Terminal deoxynucleotidyl transferase dUTP nick end labelling (TUNEL) staining of

keratinocytes also revealed features characteristic of apoptosis (Inachi et al., 1997). Keratinocyte cell death thought to occur primarily through apoptosis and later through necrosis represents a clear indicator of tissue damage in the early stage of SJS/TEN syndrome (French, 2006).

The mechanism of keratinocyte death is complicated and controversial (Stern and Divito, 2017). Although various models have been put forward in an attempt to explain how keratinocyte cell death leading to tissue damage may be occurring. The most widely accepted model stipulates that both CD8+ T cells and NK cells may be killing target cells by releasing granules containing the cytotoxic proteins such as perforin, granzymes B and by secreting granulysin via a granule-independent granulysin secretion or via the expression of Fas ligand (FasL) which binds to Fas (CD-95) receptor on target cells and can induce keratinocyte apoptosis (Posadas et al., 2002). However, a study published a few years after indicated that perforin and granzyme B are enclosed in vesicles and transported into target cells via mannose 6-phosphate receptor to induce apoptosis via multiple pathways (Veugelers et al., 2006).

Perforin creates pores approximately 16 nm in diameter in the cell membrane permitting granzyme B to enter the cell and activate the intracellular caspase cascade which consequently leads to apoptosis (Posadas et al., 2002). In further support of perforin/granzyme B and Fas/FasL mediated killing, it has been demonstrated that blocking Fas using intravenous human immunoglobulins (Viard et al., 1998) and inhibiting the perforin/granzyme B pathway (Nassif et al., 2004a)

independently protected against killing suggesting that they are important mediators of keratinocyte cell death.

Chung et al discovered that the levels of 15-kDa secretory granulysin in SJS/TEN blister fluid were two to four folds higher than that of perforin/granzyme B or soluble FasL (sFasL) (Chung et al., 2008). It was further demonstrated that depleting secretory granulysin caused a decrease in the cytotoxicity of blister fluid and a further injection of granulysin into mouse skin resulted in blistering and epidermal necrosis mimicking SJS/TEN. These findings suggest that secretory granulysin may be an important mediator of disseminated keratinocyte death in SJS/TEN (Chung et al., 2008). In addition to its cytolytic role, granulysin is a chemoattractant for various immune cells such as T lymphocytes, NK cells, monocytes and other inflammatory cells (Deng et al., 2005) which may partially account for the infiltration of CTLs and NK cells detected in skin lesion of TEN patients (Nassif et al., 2004b).

It is also known that certain cytokines of the tumour necrosis factor (TNF) family can engage specific cell surface receptors to trigger apoptosis (Wehrli et al., 2000) and more recently necroptosis (Panayotova-Dimitrova et al., 2015). Nassif et al reported elevated levels of IFN-gamma, TNF-α, sFasL, interleukins (IL) -18 and -10 in blister fluid from TEN patients and even further demonstrated that CD8+ T cells secrete interferon-gamma (IFN-γ) which sensitizes keratinocytes to express TNF-α, FasL and IL-10 (Nassif et al., 2004b). Keratinocytes can also express IL-15 which is needed for the development, maturation and function of both CD8+ T cells and NK

cells and this can have important consequences in disease pathogenesis (Fehniger and Caligiuri, 2001).

In addition to those mentioned above, other mediators of keratinocyte death include annexin A1, receptor-interacting protein kinase 3 (Panayotova-Dimitrova et al., 2015), nitric oxide (Lerner et al., 2000), calprotectin, and micro RNA 18a-5p upregulation (Ichihara et al., 2014). Interestingly, the two dominant forms of cell death, apoptosis and necrosis appear to have roles in SJS/TEN pathogenesis. Classical apoptosis and the newly described programmed necrosis (also known as necroptosis) have been proposed as pertinent cell death pathways responsible for the widespread keratinocyte death that is observed in SJS/TEN (Panayotova-Dimitrova et al., 2015).

In fact, most of the mediators of cell death discussed above have been suggested as potential mechanistic biomarkers of SJS/TEN due to their involvement in disease pathophysiological mechanisms (Kapoor, 2013) (Harris et al., 2016) (Fujita et al., 2014) (Posadas et al., 2002) (Table 1.6). There is a lack of biomarkers that can either be used in differentiating SJS/TEN from other less serious cutaneous phenotypes or used in monitoring disease prognosis (Duran-Figueroa et al., 2015). Whilst further research is still being undertaken to explore novel biomarkers involved in disease pathogenesis, there is still need to further investigate suggested existing markers of SJS/TEN.

Table 1.6: Mechanistic biomarkers proposed for detection and monitoring of SJS/TEN (Adapted from Harris et al 2016; Duran-Figueroa et al 2015; Fujita et al, 2014; Panayotova-Dimitrova et al 2015).

Marker	**Description**	**cutaneous ADR detected**
Granulysin	Pro-inflammatory cytolytic molecule released by cytotoxic T cells	SJS/TEN
Fas ligand	Transmembrane apoptotic protein	SJS/TEN
High mobility group box-1 protein	Protein released by injured or damaged cells/tissues	SJS/TEN, DRESS
Perforin	Pore forming protein produced by cytotoxic T cells	SJS/TEN, DRESS
RIPK3	Receptor-interacting protein kinase-3 involved in necroptosis regulation	SJS/TEN
Granzyme B	Serine protease found in granules of cytotoxic T lymphoctes and NK cells	SJS/TEN, DRESS
Tumour necrosis factor-alpha	Pleiotropic pro-inflammatory protein	SJS/TEN, DRESS
Micro RNA 18a-5p	Non-coding RNA involved in post-transcriptional regulation	SJS/TEN
Alpha defensin 1-3	Cationic peptides released by cytotoxic T cells	SJS/TEN

1.2.14 *In vitro* models of SJS/TEN

There is a lack of *in vitro* models to investigate the pathogenesis of SJS/TEN largely due to the complexity of the disease. In fact, in spite of numerous attempts over the years, not much has been achieved in designing good and disease mimicking *in vitro* models. Letko and colleagues devised an *in vitro* organ culture using a pool of

sera from biopsy aided diagnosed TEN patients (Letko et al., 2011). Control sera were from normal healthy patients and normal human skin, normal human conjunctiva and normal human buccal mucosa were used as substrates. These substrates were cultured in either healthy control derived sera or TEN sera. Skin and conjunctiva incubated in TEN sera showed remarkable histopathological features resembling those seen in TEN biopsy specimens.

Most of the relatively few *in vitro* models of SJS/TEN have used keratinocyte cells to investigate an aspect of disease pathogenesis. Nassif et al tested the cytotoxicity of SJS/TEN blister fluid on autologous keratinocytes (Nassif et al., 2004b). It was discovered that blister fluid can kill keratinocytes due to the presence of cytotoxic CD8+ T cells. A number of toxins have been assessed for their ability to kill keratinocytes *in vitro*. It is important to develop more *in vitro* models to study potential mediators of SJS/TEN.

Keratinocytes constitute about 95% of the cellular population in the human epidermis (Kim et al., 2015a) (Sprenger et al., 2013) (El Darzi et al., 2017) and play a vital role in the skin immune system primarily by maintaining the physical and biochemical integrity of the skin (Chikh et al., 2014). This cell type responds to diverse stimuli including cytokines, haptens and allergens including drugs by expressing and releasing immunomodulatory mediators. It has the ability to recruit immune cells to the site of injury and this is aided through the expression of various chemokines, pro-inflammatory cytokines and adhesion molecules (Kim et al., 2015a) (Barker et al., 1991) (Bos and Kapsenberg, 1993). A widely utilised spontaneously proliferating immortalised human keratinocyte cell line (HaCaT)

represents a good choice for investigation in dermatological studies as it is similar in phenotypic properties to skin epidermal keratinocytes (Schürer et al., 1993) (Schoop et al., 1999) (Colombo et al., 2017) (Chikh et al., 2014).

1.3 Death mediators and molecular mechanisms

1.3.1 Molecular definition and classification of death pathways

A cell is considered dead when either there is irreversible loss of plasma membrane integrity defined by vital dyes *in vitro* or complete fragmentation of cell including its nucleus into discrete/apoptotic bodies or its corpse has been engulfed by a neighbouring cell *in vivo* (Kroemer et al., 2005). The advent of better biochemical assays to detect precise mechanisms of cell death has changed how cell death is defined which has necessitated a re-classification of cell death types. For decades, cell death classifications have focused on morphological criteria which distinguishes cell demise as either apoptosis (also called programmed cell death) or necrosis (also known as accidental cell death). Due to the lack of consensus on the biochemical changes that precede cell demise, the Nomenclature Committee on Cell Death have now proposed more specific biochemical and molecular mechanisms of classifying cell death modalities in research (Galluzzi et al., 2012). Cell death pathways involving necrosis, necroptosis and apoptosis will be elaborated upon below.

1.3.2 Necrotic cell death pathway

Necrosis (most often known as accidental cell death) is defined as a type of cell death that lacks features of apoptosis and autophagy and is conventionally

considered to uncontrolled (Kroemer et al., 2005) (Edinger and Thompson, 2004). Necrosis is defined on the basis of morphological criteria such as early plasma membrane rupture, dilatation of cytoplasmic organelles, in particular the mitochondria and moderate condensation of chromatin, swelling of cellular organelles and cell lysis (Chen et al., 2014).

Necrosis is induced when there is an extensive failure of normal physiological pathways that are essential for cellular homeostasis such as regulation of ion transport, energy production, oxygen depletion and pH balance amongst others (Jin and El-Deiry, 2005). It has also been firmly established in the literature that inhibiting classical apoptosis signalling machineries either by pharmacological inhibition of caspases or using genetic methods can either sensitize or lead to necrosis (Jin and El-Deiry, 2005) (Golstein and Kroemer, 2007). In addition, the incomplete activation of caspase-dependent pathway can also lead to necrosis. Induction of necrosis is also cell type dependent as some cells (for example L929 murine fibrosarcoma cell line) are usually very sensitive to necrosis under certain conditions (Golstein and Kroemer, 2007).

The chronological and molecular sequence of events leading to necrosis is not fully understood. For instance, the relationship between calcium, adenosine triphosphate (ATP) and reactive oxygen species in mitochondrial mediated toxicity is complex, most likely due of the existence of self-destructive feed-forward loops (Brookes et al., 2004). Although it is important to note that each of these events alone is not specific to necrosis as indeed some can also trigger apoptosis (Kim et al., 2003). Perhaps, it is possible that the accumulation of multiple events in an

organised, programmed cascade of self-destruction might define necrosis (Golstein and Kroemer, 2007).

1.3.3 Apoptotic cell death pathway

The term apoptosis was originally coined by Kerr *et al* to describe a particular morphological aspect of cell death (Kerr et al., 1972) accompanied by rounding-up of cell, retraction of cellular volume, chromatin condensation, nuclear fragmentation and membrane blebbing (Kroemer et al., 2005) (Ouyang et al., 2012). Oligonucleosomal DNA fragmentation and caspase activation are helpful indicators in the diagnosis of apoptosis.

Apoptosis is an essential component of life for multicellular organisms that plays a vital role in development and tissue homeostasis. It is usually delicately regulated and controlled in a physiological context. However, dysregulation of apoptosis results in a myriad of pathological conditions including developmental defects, autoimmune diseases, neurodegeneration and cancer (Kam and Ferch, 2000) (Elmore, 2007). Apoptosis follows two major routes namely the extrinsic and the intrinsic pathways but there could sometimes be crosstalk between them.

1.3.4 Death-inducing ligands/receptors and extrinsic apoptosis

The extrinsic apoptosis pathway relies on extracellular stress signals from various lethal ligands such as Fas/CD95/APO-1 ligand (FasL/CD95L), tumour necrosis factor-α (TNFα), and TNF (ligand) superfamily, member 10 (TNFSF10) popularly called TNF-related apoptosis inducing ligand (TRAIL) (Locksley et al., 2001). Propagation of extracellular stimuli is carried out through specific transmembrane receptors

containing death domains (DD) (Galluzzi et al., 2012). These receptors include Fas/CD95, TNFα receptor 1 (TNFR1) and TRAIL receptor (TRAILR) 1-2.

1.3.5 Fas/FasL-induced apoptotic pathway

The FasL-Fas apoptotic signalling pathway is mediated by Fas, a cell surface death receptor belonging to the TNFR family which interacts with its ligand called Fas ligand (FasL). FasL exists in two forms, namely the membrane bound and the soluble form (sFasL) which is generated via the proteolytic cleavage of the membrane bound form. The binding of FasL to Fas promotes receptor trimerization which in turn results in intracellular clustering of death domains accompanied by its internalisation into an endosomal pathway (Strasser et al., 2009).

Fas can also pre-assemble at the plasma membrane to form functional trimers in the absence of ligand binding due to its extracellular pre-ligand binding assembly domain (PLAD), a domain also shared by TNFR1 (Danial and Korsmeyer, 2004) which is critical for ligand binding. The adaptor protein of Fas called Fas-associated death domain (DD) containing protein (FADD) which also contains a death effector domain (DED) motif is recruited to the DD of activated Fas. FADD through its DED (responsible for downstream signal transduction) located at the N-terminal tail (Nagata, 1997) allows the recruitment of initiator pro-caspase 8 (dimerised) to the CD95-FADD complex.

Pro-caspase 8 associates with FADD through its own death effector domain. The resulting multiprotein complex is called death inducing signalling complex (DISC) of which FADD and pro-caspase 8 are the key components. The interaction between FADD and pro-caspase 8 induces self-proteolysis of pro-caspase 8 into active

hetero-tetrameric caspase-8 p18/p12 fragments. This in turn is followed by the proteolytic processing of downstream effector procaspases-3/7 into their active forms (Micheau and Tschopp, 2003) (Danial and Korsmeyer, 2004). This trend to favour lethal stimulus signalling and caspase-8 activation is thought to occur in an "induced proximity" fashion made possible by elevated local levels of procaspase-8. Consequently, apoptotic substrates cleaved by activated effector caspases implement cell dismantling.

Other signalling proteins that can be recruited to the Fas DISC include receptor interacting protein kinase 1 (RIPK1, also referred to as RIP1), cellular inhibitors of apoptosis proteins (cIAPs), multiple subtypes of cellular FLICE-like inhibitory protein (c-FLIP), E3 ubiquitin ligases which on its own can inhibit apoptosis by interfering with caspase activation including pro-caspase-8/-10 (Galluzzi et al., 2012). Although, within the DISC, both cIAPs and c-FLIP exhibit a pro-survival signal, the overall decision between survival and lethal signals seems to be partly regulated by the formation of differential complex between various DD and DED proteins (Danial and Korsmeyer, 2004). Activation of Fas signalling pathway is particularly confined to apoptosis (Nagata, 1997).

A variety of human immune and non-immune cell types including human epidermal keratinocytes express Fas antigen on their surfaces (Matsue et al., 1995). Fas-induced apoptosis can occur via two independent pathways depending on cell types. In type I cells, caspase-8 cleaves and activates caspase-3/7 whereas in type II cells, caspase-8 activates pro-apoptotic BCL-2 family member BH3-interacting domain death agonist (BID) of the intrinsic apoptosis pathway (Hao and Mak, 2010)

and consequently related downstream signalling cascade relying on the mitochondrial-dependent amplification loop.

Importantly, activation of Fas can also result in non-apoptotic signalling response like cell proliferation and differentiation in normal human diploid fibroblasts and T cells. Fas-mediated proliferation tends to involve activation of FADD, caspase 8 or FLIP since mice deficient in these molecules have a defect in T cell proliferation (Strasser et al., 2009).

1.3.6 TNF-induced apoptotic pathway and receptor signalling

TNF signalling is mediated by TNF ligand through its transmembrane receptors TNFR1 and TNFR2. TNF is an important multifunctional cytokine in many biological processes and apoptosis (Micheau and Tschopp, 2003) which is primarily produced as type II transmembrane protein packaged in stable homotrimers. Moreover, TNF is expressed not only by activated immune cells like macrophages, monocytes, T cells, NK cells but also by a diverse array of non-immune cells such as endothelial cells and fibroblasts. Generally speaking, there are distinct TNFR-specific signalling pathways with extraordinary levels of complexity. The vast majority of TNFα lethal signals are propagated via TNFR1 (Vandenabeele et al., 1995) while TNFR2 is predominantly expressed by immune cells. TNFR1 is constitutively expressed, whereas TNFR2 expression is inducible. Like FasL, two forms of TNF are known: membrane bound TNF and soluble TNF which is generated via metalloproteinase-mediated proteolysis of membrane-bound TNF (Nagata, 1997) (Figure 1.4).

The ability of preassembled pre-ligand binding assembly domain (PLAD) stabilised TNFR1 to signal is occluded by binding of the silencer of death domain (SODD)

protein, an inhibitor of TNFR in the un-induced state (Wajant et al., 2003). TNF binding causes SODD to be dissociated from TNFR1 complexes thereby permitting the recruitment of the death domain-containing adaptor protein called TNFR-associated death domain protein (TRADD) via homophilic interactions of their death domains (Wajant et al., 2003). It is widely accepted that TRADD serves as a common assembly platform for the binding of TNFR-associated factor (TRAF) 2, FADD and the death domain containing RIP1. These proteins provide a scaffold allowing the recruitment of additional proteins like pro-caspase 8 to the DISC. Although TRADD lacks a DED in contrast to FADD, its C-terminal DD is used instead for downstream signalling (Hsu et al., 1996). Furthermore, unlike Fas pathway, both TNFR1 and TNFR2 pathways mandatorily require a common signal transducer, TRADD for recruiting FADD and TRAF via their DDs (Rothe et al., 1995) (Galluzzi et al., 2012).

The recruited pro-caspase 8 is activated through proteolytic cleavage and is released. The freed caspase 8 can then cleave pro-caspases-3, -6, -7 and other cytosolic substrates which can then execute apoptosis. Importantly, TNFR1-induced apoptosis consists of two sequential signalling complexes mediated by pro-survival and pro-death signalling proteins. A more elaborate discussion on TNF-α/TNFR1 signalling is provided in chapter 4 (4.1).

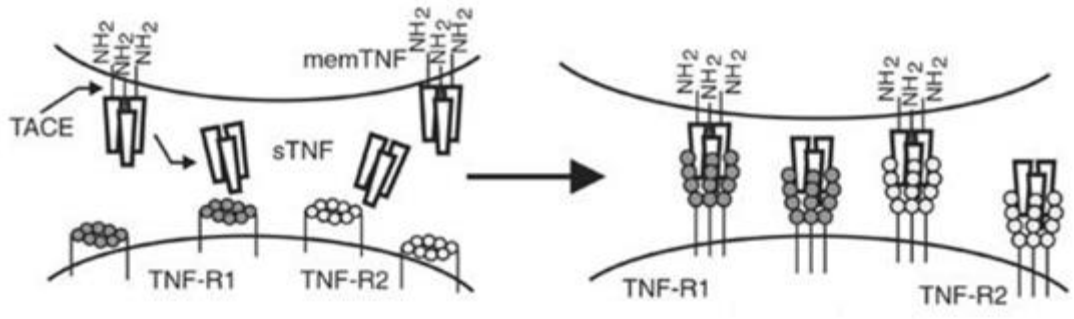

Figure 1.4: Enzymatic processing of tumour necrosis factor (TNF). Membrane-bound TNF (memTNF) is cleaved by metalloprotease TNF alpha converting enzyme (TACE) to generate homotrimeric soluble TNF (sTNF). Both memTNF and sTNF bind to the two members of TNF receptor family, TNFR1 and TNFR2. Whilst memTNF can activate both TNFR1 and TNFR2, sTNF mostly activates TNFR1 and exerts limited signalling capabilities on TNFR2. TNFR2 can only be fully activated by memTNF. Figure modified from Wajant *et al* 2003.

1.3.7 The intrinsic (mitochondrial) apoptotic pathways

Stimuli that lead to the initiation of the intrinsic apoptotic pathways usually originate from the intracellular environment. Mitochondria play a central role in orchestrating the intrinsic apoptosis. Mitochondrial outer membrane permeabilization (MOMP) is a pivotal event in the mitochondrial pathway which is regulated by the Bcl-2 protein family (Wang and Youle, 2009). There are about 20 members of the Bcl-2 family with either anti-apoptotic or pro-apoptotic functions and are divided into three categories based on the presence of conserved Bcl-2 homology (BH) domains (Wang, 2001). The anti-apoptotic members such as Bcl-2, Bcl-xL, Bcl-W, Mcl-1 and A1 containing all four BH domains promote cell survival. The pro-apoptotic members divided into two groups elicit cell death. The first group, the damage-sensing BH3-only proteins including Bid, Bad, Bim, Noxa, Puma and others which all possess the BH3 interaction domain transmit both intrinsic and

extrinsic death signals to the second pro-apoptotic multi-region BH domain proteins such as Bax and Bak (Wang, 2001). Although BH3-only proteins promote apoptosis by directly activating Bax and Bak (containing BH1-BH3 domains) at the mitochondrial outer membrane and by suppressing anti-apoptotic proteins at the mitochondria and endoplasmic reticulum; however commitment to apoptosis is controlled by Bak and Bax, both of which can cause mitochondrial outer membrane permeabilization (Wang and Youle, 2009). Bax and Bak mediated mitochondrial permeabilization causes the release of apoptogenic proteins such as cytochrome C, Smac/Diablo, apoptosis-inducing factor and endonuclease G (Wang, 2001) (Figure 1.5). Released cytochrome C binds to and activates cytosolic apoptosis protease activating factor-1 (Apaf-1) which contains a caspase recruitment domain (CARD) domain. Cytochrome C/Apaf-1 apoptosome complex triggers the activation of initiator caspase 9 which in turn cleaves and activates effector caspase 3 leading to apoptosis.

To prevent constitutive cell death, BH3-only proteins are regulated by a diverse array of mechanisms including transcription and post-translational modifications that govern how these proteins interact specifically with their targets. Also the balance between anti-apoptotic and pro-apoptotic Bcl-2 family members is believed to play a role in determining cell fate (Hata et al., 2015) (Shamas-Din et al., 2013).

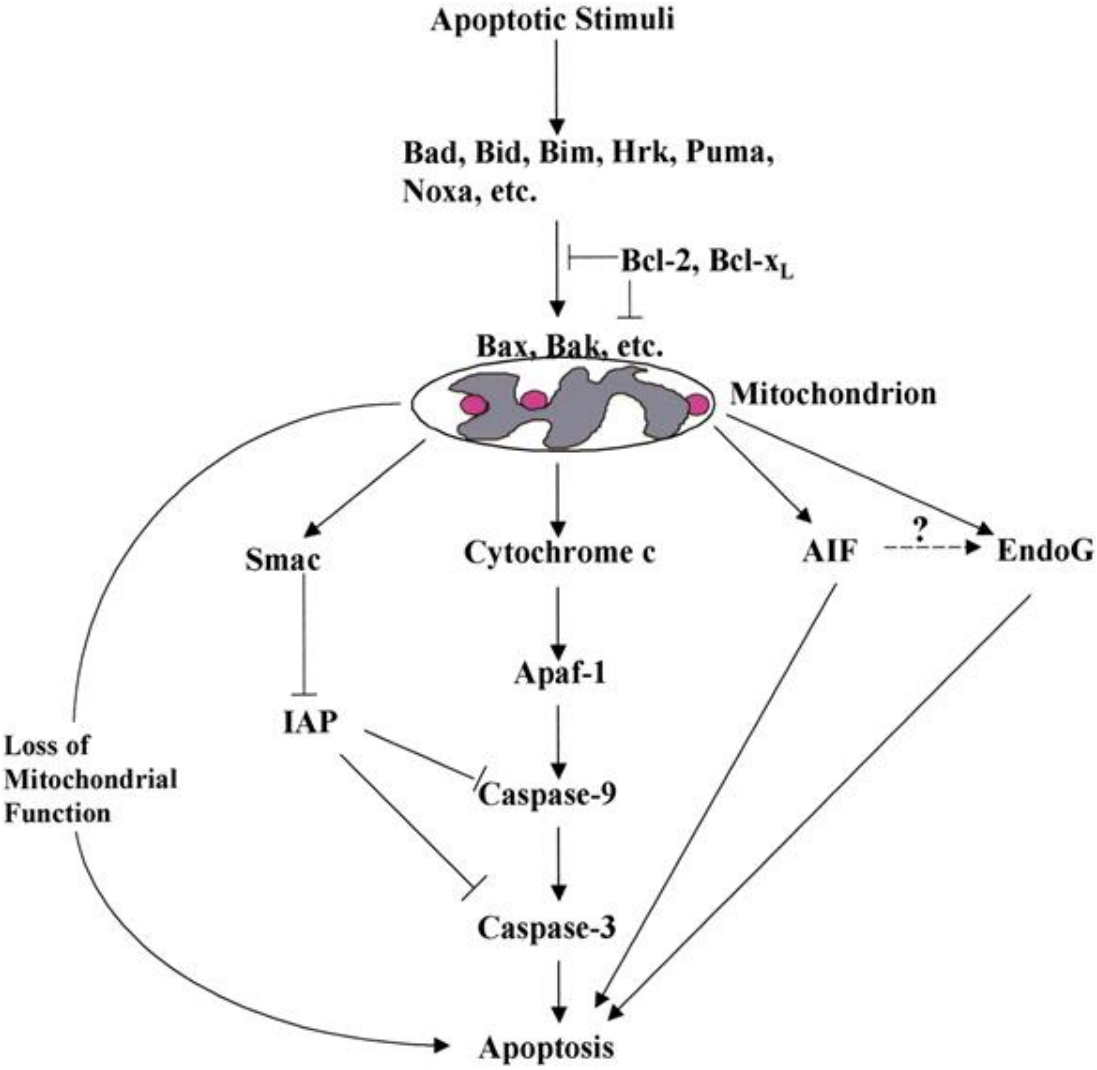

Figure 1.5: Multiple intrinsic apoptotic signals transduced by the mitochondria result in apoptosis. Intrinsic apoptotic stimuli are transmitted to the mitochondria by the BH3-only proteins such as Bim, Bid, Puma, Bad, Noxa amongst others. The signal emanating from the BH3-only proteins can either be neutralised by anti-apoptotic proteins such as Bcl-2 and Bcl-xL or further transduced to the mitochondria by the pro-apoptotic proteins such as Bak and Bax which permeabilize the mitochondrial outer membrane. Damage to the mitochondria caused by Bak or Bax triggers the efflux of apoptogenic proteins including cytochrome C, Smac/Diablo, apoptosis-inducing factor (AIF), and endonuclease G (EndoG). Cytochrome C triggers caspase 9 activation via apoptosis protease activating factor-1 (Apaf-1) and Smac/Diablo causes inhibitor of apoptosis proteins (IAPs) inhibition of caspase to be relieved potentiating caspase activation. Activated caspase 9 cleaves and activates executioner caspase 3 which cleaves downstream substrates resulting in apoptosis. AIF and EndoG promote caspase-independent chromatin condensation and fragmentation. In addition, damage to mitochondria may passively lead to cell death owing to loss of mitochondrial essential function required for cell survival. Diagram modified from Wang 2001.

1.3.8 RIPK1/RIPK3 and MLKL signalling in necroptosis

Necroptosis (programmed necrosis) is another form of programmed cell death (caspase-independent) that is regulated by key effectors which include the serine/threonine receptor interacting protein kinase 1 (RIPK1), RIP3 and the pseudo-kinase mixed lineage kinase domain-like (MLKL) protein (Sun et al., 2012). MLKL is the central core protein in necroptosis signalling (Hildebrand et al., 2014b). It has also been observed that ligation of a number of death receptors such as FAS, TNFR1, TNFR2, TRAILR1, TRAILR2 as well as Toll-like receptors (TLRs) which are known inducers of the apoptotic machinery can initiate necroptosis under certain circumstances (Vandenabeele et al., 2010b) (Tanzer et al., 2016). Some characterised biological molecules have been identified as initiators or modulators of necroptosis and these include caspase 8 inhibitors, ubiquitin E3 ligases, reactive oxygen species produced by mitochondria or NADPH oxidase 1, deubiquitinating enzymes and others (Vandenabeele et al., 2010b).

Both RIP1 and RIP3 belong to the family of serine threonine kinases and are capable of phosphorylating target substrates. This family of kinases play a vital role in innate and adaptive immunity. RIP1 is comprised of an N-terminal kinase domain (KD), an intermediate domain, a RIP homotypic interaction motif (RHIM) domain, and a C-terminal DD motif (Vandenabeele et al., 2010a) (Figure 1.6). Similarly, RIP3 is comprised of a KD and a RHIM but Its C-terminus lacks a DD (Vandenabeele et al., 2010a) (Sun et al., 1999) (Figure 1.6). RIP1 and RIP3 have been shown to interact together via their RHIM domains which enable them to form amyloid-like fibrillar structures in a higher molecular weight multiprotein complex termed the

necrosome (Li et al., 2012) (Vandenabeele et al., 2010a). Polyubiquitination of RIP1 at residue K63 by cIAP1 and cIAP2 leads to its degradation and might be crucial for cell survival (Vandenabeele et al., 2010a). Complex II apoptosis-inducing complex is converted to necroptosis-mediating complex in the presence of RIP3 in the DISC. Caspase-8 mediated cleavage of RIP-1/3 is prevented in the presence of caspase inhibitors like c-FLIP which leaves them ready for their sub-cellular kinase function (Vandenabeele et al., 2010a).

The core most terminal known effector of necroptosis, full length MLKL (FL MLKL) consists of an N-terminal four-helix bundle (4HB) domain joined to a C-terminal pseudokinase domain (PsKD) via two-helix linker termed brace helices (Murphy et al., 2013) (Tanzer et al., 2016). The PsKD motif is so-named because it possesses a conserved kinase-like fold, but lacks residues essential for catalytic activity in canonical protein kinase. Although it lacks a catalytic residue, MLKL has the ability to bind ATP but the role of nucleotide binding is not known. The structure of human MLKL has not been reported to date (Petrie et al., 2018).

RIP1 can auto-phosphorylate itself in the necrosome at serine/threonine residues. Activated RIP1 orchestrates the phosphorylation of RIP3 which then phosphorylate MLKL at threonine 357 and serine 358 residues at the PsKD domain; this is a pivotal requirement for TNF-initiated necroptosis (Yoon et al., 2016) (Chen et al., 2014). As a result, a conformational change is induced in human MLKL that causes the exposure of the 4HB executioner domain (Tanzer et al., 2016) and dissociation from the PsKD αC helix and pseudocatalytic loop to facilitate the formation of a tetramer. Subsequently, MLKL oligomerization (tetramerization) enables membrane

translocation and complex formation with lipids in the plasma membrane and ultimately necroptotic cell death (Tanzer et al., 2016). It is widely reported that the 4HB domain is responsible for lipid engagement and membrane permeabilization. Moreover, a previous report demonstrated that the 4HB domain of human MLKL binds to phosphatidylinositol phosphates (PIP) via a patch of positively charged amino acid residues at the surface of 4HB to induce leakage of PIP-containing liposomes (Dondelinger et al., 2014). The precise mechanism of MLKL-induced necroptotic death is poorly understood and still a subject of debate; however, suggested possible downstream mechanisms by which 4HB may be causing cell demise include direct permeabilization of plasma membrane/formation of a transmembrane pore, possibly through activation of ion channels (Tanzer et al., 2016) (Chen et al., 2014) and likely permeabilization of PIP-containing membranes.

Interestingly, it has been established that expressed human 4HB of MLKL (truncated MLKL) is capable of mediating necroptosis by itself through chemically enforced oligomerization (Vandenabeele et al., 2010a) (Chen et al., 2014). Collectively, both full-length MLKL and the short length 4HB-MLKL can trigger necroptosis following induction.

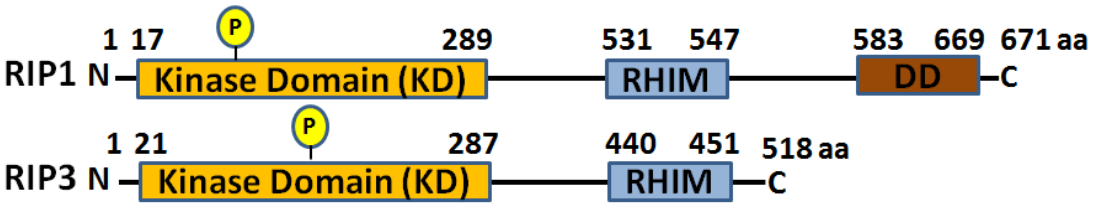

Figure 1.6: Schematic representation of the structure of human RIP1 and RIP3. The number of amino acids (aa) that make up each domain is given. RIP1 contains 671 amino acid residues while RIP3 contains 518 amino acid residues. Both RIP1 and RIP3 have an N-terminal kinase domain (KD) and an intermediate RIP homotypic interaction motif (RHIM) domain. RIP1 has a C-terminal death domain (DD) but RIP3 does not. Phosphorylation sites are located on the kinase domains for both proteins.

1.4 High mobility group box-1 (HMGB1)

1.4.1 Molecular biology and structure of HMGB1

High mobility group box-1 (HMGB1) is a non-histone chromatin binding protein with 215 amino acid sequences that is ubiquitously expressed by virtually all nucleated cell types. Structurally, HMGB1 consists of two functional domains namely the A and B boxes which are both positively charged and a negatively charged acidic C-tail (Tsuda et al., 1988) (Figure 1.7). In the nucleus, HMGB1 binds to DNA minor groove without sequence specificity and induces a bend in the helical structure of DNA to permit physical interactions with transcription factors and the chromatin. Under physiological conditions, HMGB1 expression is predominantly localised to the nucleus where it regulates a number of vital housekeeping activities such as DNA replication, repair, recombination and transcription via its action on the chromosomal architecture (Agresti and Bianchi, 2003).

HMGB1 and other relatives (HMGB2 and HMGB3) were so-named due to their high mobility in electrophoretic polyacrylamide gels (Goodwin et al., 1973). It is a highly evolutionary conserved protein with 99% identity among all mammals. HMGB1 is encoded by the *HMGB1* gene which is located on chromosome 13q12 in humans (Ferrari et al., 1996). The low affinity non-specific binding of HMGB1 to DNA confers to it a high motile property and this allows HMGB1 to shuttle between the nucleus and cytosol via nuclear pores (Pallier et al., 2003). In addition, HMGB1 can also be found within the mitochondria (Stumbo et al., 2008). Cytosolic HMGB1 plays a role in the maintenance of normal mitochondrial morphology and cellular bioenergetics. HMGB1 is also expressed on the plasma membrane of certain cell types. Membrane-bound HMGB1 controls neurite growth, smooth muscle cell, chemotaxis and tumour cell metastasis (Rauvala and Rouhiainen, 2007).

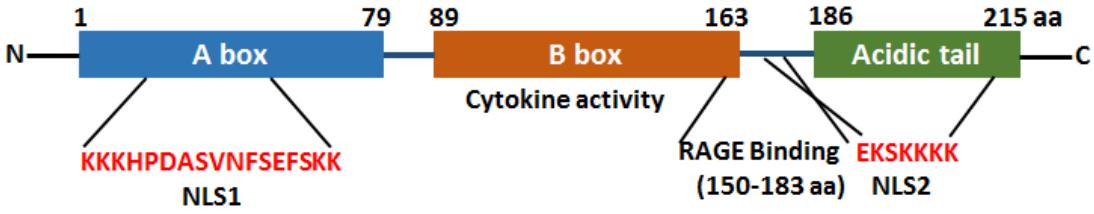

Figure 1.7: **Schematic representation of the structure of high mobility group box-1 (HMGB1) protein molecule.** HMGB1 is a single polypeptide protein with 215 amino acid (aa) residues having a molecular weight of 25kDa. The entire HMGB1 protein consists of three domains; A and B boxes and an acidic C-terminal tail with high amount of glutamic or aspartic acid residues. The number of amino acid residues that correspond to each domain is shown in the figure. HMGB1 binds to the minor groove of DNA using both its A and B boxes. The cytokine activity of HMGB1 is found within the amino acid residues of the B-box whereas the binding domain for the receptor for advanced glycation end products (RAGE) is located between residues 150 and 183. Truncated A-box shows antagonism towards HMGB1 activities. Transport of HMGB1 into the nucleus is mediated by nuclear localisation signal (NLS) -1 and -2 located on the A box and residues spanning between the connecting segment and the acidic tail respectively.

1.4.2 Extracellular release of HMGB1

For HMGB1 to act as danger signal and pro-inflammatory mediator, it must first be transported extracellularly from the nucleus. This can occur via two distinct modes i) active secretion from activated immune cells and ii) passive release from necrotic or injured or damaged cells.

Active secretion of HMGB1

HMGB1 can be actively secreted by both immune cells such as macrophages, monocytes, NK cells, dendritic cells (DCs) and non-immune cells like endothelial cells and platelets after being stimulated by pro-inflammatory stimuli including lipopolysaccharides, IL-1 and TNF-α (Bonaldi et al., 2003). HMGB1 lacks a secretory signal peptide and thus is not secreted via the Golgi apparatus/endoplasmic reticulum pathway. In monocytes and macrophages, cytoplasmic localised HMGB1 must first of all be packaged into specialized cytoplasmic vesicles that show the features of secretory lysosomes. HMGB1-containing endolysosomes fuse with cell membrane and are exocytosed following activation by extracellular lysophosphatidylcholine or ATP (Gardella et al., 2002).

Passive release of HMGB1

Passive transport of HMGB1 into the extracellular milieu can occur in necrotic cells (Bianchi and Manfredi, 2007). In contrast, apoptotic cells retain their HMGB1 bound to DNA via a mechanism involving acetylation of histones (Bell et al., 2006a). The affinity of HMGB1 for DNA is determined by the degree of acetylation of histones with a lower degree of acetylation promoting a stronger binding of HMGB1 to DNA.

1.4.3 Signalling pathways and receptors for HMGB1

Extracellular HMGB1 can signal as a damaged-associated molecular pattern (DAMP) and as a cytokine (Andersson and Tracey, 2011). DAMPs are a class of diverse signalling molecules and cellular components which are predominantly released by injured, dying or damaged cells (Davidovich et al., 2014) (Pasparakis and Vandenabeele, 2015) and can include cytokines, chemokines and alarmins which are usually recognised by pattern recognition receptors mostly present on innate immune cells (Tang et al., 2012b) (Rosin and Okusa, 2011). These receptors include the TLRs, nucleotide oligomerisation domain (NOD)-like receptors, advanced glycation end products (RAGE) and retinoic acid-inducible gene 1 (RIG-1)-like receptors (Tang et al., 2012b). In fact, HMGB1 can act as both an alarmin (a DAMP that elicits exclusively acute pro-inflammatory effects) and a cytokine (Yang et al., 2004) (Andersson et al., 2000) (Andersson et al., 2018). As a prototype DAMP, HMGB1 is perhaps the most well characterised in discriminating cell death forms (Rosin and Okusa, 2011).

HMGB1 can bind to a number of cell surface receptors to propagate pro-inflammatory signalling. They include RAGE, TLR2, -4 and -9, macrophage antigen-1, CXCR4, T-cell immunoglobulin and mucin domain-3 and others. TLR4 is the principal receptor necessary for the promotion of macrophage activation, cytokine induction and tissue damage (Yang et al., 2010) through activation of the pro-inflammatory NF-κB pathway (Tang et al., 2012b). Apart from direct receptor interaction, HMGB1 can also form hetero-complexes with various molecules which include IL-1, CXCL12, DNA, RNA, histones and lipopolysaccharide to generate stronger synergistic

responses via reciprocal receptors for HMGB1-partner molecules (Andersson and Tracey, 2011) (Harris et al., 2012). The effects of HMGB1 are mediated through various signalling pathways including mitogen activated protein kinase (MAPK), phosphoinositide-3-kinase (PI3K)/Rac-a serine/threonine-protein kinase (Akt) (PI3K/Akt) and nuclear factor-kappa B (NF-Kb) (Gong et al., 2010).

1.4.4 Post-translational modifications of HMGB1

Following translation, newly synthesized HMGB1 undergoes extensive modifications including acetylation, terminal cysteine oxidation, phosphorylation, methylation, adenosine diphosphate (ADP)-ribosylation and to a lesser degree glycosylation and these do have functional consequences (Richard et al., 2017). For instance, acetylation within the A and B box motifs is functionally vital as it can influence DNA-binding affinity, histone interaction and shuttling between the nucleus and cytoplasm (Bonaldi et al., 2003). Emphatically, acetylation at certain lysine residues of HMGB1 proximal to the nuclear localisation signal promotes its translocation from the nucleus to the cytoplasm and prevents a nuclear re-entry which is a requirement for extracellular secretion (Lotze and Tracey, 2005). Moreover, phosphorylation of HMGB1 has been reported to modulate its transcriptional factor regulatory activity as well as influencing its stability configuration and DNA-binding avidity (Wolffe, 1994).

1.4.5 Redox status of HMGB1 determines extracellular functions

Redox states of HMGB1 regulate its extracellular functions. HMGB1 contains three conserved key cysteines (C); C23, C45 (box A) and C106 (box B) which are sensitive

to oxidation (Hoppe et al., 2006) (Figure 1.8). The redox states of these cysteines dictate the extracellular activity of HMGB1 (Tang et al., 2012a). In mild oxidative conditions, C23 and C45 readily form an intramolecular disulphide bridge, while C106 usually remains unpaired (reduced) (Hoppe et al., 2006). Thus three distinct redox forms of HMGB1 (all-thiol-HMGB1, disulphide-HMGB1, and oxidised-HMGB1) were generated using bacterial expression systems (Venereau et al., 2012).

The three redox forms were reported to have a differential function in cytokine-stimulating and chemoattractant activities (Venereau et al., 2012) (Figure 1.8). Importantly, disulphide-HMGB1 promoted production of pro-inflammatory cytokines via the NF-κB pathway activation. In contrast, all thiol-HMGB1 failed to induce a pro-inflammatory response but instead showed a chemoattractant activity (Venereau et al., 2012). Interestingly, reactive oxygen species-mediated oxidised-HMGB1 causes immune tolerance (Kazama et al., 2008) (Lotfi et al., 2009). Collectively, these findings establish a vital role for redox in the control of HMGB1 role in inflammation and migration (Tang et al., 2012a).

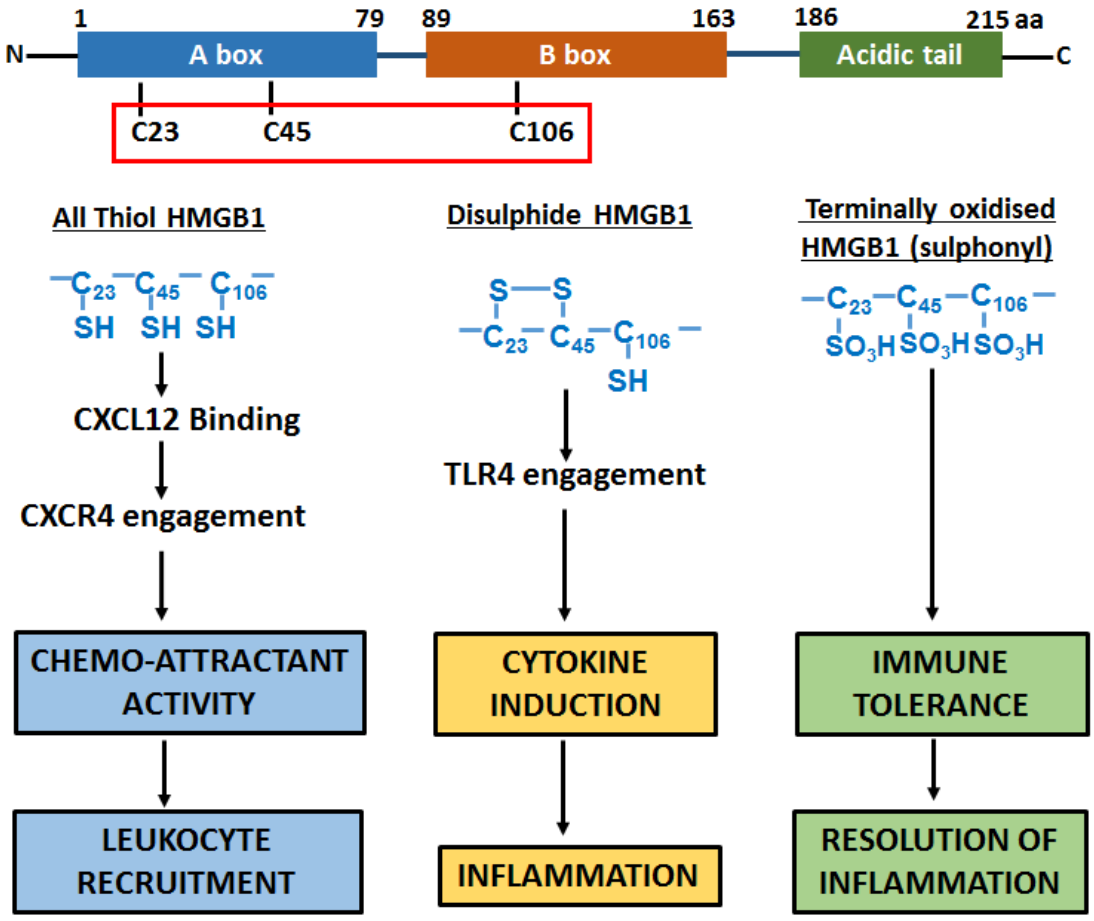

Figure 1.8: Redox regulation controls HMGB1 activity. The activities of extracellular HMGB1 are redox-dependent. The HMGB1 molecule contains three key cysteine residues located on the A box (C23 and C45) and B box (C106) that undergo redox modifications. All thiol-HMGB1 (reduced HMGB1) forms complex with CXCL12 and interacts with CXCR4 receptor to promote chemokine production and leukocyte recruitment. Disulphide-HMGB1 secreted by infiltrating leukocytes interacts with TLR4 to promote release of pro-inflammatory cytokines and thus participates in in the inflammatory process. Terminally oxidised-HMGB1 generated via the oxidising reaction of reactive oxygen species originating from leukocytes shows immune tolerance and thus mediates resolution of inflammation.

1.5 Nitric oxide

Nitric oxide (also known as nitrogen monoxide, NO) is a diatomic free radical endogenously synthesised in mammals mainly through the action of nitric oxide synthase (NOS) enzymes (Förstermann and Sessa, 2012). NO synthesis by NOS enzymes requires the presence of both co-substrates and co-factors. The co-substrates include molecular oxygen and reduced nicotinamide adenine dinucleotide phosphate (NADPH) while the co-factors include flavin adenine dinucleotide (FAD), flavin mononucleotide (FMN) and tetrahydrobiopterin (BH4) (Förstermann and Sessa, 2012). NO exhibits weak intermolecular interactions and is a gas at 1 atm and 25^{o}C (Moller et al., 2019). It is scarcely soluble in water but readily dissolves in organic solvents and can rapidly diffuse through cell membranes once produced. The effects of NO are exerted either through direct interactions with specific biological targets (example soluble guanylyl cyclase) or indirectly via NO-derived oxidants (Förstermann and Sessa, 2012).

NO is a known physiological mediator in the vascular, nervous and immune systems and can regulate gene transcription and messenger RNA translation (for instance by binding to iron responsive elements) (Förstermann and Sessa, 2012) (Moller et al., 2019). NO production is tightly regulated under physiological conditions but dysregulated under pathophysiological conditions (Moller et al., 2019). Dysregulation of NO homeostasis has been linked to neurodegeneration, cardiovascular disease, cancer and inflammation (Moller et al., 2019). The pathological role of NO in driving keratinocyte cell death and inflammation shall be discussed in detail in chapter 3.

1.6 Aims of thesis

The pathogenesis of SJS/TEN is complicated and despite intense research efforts, it is yet to be fully resolved. SJS/TEN is said to be due to inflammation and fulminant death of epidermal keratinocytes (Panayotova-Dimitrova et al., 2015). The mechanisms of SJS/TEN are poorly understood and require further investigation. HMGB1 sits at the intersection between cell death and inflammation. It is therefore necessary to investigate mediators of cell death and inflammation that may be involved in disease pathogenesis. Further research is therefore needed to generate adequate *in vitro* models for SJS/TEN to further investigate the mechanisms of keratinocyte death. This study employed both clinical samples and *in vitro* HaCaT models to study SJS/TEN mechanisms.

The overall aims of this thesis were therefore:

a) To investigate HMGB1 as a putative biomarker of SJS/TEN by analysing HMGB1 serum and blister-fluid profiles and expression in skin biopsy samples from SJS/TEN patients versus controls.
b) To investigate the mechanism of nitric oxide-induced keratinocyte cell death and evaluate HMGB1 translocation and release *in vitro*.
c) To investigate the mechanisms of TNF-α induced keratinocyte death and determine their impact on extracellular HMGB1 levels.
d) To generate and characterise stable HaCaT necroptotic and apoptotic models using molecular gene cloning of MLKL, RIPK3 and Bak and assess their contribution to extracellular HMGB1 release.

CHAPTER 2

HIGH MOBILITY GROUP BOX-1 SERUM AND BLISTER-FLUID PROFILES AND SKIN EXPRESSION IN DRUG-INDUCED STEVENS-JOHNSON SYNDROME AND TOXIC EPIDERMAL NECROLYSIS.

Contents

2.1 Introduction

Stevens Johnson Syndrome (SJS) and toxic epidermal necrolysis (TEN) are serious immune-mediated blistering cutaneous adverse drug reactions (cADRs) with a manifestation of extensive epidermal detachment and mucosal sloughing due to keratinocyte death (Bastuji-Garin et al., 1993) . Drugs are the most common causes of SJS/TEN as over 80% of cases have drug aetiology (Roujeau et al., 1995) (Guillaume et al., 1987). A number of circulating cytotoxic proteins found at high levels in SJS/TEN patient sera and/or blister fluids have been identified and are being investigated for their utility as potential candidate biomarkers for the early diagnosis of SJS/TEN. They include granulysin (Chung et al., 2008), soluble Fas ligand (sFasL) (Posadas et al., 2002) (Abe et al., 2003), tumour necrosis factor-α (TNF-α)(Wang et al., 2018b), interleukin (IL)-15 (Su et al., 2017) and -17 (Morsy et al., 2017). Although granulysin and FasL are considered to be among the key players in SJS/TEN pathogenesis (Su and Chung, 2014), however, Nakajima *et al.* has argued that given their short duration of elevation, they may be susceptible to interpretation bias due to false negatives (Nakajima et al., 2011).

High mobility group box-1 (HMGB1) is a DNA binding protein that is present in virtually all nucleated cells. It is actively secreted to the extracellular milieu by activated immune cells or passively released by necrotic or damaged/injured cells or tissues (Figure 2.1). HMGB1 is one example of a protein known as a damage-associated molecular pattern (DAMP) (Zitvogel et al., 2010) which provides a link between tissue injury and inflammation arising from activation of the innate immunity (Yang et al., 2015). A pioneer study by Nakajima *et al* reported that

HMGB1 serum profiles were significantly elevated during the acute stage of SJS/TEN compared to milder forms of cutaneous reactions (erythema multiforme and maculopapular exanthema) (Nakajima et al., 2011). Subsequently, serum HMGB1 and cytokine profiles in various cutaneous adverse drug reaction was investigated (Fujita et al., 2014). However, to the best of our knowledge, no study has investigated HMGB1 distribution in SJS/TEN patient blister fluid and skin biopsy.

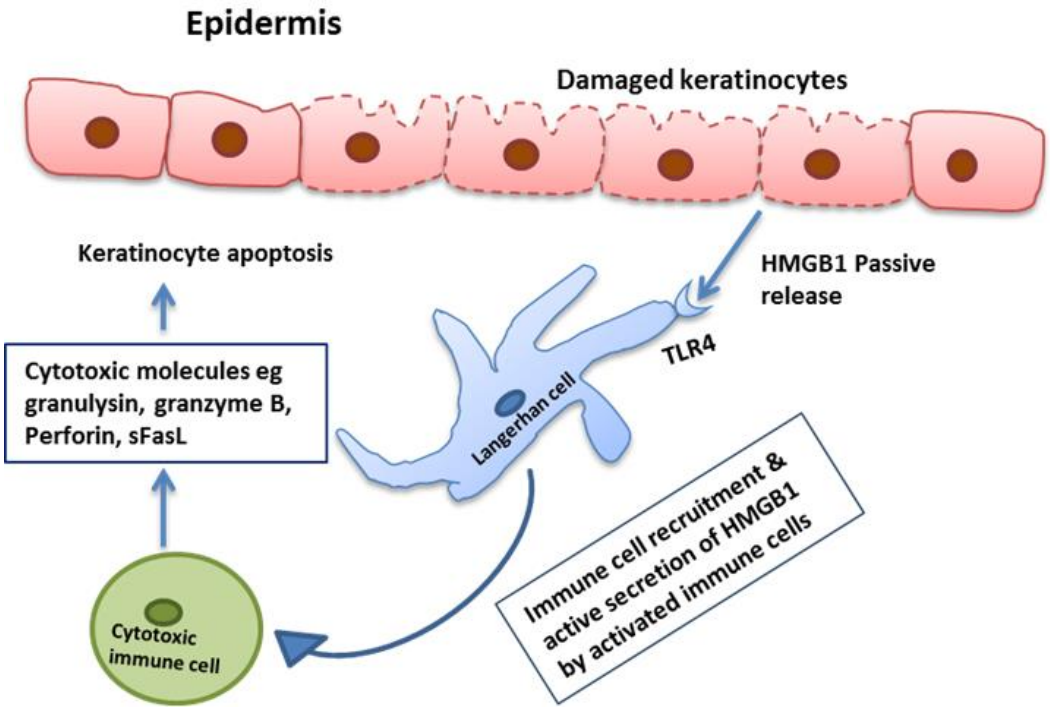

Figure 2.1: A simplified schematic representing a putative HMGB1-mediated, mechanism of epidermal keratinocyte damage in Stevens-Johnson syndrome (SJS) and toxic epidermal necrolysis (TEN). Damaged keratinocytes passively release HMGB1 into the extracellular space that can interact with cell surface receptors such as toll-like receptor 4 (TLR4) on antigen presenting dendritic cells (for example Langerhans cell, the skin's resident antigen presenting cell) and trigger cytotoxic T lymphocyte and natural killer cell recruitment (source of actively secreted HMGB1) and consequently apoptotic cellular degradation via the secretion of cytotoxic molecules such as granzyme B, perforin, soluble Fas ligand (sFasL) and granulysin. Thus more HMGB1 can create a feedback mechanism which can exacerbate damage to epidermal keratinocytes.

The aim of this chapter was to evaluate total HMGB1 levels in sera from 3 independent SJS/TEN patient cohorts and in blister fluid from a subgroup of a Spanish cohort. In addition, this chapter also aimed to determine HMGB1 protein expression in formalin-fixed paraffin embedded SJS/TEN skin biopsies.

2.2 Patients and methods

2.2.1 Nevirapine treated HIV positive Malawian patient cohort

Nevirapine exposed HIV positive patient cohort recruitment was prospectively conducted as previously described (Carr et al., 2013). The study recruited a total of 1117 HIV-positive patients who were naive to antiretroviral therapy from the Queen Elisabeth Central Hospital, Blantyre in Malawi. The study was carried out from March 2007 to December 2008. All patients recruited to this facility gave an informed consent and were of black-African ancestry, all over the age of 16 with no reported baseline jaundice. At the time of diagnosis, all patients were at HIV clinical stage 3 or 4 or had undergone a CD4+ cell counts (<250 cells per µl). They were all commenced on a triomune antiretroviral regimen containing a fixed dose of nevirapine (NVP) and variable doses of lamivudine and stavudine. Blood samples were taken before the commencement of antiretroviral therapy (week 0) and at weeks 2, 6, 10, 14, 18 and 22. Also, both CD4+ cell counts and liver function test were determined at 0, 6, 14 and 18 weeks in order to monitor disease progression and patient prognosis. Treatment was discontinued immediately following a patient presentation with nevirapine-induced hypersensitivity and samples were taken at

that point. A total of 51 patients who developed nevirapine-induced cutaneous hypersensitivity presented one or more of the following phenotypes and were categorised using the following criteria:

Maculopapular exanthema (MPE), also known as acute generalised exanthematous pustulosis (AGEP): widespread rash; with no systemic manifestations

- Drug rash with eosinophilia and systemic symptoms (DRESS): systemic manifestations included cough, fever or abnormal liver function test.
- SJS: extensive rash, affecting ≥2 mucous membranes or blistering reactions affecting < 10% of total body surface area.
- TEN: blistering eruptions affecting >30% of total body surface area

  Patients with SJS/TEN overlap had blistering reactions on 10-30% of their body surface area.

Two NVP-tolerant controls were matched for age and gender to each of the 51 cutaneous hypersensitivity cases. Serum was isolated from whole blood for all samples and frozen down at -80°C until needed for analysis.

2.2.2 Taiwanese SJS/TEN cohort

The recruitment of patients for the Taiwanese SJS/TEN cohort was undertaken as follows. Han Chinese patients (n=73) with SJS/TEN recruited between 2009 and 2015 through the Chang Gung Memorial Hospital (CGMH), Taiwan were enrolled on this study. All patients in this cohort were usually those who had received referrals from other Taiwan national hospitals including National Taiwan University Hospital, Taichung Veterans General Hospital, National Cheng Kung University Hospital,

Kaohsiung Medical University, and Chung-Ho Memorial Hospital. Written informed consent was given by all patients enrolled on this study with the approval of the Institutional Review Board (IRB) and ethics committee of CGMH in line with Taiwan law (IRB No.97-0509B, No.100-4657A3, No.103-2562C, and No.105-3600C). Screening of patients with SJS/TEN was based on presented phenotypes in the form of rapidly blistering MPE associated with mucosal and skin detachment. Diagnosis of SJS/TEN was based on both phenotypes and on the criteria proposed by the European registry of severe cutaneous adverse drug reaction (RegiSCAR) project group (Auquier-Dunant et al., 2002) (Roujeau, 2005). Serum samples were taken from SJS/TEN patients during the acute, maximum and recovery stages of the disease and all samples were frozen at -80°C. In each individual patient, the time to onset of illness was carefully considered as well. When the time to onset of illness was less than 6 days it was termed the “acute”stage; while the time from onset to maximal skin detachment (with no further progression of skin detachment) was termed the “maximum” stage and lastly the “recovery” phase was the time at which full skin healing had occurred.

2.2.3 Spanish SJS/TEN and DRESS cohort

Patients in the Spanish cohort were recruited from a number of hospitals in Madrid, Spain which belong to the PIELenRed Consortium. A total of 23 cases diagnosed with severe cutaneous hypersensitivity including SJS, TEN, SJS/TEN overlap or DRESS overlap were enrolled on this study. Approval for this study was obtained from the Research Ethics Committee of Príncipe de Asturias University Hospital (coordinating centre of the national PIELenRed Consortium), Spain. Notably, in 2011, PIELenRed Consortium joined the RegiSCAR group (González-Herrada et al.,

2017) and so, some of the patients included in this study are documented in the multinational registry (RegiSCAR, 2018). All patients or their legal representatives gave written informed consent. Serum and blister fluid samples were obtained at the acute stage of severe cutaneous adverse drug reactions and frozen down at -80°C.

2.2.4 Assessment of total serum and blister fluid HMGB1 by ELISA

All serum and blister fluid samples were assessed for total HMGB1 in the Wolfson Centre for Personalised Medicine, University of Liverpool, UK. The concentrations of total HMGB1 protein in serum and blister fluid (where applicable) were determined by ELISA in accordance with the manufacturer's protocol (Oxford Biosystems, UK). Briefly, frozen samples were thawed at room temperature and HMGB1 standards (0-80 ng/ml) were made by reconstituting HMGB1 stock with the appropriate volume of sample diluent and this was allowed to stand for 10 mins. Samples, standards and positive control were added to the required well in an anti-HMGB1 polyclonal antibody coated plates in duplicates. Blister fluid samples were determined firstly neat, before diluting appropriately until reading was quantifiable within the detection limit of the assay. Plates were sealed and incubated at 37°C for 20-24 hr with gentle shaking. The following day, plate contents were discarded and the manufacturer's instruction was followed throughout until the reaction was stopped. Plates were read at 450 nm using a DTX880 Plate Reader (Beckman Coulter Incorporated, High Wycombe, UK) and results were determined in accordance with ELISA protocol. Samples that fell below the manufacturer's lower

limit of quantification (0.2ng/ml) or showed discrepancies >15% in replicates were excluded.

2.2.5 Formalin-fixed paraffin-embedded (FFPE) skin biopsies

Skin biopsy samples (healthy controls n=5, drug-induced rash n=7, SJS/TEN n=7) which had been preserved using formalin-fixed paraffin-embedded (FFPE) protocol and archived from 2013 to 2016 were obtained from the histology database belonging to Cleveland Clinic (Cleveland Clinic, Ohio). The Medical Subject Headings (MeSH) terms used to retrieve the samples from archive were “Stevens-Johnson Syndrome” or “toxic epidermal necrolysis” and drug eruption/drug reaction and “dermal hypersensitivity reaction”. The cases that were selected for SJS/TEN or MPE were backed up by clinical diagnosis with well documented clinical notes. Healthy control samples were derived from excised specimens from normal skin donors. All FFPE skin samples were accessed in January 2017.

2.2.6 Immunohistochemistry detection of HMGB1

Immunohistochemistry (IHC) was generously performed by Valerie Tilston from the Department of Veterinary Pathology, Institute of Veterinary Science (Cleveland Clinic Foundation, Ohio). Slides from SJS/TEN, MPE and healthy controls along with negative controls were heated for 20 min at 98°C and de-paraffinized from xylene to water and then subjected to antigen retrieval in Dako PT high pH buffer (Agilent Technologies Ltd, UK) via a computer managed antigen retrieval workstation (PT Link; Agilent Technologies Ltd, UK). Endogenous peroxidases were quenched by incubating skin sections in 3% hydrogen peroxide and Tris Buffered Saline (TBS) for 5 min, followed by a further 5 min in TBS. Skin sections were stained with HMGB1

primary antibody (Rabbit polyclonal, ab18256, Abcam, Cambridge, UK) at a 1:1,000 dilution for 1 h at room temperature using an automated immunostainer (Link 48; Agilent Technologies Ltd, UK). Negative control slides were derived from sections incubated with non-immune rabbit serum. This was then followed by a further incubation using a polymer peroxidase-based detection system (Anti Mouse/Rabbit Envision Flex+, Agilent Technologies Ltd, UK) for 30 min at room temperature. The reaction was visualised using diaminobenzidine (Agilent Technologies Ltd, UK). Reactions that were deemed positive showed a characteristic brown colour that was predominantly nuclear but rarely cytoplasmic. This was located at the site of the epidermis and hair follicle in normal skin.

The intensity of expression of HMGB1 and its distribution was semi-quantitatively evaluated by a histopathologist. The following terms were used to describe the stain intensity; negative, minimal, moderate and strong. Negative stain (-) described the complete absence of specific brown colour whereas minimal stain (+/-) described almost invisible characteristic brown colour. Moderate (+) and strong (++) stains represented clearly visible brown colour but milder in appearance compared to keratinocytes from normal skin (positive control) and clearly visible brown colour comparable to keratinocytes stains from normal skin respectively.

2.2.7 *Statistical analysis*

Statistical analysis was performed using Prism 5 software (GraphPad Incorporated) and Rstudio version 1.1.414. To Compare differences in HMGB1 serum and blister fluid profiles for the Spanish cohort and HMGB1 levels at the different stages of SJS/TEN disease in the Taiwanese cohort, linear mixed effects models fitted to Imer

function in R package Ime4 was used. To check for normality for the residual models, concentration values from HMGB1 Spanish cohort were log-transformed. For comparing between samples at the time of hypersensitivity reactions for unpaired sample groups, Kruskal-Wallis test was adopted. HMGB1 concentrations above baseline (>2.3ng/ml) determined using a 97.5% interquartile range were considered elevated. Analysis of constructed binary outcome was determined by Chi-square test. Multiple testing was adjusted for using the Bonferroni corrections. Values of p less than 0.05 were considered statistically significant.

2.3 Results

2.3.1 Measurement of serum and blister fluid HMGB1 levels

Different patient cohorts with SJS/TEN were screened and HMGB1 concentrations in the serum and blister fluid were investigated. The results of the investigation are presented below on a cohort by cohort basis.

HMGB1 concentrations in Nevirapine treated SJS/TEN cohort

To measure differences in HMGB1 levels in cutaneous hypersensitivity phenotypes, only 40 nevirapine-induced hypersensitivity cases (MPE n=22, DRESS n=9, SJS/TEN n=9) were selected from the 51 total observed cases. In addition, 70 tolerant controls out of 102 tolerant controls whose sera were available and adequate for total HMGB1 analysis by enzyme-linked immunosorbent assay (ELISA) were also selected. The data showed that the mean (±SD) total HMGB1 serum concentrations were elevated but not significant ($p>0.05$) in 3 cutaneous adverse drug reaction cases including MPE (3.92±2.17 ng/ml), DRESS (5.25±2.65 ng/ml), SJS/TEN (3.98±2.17 ng/ml) and combined phenotype (4.17±2.81) compared to tolerant controls (2.97±3.00 ng/ml) (Figure 2.2A) as determined by the Kruskal-Wallis test. Using Chi-squared test to consider each case of hypersensitive phenotype alone versus the tolerant controls, the percentage of individuals with elevated HMGB1 profile (>2.3ng/ml threshold cut off) was higher in all hypersensitive categories: MPE (72%, $p=0.027$), DRESS (89%, $P=0.029$) and SJS/TEN (78%, $p=0.042$) in comparison to the tolerant category (46%) (Figure 2.2B). However, following the

application of Bonferroni test to account for multiple testing, only the combined hypersensitive category was unaffectedly significantly higher ($p<0.0125$) compared to tolerant controls.

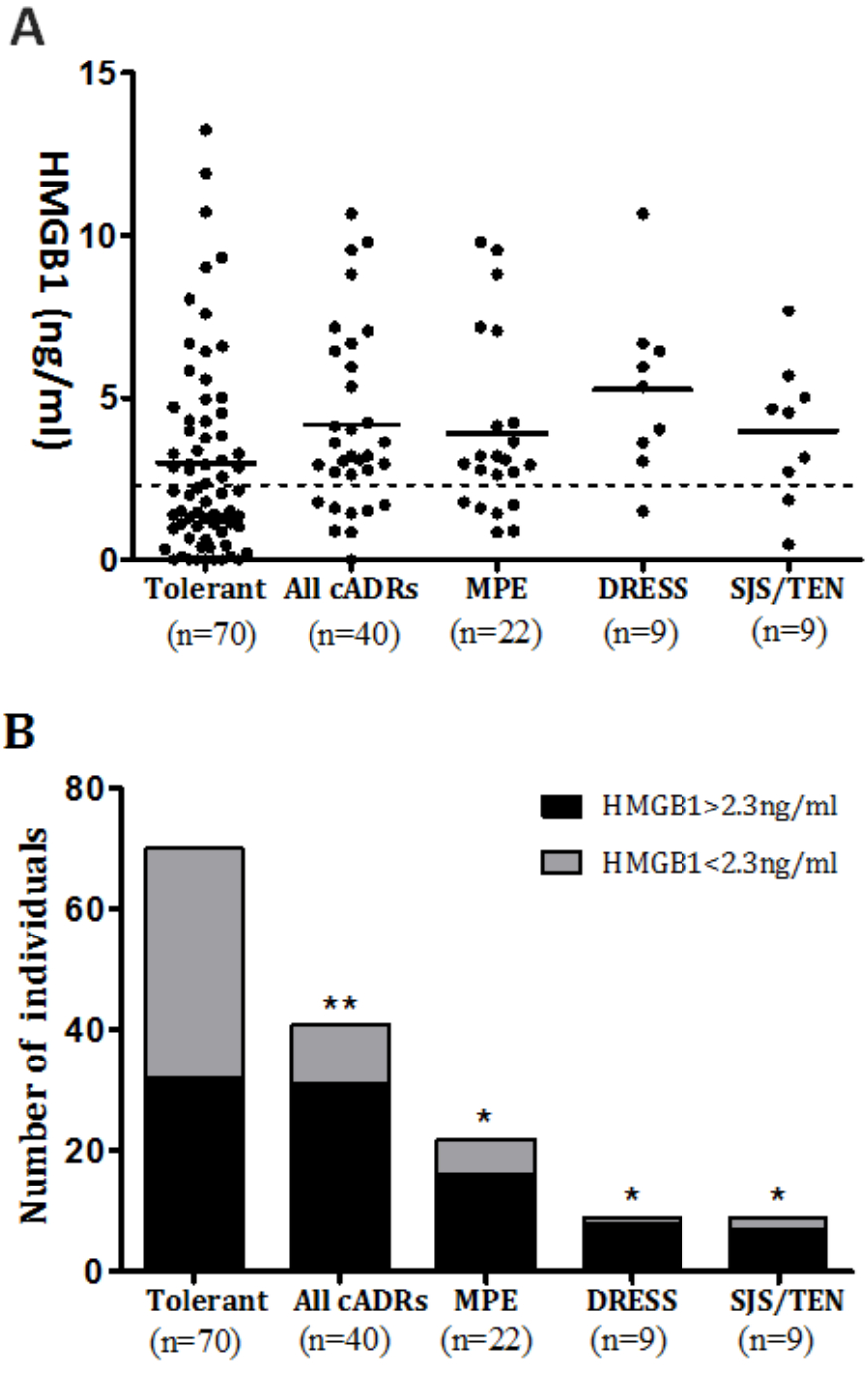

Figure 2.2: Quantification of total serum high mobility group box-1 (HMGB1) protein in HIV positive Malawian patients presented with nevirapine-induced cutaneous adverse drug reaction A) Serum HMGB1 values of all hypersensitive

phenotypes and tolerant controls exceeding threshold B) Binary outcome representation of the number of individuals with HMGB1 below or above the upper limit of normal (ULN, 2.3 ng/ml) in various cutaneous adverse drug reactions (cADRs). Enzyme-linked immunosorbent assay was used to quantify serum HMGB1 samples. Results represent duplicate ELISA readings with less than 15% discrepancy. Statistical analyses on data presented here were carried out using Kruskal-Wallis test (**A**) and Chi-squared test (**B**) and significance indicated (*p<0.05, **p<0.01).

HMGB1 profile in Taiwanese SJS/TEN patient cohort

To determine if there were any differences in HMGB1 profiles as SJS/TEN progresses, serum HMGB1 measurement in the acute, maximal and recovery phases of SJS/TEN in the Taiwanese cohort was undertaken. To conduct this particular study, sera from 73 Taiwanese SJS/TEN was subjected to HMGB1 profiling by ELISA (Figure 2.3). Patients at different stages of SJS/TEN categorized into acute (n=73), maximal (n=59) and recovery (n=66) had their serum taken and total HMGB1 measured. Interestingly, a significant difference was observed in the mean (±SD) total serum HMGB1 levels at the acute stage of reaction (32.6±26.6 ng/ml) versus both the maximal (19.7±23.2ng/ml; p=0.0002) and recovery (24.6±25.3ng/ml; p=0.0003) stages as revealed by the linear mixed modelling. Interestingly, both differences remained statistically significant (p=0.017) even after applying the Bonferroni corrections. When the difference in the levels of serum HMGB1 between the maximal and recovery phases were compared, it was not statistically significant.

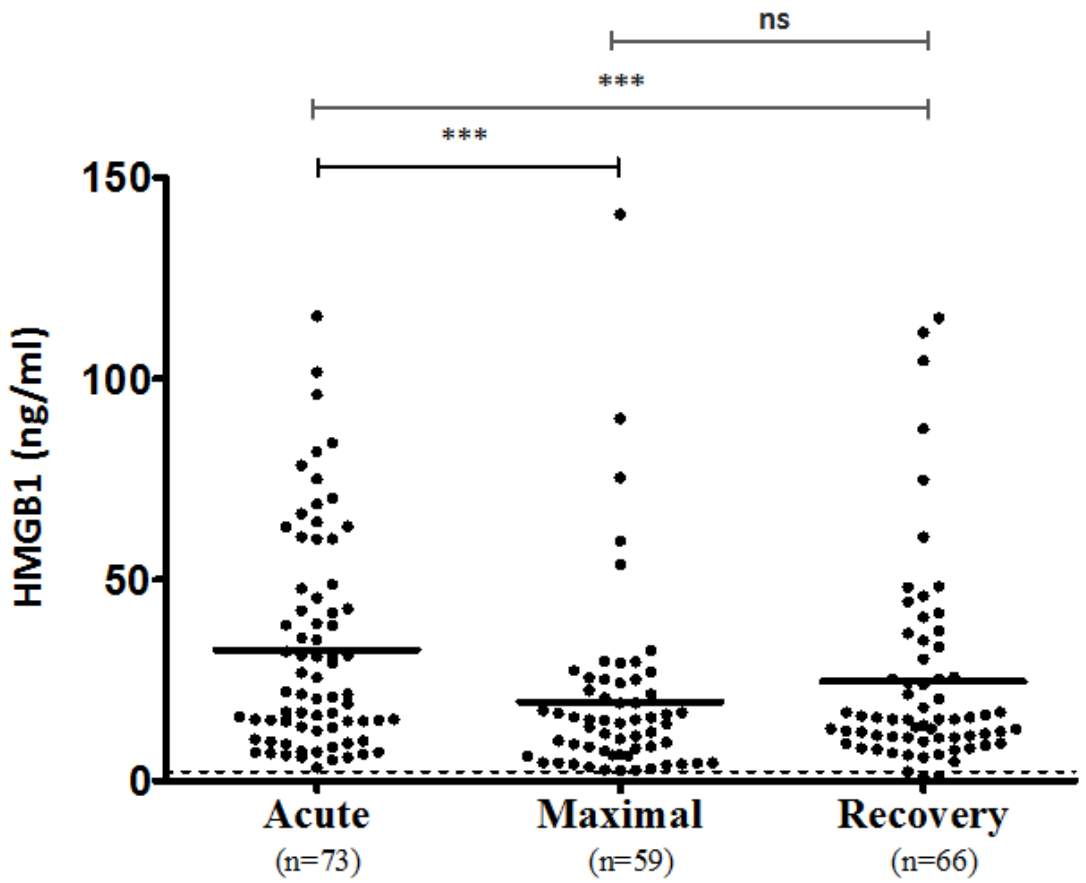

Figure 2.3: Measurement of serum high mobility group box-1 (HMGB1) concentration at different phases of Stevens-Johnson syndrome/ toxic epidermal necrolysis (SJS/TEN) in Taiwanese cohort. Sera from patients at the acute, maximal and recovery stages of SJS/TEN were analysed for total HMGB1 by enzyme-linked immunosorbent assay. The broken line represent the notional upper limit of normal (ULN; 2.3 ng/ml) while the abbreviation ns denotes non-significant difference. A statistically significant difference indicated by *** $p<0.0001$ was determined by linear mixed effect model.

HMGB1 concentration in the Spanish SJS/TEN and DRESS cohort

To determine HMGB1 serum and blister fluid profiles in the Spanish SJS/TEN and DRESS cohort, mean total HMGB1 from a total of 23 patients were quantified. Serum samples were taken from 22 SJS/TEN and DRESS patients, out of which 12 patients also had blister fluid samples taken. Blister fluid was available from one additional patient which brought the total number of blister fluid samples to 13.

Both serum and blister fluid samples were analyzed for total HMGB1 by ELISA. HMGB1 profiles were different in the serum and blister fluid as expected. The mean serum total HMGB1 was 8.8±7.6ng/ml and the mean total blister fluid HMGB1 concentration was 486.8±687.9ng/ml (Figure 2.4). When we compared serum and blister fluid total HMGB1 levels from all patients by linear mixed modelling analysis, we discovered that blister fluid HMGB1 levels were significantly higher ($p<0.001$) than serum HMGB1 levels. However, no correction was found (data not shown; $R^2=0.036$) for the 12 patient blister fluid HMGB1 levels matched against serum HMGB1 levels.

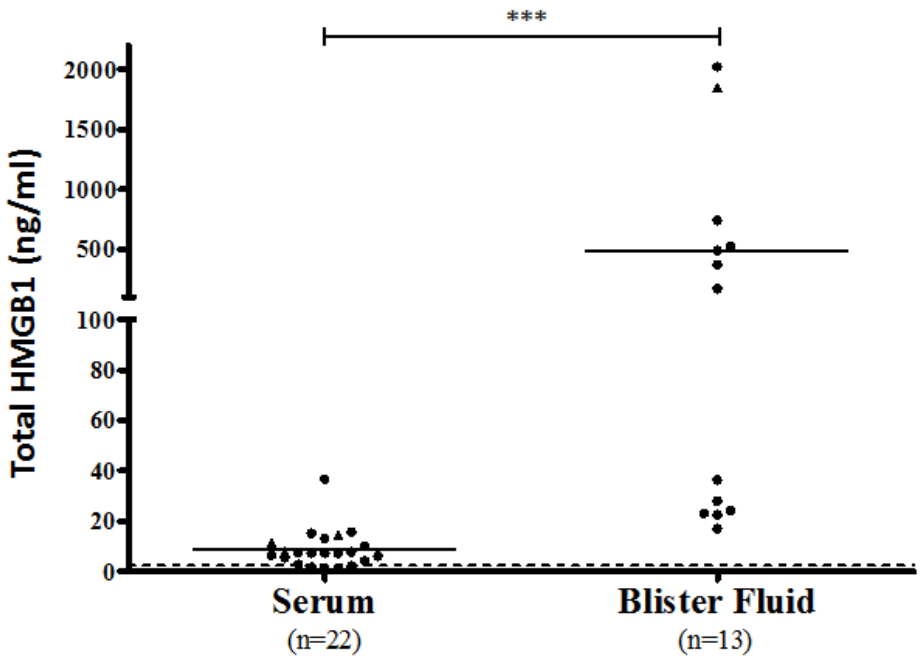

Figure 2.4: Measurement of total high mobility group box-1 (HMGB1) in serum and blister fluid from Stevens-Johnson syndrome/toxic epidermal necrolysis (SJS/TEN) and drug rash with eosinophilia and systemic symptoms (DRESS) Spanish cohort. Serum (n=22) and blister fluid (n=13) samples from Spanish SJS/TEN cohort were analysed for total HMGB1 by enzyme-linked immunosorbent assay. Differences in HMGB1 levels were compared for patients (n=12) who had both serum and blister fluid available for HMGB1 measurement. Circles were used to indicate SJS/TEN samples and triangles represented DRESS/TEN overlap patients.

The broken line denotes the ULN (2.3 ng/ml). Statistical significance was determined by linear mixed model and ***p<0.001 indicate significance.

2.3.2 HMGB1 expression in the skin

In SJS/TEN, the dermis is separated from the epidermis at the dermal-epidermal junction. It was therefore necessary to carry out skin biopsy that will allow us to examine if there is any difference in the expression patterns of HMGB1 at different layers of the skin. In order to do this, immunohistochemical staining for HMGB1 was performed on FFPE skin sections. There was a significantly less nuclear expression of HMGB1 in both the MPE skin and the non-blistered SJS/TEN skin compared to the healthy control skin (Figure 2.5). In all SJS/TEN skin sections (both the non-blistered and blistered), it seemed that HMGB1 expression was confined to the basal/suprabasal layer (Figure 2.6). HMGB1 expression pattern was different in both the blistered SJS/TEN skin and the non-blistered SJS/TEN skin compared to the healthy control skin. Blistered SJS/TEN skin had less basal/suprabasal HMGB1 expression than non-blistered SJS/TEN skin indicating that HMGB1 might have leaked out from keratinocytes in detached epidermis. Another interesting observation was a dominant expression of HMGB1 by inflammatory cells that have infiltrated the skin in both the MPE skin and the SJS/TEN skin (

Table **2.1**).

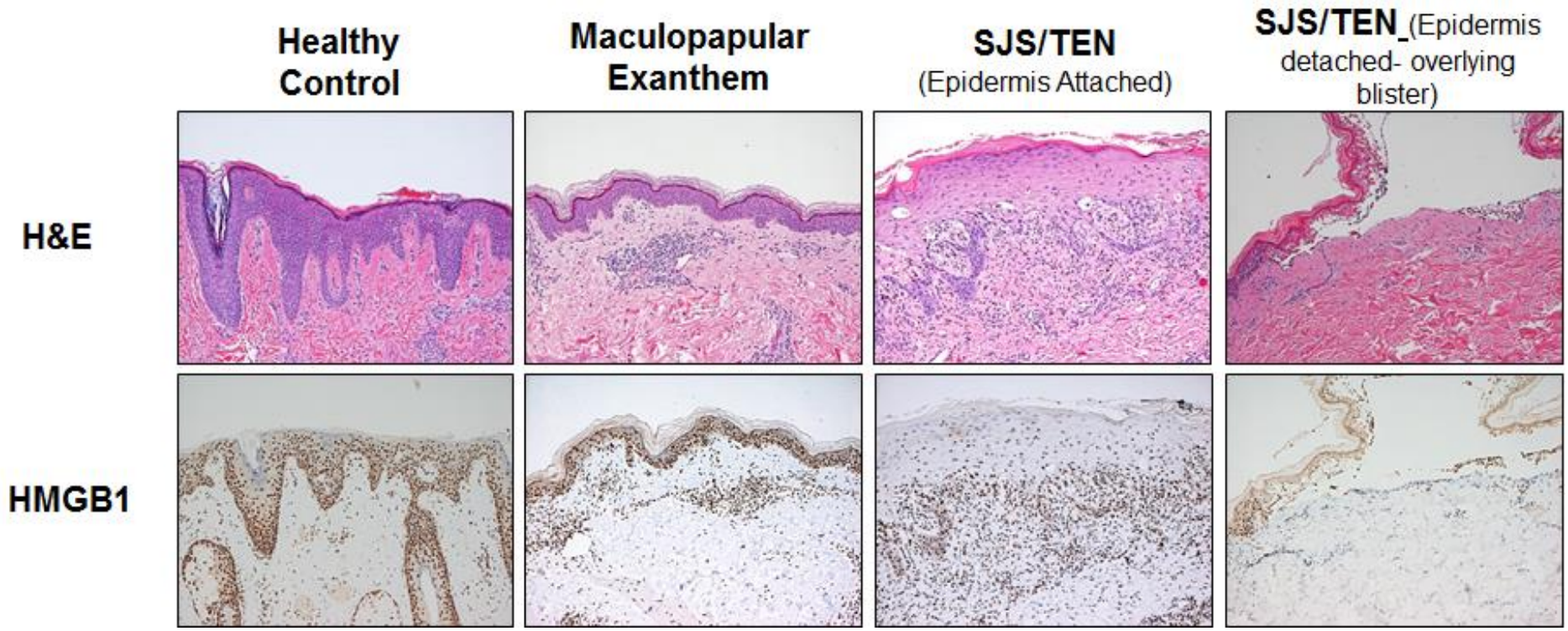

Figure 2.5: Haematoxylin and eosin stain presented alongside immuno-histochemical staining of high mobility group box-1 (HMGB1) for skin biopsies from cutaneous adverse drug reaction patients (maculopapular exanthema and Stevens-Johnson syndrome/toxic epidermal necrolysis) and healthy donor. Cell nuclei and cytoplasmic structures are stained purple and pink respectively. Intense HMGB1 (brown) staining is localised to the nucleus in healthy donor but reduced in cutaneous adverse drug reaction cases. These images were captured at 100x magnification.

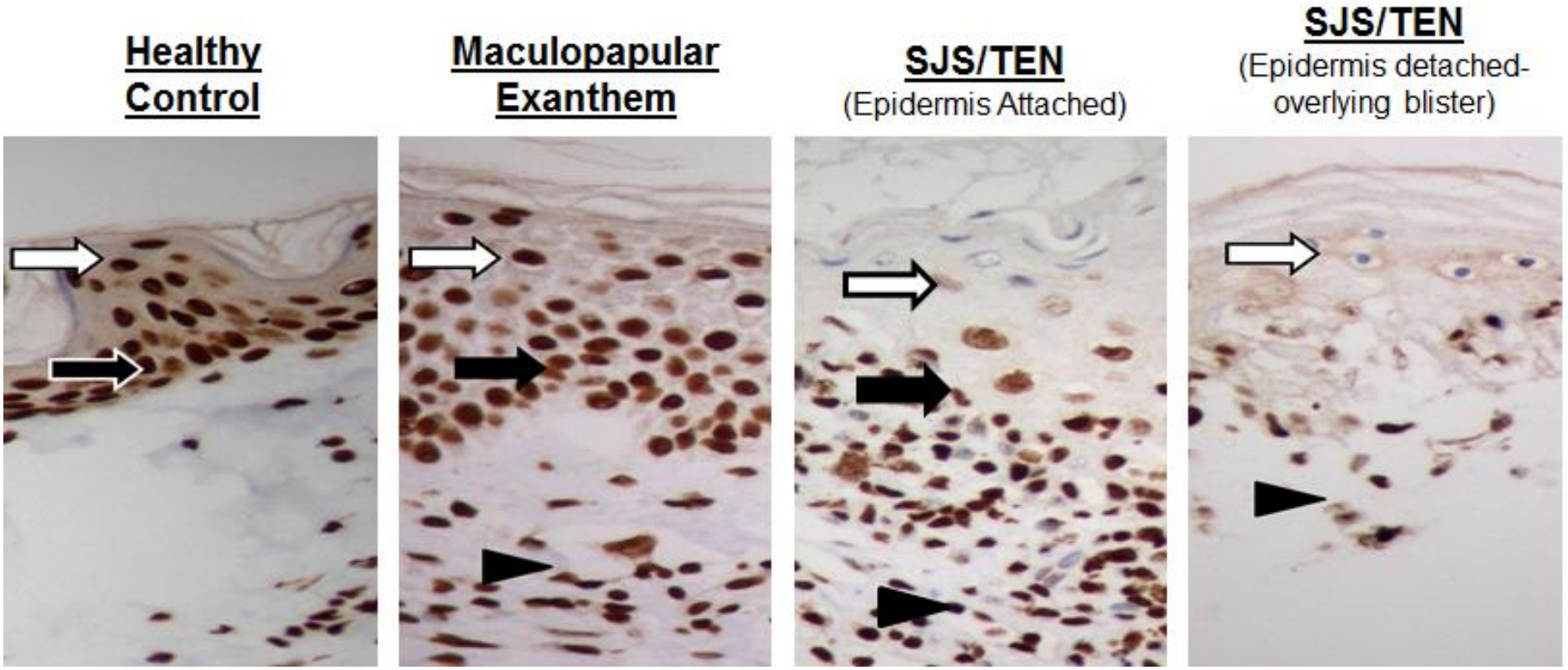

Figure 2.6: Immunohistochemically stained high mobility group box-1 (HMGB1) in skin sections prepared from skin biopsy specimens from healthy donors and cutaneous adverse drug reaction patients. The white arrow shows the stratum spinosum, while the black arrow shows the stratum basale. Inflammatory infiltrates are indicated by the arrowheads. HMGB1 (brown) at different layers of the skin is also indicated. The images presented here were captured at 400x magnification. Data is representative of n=7 replicate samples for cutaneous hypersensitivity cases and n=5 for healthy control skin samples.

Table 2.1: **High mobility group box-1 immunostained biopsy skin sections from healthy control, maculopapular exanthema, Stevens-Johnson syndrome/toxic epidermal necrolysis semi-quantitatively analysed.** N.P. (not present) indicates biopsy samples without any inflammatory infiltrate detected. Staining intensities were defined as negative (-), minimal (-/+), moderate (+) and strong (++) according to a histopathologist.

					IHC HMGB1 Expression				
Phenotype	Biopsy Site	Age	Gender	Causal Drug	Epidermis	Nuclear stain within Epidermis	Follicle/ Adnexae	Dermis	Inflammatory Infiltrate
Healthy	Thigh	23	F	n/a	++	all layers	++	+/-	N.P.
Healthy	Forehead	19	M	n/a	++	all layers	++	+	N.P.
Healthy	Arm	61	F	n/a	++	all layers	++	+/-	N.P.
Healthy	Back	58	F	n/a	++	all layers	++	+/-	N.P.
Healthy	Inferior Breast	40	F	n/a	++	all layers	N.P.	+	N.P.
MPE	Arm	81	F	vancomycin	+	all layers	++	+	++
MPE	Arm	61	M	meropenem	++	all layers	++	+/-	++
MPE	Arm	59	F	simvastatin	++	all layers	++	+/-	++
MPE	Arm	22	M	apiprazole	++	all layers	++	+/-	++
MPE	Scalp	78	F	undetermined	++	all layers	++	+/-	++
MPE	Abdomen	59	F	levetiracetam	++	all layers	++	+	++
MPE	Abdomen	62	M	piperacillin /tazobactam	++	all layers	++	+	++
SJS	Back	62	M	ceftaroline	+/-	Basal/Suprabasal layer	++	+/-	++
SJS	Arm	51	M	vancomycin	+/-	Basal/Suprabasal layer	N.P.	+/-	++
SJS	Lip	23	F	sulfamethoxazole/ trimethoprim	+/-	Basal/Suprabasal layer	N.P.	+	++
SJS/TEN	Thigh	54	M	vancomycin	+/-	Basal/Suprabasal layer	++	+/-	++
SJS/TEN	Abdomen	39	F	piperacillin/ tazobactam	+/-	Basal/Suprabasal layer	++	+/-	++
TEN	Arm	24	F	ketorolac	+/-	Basal/Suprabasal layer	+/-	-	++
TEN	Chest	28	F	sulfamethoxazole/ trimethoprim	+/-	Basal/Suprabasal layer	++	+/-	++

2.4 Discussion

The goal to identify biomarkers that may aid the diagnosis and/or prognosis of SJS/TEN is an ongoing research need that warrants more focused investigation. Following a previous report that HMGB1 was significantly elevated in SJS/TEN but not in DRESS and MPE and could serve a diagnostic role if given extensive validation, we undertook a study to investigate HMGB1 levels in 3 independent SJS/TEN patient cohorts.

Total serum HMGB1 was more elevated in SJS/TEN and DRESS patients at time of reaction, though not in a significant manner compared to MPE and tolerant control patients in our nevirapine cohort from Malawi. This implies that HMGB1 levels cannot completely differentiate between cADR phenotypes in this patient cohort. Although, the construction of a binary outcome with the data (cut off threshold exceeding 2.3ng/ml) provided a possibility that HMGB1 levels might be used to differentiate between hypersensitivity phenotypes but only to a lesser extent. This observation was contrary to Nakajima et al finding which demonstrated that serum HMGB1 levels were significantly higher at the acute stage of SJS/TEN than in DRESS and MPE patients (Nakajima et al., 2011). The fact that low levels of serum HMGB1 were observed in our nevirapine treated Malawian cohort is perhaps not too surprising given that they were HIV positive patients. At the time of recruitment for this study, patients were already clinically diagnosed with advanced stage 3/4 HIV infection (CD4+ count <250 cells/µl). Available evidence suggests that HIV infection raises HMGB1 plasma levels (Nowak et al., 2007) (Nowak et al., 2012) and that HMGB1 protein might be released from necrotic or apoptotic HIV infected cells. In

return, HIV viral replication is aided by HMGB1 (Trinh et al., 2016). In addition, the fact that the patients were placed on antiretroviral therapy (ART) could also be another reason for low HMGB1 serum levels. It has been reported that prolonged use of ART seems to reduce HMGB1 plasma levels (Troseid et al., 2010), but there is little evidence on its use in the short term especially in advanced stage of HIV pathology.

With the Taiwanese cohort, our data showed that serum HMGB1 levels were significantly higher in the acute stage of SJS/TEN reaction, than at the maximal and recovery stages. This indicates that at the onset of SJS/TEN reaction prior to treatment, massive tissue damage is rapidly occurring causing high amount of HMGB1 to be released and/or secreted into the systemic circulation. Further evidence accounting for HMGB1 serum elevation was the discovery of drug-specific T cells in SJS/TEN which were strongly linked to the destruction of epidermal keratinocytes in the acute stage of the disease (Correia et al., 2002b) (Leyva et al., 2000). The commencement of treatment (both palliative and targeted disease-modifying therapy), may bring about alteration in HMGB1 serum levels. Also HMGB1 serum levels were unexpectedly higher, though not significant in the recovery phase than in the maximal phase of SJS/TEN. The actual reason for this is not completely clear but however, sampling governance, phenotype definition and ethnicity differences perhaps might have accounted for differences in levels. Comparatively, HMGB1 serum profiles in our Taiwanese cohort were several folds higher than their Malawian counterpart. As we have already highlighted, HIV infection and ART and probably ethnicity differences might have been responsible for the observed HMGB1 serum profile differences. It is noteworthy to state here

that the samples for all cohorts from which HMGB1 was measured came from distinct study designs conducted retrospectively, initially set up to test different outcomes on HMGB1 elevation and that this heterogeneity does not allow comparison of HMGB1 levels amongst cohorts.

The HMGB1 content of blister fluid from SJS/TEN patients (n=12) from Spain was exceptionally high compared to levels in serum. Remarkably, this is a pioneer observation which suggests that this super-elevated blister fluid HMGB1 is significantly higher (55-fold) than serum HMGB1 originated from damaged epidermal keratinocytes. By contrast, α-defensins 1-3, a cytotoxic protein thought to have a role in SJS/TEN is approximately 3 times higher in blister fluid than in serum (Morel et al., 2011) which is less in magnitude in comparison to our finding with HMGB1. Since granulysin levels in blister fluid are a good indicator and determinant of both disease severity and mortality compared to levels in serum (Chung et al., 2008), it is then perhaps necessary for other researchers to investigate HMGB1 levels in blister fluid and serum from matched SJS/TEN subjects and determine if there is any association between blister fluid HMGB1 and disease severity and deaths.

We showed for the first time through our skin biopsy data that HMGB1 nuclear expression was diminished in the epidermis of non-blistered SJS/TEN skin but confined to the basal/suprabasal layers in blistered SJS/TEN skin. This decline in epidermal nuclear HMGB1 might most probably be due to keratinocyte death, and as a consequence, lead to the upsurge of total serum HMGB1 in the circulation. However, given that from a histological standpoint, the detachment of the

epidermis from the dermis is a hallmark of SJS/TEN (Harr and French, 2010), the reason for HMGB1 retention at the suprabasal/basal layers should be questioned and thoroughly investigated. A previous report by Nakajima *et al* revealed that HMGB1 epidermal expression in SJS skin specimens was diffused (Nakajima et al, 2011). The marked difference in HMGB1 distribution in the epidermis of SJS/TEN skin compared to MPE skin and healthy control skin nominates HMGB1 analysis by IHC as a possible diagnostic tool for SJS/TEN, but this would need to be further verified. In addition, our data also suggest that HMGB1 release by keratinocytes in SJS/TEN precedes separation of the epidermis from the dermis, which may serve as an early indicator of tissue damage in SJS/TEN. This observation is also a subject for further investigation.

There are a number of pathologies apart from SJS/TEN in which HMGB1 is significantly elevated in the serum/plasma or showed marked tissue expression at the site of the disease. They include HIV (Nowak et al., 2007), epilepsy (Zhu et al., 2018) and several inflammatory and autoimmune diseases (Magna and Pisetsky, 2014) including but not limited to psoriasis vulgaris (Chen et al., 2013a), traumatic brain injuries (Parker et al., 2017), cognitive dysfunction (Paudel et al., 2018). Thus we are aware that serum HMGB1 levels alone cannot be used as a specific biomarker for SJS/TEN in a scenario where other morbidities that may lead to alteration in HMGB1 levels have not been clinically ruled out. This can present a limitation for the use of HMGB1 serum elevation to diagnose SJS/TEN disease.

A limitation in our data emanated from the fact that only total HMGB1 and not its post-translationally modified isoforms was measured. Post-translational

modifications can have a large impact on HMGB1 biological function. The redox and acetylation status of HMGB1 can confer a different biological property to the molecule (Andersson et al., 2014). A variety of cell types of immune origin such as NK cells, macrophages, dendritic cells and monocytes can secrete acetylated HMGB1 as a cytokine into the extracellular milieu (Bianchi and Manfredi, 2007). Also, necrotic cells release the un-acetylated HMGB1 isoform. Both forms of HMGB1 can contribute to extracellular HMGB1 levels and by extension serum levels seen in SJS/TEN.

Given that keratinocyte death is not seen or rarely seen in both MPE and DRESS, it is possible to be able to use HMGB1 un-acetylated isoform profile to distinguish SJS/TEN which is characterized by fulminant keratinocyte death from the less severe cutaneous phenotype. And so the development of an assay to discriminate and characterize specific HMGB1 isoform levels would be a useful tool in further delineating the dominant source of HMGB1 measured in SJS/TEN patient serum. Secondly, a much larger cohort of SJS/TEN cases is needed which would give the required sample size power to be able to make far reaching conclusion. This is currently a setback, as SJS/TEN is rare and the patients might have comorbidities that may perturb data interpretation.

Taken together, this chapter has demonstrated that HMGB1 is significantly increased in SJS/TEN patient serum at the acute stage and that level in blister fluid is even higher than in serum. However, with the caveat that SJS/TEN patients with comorbidities (like HIV disease) may have altered levels of HMGB1 that may not truly reflect the reality in SJS/TEN pathology. In addition, our data did not provide

any evidence that total HMGB1 serum levels could be used as a prognostic marker. Finally, we have shown for the first time that HMGB1 skin expression is decreased in the SJS/TEN epidermis but reserved in the basal/supra-basal layers giving an indication that it might play a role in the pathogenesis of epidermal detachment and possibly exacerbation of keratinocyte death within the suprabasal layer. Therefore this finding highly suggests that HMGB1 analysis by IHC could serve a putative diagnostic role in SJS/TEN pathogenesis but this requires further investigation. Overall, this chapter has demonstrated that HMGB1 is markedly increased in the serum and blister fluid of SJS/TEN patients and in addition decreased in the epidermis but retained at the suprabasal layer of SJS/TEN skin. This strongly suggests a potential role for HMGB1 in the pathogenesis of SJS/TEN. Taken together, our data suggest a potential putative role for HMGB1 in SJS/TEN pathogenesis; however, additional studies are required to address the limitations of this chapter.

CHAPTER 3

ROLE OF NITRIC OXIDE INDUCED NITROSATIVE STRESS IN KERATINOCYTE DEATH

Contents

3.1 Introduction

Cells can undergo stress resulting from the accumulation of both reactive oxygen species (ROS) and reactive nitrogen species (RNS). ROS and RNS are free radicals with a single unpaired electron derived from molecular oxygen and nitrogen (Pham-Huy et al., 2008). RNS can be generated in the presence of superoxide ($O_2^{\cdot -}$) and nitric oxide (NO) to form peroxynitrite ($ONOO^-$/ONOOH). Peroxynitrite is a highly reactive species that can target and cause damage to cellular components such as proteins, membrane lipids, DNA and ultimately cell injury (Pham-Huy et al., 2008) (Janko et al., 2014) (Figure 3.1).

NO is a small free radical molecule that is synthesised by the action of nitric oxide synthase (NOS) through the oxidation of L-arginine into L-citrulline (Shimaoka et al., 1995). There are three isoforms of NOS known; neuronal NOS (nNOS), endothelial NOS (eNOS) and inducible NOS (iNOS) (Daniela et al., 1998). iNOS is responsible for the generation of substantial amounts of NO that may elicit toxic effects (Lerner et al., 2000). Under physiological conditions, NO is produced in micromolar and nanomolar quantities with a short half-life and exerts pleiotropic functions (Shimaoka et al., 1995). NO is expressed by most human cell types including keratinocytes (Weller, 1997).

Nitrosative stress has been implicated in the pathogenesis of several pathologies including SJS/TEN where NO has been implicated in the destruction of the epidermis by apoptosis (Schwartz et al., 2013a) (Nassif et al., 2004b). An earlier study performed on SJS/TEN skin biopsies had identified strong expression of iNOS both in the lower and upper epidermal layers (Lerner et al., 2000). It has also been

reported that cytokines such as tumour necrosis factor alpha (TNF-α) and interferon gamma (IFN-γ) are potent inducers of iNOS in TEN (Viard-Leveugle et al., 2013).

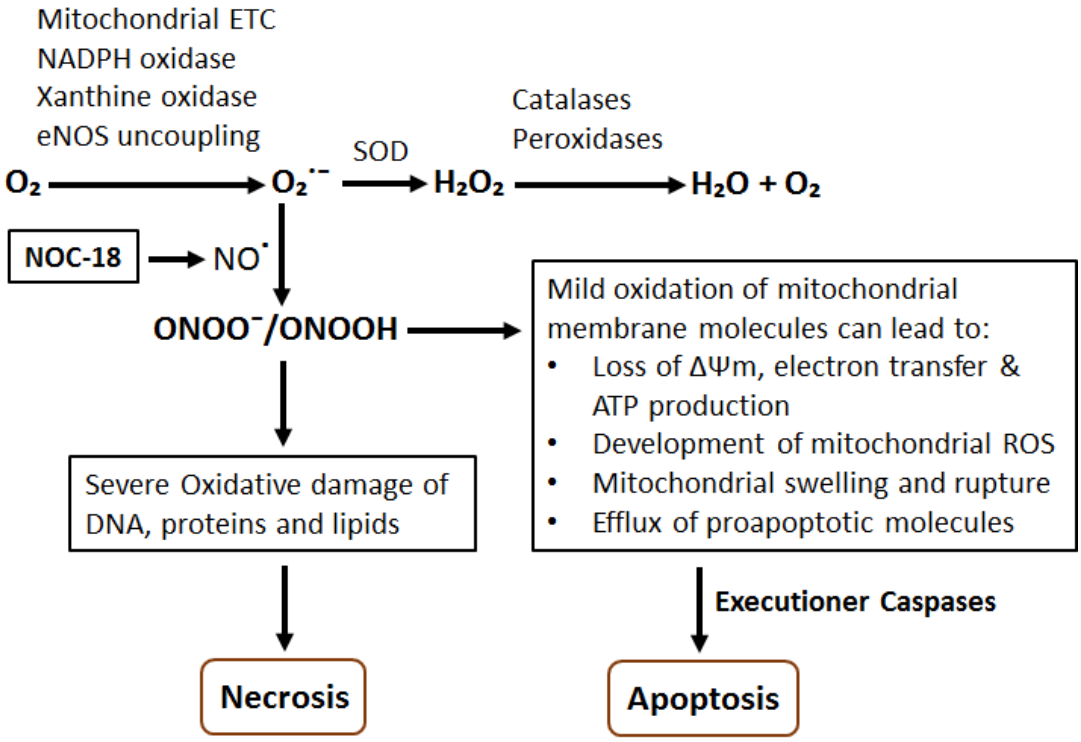

Figure 3.1: Generation of reactive oxygen species (ROS) and reactive nitrogen species (RNS). Leakage of electrons from the mitochondrial electron transport chain (ETC), NADPH oxidase, xanthine oxidase and uncoupling of nitric oxide (NO) synthases can result in the development of superoxide ($O_2^{\bullet-}$). Peroxynitrite ($ONOO^-$/ONOOH) is generated by the reaction between nitric oxide (NO) and superoxide. ROS can be detoxified by catalase, peroxidase and superoxide dismutase (SOD). Un-detoxified ROS and RNS can cause oxidative damage to DNA, proteins and lipids leading to necrosis. ROS and RNS can also lead to the loss of mitochondrial membrane potential (ΔΨm) through damage to mitochondria resulting in the activation of caspase-dependent apoptosis. Under experimental conditions, NO is derived from NOC-18. Figure was adapted from Janko *et al.,* 2014.

Keratinocyte cell death by apoptosis has been previously reported as the mechanism of cell death in TEN (Paul et al., 1996). However, current evidence now suggests that two major forms of death, apoptosis and necroptosis play a role in keratinocyte death based on histological findings from biopsy specimens and skin

lesions from SJS/TEN patients (Panayotova-Dimitrova et al., 2015) (Marzano et al., 2007) (Su and Chung, 2013) (Kim et al., 2015b).

Necrosis and necroptosis are characterized by the massive release of DAMPs which act to trigger or potentiate inflammation, further exacerbating cell death (Pasparakis and Vandenabeele, 2015) (Yang et al., 2015). High mobility group box-1 (HMGB1) protein is a prototype DAMP that is widely utilised to discriminate cell death forms (Rosin and Okusa, 2011) (Zitvogel et al., 2010).

It has not yet been established whether NO can mediate both apoptosis and necroptosis in keratinocytes and the potential impact this has on HMGB1. Using NOC-18, a molecular carrier that donates NO which has been shown to trigger either apoptosis or necrosis or both depending on the cell type and concentration (Murphy, 1999) (Bal-Price et al., 1999) (Bal-Price and Brown, 2000). Additionally, NOC-18 has been reported to act as a pro-apoptotic Fas/FasL inducer (Stassi et al., 1997) (Fukuo et al., 1996) (Viard-Leveugle et al., 2013). The aim of this chapter was to characterise keratinocyte cell death caused by NO and determine its effect on extracellular HMGB1 release.

3.2 Materials and methods

3.2.1 Materials

DETA/NO, 2-2'-(Hydroxynitrosohydrazino) *bis*-ethanamine,DETA NONoate (NOC-18) (#487957) was purchased from Calbiochem (UK). zVAD.fmk (Benzyloxycarbonyl-Val-Ala-Asp (O-Me) fluoromethyl ketone) (# ab120382) (zVAD), anti-HMGB1 (#ab18256), anti-actin (AC-15) (#Ab6276), and Hoechst 33342 (ab145597) were

purchased from Abcam (Cambridge, UK). Necrostatin-1 (#BML-AP309) was purchased from Enzo Life Sciences, Exeter, UK. Staurosporine, dimethyl sulfoxide (DMSO), 3-(4,5-dimethythiazol-2-yl)-2,5-diphenyl tetrazolium bromide (MTT), dimethylformamide, RIPA lysis buffer (#R0278), sodium dodecyl sulphate (SDS), 0.25% Trypsin-EDTA Solution , protease inhibitor cocktail (# P8340), Dulbecco's modified eagle's medium (DMEM)-high glucose (# D5796), Hanks' balanced salt solution (#H8264) (HBSS), phosphate buffered saline (PBS), antibiotic-antimycotic solution (100x) (#A5955), penicillin-streptomycin (# P4333) and Anti-rabbit IgG HRP conjugate (A0545) were obtained from Sigma-Aldrich, Poole UK. Anti-mouse IgG HRP-linked secondary antibody (#7076S), anti-MLKL (D216N) antibody (#14993), anti-PARP (#9542) were purchased from Cell Signalling Technology (CST), Leiden, Netherland. *ProLong Gold Antifade (P36935),* fetal bovine serum (FBS), 96 and 12 and 6 multi-well polystyrene plates, T75, T175 flasks and other cell culture materials were purchased from Thermo Fisher Scientific, Texas, USA. Clarity Western ECL substrate (1705060) was obtained from Bio-Rad, France.

3.2.2 Cell culture

HaCaT cells were a generous gift from Dr Ross Kehinde (Liverpool John Moores University, Liverpool UK) and the HEK293T cell line was obtained from Dr Nicholas Harper (University of Liverpool). All cells were cultured and maintained in either T75 or T175 flasks in DMEM containing 10% sterile-filtered FBS, antibiotic solution (penicillin 100 U/ml, streptomycin 0.1 mg/ml), and an antibiotic-antimycotic solution (20 U/ml penicillin, 20 µg/ml streptomycin, 0.25 µg/ml amphotericin B). All

cells were grown at 37°C in a humidified environment containing 5% CO_2 and maintained by periodic passage at 75-80% confluency every 2-5 days.

3.2.3 Cell passage

Detachment of cells grown in T75 flasks was performed by discarding spent media and gently washing cells with 15 ml of HBSS. Following washing, 10 ml trypsin-EDTA was added and flasks incubated at 37°C/5% CO_2 for 10 minutes to detach cells. Gentle agitation of flasks aided the dislodging process. Cell suspensions were transferred to universal tubes and trypsin neutralised by adding 10 ml DMEM. The tubes were then spun at 1300 rpm for 5 min to pellet cells. Supernatant was discarded, and the cell pellet re-suspended in 5 ml DMEM.

3.2.4 Cell counting

Cell suspension (10 µl) was loaded into a Countess Cell chamber slide and cell density and viability was determined using the Countess Cell Counter (Thermo Fisher Scientific, TX, USA) according to the manufacturer's instruction. Cells were seeded at 1x 10^6 per T75 flask for routine culture.

3.2.5 Freezing and thawing cells

Cell pellets were re-suspended in freezing media made up of FBS supplemented with 10% DMSO. Aliquots of cells (1 ml) in freezing media containing approximately 5x10^6 cells/ml were transferred to 1.8 ml Cryo Vials and placed into "Mr Frosty" freezing containers containing Isopropanol (Thermo Fisher Scientific, TX, USA). This was then frozen at -80°C which allows cells to cool slowly at the rate of -1°C per minute. Following overnight or 1-7 days storage, cells were transferred to liquid

nitrogen. When required, frozen cells were thawed rapidly in a 37°C water bath for 1 minute and slowly diluted in 20 ml DMEM in a T75 flask and incubated at 37°C.

3.2.6 Assessment of cell viability using an MTT assay

Cell viability was determined using the MTT Assay. This assay is based on the reduction of the yellow MTT solution into an insoluble dark purple formazan product by the mitochondrial NADP(H) dependent oxidoreductase enzymes exclusively present in the active state in metabolically competent cells (Mosmann, 1983). The amount of formazan formed is directly related to the number of living cells which gives an indication of the viability of the cells.

HaCaT cells were seeded into a 96-well plate at a density of $2.5x10^4$ cells per well overnight in DMEM. Cells were treated with either NOC-18 (0-15 mM) or staurosporine (0-10 µM) for 12 hours (h) and TNF-α (0-10 ng/ml) for 8 h in serum-free DMEM supplemented with penicillin-streptomycin. Twenty microlitres MTT solution (2 µg/µl final concentration) was added per well and incubated for 2 h at 37°C. Following this, 100 µl of lysis buffer (20% (w/v) SDS in 50% (v/v) dimethylformamide) was added per well and plates incubated for 3 h or overnight to solubilise cells. The optical density (absorbance) of plates was measured at 595 nm using multimode plate spectrophotometer (Beckman Coulter, CA, USA). The percentage viability of cells was calculated as the absorbance of treated wells normalised to the untreated control.

3.2.7 Assessment of caspase luminescence activity using caspase-Glo^{R} 3/7 Assay.

Measurement of caspase 3/7 activity in NOC-18 exposed HaCaT cells was performed using caspase-Glo 3/7 assay kit (Promega, USA). The pro-luminescent substrate contains a DEVD sequence which is cleaved by caspase-3 and/or -7. Following cleavage, a substrate for luciferase (aminoluciferin) is released which results in luminescence. Caspase-Glo substrate is mixed with caspase-Glo buffer to obtain caspase-Glo Reagent. Caspase-Glo Reagent (50 µl) was added per well to cells already dosed with NOC-18 (0-10 mM) for 12 h and mixed thoroughly on a plate shaker for 30 seconds before then incubating at 37°C for 1 h. Luminescence was measured at 535 nm using the multimode plate spectrophotometer.

3.2.8 Preparation of lysates for Western blotting

Cell lysates were prepared in either SDS sample buffer (50 mM Tris/HCl pH 7.5, 4% SDS containing 0.01 % Bromophenol Blue) or RIPA buffer supplemented with a protease inhibitor cocktail (P8340 Sigma-Aldrich). When preparing RIPA lysates, cell pellets were lysed on ice for 30 min followed by sonication to increase protein yield. Lysates (supernatants) were separated from cellular debris by centrifugation at 12,000 rpm for 20 min at 4°C. For SDS buffer lysates, samples were sonicated in SDS sample buffer to aid cell lysis after which 4 µl of 2-mercaptoethanol per 1 ml sample buffer was added. Protein concentration determined using a bicinchoninic acid assay (BCA) assay (#23227, Thermo Fisher Scientific, Rockford, USA) with bovine serum albumin (BSA) (0-2 mg/ml) as standards. The working reagent was prepared by mixing reagent B to reagent A (1:50). 200 µl of working reagent was added to 10

µl of lysates in triplicates. The plate was mixed by shaking for 30 seconds followed by incubated at 37°C for 30 minutes and absorbance was measured at 595 nm.

3.2.9 Preparation and harvesting of supernatants

Supernatants from drug treated HaCaTs were collected and centrifuged at 5000 rpm for 5 mins to pellet any cell debris including dead cells. Cell free supernatants were then aliquoted and stored at -80°C until needed for Western blotting.

3.2.10 Western blotting analysis

SDS-PAGE

A total of 10-20 µg of total protein for lysates and 25-30 µl for cell culture supernatants were mixed with 5-7 µl of SDS sample buffer and sample reducing agent mixture (7:3) Samples were then heated at 85°C for 5 min, cooled on ice and loaded onto 4-12% NUPAGE pre-cast gels (Life Technologies) together with a protein molecular weight marker (Precision Kaleidoscope marker, 161-0375: Bio-Rad or SEEBLUE PLUS 2, LC5925: Life Technologies). The gel was electrophoresed in MOPS running buffer (NP MOPS, Applied Biosystems Life Technologies) at 90V (15 min), then 180V (50-60min).

Western blotting

Transfer of immobilized proteins to nitrocellulose membrane was carried out at 100V for 1 h. The membrane was blocked in Tris buffered saline-tween (TBST) containing 10% dried-milk powder for 1 h at room temperature to minimize non-specific binding of antibodies. Primary antibodies were diluted as indicated below (Table 3.1) in either 2% milk/TBST or 1x TBST and then incubated overnight at 4°C.

5 washes in TBST were carried out to wash off unbound antibodies. Diluted secondary antibodies were incubated for 1 h at room temperature. Washed membranes were developed and visualized using enhanced chemiluminescent substrate (ECL) and either film or a Chemidoc Touch Imaging System (Bio-Rad, CA, USA). Where applicable, quantitation of bands were performed either using Image Lab Software or Image J software.

Table 3.1: Summary of antibodies including dilutions used in Western blotting for the detection of target proteins

Antibody (Product number)	Source	Species	Dilution
MLKL (14993)	CST	Rabbit	1:1,000
Caspase 3 (9661)	CST	Rabbit	1:1,000
PARP (9542)	CST	Rabbit	1:1,000
HMGB1 (ab18256)	Abcam	Rabbit	1:5,000
B-actin (AC-15) (Ab6276)	Abcam	Mouse	1:20,0000
Caspase 3 (9662)	CST	Rabbit	1:1,000
cIAP1 (ab154525)	Abcam	Rabbit	1:2,000
cIAP2 (ab137393)	Abcam	Rabbit	1:2,000
Caspase 7 (9494)	CST	Mouse	1: 1,000
Caspase 8 (9746)	CST	Mouse	1:1,000
Caspase 9 (9502)	CST	Rabbit	1:1,000
StrepMab -Classic (2-1507-001)	IBA	Mouse	1:4,000
Anti-mouse IgG HRP conjugate (7076S)	CST	Horse	1:10,000
Anti-rabbit IgG HRP conjugate (A0545)	Sigma	Goat	1:10,000

3.2.11 Immunofluorescence staining and imaging

Cells were seeded at $2.5x10^5$ density per well in 12-well plates on 13mm cover slips pre-coated with 0.5% gelatin and incubated overnight at 37°C/5% CO_2 for cells to adhere. The following day, cells were dosed and thereafter washed twice in PBS and fixed with 2% paraformaldehyde (PFA) for 15 min at room temperature. The wells were washed once with 50 mM ammonium chloride (NH_4Cl) (500 µl per well) and incubated for 10min in fresh NH_4Cl. After 3x washes in PBS, cells were permeabilized using 0.2% Triton X-100 (Sigma-Aldrich) for 10min at room temperature. To block non-specific binding of antibodies, cells were incubated for 1 h at room temperature in a solution containing 1% BSA, 0.1% Tween-20 and 5% donkey serum in TBS. Blocking buffer was washed off using TBST. Ant-HMGB1 primary antibody diluted in TBST/1% BSA (1:1000) was added to cells and incubated for 1 h at room temperature. Following washing in TBST, a fluorescently conjugated secondary antibody (Alexa Fluor 488 donkey anti-rabbit, ab150073, Abcam) and anti-actin (Phalloidin) (Alexa Fluor 568, ab208143, Abcam) were used at 1:1000 and 1:250 dilutions respectively. Incubations were performed at room temperature for 1 h in the dark. After 2x washes in TBST, 2 µg/ml Hoechst 33342 (200 µl per well) was added and cells incubated at room temperature for 10 min. Cells were again washed In TBST and 10 µl of ProLong Gold Antifade reagent was used to mount each cover slip. A transparent nail varnish was used to hold cover slip in place and slides were stored in the dark at 4°C until imaged.

Z-stacked Images of stained cells were captured using 40X objective Apochrome on the Zeiss Axio Observer Z.1 microscope (Zeiss, Oberkochen, Germany). The filter

sets Alexa 488 (Green), Alexa 568 (Red) and Alexa 349 (blue) were used for HMGB1, actin (Phalloidin) and Hoechst stains respectively. Images were retrieved both in single filter channels and merged channels with a 20 μm cell diameter scale bar applied.

3.2.12 Stripping and re-probing of membrane

Membranes were stripped and re-probed for other target proteins including β-actin endogenous loading control using a mild stripping buffer (15 g glycine, 1 g SDS, 10 ml Tween 20, pH 2.2, volume adjusted to 1 litre with distilled H_2O). Membrane was covered in sufficient volume of stripping buffer and incubated at room temperature for 10 min. Spent stripping buffer was discarded and this was repeated with fresh stripping buffer. Membrane was then washed twice in 1X PBS for 10 min each and then washed twice in 1X TBST for 5 min each. Once washings were completed, membrane was blocked as documented in this thesis and re-probed with the intended antibody.

3.2.13 Statistical analysis

All experimental data were expressed as mean ± SEM. A two sample (unpaired) t-test was used to determine whether the means of the control and experimental groups are equal. This test works on the assumption that the dependent variable (mean) in the groups is normally distributed. When the data did not follow a normal distribution based on the test for normality, the non-parametric Mann-Whitney U test was used to check the difference in Rank Sum and U statistic and significance established when the U critical value exceeded the U statistic. A two-tailed analysis

of variance was calculated on the variables in the groups whilst assuming equal variances between groups. All tests were performed using Stats Direct 3 software. Quantification of protein band density was achieved using ImageJ software. Results were considered significant when two sided P-values yielded a value less than 0.05. *=P<0.05, **=P<0.01, ***=P<0.001 were used to indicate different degrees of significance.

3.3 Results

3.3.1 Effect of nitric oxide-donating compound NOC-18 on HaCaT cellular viability.

The effect of NOC-18 on HaCaTs was investigated in order to identify the optimal dose required for maximal toxicity as measured using an MTT assay. NOC-18 mediated HaCaT cell death in a dose-dependent manner with 10 mM dose exhibiting optimal cell death (Figure 3.2A) selected for subsequent experiments. Staurosporine, a well-known apoptosis-inducing compound (Belmokhtar et al., 2001), was tested at concentrations ranging from 0 to 20 µM (Figure 3.2B). Similarly, this also induced a dose-dependent decrease in HaCaT viability. 5µM Staurosporine was selected for subsequent experiments as a positive control for apoptosis.

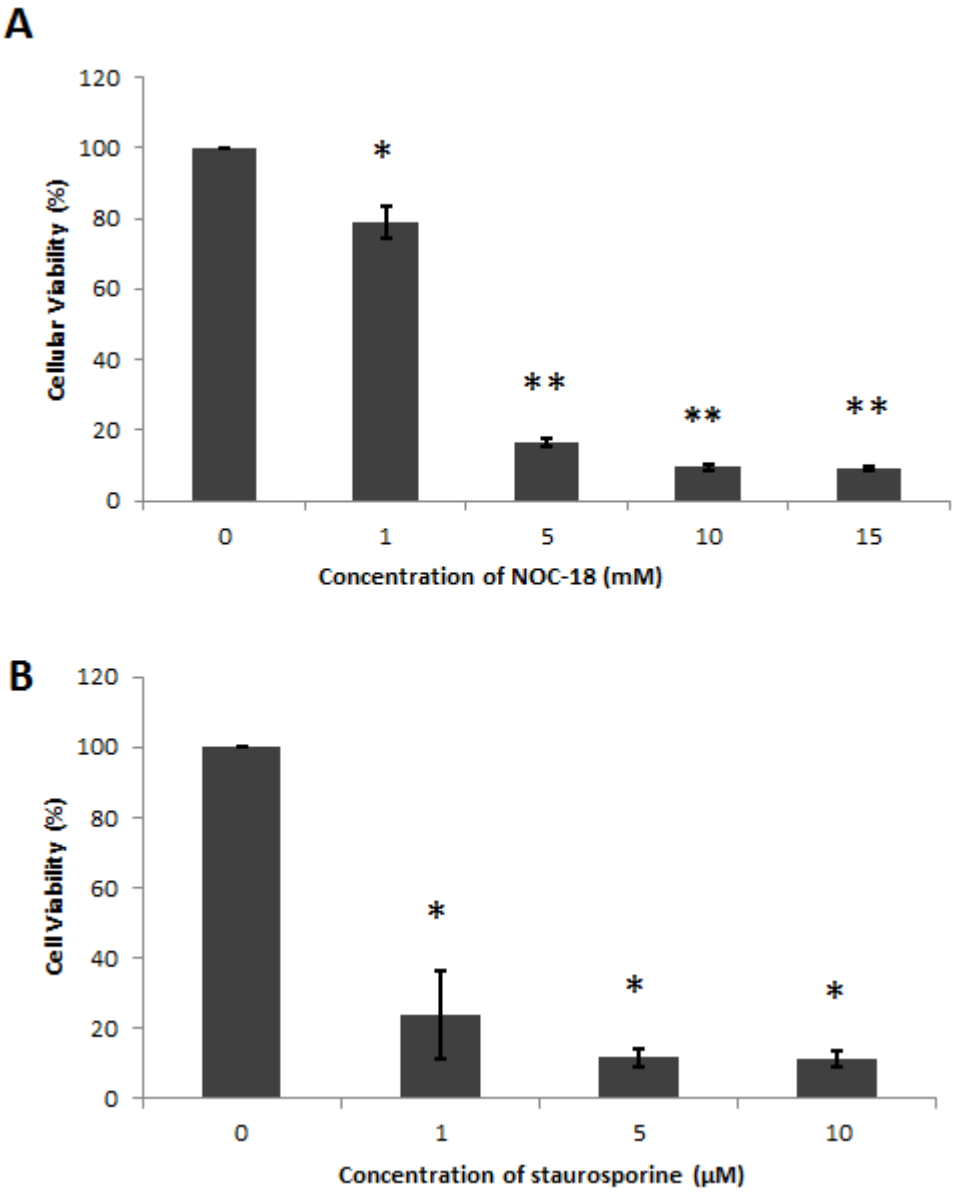

Figure 3.2: Effect of NOC-18 and Staurosporine on cell death in HaCaTs. A) NOC-18 on HaCaT cellular viability B) Staurosporine on HaCaT viability**.** Cell viability was corrected relative to untreated controls. The number of dead or dying cells was measured using an MTT assay following 12h of incubation. Treatments were performed in triplicate with each experiment performed independently three times. Data represent mean ± SEM and statistical analysis significance from Mann-Whitney U test compared to vehicle control (*P<0.05, **P<0.01).

3.3.2 Effect of zVAD and Nec-1 on HaCaT cells

Small molecule inhibitors of caspases (zVAD.fmk, zVAD) and RIP1 (necrostatin-1, Nec-1) are routinely used to discriminate specific molecular death pathways activated by toxins in cells (Bergamaschi et al., 2019). zVAD is a cell-permeable pan-caspase inhibitor that irreversibly binds to the catalytic site of caspases blocking the induction of apoptosis while Nec-1 is a small molecule that selectively binds and inhibits the kinase domain of RIP1. In order to identify suitable doses of zVAD and Nec-1 with no or minimal toxicity to HaCaT cells, a dose response curve was constructed. zVAD showed little toxicity to HaCaT cells at 50 µM after 12 hours of treatment (Figure 3.3A) whereas Nec-1 at 50 µM showed no toxicity to HaCaT cells (Figure 3.3B). The dose of 50 µM for both Nec-1 and zVAD was chosen for further studies.

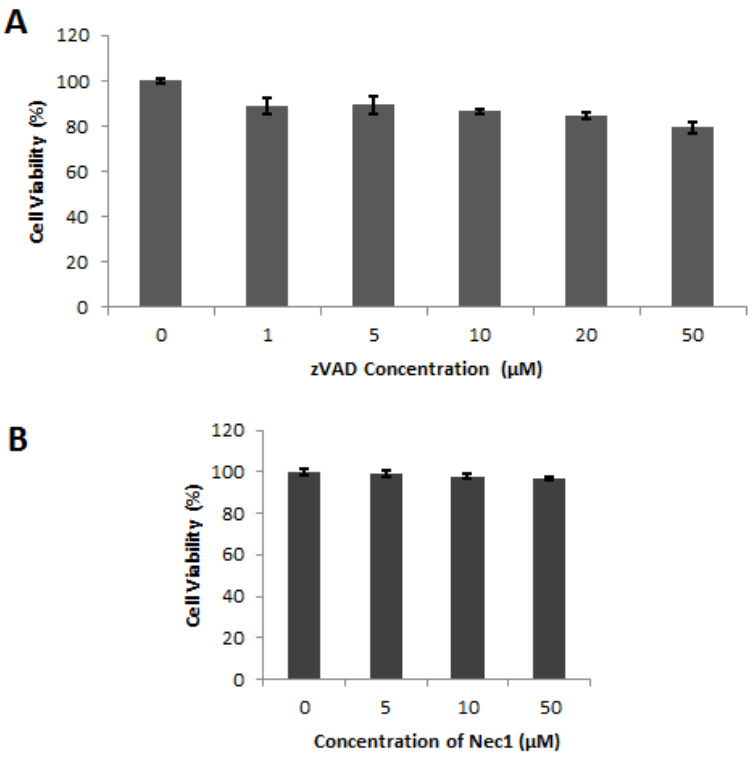

Figure 3.3: Effect of zVAD (A) and Nec-1 (B) on HaCaT viability. HaCaT cells were treated with the indicated doses of either zVAD or Nec-1 for 12 h after which time cell viability was measured using the MTT assay. All results represent mean ± SEM of triplicate samples from 3 independent experiments.

3.3.3 Effect of RIPK1 and caspase inhibition on NOC-18-induced HaCaT cell death

Apoptosis has been identified as the preferential mechanism by which NOC-18 causes cell death. To address whether the cell death that was observed with HaCaT cells is apoptosis or necroptosis, an MTT cell death assay was performed following treatment with NOC-18 in the presence of Nec-1 or zVAD. Surprisingly, neither Nec-1 nor zVAD pre-treatment rescued HaCaT cell death (Figure 3.4). More surprising was the lack of effect by zVAD to offer some protection to HaCaT cells treated with staurosporine.

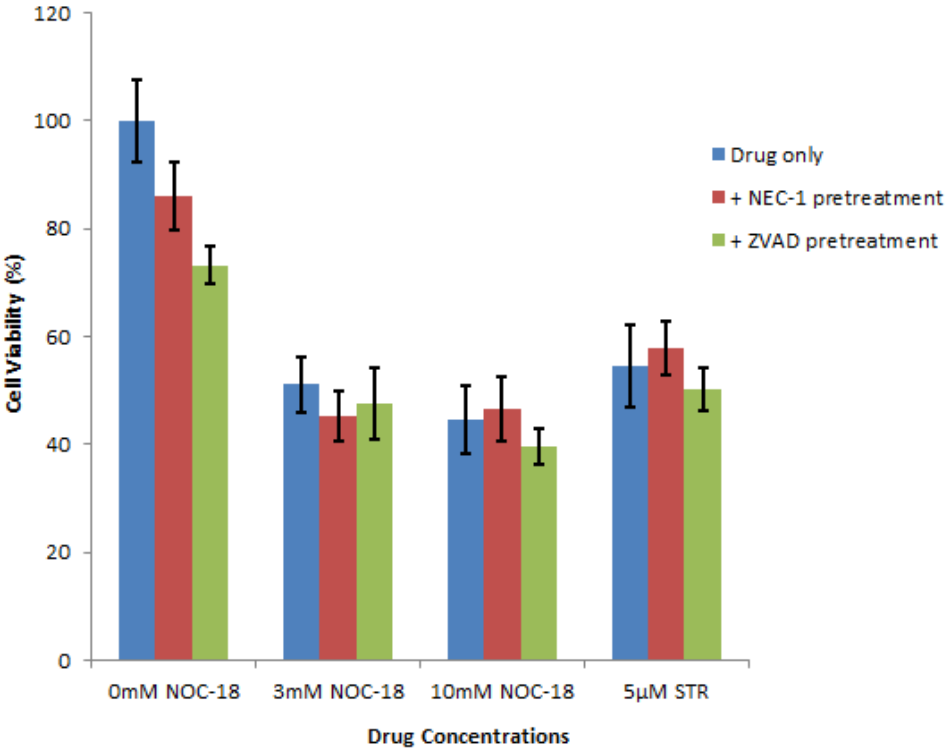

Figure 3.4: Effect of RIPK1 and caspase inhibition on keratinocyte cell death following NOC-18 treatment. MTT assay assessment of NOC-18-induced cell death in the presence of caspase and RIPK1 inhibition. HaCaTs were either pre-stimulated with 50 µM zVAD or 50 µM Nec-1 for 1h followed by 12h with NOC-18. Data represent triplicate measurements of three independent experiments expressed as mean ± SEM.

3.3.4 Effect of NOC-18 on end-point cell death markers

To determine caspase-dependent apoptotic involvement in NOC-18 induced HaCaT cell death, caspase 3/7 activity was measured in NOC-18 treated HaCaT cells using a luminometric-based probe. This assay provides a homogenous luminescent measurement of caspases-3 and -7 activities. The probe utilises the ability of these caspases to specifically recognise and cleave a DEVD tetra-peptide motif. Following 12 h of drug incubations, caspases 3/7 activity was significantly increased 2-fold in the 5 mM dose of NOC-18 but with the lower doses (Figure 3.5A). As expected, pre-stimulation with zVAD reduced caspase 3/7 activity in NOC-18 treated HaCaT cells

indicating the activation of these caspases. Staurosporine was used as a positive control for apoptosis and this also caused an increase in luminescence which was blocked by zVAD. In addition, necroptosis terminal effector mixed lineage kinase domain like (MLKL), and caspase 3 processing were investigated. Lysates from NOC-18 treated cells were subjected to Western blotting for the detection of cleaved caspase-3 fragments and MLKL. The detection of caspase-3 cleavage from the catalytically inactive p32 pro-form into the catalytically active 19kDa and 17kDa fragments was used as a marker for apoptosis whereas the elevation in the levels of MLKL was used as a marker for necroptosis. Cleaved caspase-3 fragments were more visible after 10mM of NOC-18 indicating caspase-3 processing with this concentration (Figure 3.5B and Figure 3.5C). MLKL was also slightly increased compared to untreated cells. Slight elevation of MLKL protein was seen at 5 mM and down-regulation at 10mM indicating the possibility of necroptosis involvement (Figure 3.5B and Figure 3.5C). Differences in cleaved caspase 3 and MLKL levels between treatments were non-significant (Figure 3.5C) as determined by unpaired t test. β-actin was used as a loading control to determine protein transfer efficiency.

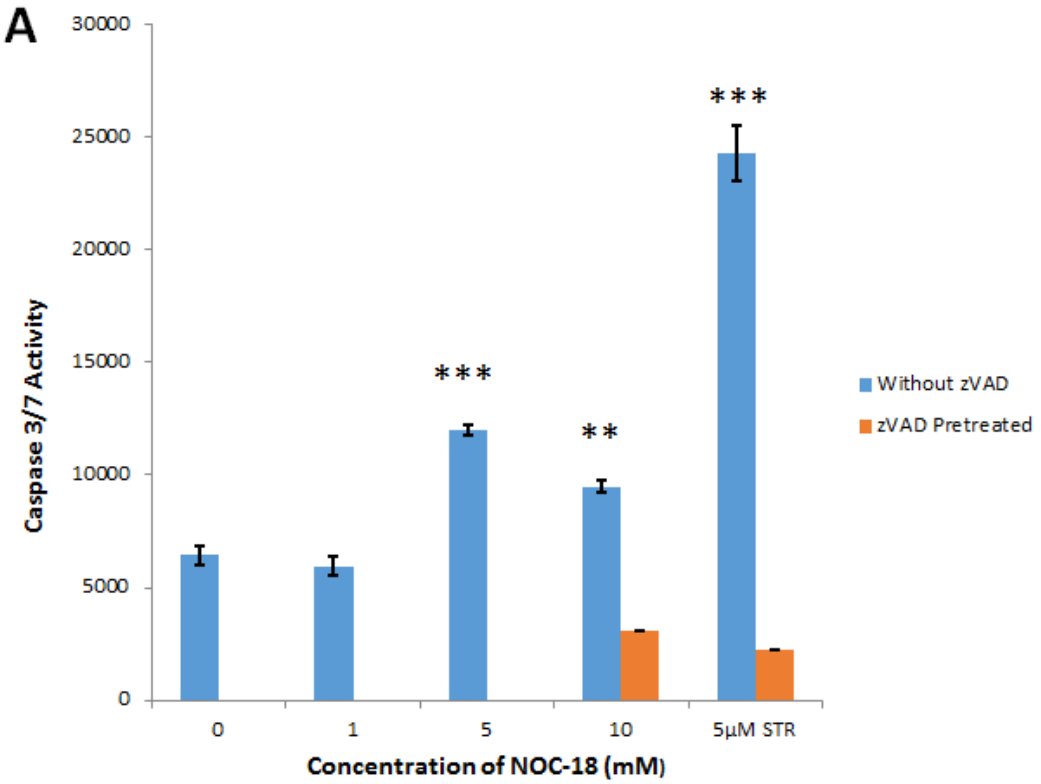
A
30000
25000
20000
15000
10000
5000
0
Caspase 3/7 Activity
***
**
***
Without zVAD
zVAD Pretreated
0
1
5
10
5µM STR
Concentration of NOC-18 (mM)

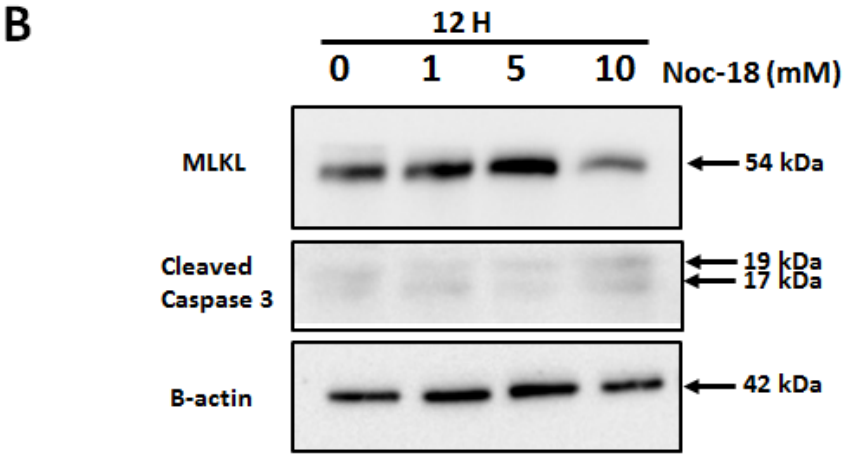
B
12 H
0
1
5
10
Noc-18 (mM)
MLKL
54 kDa
Cleaved
Caspase 3
19 kDa
17 kDa
B-actin
42 kDa

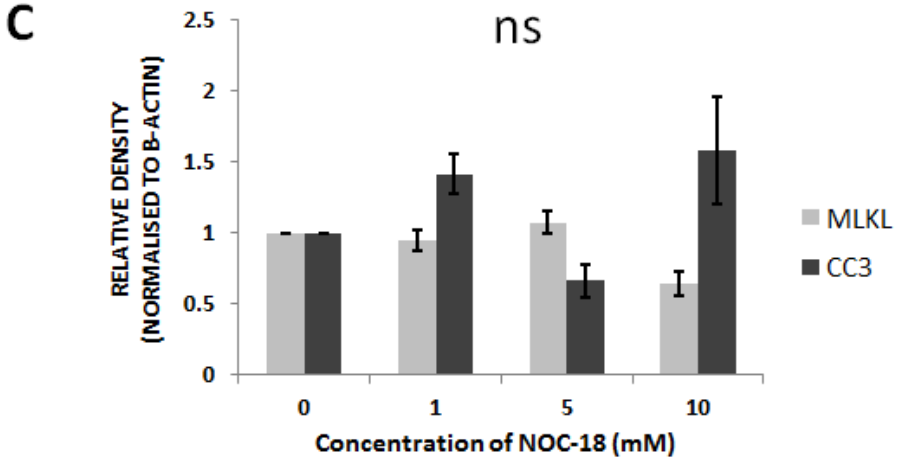
C
ns
2.5
2
1.5
1
0.5
0
RELATIVE DENSITY
(NORMALISED TO B-ACTIN)
MLKL
CC3
0
1
5
10
Concentration of NOC-18 (mM)

Figure 3.5: Investigation of apoptotic and necroptotic markers in NOC-18 treated HaCaT keratinocytes A) Effect of NOC-18 on caspase-3 and -7 activation in HaCaT cells as determined by caspase-Glo^{R} 3/7 assay B) Western blot analysis of MLKL expression and caspase-3 cleavage C) ImageJ analysed Western blotting result from B (n=2) showing MLKL and cleaved caspase 3 levels relative to β-actin levels. Drug incubations were carried out with or without zVAD (50 μM, pre-treatment for 1 h) and caspase-3/7 activity was measured after 12 h of NOC-18 treatment using caspase-Glo 3/7 assay. Staurosporine (5 μM) was used as a positive control. zVAD (50 μM) was included as indicated to block caspase activity. Data are shown as mean ± SEM from three sets of independently conducted experiments performed in triplicate. Significance indicated by unpaired t test (*P<0.05, **P<0.01, ***P<0.001). STR; staurosporine. MLKL and cleaved caspase-3 levels in total HaCaT cell lysates exposed to increasing doses of NOC-18 for 12 h were measured using Western blotting. β-actin levels were used as loading control. Blots are representative of two independent experiments. Abbreviations CC3 and ns indicate cleaved caspase 3 and non-significant result respectively.

3.3.5 Effect of NOC-18 on HMGB1 subcellular localisation

HMGB1 is a transcription factor whose subcellular location determines its function (Martinotti et al., 2015). Under normal physiological conditions, the protein is predominantly nuclear in most cell types but it can relocate during cell death (Bianchi and Manfredi, 2007). Immunofluorescence was employed to visualise the subcellular location of HMGB1 in both untreated and NOC-18 treated HaCaT cells (Figure 3.6). In untreated controls, HMGB1 (green) was confined to the nucleus (blue) as revealed by immunofluorescence staining. The nuclei of the cells were also intact having the spherical morphology typical of cells that have not undergone any cell death. There was a dose-dependent decrease in expression of HMGB1 in the nucleus of HaCaT cells as translocation from nucleus to cytosol and then to extracellular space was induced by NOC-18 treatment (Figure 3.6). 5 mM and 10 mM doses of NOC-18 caused a marked down-regulation in the nuclear expression of HMGB1. Some of the nuclei of HaCaT cells exposed to higher doses (≥ 5 mM) of

NOC-18 showed both shrinkage and destruction of the nuclear integrity whereas others appear relatively spherical with little observation of nuclear membrane condensation.

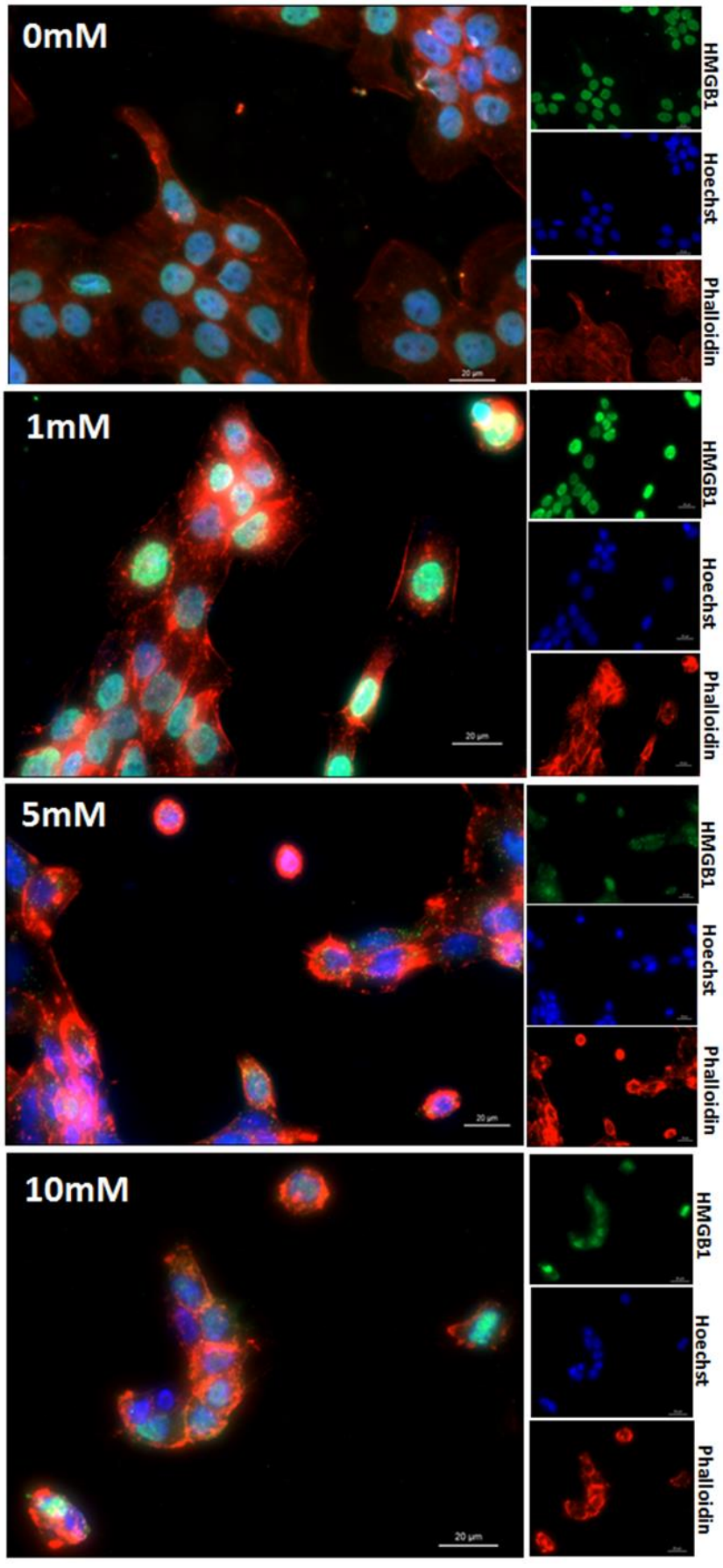

HMGB1 Fluorescent intensity measurement for NOC-18 treated wildtype HaCaT cells			
[NOC-18] (mM)	Mean gray value	AV	SEM
0	6.897	6.119	0.3962
	5.860		
	5.600		
1	7.168	5.781	0.7240
	5.446		
	4.728		
5	2.994	3.504	0.5000
	4.504		
	3.014		
10	2.177	2.601	0.2128
	2.782		
	2.844		

Figure 3.6: **Merged and single channel immunofluorescence images of HaCaT cells exposed to increasing doses of NOC-18.** HMGB1 was almost exclusively expressed in the nucleus of unstimulated HaCaT cells. Treatment with NOC-18 led to translocation from the nucleus to the cytoplasm. HMGB1 was stained with alexa488 (green), the nucleus with Hoechst (blue) and the actin cytoskeleton alexa568-Phalloidin (red). Images shown are representative of 3 separate experiments. Fluorescent intensity measurement in different samples was performed using ImageJ software. Mean gray level (0-255) of selected pixels representing intensity of HMGB1 staining per unit area in arbitrary units was determined for 3 separate experiments. AV and SEM represent average and standard error of mean.

3.3.6 Effect of NOC-18 on extracellular total HMGB1 levels

Extensive release of HGMB1 from dying or injured cells into the extracellular space may be a useful marker for cell death by both necrosis and necroptosis (Kaczmarek et al., 2013). Supernatants from HaCaT cells exposed to varying doses of NOC-18 in the absence of both zVAD and Nec-1 were analysed for the presence of HMGB1 by Western blotting. Results revealed a dose-dependent increase in HMGB1 levels in the supernatants from NOC-18 treated HaCaT cells compared to vehicle treated controls although only the 10mM dose of NOC-18 showed a statistically significant difference ($p<0.05$) (Figure 3.7).

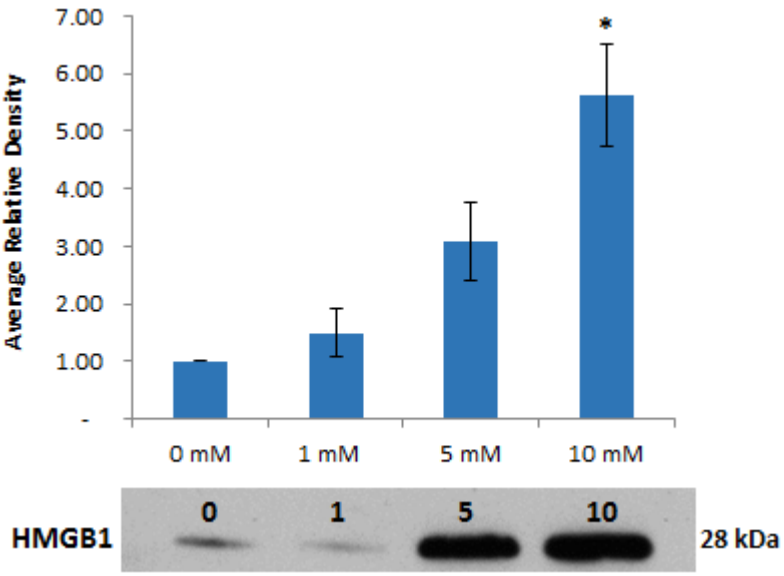

Figure 3.7: HMGB1 profiling in supernatants from NOC-18 treated HaCaTs analysed by Western blotting. Supernatants (25 µl) collected from NOC-18 treated HaCaT cells in the absence of both zVAD and Nec-1 were subjected to Western blotting for HGMB1 detection. Densitometric analysis was carried out on n=3 experiments via ImageJ software and statistical significance determined using Mann-Whitney U test. *p<0.05 is indicative of significance.

3.4 Discussion

The aim of this chapter was to determine the mechanism of NO-dependent keratinocyte death and investigate its effect on extracellular HMGB1 levels. In the previous chapter, it was demonstrated that HMGB1 serum and blister profiles stratified cutaneous hypersensitivity phenotypes from tolerant controls in all patient cohorts examined. Our wish was to assess the contribution that NO may have on HMGB1 release in keratinocytes and relate this to its potential pathologic role in SJS/TEN disease mechanisms.

It was shown that NOC-18-mediated killing of HaCaT keratinocytes in culture was likely caspase 3/7 dependent, as revealed by caspase 3/7 luminescence assay and this was accompanied with caspase 3 cleavage especially with the 10 mM NOC-18

dose. This suggests that caspase-dependent apoptosis could be contributing to NO-induced HaCaT cell death. To support this, the presence of cleaved caspase 3 fragments was confirmed which further suggests the activation of caspase dependent apoptosis. In contrast, our data on the viability of NOC-18 treated HaCaTs determined by MTT did not show any cell death rescue effect by both zVAD and Nec-1. This may suggest that although caspase is activated, NO may be causing toxicity via other mechanisms as blocking one death pathway may sometimes unmask a secondary process of cell death (Bal-Price et al., 1999). There was no observable zVAD effect on staurosporine induced HaCaT cell death at 12 hour incubation. A probable explanation for our observation could likely be that staurosporine induces late apoptosis through a caspase-independent mechanism similar to that reported by Belmokhtar *et al* 2001 in mouse leukemia L1210/0 cells (Belmokhtar et al., 2001). Also, other publications have demonstrated that inhibiting caspase activities in mammalian apoptotic systems using zVAD sometimes fail to prevent cell death (Xiang et al., 1996) (Miller et al., 1997) (Lavoie et al., 1998).

Our data did not show poly (ADP-ribose) polymerase (PARP) cleavage at 12 h (data not shown) indicating that PARP was not cleaved during HaCaT cell death induced by NOC-18. Perhaps detection of cleaved PARP fragments in certain cell types upon NOC-18 death induction is time dependent. In agreement one study only observed NOC-18-induced PARP cleavage in human neuroblastoma SH-5Y cells at 24 h but not at earlier time-points (Uehara et al., 1999). PARP cleavage is primarily mediated by effector caspases -3 and -7 (Boulares et al., 1999). A rise in the activity of caspase-3 like protease preceding mitochondrial cytochrome C release was demonstrated upon induction of apoptosis in SH-5Y cells using NOC-18 (Uehara et al., 1999).

Furthermore, our data showed a marginal increase in MLKL protein expression following NOC-18 treatment indicating its possible involvement as a necroptosis effector in the execution of HaCaT cell death. Although RIPK1 inhibition by Nec-1 did not offer any protection to HaCaT cells from NO mediated cell death suggesting that necroptosis induction by MLKL was RIPK1-independent. Perhaps, RIPK1 inhibition does not completely prevent MLKL upregulation. This is supported by a recent study that demonstrated Nec-1 could block RIPK1-dependent necroptosis but not RIPK1 phosphorylation (Alturki et al., 2018).

NO and RNS can kill cells by a variety of yet poorly defined mechanisms which are cell type and experimental conditions dependent (Brown and Borutaite, 2001) (Murphy, 1999). Cell death mediated by NO can be distinguished on the basis of the energy status of the cell into energy depletion-induced necrosis and oxidant-induced apoptosis (Brown and Borutaite, 2001). The energy depletion-necrosis induction causes ATP depletion through four mechanisms: a) inhibition of mitochondrial respiration b) induction of mitochondrial permeability transition c) inhibition of glycolysis at glyceraldehyde-3-phosphate dehydrogenase and d) activation of PARP (Brown and Borutaite, 2001). Apoptosis mediated by NO is mostly through the mitochondrial pathway and can be accomplished by various molecular mechanisms that include up-regulation of tumour suppressor P53 (Messmer et al., 1994), activation of MAPK (Bosca and Hortelano, 1999) and mitochondrial permeability transition (MPT) (Snyder et al., 2009). Cytochrome c is then released which leads to caspase activation leading to apoptosis (Yabuki et al., 1997) (Brockhaus and Brune, 1998). Chromatin condensation and DNA fragmentation have also been observed (Brüne et al., 1998).

Studies aimed at gaining further insights into the mechanism of NO-induced apoptosis have also implicated the death receptor, Fas. A link between NOC-18 and Fas-mediated apoptosis emerged with an observation that HaCaT cells stimulated with NOC-18 showed both an increase in cell surface FasL together with an increase in Fas mRNA levels (Viard-Leveugle et al., 2013). Viard-Leveugle et al (2013) further demonstrated that increasing NO synthesis in keratinocytes isolated from TEN patients resulted in increased FasL expression and consequently lead to the activation of Fas and caspase-8 mediated apoptosis. Under physiological conditions, other studies have shown that mRNAs of key apoptotic pathway players like Fas, FADD and caspase-8 are detectable in the epidermis, primary keratinocyte culture and keratinocyte cell line and that both Fas and FasL are co-expressed by epidermal keratinocytes (Viard-Leveugle et al., 2003).

In tissues, NO toxicity may be greatest in the epidermis where haemoglobin which is thought to be the major scavenger of NO is either very low or absent (Qureshi et al., 1996). NO can trigger both apoptosis and necrosis *in vitro* (Mitrovic et al., 1995). Together, these data suggest that both caspase-dependent apoptosis and necroptosis may play a role in NO mediated nitrosative stress that culminates in keratinocyte cell death.

Our data revealed the translocation of HMGB1 from the nucleus to the cytosol and finally to the extracellular space upon NOC-18 mediated keratinocyte death. We further showed dose related marked release of HMGB1 into culture media following stimulation with NOC-18. This observation implies that an increase in NO has a huge impact on the active cellular translocation of HMGB1. In agreement with this,

blocking INOS in Raw 264.7 cells (macrophages) attenuated NO-induced HMGB1 translocation and release (Jiang and Pisetsky, 2008). We did not carry out further investigation in the regulation of HMGB1 translocation, however, other studies have shown that HMGB1 translocation occurs through the c-Jun N-terminal kinase (JNK) pathway (Wu et al., 2013) (Wu et al, 2006) (Cheng et al., 2017) (Wang et al., 2017) (Jiang and Pisetsky, 2008).

Interestingly, our immunofluorescence data on the morphology of NOC-18-mediated HaCaT cell death tended to show more morphological features of necrosis than apoptosis. In agreement with this, a study performed on PC12 cells using NOC-18 yielded results that were predominantly of necrotic nuclear morphology (Bal-Price and Brown, 2000). This may suggest that more HaCaT cells were dying by either necrosis or necroptosis or perhaps both.

Our Western blotting data on supernatants revealed a significant release of HMGB1 during NOC-18-mediated keratinocyte death. The level of HMGB1 observed would be unlikely if apoptosis was the dominant pathway in this model. Notably, it is difficult to achieve accurate quantification of HMGB1 in supernatants by Western blotting because the software used to estimate protein band density is more user-dependent and Western blotting is generally considered as a semi-quantitative technique (Ghosh et al., 2014) (Mahmood and Yang, 2012) (Taylor et al., 2013). A more sensitive and accurate quantification of HMGB1 concentration can be achieved via enzyme linked immunosorbent assay (ELISA) technique. However, there was no suitable and compatible ELISA kit that could be used to measure HMGB1 in cell culture supernatant at the time of this investigation. With recent

advances in ELISA development, HMGB1 in cell supernatants can now be determined by ELISA using commercially available HMGB1 ELISA Kit II (Shino-Test Corp, Sagamihara, Japan). Thus this offers us the opportunity in the future to precisely measure HMGB1 in supernatants by ELISA and make comparison with serum and blister fluid HMGB1 levels from SJS/TEN patients discussed in chapter 2.

This study was unable to achieve precise characterisation of the mechanisms of NO-mediated keratinocyte death. However, like other studies, we have demonstrated that NO can activate multiple death pathways and that these pathways altogether result in a marked release of HMGB1. Thus NO expression in SJS/TEN might contribute to epidermal keratinocyte damage and consequently HMGB1 elevation. Taken together, findings from this study suggest that NO and its mediators plays a key role in driving keratinocyte death, and that damaged keratinocytes release HMGB1 which may further exacerbate inflammation in SJS/TEN.

CHAPTER 4

MECHANISM OF TUMOUR NECROSIS FACTOR ALPHA INDUCED KERATINOCYTE DEATH AND HMGB1 RELEASE

Contents

4.1 Introduction

Extracellular stress signals conveyed by cytokines of the tumour necrosis factor (TNF) receptor superfamily engage and activate cell surface death receptors (Galluzzi et al., 2012). A number of these cytokines such as TNF, Fas ligand (FasL) and TNF-related apoptosis-inducing ligand (TRAIL) can initiate either apoptosis or necroptosis depending on the levels of the intracellular signalling proteins recruited to their death-inducing signalling complexes (DISC) (Vandenabeele et al., 2010b) (Tanzer et al., 2016).

TNF-α is mainly produced by macrophages and exhibits pleiotropic roles in immunity, inflammation, regulation of proliferation, differentiation and cell death (Micheau and Tschopp, 2003). TNF-α action is exerted through its receptors: TNF receptor-1(TNFR1) and -2 (TNFR2) which are expressed by virtually all nucleated cell types (Vandenabeele et al., 1995) (Figure 4.1). TNF, through TNFR1, can signal both for cell survival and cell death via two distinct complexes (Hsu et al., 1995) (Wiegmann et al., 1992).

The pro-survival complex I forms at the cell surface when TNFR1 is triggered leading to binding of the adaptor proteins TNFR-associated death domain protein (TRADD), TNFR-associated protein 2 (TRAF2), receptor-interacting protein kinase 1 (RIPK1) and the cellular inhibitor of apoptosis proteins, cIAP1 and cIAP2. This leads to recruitment and activation of the IKK signalosome and activation of the pro-survival nuclear factor κB (NF-κB) pathway (Shu et al., 1996). The pro-death signalling complex, complex II, is activated following receptor internalization of complex I which then recruits Fas-associated death domain containing protein (FADD) and

caspase 8 to generate the death inducing signalling complex (DISC) (Micheau and Tschopp, 2003) (Rothe et al., 1995) (Galluzzi et al., 2012). The recruitment of RIPK3 to the DISC by RIPK1 in the absence of c-FLIP and cIAPs is a key determinant for necroptosis signalling (Chen et al., 2014) (Vandenabeele et al., 2010a). The amount of procaspase-8 recruited is also critical as this will determine whether the signal will be apoptotic or necroptotic probably through cleavage of RIPK3 (O'Donnell et al., 2011).

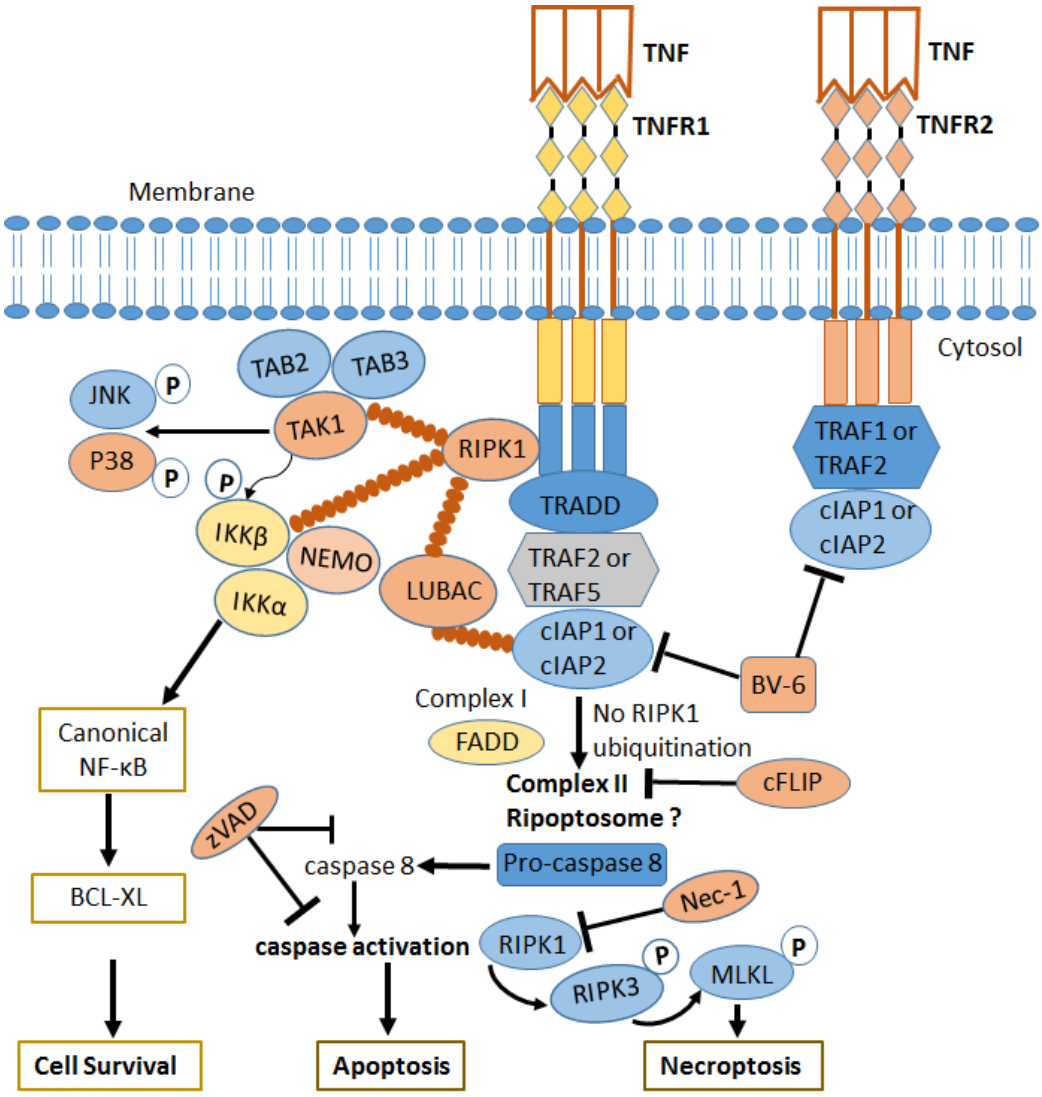

Figure 4.1: **Schematic representation of apoptosis and necroptosis extrinsically activated by TNF death receptor signalling**. Ligation of both transmembrane tumour necrosis factor receptor 1 (TNFR1) and 2 (TNFR2) by tumour necrosis factor

(TNF) leads to receptor activation through trimerization. Activated TNFR1 binds to adaptor protein, TNFR-associated death domain protein (TRADD) which then recruits receptor interacting protein kinase 1 (RIPK1), TNFR-associated protein 2 (TRAF2) or TRAF5 and cellular inhibitor of apoptosis protein 1 (cIAP1) or cIAP2 to form TNFR1 signalling complex I. Activated TNFR2 can also directly interact with TRAF1 or TRAF2 to recruit cIAP1 or cIAP2. Both cIAP1 and cIAP2 are E3 ubiquitin ligases responsible for adding K63-linked polyubiquitin chains to RIPK1 and possibly other components of the signalling complex. The ubiquitin ligase activity of cIAP1 and cIAP2 is utilised to further recruit linear ubiquitin chain assembly complex (LUBAC) to complex I. Upon recruitment, LUBAC stabilises complex I through the catalytic attachment of a linear M1-linked polyubiquitin chain most often to RIPK1. K63-polyubiquitinated RIPK1 recruits TGFβ-activated kinase 1 (TAK1) and MAP3K7 binding protein 2 (TAB2)-and 3 (TAB3), which activate signalling through JUN N-terminal kinase (JNK) and p38 including IκB kinase (IKK) complex. The IKK complex consists of three subunits: two kinases; IKKα and IKKβ and the regulatory subunit, nuclear factor κB (NF-κB) essential modulator (NEMO). Thereafter, the IKK complex activates NF-κB which in turn leads to the transcription of numerous anti-apoptotic target genes such as BcL-XL (also referred to as BcL2L1) and the long isoform of FLICE-like inhibitory protein ($FLIP_L$), which collectively act to promote cell survival. The formation of the cytosolic pro-death complex II begins with receptor internalisation of complex I, which is dependent on non-ubiquitinated RIPK1. Non-ubiquitinated RIPK1 dissociates from complex I and migrates into the cytosol, where it assembles with the adaptor protein FADD and recruits pro-caspase 8 and cellular FLIPL ($cFLIP_L$) to form a death inducing signalling complex (DISC). Pro-caspase 8 can form both homodimers with itself or heterodimers with $cFLIP_L$. Apoptotic or necroptotic signalling depends on the levels of pro-caspase 8 recruited to the DISC. High levels of pro-caspase 8/$cFLIP_L$ heterodimer or pro-caspase 8 homodimer facilitates self-processing and activates caspase 8, thereby inactivating RIPK1 through cleavage. Thus caspase 8 can further cleave downstream executioner caspases leading to apoptosis. RIPK1 recruits and activates RIPK3 via phosphorylation in a complex called ripoptosome only when the level of pro-caspase 8 is low, which then leads to necroptotic signalling. Activated RIPK3 activates the terminal effector of necroptosis, mixed lineage kinase domain like (MLKL) protein, via phosphorylation. BV-6 and Nec-1 inhibits the cIAPs and RIPK1 respectively, while zVAD (zVAD.fmk) is a pan caspase inhibitor.

The aberrant production of TNF-α by cytotoxic T lymphocytes has been implicated in SJS/TEN pathology with TNF-α thought to play a key role in driving TEN pathology (Paquet et al., 1994) (Panayotova-Dimitrova et al., 2015). Also, a number of studies have shown evidence for the use of TNF-α antagonist etanercept as a therapy for SJS/TEN (Paradisi et al., 2014) (Lee et al., 2013) (Wang et al., 2018a) (Gavigan et al.,

2018) (Zhang et al., 2019). TNF-α is also found at high levels in the serum and blister fluid from SJS/TEN patients (Wang et al., 2018c) (NOMURA et al., 2011) (Correia et al., 2002a). However, it is not well established whether TNF-α plays a role in HMGB1 elevation following destruction of the epidermis in SJS/TEN.

HMGB1 is an established marker of cell death and inflammation (Bell et al., 2006a) and elevated HMGB1 levels have been observed in serum and blister fluid from patients with SJS/TEN.

The aim of this chapter was to investigate the mechanism of TNF-α mediated keratinocyte death and determine extracellular HMGB1 release from characterised death pathways.

4.2 Materials and methods

4.2.1 Materials

Recombinant Human TNF-α (#210-TA-020) was supplied by R&D SYSTEMS (Abingdon, UK). Anti-cIAP1 (#ab154525) and anti-cIAP2 (#ab137393) were purchased from Abcam (Cambridge, UK). BV-6 (#S7597) was obtained from Selleckchem (Munich, Germany). Anti-caspase-3 (Asp 175) antibody (#9661, #9662), anti-PARP antibody (#9542) were all purchased from Cell Signalling Technology (Leiden, Netherlands). Anti-rabbit IgG HRP conjugate (A0545) was obtained from Sigma-Aldrich (Poole, UK). Annexin V and Propidium Iodide were obtained from Dr Shankar Varadarajan of the University of Liverpool. Other reagents used in this chapter have been presented in chapter 3 (3.2.1).

4.2.2 Cell culture

Cell culture was performed as outlined in materials and methods of chapter 3 (3.2.3)

4.2.3 Transfection of cIAP2 construct into HEK293T cells

In order to have a positive control for cIAP2 protein detection by Western blotting, a Flag-tagged cIAP2 plasmid generously provided by Dr Nicholas Harper was transiently expressed in HEK293T cells. Briefly, 1µg of DNA was transfected into HEK293T cells for 24 hours using jetPEI DNA transfection reagent (101-10, Polyplus, France). HEK293T cells were seeded at a density of $3.0x10^5$ cells per well into a 6-well plate and allowed to adhere overnight. Following the Polyplus transfection protocol, 100 µl of 150 mM NaCl was thoroughly mixed with 4 µl of JetPEI. Another 100 µl of NaCl was used to dilute 1 µg of the cIAP2 plasmid. Diluted JetPEI was then added dropwise to diluted DNA, vortexed and left to incubate at room temperature for 20 min. 200 µl of DNA/JetPEI complexes was then added dropwise to cells and allowed to incubate at 37°C, 5% CO_2 for 24 h. Cells were lysed in SDS sample buffer and western blotting performed. Detailed information on antibodies used has already been presented in Table 3.1.

4.2.4 MTT assay

Cell viability of both control and TNF-α treated HaCaTs was determined using the MTT assay as described in materials and methods of chapter 3 (3.2.6).

4.2.5 Annexin V/Propidium Iodide staining

In healthy cells, phosphatidylserine (PS) is preferentially located on the cytoplasmic leaflet of the plasma membrane (Leventis and Grinstein, 2010). Early apoptosis causes the externalisation of PS to the outer leaflet of the cell plasma membrane exposing it to the external milieu. Annexin V conjugated with fluorescein isothiocyanate (FITC) (annexin V-FITC conjugate) binds to the externalised phosphatidylserine in the presence of Ca^{2+} and therefore detects early apoptosis. Propidium iodine (PI) detects late apoptosis and necrosis by binding to DNA exposed only after both plasma and nuclear membranes have ruptured. Cells were seeded at a density of 5x 10^5 per well into 6-well plates and allowed to adhere overnight. They were then treated with either DMSO, TNF/BV-6, TNF/BV-6 + Nec-1, TNF/BV-6 + zVAD and TNF/BV-6 + Nec-1 + zVAD for 8 h. After 8 h incubations, cell supernatants for all cells used in this assay were retained in order not to lose floating dead cells. Cells were washed with HBSS, detached using trypsin and cell mixture returned to their corresponding tube. Trypsin was inactivated using serum DMEM. All cells were pelleted at 2000 rpm for 5 min at room temperature, washed in PBS and re-centrifuged. Cell pellets were re-suspended in 1X annexin binding buffer (10 mM HEPES, 140 mM NaCl and 2.5 mM $CaCl_2$, pH 7.5). Staining was then carried out with annexin V (2.5 µg/ml final concentration) for 10 min in the dark and on ice. Afterwards, PI (0.1 mg/ml in PBS) was added to a final concentration of 0.25 µg/ml, and cells were incubated for a further 5 min on ice. Cell death analysis was performed by flow cytometry using Attune Acoustic Focusing Cytometer (Applied Biosystems).

4.2.6 Running SDS-PAGE

SDS-PAGE was used to separate proteins on the basis of molecular size. SDS-PAGE was performed as previously described (3.2.10).

4.2.7 Western blotting

Cell lysates and cell culture supernatants from TNF-α treated cells in the absence or presence of inhibitors were subjected to Western blotting (3.2.10).

4.2.8 Statistical analysis

The statistical significance of results presented in this chapter was performed as previously described (3.2.13). In addition, a two way ANOVA was used to determine statistical significance of results where two independent variables were involved. A p value less than 0.05 was considered significant.

4.3 Results

4.3.1 Degradation of inhibitor of apoptosis proteins (IAPs) using BV6, an IAP inhibitor

TNF-α, on its own cannot cause cell death in many mammalian cell lines unless the NF-kB pathway is blocked either by using an IKK or protein synthesis inhibitor such as cycloheximide (Locksley et al., 2001). Inhibition of IAPs is also a recognised sensitizer stimulus as this can also block NF-kB activation at the level of the death inducing signalling complex (DISC) (Feoktistova et al., 2011). BV-6, a bivalent SMAC

mimetic promotes auto-ubiquitination of cIAP-1 and -2 and X-linked IAP (XIAP) and subsequent degradation by the proteasome.

In order to block IAPs and ultimately determine the role of TNF-α in HaCaT cell death, doses of BV-6 that could completely deplete IAPs in HaCaT cells were tested. Treatment of HaCaTs with BV-6 for 30 min led to the complete degradation of cIAP-1 (Figure 4.2A) and cIAP-2 (Figure 4.2B) proteins even at 1 µM. The selected inhibitory dose of BV-6 for IAP deletion was 5 µM since this dose did not cause toxicity to HaCaT cells at 1 h as determined via MTT (Figure 4.2C).

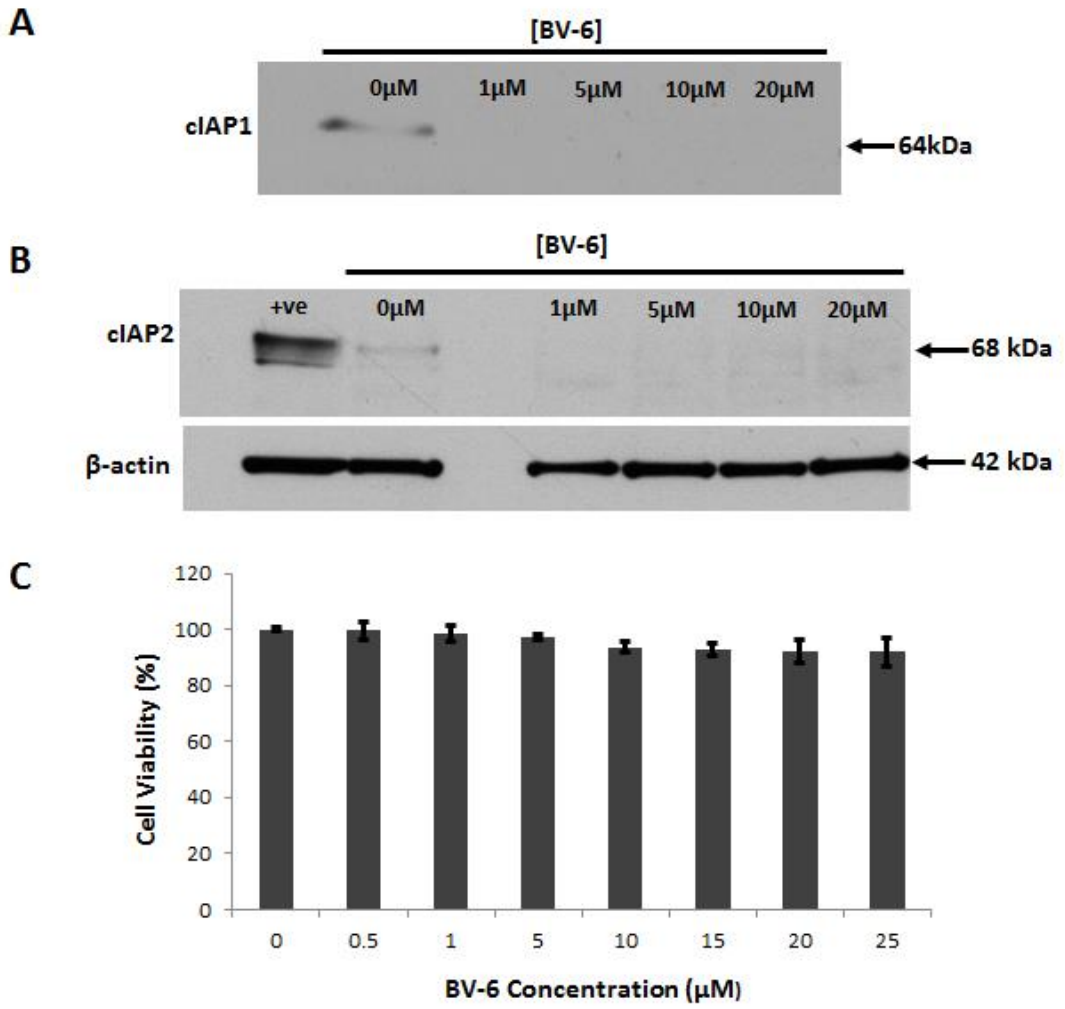

Figure 4.2 Determining the optimal dose of BV-6 on HaCaT cells A) inhibition of c-IAP1 **B**) inhibition of c-IAP2 **C**) assessing cell viability post treatment via MTT assay. Total lysates (10 µg) from BV-6 treated HaCaTs (30 min) were subjected to

immunoblotting. Positive control lysate was derived from a flag-tagged c-IAP2 plasmid transiently expressed in HEK293T cells. The MTT assay was used to determine the viability of HaCaT cells treated with BV-6 (1 h). Data was normalised to untreated control represented as mean ± SEM of three separate experiments with each carried out in triplicate.

4.3.2 Degradation of IAPs sensitizes HaCaTs to TNF-α induced killing.

To understand the role of cIAPs in TNF-α signalling in HaCaTs, cells were pre-stimulated with either BV6 or DMSO for 1 h, then incubated with different doses of TNF-α (0-10 ng/ml) for 8 h. Cell viability was then determined using the MTT assay. Results showed that loss of cIAPs in HaCaTs sensitized HaCaT cells to TNF-α mediated killing. In contrast, cIAP inhibition had no effect on staurosporine mediated HaCaT cell death. TNF-α at 1 ng/ml in combination with BV-6 caused about 40% of HaCaT cell death (Figure 4.3) and this dose was selected for routine experiments.

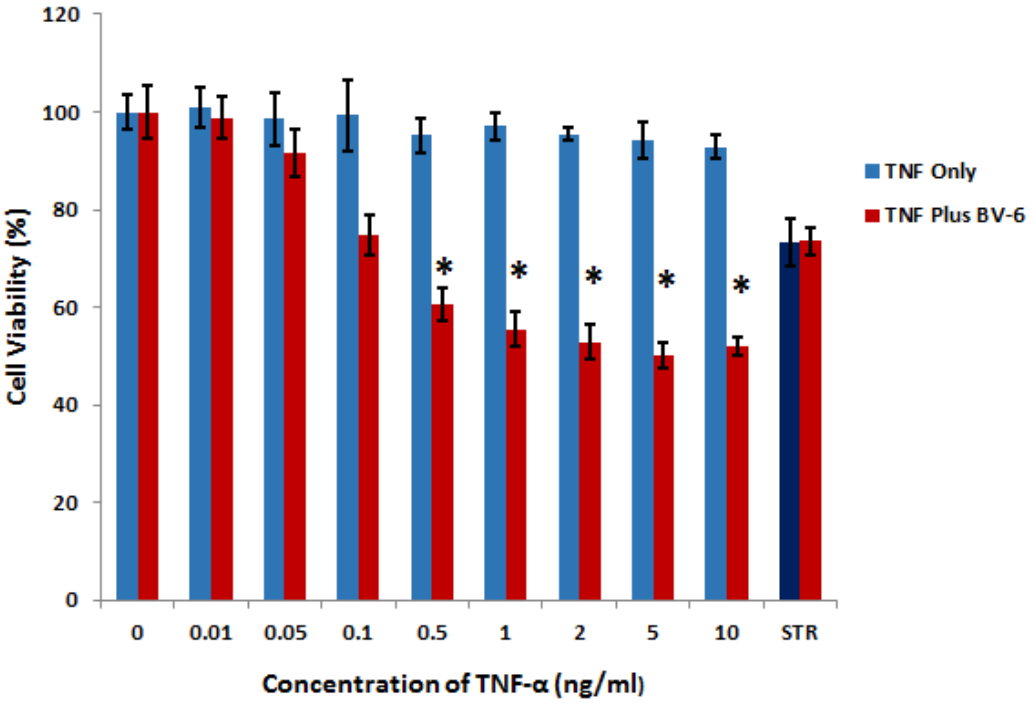

Figure 4.3: c-IAP inhibition sensitises HaCaT cells to TNF-α-induced cell death. HaCaT cells were pre-incubated with BV-6 (5 µM) for 1 h. This was followed by incubation with TNF-α (0-10 ng/ml) for 8 h or 1 µM staurosporine for 8 h. Cell death was measured using MTT. Results are mean ± SEM of three independent experiments carried out in triplicate. STR; staurosporine. Mann-Whitney U test was used to determine statistical significance of treated samples versus vehicle control (*P<0.05).

4.3.3 Assessment of TNF-α induced apoptosis using annexin V and Propidium Iodide staining

To understand the molecular events of death, and characterise both primary and secondary apoptosis induction by TNF-α in keratinocytes, HaCaT cells deficient in cIAPs were treated with TNF-α (1 ng/ml) in the presence or absence of Nec-1 or zVAD or both for 8 h. Annexin V and propidium iodide double staining was then performed and samples were analysed by flow cytometry. Annexin V binding indicates early apoptosis whereas Annexin V/propidium iodide double positivity indicates late apoptosis and necrosis. TNF-α induced a significant number of early

apoptotic keratinocytes indicated by annexin V positive (AV+, PI-) fluorescence channel but was marginally rescued through RIPK1 inhibition using Nec-1 (Figure 4.4). Interestingly, the addition of either zVAD or Nec-1/zVAD resulted in a significant protection from apoptosis. For late apoptosis (AV+, PI+), there was no difference in the different groups except for the group with zVAD pre-treatment in which a non-significant difference was seen.

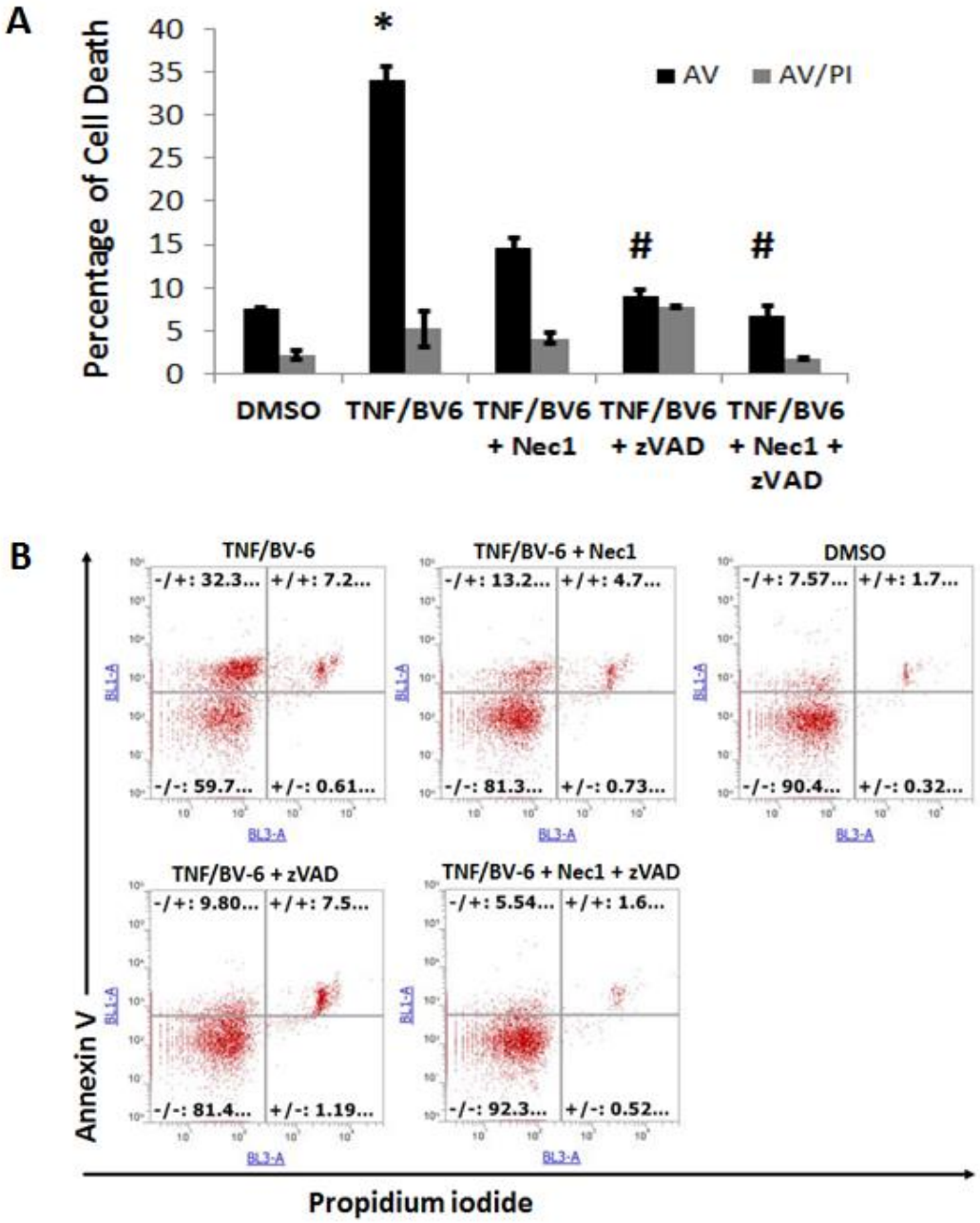

Figure 4.4: Flow cytometric detection of TNF-α induced apoptosis identified via annexin V and propidium iodide double stained HaCaT cells A) percentage analysis plot of apoptotic cells from gated controls B) Representative scattered plots showing quadrants. TNF-α (1 ng/ml) treated cells with or without Nec-1 or zVAD or Nec-1/zVAD pre-treatment were harvested and re-suspended in 1X annexin V binding buffer containing both annexin V-FITC conjugate at a final concentration of 2.5 µg/ml and propidium iodide at a final concentration of 0.25 µg/ml. The samples were then analysed via flow cytometry. Polygon gating was performed on 10, 000 cells. BL3 channel was used to capture PI positive cells whereas BL1 channel was used to capture AV positive cells. Data represent mean ± SEM of 2 independent experiments performed in duplicates. Statistical significance was determined using two-way ANOVA (*/$^{\#}$p<0.05). *denotes significance difference in death induction whereas # indicates the ability of inhibitors to offer significant protection to TNF-α treated cells. AV denotes annexin V while PI represents propidium iodide.

4.3.4 The role of RIPK1 and caspase inhibition in TNF-α mediated keratinocyte death

To characterise the pathway by which TNF-α mediates its cytotoxic action on keratinocytes, a small molecule inhibitor of RIPK1, necrostatin-1 (Nec-1) and zVAD were used. HaCaT cells were pre-stimulated with Nec-1, zVAD, or both in combination together with BV-6 for 1 h, then treated with TNF-α for 8 h. An MTT assay revealed marked protection from TNF-α-induced death by both Nec-1 and zVAD individually and complete protection when used together (Figure 4.5). This result indicated that TNF-α activates apoptosis and necroptosis and that they both account for keratinocyte death.

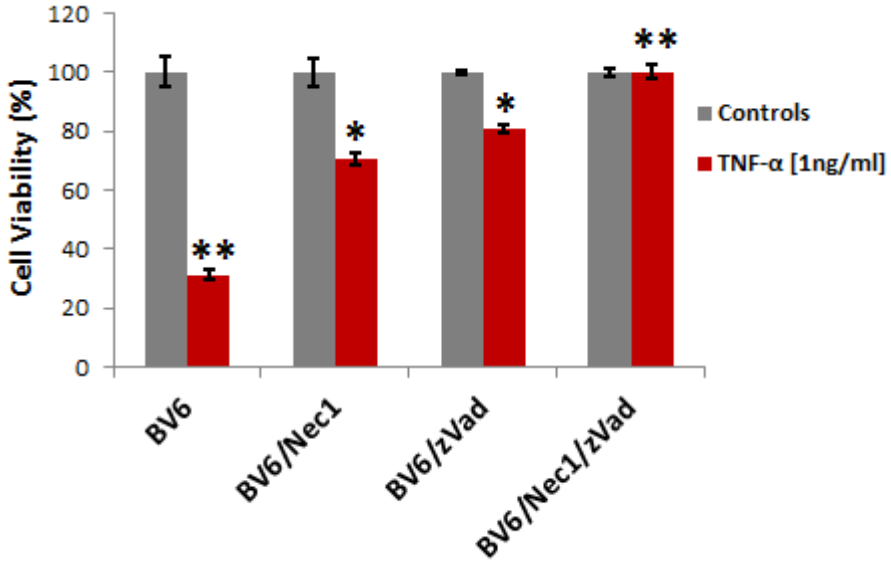

Figure 4.5: Effects of Nec-1 and zVAD on TNF-α mediated HaCaT death. All cell categories were pre-treated with BV-6 (5 µM) while select cell categories were pre-treated with 50 µM Nec-1 and 40 µM zVAD either separately or in combination for 1 h. Data represent mean ± SEM of 3 experiments conducted separately in triplicates and statistical analysis significance was determined by Mann-Whitney U test comparing different treatment conditions to untreated control (*P<0.05, **P<0.01).

4.3.5 PARP and Caspase-3 processing during TNF-α mediated keratinocyte death

To further characterise the mechanism of TNF-α induced keratinocyte death, we looked at PARP and Caspase-3 cleavage and, also levels of MLKL by Western blotting. In TNF-α and BV6 treated HaCaT cells, PARP was cleaved to the 89 kDa fragment which is usually generated by both Caspase-3 and/or -7.

Blocking RIPK1 with Nec-1 did not affect processing of PARP as expected (Figure 4.6A), however, zVAD completely inhibited its processing. Similar patterns were observed with the processing of caspase-3 into the p17 and p19 subunits. MLKL levels were minimally increased by TNF-α treatment and levels remained the same even with Nec-1 mediated RIPK1 inhibition (Figure 4.6A and Figure 4.6B). Treatment with zVAD and Nec-1 concomitantly appeared to drop MLKL levels almost to baseline (Figure 4.6B).

Performing Mann-Whitney U test revealed significant differences in both PARP and caspase 3 cleaved fragment sizes for BV-6 sensitized TNF-α treated HaCaT cells which remained largely unchanged when RIPK1 was inhibited using Nec-1 (Figure 4.6B).

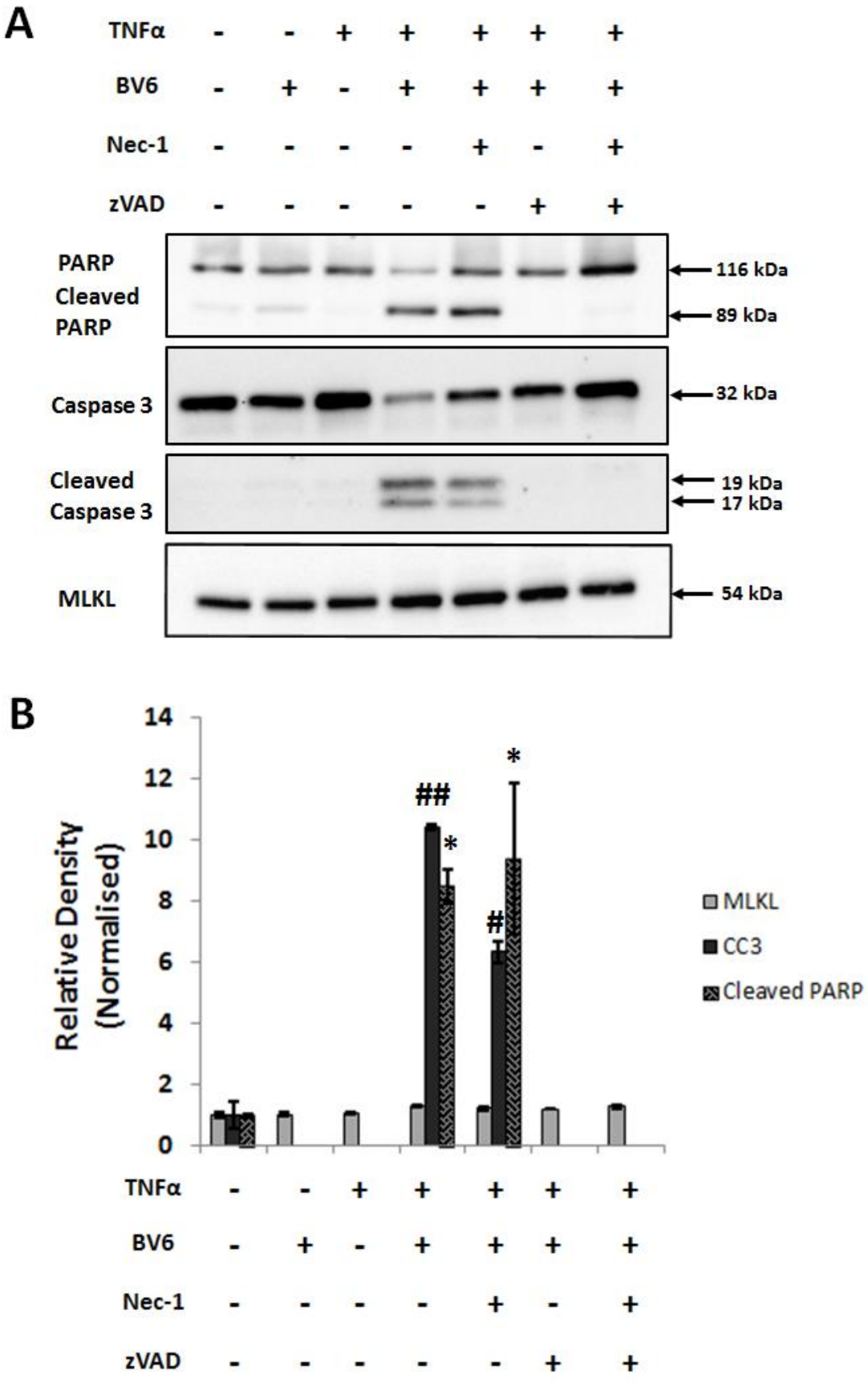
A
TNFα - - + + + + +
BV6 - + - + + + +
Nec-1 - - - - + - +
zVAD - - - - - + +
PARP
Cleaved
PARP
116 kDa
89 kDa
Caspase 3
32 kDa
Cleaved
Caspase 3
19 kDa
17 kDa
MLKL
54 kDa
B
Relative Density
(Normalised)
14
12
10
8
6
4
2
0
##
*
#
*
MLKL
CC3
Cleaved PARP
TNFα - - + + + + +
BV6 - + - + + + +
Nec-1 - - - - + - +
zVAD - - - - - + +

Figure 4.6 : Cleavage of PARP and Caspase 3 during TNF-α mediated cell death in HaCaT cells A) Western blotting detection of protein levels B) Densitometric analysis of protein levels normalised against untreated control. Total protein lysates (10 µg) from TNF-α treated HaCaT cells were subjected to immunoblotting. HaCaT cells were treated with 1 ng/ml TNF-α following pre-treatment with either Nec-1 (50 µM) and/or zVAD (50 µM). Antibodies against caspase 3 (both intact and cleaved forms), PARP and MLKL proteins were used to determine the expression of these proteins. Blots are representative of two independent experiments. ImageJ was used to quantify protein relative density and Mann-Whitney U test was used to determine statistical significance (*/#$p<0.05$, ##$p<0.01$). The abbreviation CC3 denotes cleaved caspase 3.

4.3.6 Extracellular HMGB1 release during TNF-a mediated HaCaT cell death

To understand the effects of TNF-α mediated HaCaT cell death on the extracellular release of HMGB1, a transcription factor whose release is indicative of cell death and once outside the cell can adopt a cytokine role (Bell et al., 2006a), supernatants from TNF-α treated HaCaT cells were harvested and screened for HMGB1 by Western blotting.

Levels of HMGB1 in supernatants from TNF-α and BV6 treated HaCaTs were significantly higher compared to untreated (DMSO) control (Figure 4.7). HMGB1 level remained high and was unaffected by zVAD. RIPK1 inhibition with Nec1 significantly decreased extracellular HMGB1 levels. The inhibition of both RIPK1 and caspases completely attenuated extracellular HMGB1 release.

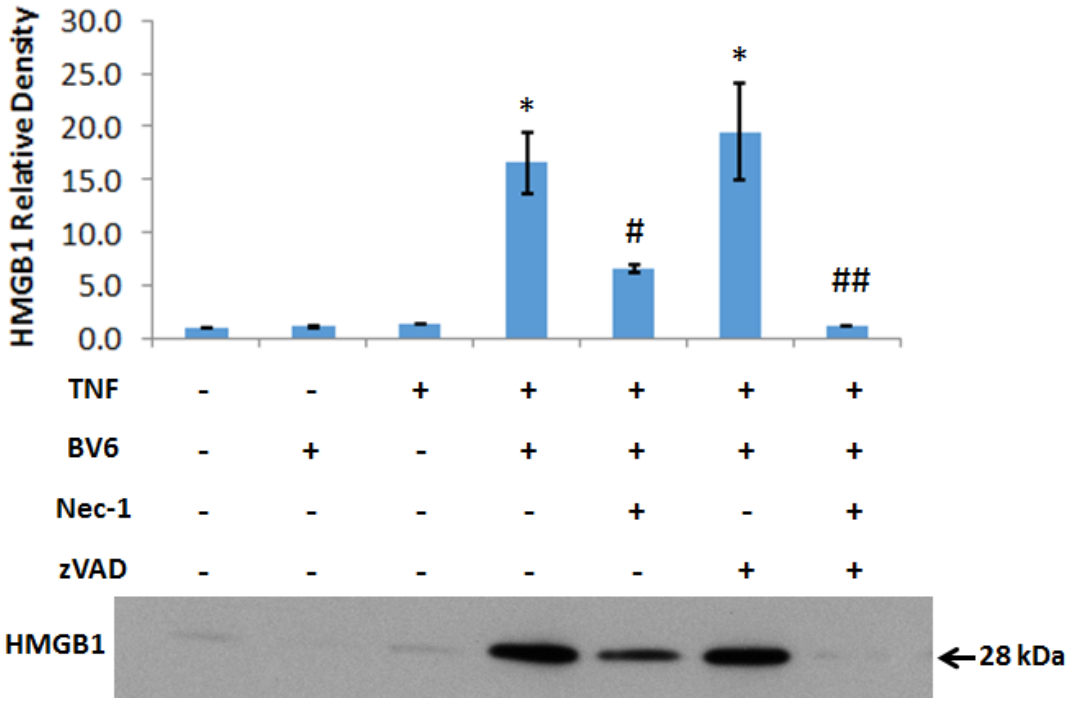

Figure 4.7: Profiling of HMGB1 in supernatants from TNF-α treated HaCaT cells. Supernatants (30 µl for each) from TNF-α treated HaCaTs in the presence of different combinations of inhibitors (zVAD 40µM, Nec-1 50 µM and BV-6 5 µM) were immunoblotted for HMGB1. Densitometric analysis was performed on three independent blots using ImageJ software whereas statistical analysis was performed using Mann-Whitney U test. */$^{\#}$p<0.05, $^{\#\#}$p<0.01 represent degrees of significance. *Statistical representation of the ability of treatments to induce HMGB1 release while #/## represents the ability of inhibitors to block HMGB1 exit from HaCaT cells.

4.4 Discussion

In this chapter, the role of TNF-α in SJS/TEN disease was investigated. Destruction of the epidermis comprising of mostly keratinocytes is a characteristic marker of this disease. To achieve this, we utilised an in-vitro keratinocyte cell line model and studied the mechanisms by which TNF-α induces HaCaT death.

The induction of cell death by TNF-α *in vitro,* although fairly well characterised, is complex and controversial. cIAP-1 and 2 play an important role in the regulation of TNF-α mediated cell killing *in vitro*. A number of studies have demonstrated that loss of cIAPs is required for the spontaneous formation of the ripoptosome, a death signalling complex that can sensitize cells towards death but is not capable by itself to execute death without an additional external death stimulus (Feoktistova et al., 2011) (Tenev et al., 2011) (Schilling et al., 2014).

Our data showed complete depletion of both cIAP-1 and -2 at 30 mins by BV-6 (IAP antagonist). BV-6 induces the rapid autoubiquitination of c-IAPs targeting them for degradation by the proteasome (Dueber et al., 2011) (Labbé et al., 2011). BV-6 binds to the surface groove on select baculovirus IAP repeat (BIR) domains of cIAP1 causing a conformational change that triggers dimerization and activation of the E3 ligase RING domain (Dueber et al., 2011) (Feltham et al., 2011). This promotes the activation of caspases that are usually inhibited by cIAPs leading to proteolytic cleavage of substrates (Feoktistova et al., 2011).

It was further demonstrated that cIAP inhibition in HaCaTs promotes dose dependent TNF-α mediated HaCaT killing. Our result is consistent with data from other studies where this same effect has been replicated in several other cell lines

(Welsh et al., 2016) (El-Mesery et al., 2016). Additionally, we showed that cell death mediated by TNF-α in cIAP-depleted HaCaTs was attenuated by both Nec-1 and zVAD. This indicates that both RIPK1-dependent necroptosis and caspase-dependent apoptosis may play a role in TNF-α HaCaT cell death induction. Our finding is in agreement with a previous report which demonstrated that TNF-α mediated HaCaT keratinocyte death occurs via both necroptosis and apoptosis (Feoktistova et al., 2011). In contrast, there are cases whereby a single death pathway (either necroptosis or apoptosis) which can switch between the other may be activated in some cell lines (Vanlangenakker et al., 2011) (El-Mesery et al., 2016).

Cell surface PS exposure is a classical feature of apoptosis that serve as an "eat me signal" to permit the recognition and phagocytosis of apoptotic bodies (Wlodkowic et al., 2009). We utilised flow cytometric analysis to detect annexin V and propidium binding to phosphatidylserine and DNA respectively. PS externalisation is an early event that occur during apoptosis triggered by a variety of stimuli which has been used as an early indicator of apoptosis compared to DNA based assays (Hotz et al., 1994) (Wlodkowic et al., 2009) (Zhang et al., 1997). In agreement with the literature, our data indicated that TNF-α induces early apoptosis in keratinocytes and it can be blocked through either caspase inhibition or through concomitant inhibition of caspase and RIPK1. This data perhaps suggests that RIPK1 might play a role in apoptosis or have necroptosis-independent functions. This is partially supported by studies that have reported that RIPK1 depletion suppresses apoptosis. In these studies, it was demonstrated that mice deficient in RIPK1 shows aberrant caspase-8 dependent apoptosis (Kaiser et al., 2014) (Dillon et al., 2014).

Interestingly, the concomitant use of Nec-1 and zVAD completely protected HaCaTs from TNF-α induced death further suggesting that RIPK1 dependent necroptosis and caspase dependent apoptosis culminate in the complete killing of HaCaT cells. This implies that extensive epidermal keratinocyte death as well as destruction of the epidermis seen in SJS/TEN may be occurring via both RIPK1 and caspase dependent death which may be driven to a large extent by TNF-α. In agreement with this, other studies have also earlier implicated that both apoptosis and necroptosis were effector pathways that drive TNF-α induced keratinocyte death in SJS/TEN (Saito et al., 2014) (Panayotova-Dimitrova et al., 2015) (Paquet et al., 1994) (Paquet et al., 2000).

Further probing into the mechanism of HaCaT cell death upon TNF-α induction, we observed both caspase 3 and PARP processing in TNF-α treated HaCaTs suggesting apoptosis. PARP is a nuclear protein which is activated by DNA strand breaks and its cleavage is primarily mediated by caspases -3 and -7 during apoptosis (Lazebnik et al., 1994) (Woo et al., 1998) (Boulares et al., 1999). These Caspases cleave PARP at a DEVD/G tetra-peptide motif (Martins et al., 1997). TNF-α induces the up-regulation and activation of iNOS in the skin of TEN patients (Viard-Leveugle et al., 2013). Clinical studies have found high levels of TNF-α in skin biopsies, sera and blister fluids from SJS/TEN patients (Posadas et al., 2002) (Paquet et al., 2000) (Wang et al., 2018c) (NOMURA et al., 2011). These clinical findings in conjunction with our *in vitro* data together highlight a vital role for TNF-α in SJS/TEN pathogenesis and as a consequence keratinocyte death.

A number of studies have shown that when cells undergo either apoptosis or necrosis, they release HMGB1 which appears to play a bi-functional role, firstly it acts as a transcription factor but during cell death when released from the cell it has the capacity to activate inflammatory cascades (Bianchi and Manfredi, 2007) (Sims et al., 2010) (Nakajima et al., 2011). SJS/TEN pathogenesis has an inflammatory component thought to be initiated by cytotoxic T lymphocytes (Harr and French, 2010) and we have shown elevated levels of HMGB1 in serum and blister fluid samples in comparison to controls in chapter 2.

Remarkably, data from TNF-α pathway characterisation and HMGB1 modulation indicated differential modulation of HMGB1 by specific cell death forms. In a novel finding, we demonstrated that TNF-α driven extracellular HMGB1 levels was significantly higher in necroptosis compared to apoptosis in keratinocytes. This suggests that necroptosis may be the major regulator and driver of HMGB1 exocytosis from dying keratinocytes. Possible explanations why necroptosis tends to favour HMGB1 release is perhaps because HMGB1 binding to chromatin is weak and so can easily exit the nucleus due to its high mobility (Jiang and Pisetsky, 2006). Also, necroptosis involves rapid permeabilization of plasma membrane consequently leading to the emptying of cellular contents including but not exclusive to DAMPs (Kaczmarek et al., 2013) (Christofferson et al., 2012) (Vercammen et al., 1997). By contrast, apoptosis involves the orderly and tighter packing of organelles and nuclear chromatin condensation which do not allow for the escaping of cellular contents and DAMPs (Jiang et al., 2007) (Tang et al., 2010). (Maeda and Fadeel, 2014).

Overall, this chapter has demonstrated that TNF-α can trigger both keratinocyte apoptosis and necroptosis and that necroptosis has a more significant contribution to extracellular HMGB1 levels than apoptosis and that necroptosis perhaps could be the major source of HMGB1 seen in SJS/TEN.

CHAPTER 5

MOLECULAR AND FUNCTIONAL CHARACTERISATION OF CORE DEATH EFFECTORS IN HUMAN KERATINOCYTE *IN VITRO* MODEL

Contents

5.1 Introduction

Necroptosis has been implicated in the pathogenesis of several pathologies including SJS/TEN. Saito et al, discovered that the binding of annexin A1 to its receptor formyl peptide receptor 1 (FPR1) which is abundantly expressed by SJS/TEN keratinocytes triggers RIPK1/RIPK3 dependent necroptosis (Saito et al., 2014). Two independent studies have reported that RIPK3 was highly up-regulated in TEN lesional skin samples (Kim et al., 2015b) (Panayotova-Dimitrova et al., 2015). Kim *et al* suggested that the high levels of RIPK3 expression coupled with the increased MLKL phosphorylation in TEN epidermis indicated RIPK3-mediated keratinocyte necroptosis (Kim et al., 2015b). Clinical findings have also strongly suggested that RIPK3 may play an important role in SJS/TEN pathogenesis.

Necroptosis is regulated by RIPK1, RIPK3, c-FLIP and procaspase-8 with MLKL being the key effector protein. Both RIPK1 and RIPK3 are serine/threonine kinases and they play a vital role both in the innate and adaptive immunity signalling pathways (Yang et al., 2015). RIPK3 is comprised of an N-terminal kinase-like domain (KD) and an RIP homotypic interaction motif (RHIM) domain but its C-terminus lacks a death domain (DD) (Sun et al., 1999) (Vandenabeele et al., 2010a). RIPK1 can be induced by auto-phosphorylating itself in the necrosome thus activating RIPK3, which is then able to phosphorylate and activate MLKL (Sun et al., 1999). Activated MLKL punctures the plasma membrane leading to cell death (Tanzer et al., 2016).

The intrinsic apoptosis pathway is controlled and regulated by the mitochondria and can be triggered by a wide range of non-receptor mediated stimuli (Elmore,

2007). Bcl-2 family of proteins participates in the regulation of this pathway (Adams and Cory, 2007). Two members Bak and Bax determine the commitment of cells to apoptosis (Brunelle and Letai, 2009) whilst Bcl-2, Bcl-XL, Mcl-1 and others act to regulate this. Bak promotes apoptosis by inducing mitochondrial membrane permeabilization leading to cytochrome c release and ultimately apoptosome formation leading to activation of caspases-9 and -3 (Adams and Cory, 2007).

HMGB1 is a well-known cell death marker that regulates different cell death modes. Necroptosis, necrosis and apoptosis are pivotal in HMGB1 extracellular release (Bell et al., 2006b) (Kaczmarek et al., 2013). Extracellular HMGB1 plays important roles in the pathogenesis of human diseases and potentially in SJS/TEN (Nakajima et al., 2011).

Triggering necroptosis in cell lines has proved to be problematic as many stimuli result in a mixture of apoptosis and necroptosis. There is therefore a need to develop good *in vitro* models in order to study the role of RIPK3 in keratinocyte necroptosis as well as the contribution of necroptosis to HMGB1 levels in the extracellular milieu.

The aims of this chapter are to establish necroptotic models in HaCaT cell lines by stably overexpressing Tet-inducible RIPK3, MLKL and Bak. Secondly, the cell death phenotype will be studied based on the different effector proteins namely RIPK3, Bak and MLKL in HaCaT cells. Finally, HMGB1 levels in supernatants will be measured following induction of apoptosis and necroptosis by cell death effectors.

5.2 Materials and methods

5.2.1 Material

The chemical (2*E*)-*N*-[4-[[(3-Methoxy-2-pyrazinyl) amino]sulfonyl]phenyl]-3-(5-nitro-2-thienyl)-2-propenamide (necrosulfonamide, S8251) was obtained from Selleckchem, Munich, Germany and N-5-Benzothiazolyl-6-[(1-methylethyl)sulfonyl]-4-quinolinamine (GSK'872, #6492/10) was purchased from R&D SYSTEMS, Abingdon, UK. Midori Green Advance DNA stain, 10X BlueJuice Gel Loading Buffer, 1 Kb Plus DNA Ladder, 100 bp DNA ladder and 10 Kb plus DNA ladder and carbenicillin disodium were purchased from Thermo Fisher Scientific, UK. The Wizard® SV Gel and PCR Clean-Up System was purchased from Promega UK. NEBuffer 2.1, T4 DNA Ligase, Phusion High-Fidelity DNA Polymerase, Deoxynucleotide (dNTP) Solution Mix and OneTaq DNA polymerase were obtained from New England BioLabs (NEB), Ipswich, UK. Doxycycline was a kind gift from Dr Nicholas Harper. Other reagents used in this chapter including antibodies have already been presented in chapter 3 and 4 materials and methods.

5.2.2 Plasmids

pCMV hpyPBx100 containing the hyperactive Sleeping Beauty Transposase and pSB-Tet Blast which contains a tetracycline inducible expression cassette flanked by Sleeping Beauty transposon IR/DRs containing ampicillin resistance and blasticidin selection markers and pcDNA3 Strep-tagged Bak were a kind gift from Dr Nicholas Harper of the University of Liverpool, UK. pFRT flag-tagged human MLKL plasmid was obtained from associate Prof James Murphy (WEHI, Melbourne Aus). pCW57.1

containing MLKL insert was obtained from Dr Nicholas Harper whereas hRIP3 GFP wt plasmid (#41387) submitted by Francis Chan was purchased from Addgene, UK. All plasmids used in cloning contained a SfiI recognition sequence.

5.2.3 Cloning and sub-cloning of DNAs

Coding sequences for full length human RIPK3 (NM_006871.3), MLKL (NM_152649.3) and Bak (NM_001188.3) were identified from the NCBI database (https://www.ncbi.nlm.nih.gov/nucleotide). Flanking primers (Integrated DNA Technologies, Belgium) were then designed through the NCBI database (https://www.ncbi.nlm.nih.gov/) for all the human cDNA containing SfiI restriction sites (GGCCNNNN/NGGCC) (Table 5.1). Primers were designed to have a melting temperature (T_m) between 64-70°C and extra nucleotides were added before the SfiI recognition sequence to keep the ORF in frame and a 5'-overhang to facilitate restriction enzyme binding. ThermoFisher Scientific Tm calculator tool was used to determine both T_m and annealing temperature (Ta). All primers were diluted to a working concentration of 10 µM. The selected DNA regions of interest were amplified with Phusion High Fidelity DNA polymerase using polymerase chain reaction. Using both forward and reverse primers containing SfiI restrictions, amplified insert DNAs were generated with flanking SfiI restriction sites on both sides. This technique allows for the use of a single restriction enzyme in restriction digest cloning.

Table 5.1: PCR primers used to amplify cDNAs

Bak	Forward	5’ AAAGGCCTCTGAGGCCACCATGGCTTGGAGCCAC-3’
	Reverse	5’ GCTTGGCCTGACAGGCCTCATGATTTGAAGAATCTTCGTACCAC 3’
RIPK3	Forward	5’ AAAGGCCTCTGAGGCCACCATGTCGTGCGTCAAGTTATG 3’
	Reverse	5’ AAGCTTGGCCTGACAGGCCTCATGCTTTTTCGAACTGGGGGTGGC 3’
MLKL	Forward	5’ AAGGCCTCTGAGGCCACCATGGAAAATTTGAAGCATATTATCACC 3’
	Reverse	5’ AAGCTTGGCCTGACAGGCCTCATGCCTTTTCGAACTGCGGGTGGC 3’

5.2.4 Polymerase chain reaction (PCR) cloning

Strep tag II (Trp-Ser-His-Pro-Gln-Phe-Glu-Lys) coding sequence was introduced at the carboxyl-terminus of RIPK3 DNA by PCR cloning whereas Bak and full length MLKL DNAs had strep tag II coding sequence fused at the amino-terminal ends. For all genes, a two amino acid spacer was allowed between the target sequence and the tag to allow for accessibility of tag. A stop codon was introduced downstream of the insert or immediately following a strep tag coding sequence. The strep-tag coding sequence was introduced to enable detection of translated protein product using strep-Tactin antibody.

5.2.5 Polymerase Chain Reaction (PCR)

Thermocycling parameters were selected based on the estimated product size and estimated G:C ratio of primer used. OneTaq DNA polymerase and Phusion High Fidelity DNA polymerase (NEB) were frequently chosen for PCR throughout this

thesis. To amplify insert for downstream applications, Phusion High Fidelity polymerase was used whereas for a regular PCR amplification, OneTaq DNA polymerase was used. This was because Phusion High Fidelity polymerase is very efficient in DNA proof reading and less prone to errors. A typical PCR mix is represented on the table below (Table 5.2).

Table 5.2: Representation of a typical PCR mix with both DNA polymerases

Polymerase	**OneTaq**	**Phusion**
NE Buffer	5 µl (2x)	10 µl (5x)
Nuclease free H_2O	2.5 µl	31 µl
dNTPs (10 µM)	N/A	1 µl
Forward and Reverse primer mix (10 µM)	0.5 µl	5 µl
Template DNA (200 ng)	2 µl	2 µl
Polymerase	N/A	1 µl
Final reaction volume	10 µl	50 µl

Reactions were initially denatured at 95 °C for 2 min then cycled at 95 °C for 30 min, 65 °C for 30 min and 72 °C for 1 min for 35 cycles in an Applied Systems SimpliAMP Thermal Cycler (Applied Biosystems, Thermo Fisher).

5.2.6 Restriction digestion of plasmid DNA and vector DNA

The destination plasmid vector (code named pSBTET) had a cassette which has been modified to contain duplexes with SfiI recognition site within the multiple cloning sites upstream of the promoter. SfiI endonuclease is a tetramer that ideally must bind two copies of its recognition site for DNA cleavage to occur but can also cleave

with one recognition site by forming a synaptic complex containing two of such duplexes bound to it (Williams and Halford, 2001) (Wentzell et al., 1995). 1 µg of either PCR amplified DNA fragment (denoted the "insert") or 5 µg of pSBTET vector DNA was digested using SfiI in CutSmart buffer (New England BioLabs, UK) (Table 5.3). Control samples were set up without a restriction enzyme in order to observe a no cleavage product. All samples were incubated at 50°C for 4 hours before performing gel extraction or PCR purification using the Wizard SV gel and PCR clean-up system (Promega). Agarose gel electrophoresis was carried out to determine whether the expected product size has been obtained.

Table 5.3: Representation of a typical restriction digest reaction

Components	**Amount**
Plasmid vector	5 µg
Insert DNA	1 µg
CutSmart (10x)	8 µl
Sfil Restriction Enzyme	2 µl
Nuclease free H_2O	to 80 µl

5.2.7 DNA electrophoresis: Agarose and PAGE

UltraPure Agarose (Invitrogen, ThermoFisher Scientific) was weighed and melted in 1x TAE buffer (40 mM Tris/20 mM Acetic acid/1 mM EDTA). Agarose powder (1-2 g) corresponding to agarose gel (1-2%) was weighed and dissolved in 1x TAE buffer depending on the PCR product sizes. Typically, 1% agarose gel for a 400-500 bp insert and 6.5-7.0 kb vector. The mixture was heated to obtain a completely clear

molten agarose solution, cooled slightly and ethidium bromide (EtBr) added before pouring. EtBr is a DNA intercalating dye which fluoresces on exposure to ultraviolet light (Waring, 1965) and thus enables DNA visualisation. The DNA samples were separated alongside a DNA molecular weight marker (1 Kb) at 135 V for approximately 45 mins or until sufficient separation was observed. Separation of DNA fragments was visualised through exposure to UV light.

5.2.8 Purification of PCR and restriction digest products using the Wizard SV gel and PCR clean-up system

The Wizard® SV Gel and PCR Clean-Up System is a membrane based system that was used to extract DNA fragments of 100bp to 10kb from agarose gels in Tris acetate (TAE) and also to purify PCR products directly from an amplification reaction. Following DNA electrophoresis**,** the DNA band was excised from the gel using a scalpel into 1.5 ml Eppendorf tubes. Membrane binding solution was added to gel slice, mixed and incubated at 55°C until dissolution was fully accomplished. The dissolved gel or PCR product was transferred to the spin-column and incubated at RT for 1 min. Following centrifugation at 16, 000 g for 1 min the flow-through was discarded and column reinserted into collection tube. This was washed twice with membrane wash solution and the centrifugation step was repeated but with a slight variation in centrifugation time; 1 min for the first and 5 min for the second. The column assembly was re-centrifuged and residual ethanol evaporated. Finally, DNA was eluted with nuclease free water incubated at RT for 1 min before centrifugation. Eluted DNA was stored at -20°C until needed.

5.2.9 Ligation of digested DNA fragments

Sfil-digested vector plasmids and Sfil-digested inserts were subjected to a ligation reaction. Ligation reactions were performed as highlighted in the table below (Table 5.4). The reactions were incubated at 4°C overnight in a 1.5 ml Eppendorf and then set aside for transformation.

Table 5.4: A typical ligation reaction

Component	**Vector + Ligase**	**V:I (1:2)**	**V:I (1:4)**
Vector	25 ng	25 ng	25 ng
Insert	n/a	100 ng	200 ng
T4 DNA ligase	0.5 µl	0.5 µl	0.5 µl
10x ligase buffer	1 µl	1 µl	1 µl
H_2O	Up to 10 µl	Up to 10 µl	Up to 10 µl

5.2.10 Transformation of chemically competent *E.coli*

NEB Stable competent E.coli and DH5 alpha competent E. coli were used to carry out all transformations. NEB Stable is a RecA- line and is required when using plasmids containing repeated sequences (such as the Sleeping Beauty transposon plasmids). 2-20 ng of plasmid DNA was added to 50 µl aliquot of competent *E.coli* and incubated on ice for 20 min. E.coli was then heat-shocked at 42°C for 1 min and allowed to recover on ice for 5 min. 350 µl of SOC medium (SOB including 1% glucose) was then added and the cells were grown at 37°C with shaking for 1 hour. 50-150 µl of transformed cells was then plated onto a Luria Broth Agar plate containing ampicillin (1 µg/ml final concentration) for positive colony selection.

Plates were incubated overnight at 37°C to allow clones to grow out. Positive clones were amplified by colony PCR before being amplified in sterile LB Broth solution already containing 1 μg/ml ampicillin.

5.2.11 Colony PCR

Colony PCR was used to determine if the desired insert had been successfully cloned into the required plasmid. Bacterial colonies were picked and PCR screening was performed on lysed bacterial supernatants which provided template DNA using OneTaq DNA polymerase and vector and insert-specific primers. Four positive clones were identified per plasmid construct and these were used to inoculate overnight bacterial cultures.

5.2.12 Isolation of plasmid DNA from overnight bacterial cultures

Miniprep and Maxiprep plasmid DNA isolation protocols were used to isolate plasmid DNA from bacterial cultures depending on the amount of DNA desired. Low amount of DNA was extracted with Miniprep whereas high amount of DNA was extracted using Maxiprep.

Plasmid DNA isolation by Miniprep

DNA Mini-preps were performed using the Qiaprep Spin Mini-Prep kit (Qiagen, UK) following the manufacturer's instructions but with slight modifications. Mini-prep was performed when a small amount of plasmid DNA was required. Briefly, about 4 ml of an overnight bacterial culture was centrifuged at 4600 rpm for 10 min. Pelleted bacterial cells were re-suspended in 250 μl Buffer P1. Cells were then lysed

in 250 µl of Buffer P2 for 5 min. Proteins and plasmid DNA were precipitated with Buffer N3 and the tube was centrifuged. 800 µl of supernatant was added to the spin columns. The spin columns were centrifuged and the flow-through discarded, this step was repeated for the remaining supernatant. Columns were then washed in sequence with Buffers PB and PE. The columns were transferred to collection tubes re-centrifuged to get rid of residual wash buffer. With columns placed in Eppendorf tubes, elution of plasmid DNA was achieved using ultrapure (Milli Q) water.

Plasmid DNA isolation by Maxiprep

MAXI-Preps were performed using the PureLink HiPure Plasmid Purification Maxiprep Kit (Invitrogen, ThermoFisher Scientific, UK). These were carried out when large amount of plasmid DNA was required. Plasmid maxi-prep was performed in accordance with the manufacturer's protocol. Firstly, 1 ml of bacterial cells from a bacterial starter culture was used to inoculate a 200 ml LB culture (containing carbenicillin) and this was shaken overnight at 37°C. The culture was centrifuged at 4000 g for 5 min to pellet cells. Cell pellets were re-suspended in Resuspension Buffer R3 (supplemented with RNaseA) and then lysed with Lysis Buffer L7 while incubating at room temperature for 5 min. Proteins and plasmid DNA were precipitated with Precipitation Buffer N3. Lysate was carefully separated by centrifugation at 13 000 g for 10 min at room temperature and the resulting supernatant was obtained. The supernatant was applied to the provided Maxiprep columns which has already been pre-equilibrated and allowed to drain by gravity flow. The columns were washed with Wash Buffer W8 and the flow-through was

discarded. The DNA was eluted into a sterile collection tube using Elution Buffer E4. Precipitation of eluted DNA was done by the addition of isopropanol and this was stored at -20°C overnight to achieve sufficient precipitation. Precipitated DNA was pelleted by centrifugation at 13000 g for 30 min at 4°C and the (isopropanol) removed and discarded. DNA pellet was washed in 70% ethanol before being re-centrifuged to remove the ethanol. In the end, pellet was air dried and re-suspended in ultrapure water. Pure plasmid DNA was stored at -20°C until needed for further analysis.

5.2.13 Quantification of DNA

DNA was quantified using NanoDrop 8000 spectrophotometer (Thermo Scientific). Values from DNA peak curve with an A260/280 value with range 1.8-2.0 were judged as good. DNA concentration was recorded in ng/µl.

5.2.14 Transient transfection of plasmids into HEK293T cells

Plasmids isolated from positive clones that showed the presence of the insert following colony PCR and sequencing were transiently transfected into HEK293T cells. Transfections with the Sleeping Beauty transposon tetracycline inducible vector (pSBTET) construct were co-transfected with the Sleeping Beauty transposase SB100 expression vector. Delivery of gene into the genome is through transposase. HEK293T cells were seeded at a density of 2.5x 10^5 cells per well in a 6-well plate overnight. Cells were seeded in 2 ml serum containing media without antibiotics. For all transient transfections, 1µg of plasmid DNA was transiently expressed in HEK293T cells for 24 hours using jetPEI DNA transfection Reagent (101-

10, Polyplus, France). For pSBTET constructs, 100 ng of SB100 transposase was added to the reaction tube for every 1 µg of plasmid DNA. Briefly, $3.0x10^5$ HEK293T cells seeded into a 6-well plate were allowed to adhere overnight. Following Polyplus transfection protocol, 100 µl of 150 mM NaCl buffer was thoroughly mixed with 4 µl of JetPEI. Plasmid DNA (1 µg) was diluted in 100 µl of 150 mM NaCl buffer. Buffer diluted JetPEI was then added dropwise to diluted DNA, vortexed and allowed to incubate at room temperature for 20 min. DNA/JetPEI complexes (200 µl) was then added dropwise to cells immediately followed by doxycycline addition to select wells and plates were allowed to incubate at 37°C, 5% CO_2 for 24 h. Doxycycline (dox) (to 5 µg/ml final concentration) was used to activate transcription of transgenes under a tet-inducible promoter. Cells were then scraped into Eppendorfs and centrifuged at 2000 rpm to obtain pellets. Pellets were washed twice in PBS and then lysed in SDS sample buffer. Finally, Western blotting was performed on lysates to determine protein expression.

5.2.15 Sequencing of pSBTET plasmid constructs

Sequencing of pSBTET plasmid constructs was performed to ensure correct insert sequence. Plasmids that have been checked for protein expression were sequenced by Sanger Sequencing (Source Bioscience, Rochdale UK). Sequencing was performed using vector specific primer; pCEP forward primer (5' AGAGCTCGTTTAGTGAACCG 3') and EBV reverse primer (5' GTGGTTTGTCCAAACTCATC 3'). Primers were diluted to 3.2 µM and plasmid DNAs were diluted to 100 ng/µl before being sent off for sequencing. Sequence reads were compared to the following NCBI accession

numbers NM_006871.3 (RIPK3), NM_152649.3 (MLKL) and NM_001188.3 (Bak) using Chromas trace viewer 2.6 (Technelysium Pty Ltd, South Brisbane, Australia).

5.2.16 Transfection of pSBTET plasmids into HaCaT cells

HaCaT cells were seeded at a density of 2.5x 10e5 cells in 2 ml serum containing DMEM in 6-well plates and allowed to adhere overnight. Fresh media was used to replace the spent media prior to transfection. 3 μg of plasmid DNA was co-transfected with 300 ng of the SB100 transposase. Transfection was carried out as described above with jetPEI. However, no dox was added to wells, and plates were incubated for 24 h at 37^{o}C/5% CO_2. After 24 h, transfected cells were passaged and re-seeded into 6-well plates for antibiotic selection.

5.2.17 Isolation of Blasticidin positive HaCaT cells

To isolate blasticidin positive HaCaT clones, transfected HaCaT cells were initially treated with 1.5 μg/ml blasticidin (InvivoGen, France) for 2 days to allow for blasticidin resistance gene expression. There were dose adjustments with blasticidin subsequently. HaCaT cells were further exposed to 5 μg/ml blasticidin (final concentration) for a period of 6 days with fresh drug applied every 2 days. Later, blasticidin concentration was raised to 10 μg/ml for a period of 2 days and finally to 15 μg/ml for a total of 6 days with fresh drug applied every 2 days. The antibiotic resistant population of HaCaT cells were considered polyclonal stable HaCaT cells for the different transgenes namely RIPK3, Bak and MLKL generated in this chapter.

5.2.18 Experimental design with stably transfected HaCaT cells

Different time points were selected in order to determine the optimal time for gene expression for all stable HaCaT cell lines including RIPK3, Bak and FL MLKL. The specific time point at which protein expression was optimally observed for the transgenes was noted and used for cell death optimisations and other assays.

5.2.19 MTT cell viability assay

The MTT assay was performed with stably transfected HaCaT cells in the absence of presence of gene induction. The MTT assay was conducted as previously described (3.2.6).

5.2.20 Western blotting analysis

RIPK3, Bak and FL MLKL transgenic HaCaT cells were optimised for dose and time at which protein expression was recorded. Western blotting was performed as previously described. A comprehensive list of antibodies used and their dilution has already been summarised in chapter 3 (3.2.10). Streg-tag 11 antibody was reconstituted with PBS to a stock of 1 mg/ml.

5.2.21 Immunofluorescence staining of cells

Immunofluorescence was performed on both stably transfected and wild-type HaCaT cells after dosing with either dox or DMSO for 12 h following already described protocol (3.2.11).

5.2.22 Statistical analysis

Statistical analysis was determined as previously described (3.2.13).

5.3 Results

5.3.1 Screening of transformed ligation products by colony PCR

In order to determine correct ligation of insert using vector insert-specific primers, four bacterial clones were picked and subjected to colony PCR. PCR products were then ran on an agarose gel to analyse for the right product size. For RIPK3, only clones A, C and H showed bands at the expected product size (~ 450 bp) indicating positive products (Figure 5.1). However, for clone B, no band was seen indicating a negative result. On the other hand, for Bak, only #2 and #4 showed bands at the predicted product size (~400 bp). Similarly, clones #1 and #3 for Bak did not show any band which indicated a negative result.

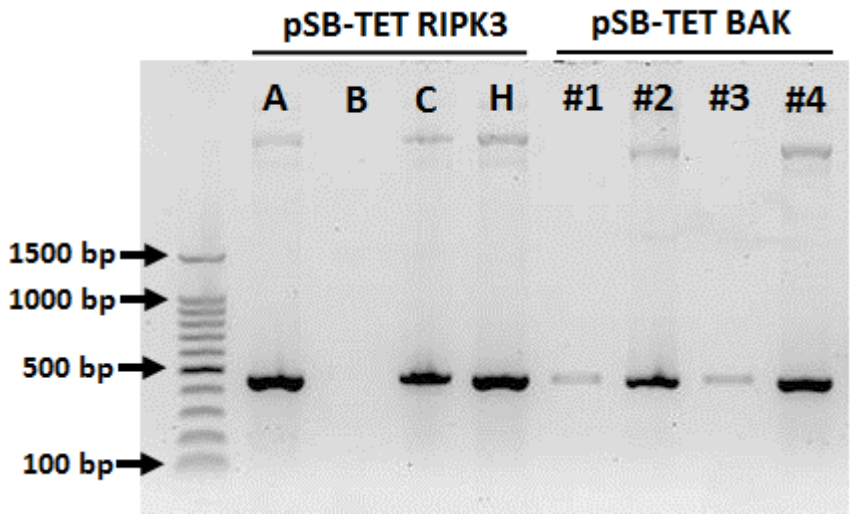

Figure 5.1: **Colony PCR screening for positive bacterial clones for RIPK3 and Bak gene constructs.** Selected bacterial colonies were picked and lysed in TE buffer. The supernatants (1 µl per reaction) were added to PCR tube already containing adequate PCR components. These were thermal cycled using standard cycling conditions. PCR products were analysed for predicted size on 1% agarose gel alongside a 100 bp DNA ladder. Clones A, C and H were positive for RIPK3 whereas clones #2 and #4 were positive for Bak.

5.3.2 Verifying the insert Sequences of RIPK3, MLKL and Bak with Sanger sequencing

The insert sequences of RIPK3, MLKL and Bak constructs were determined for the correct sequence through Sanger sequencing. Data (not shown) indicate that all sequences matched identically with the NCBI reference accession sequences as described (5.2.15).

5.3.3 Assessment of RIPK3 and BAK protein overexpression in HEK293T cells transiently transfected with RIPK3-pSBTET and Bak-pSBTET plasmids

Protein expression for strep-tagged RIPK3 and strep-tagged Bak was determined by Western blotting. Detection of over-expressed proteins was seen at approximately 60kDa for RIPK3 and about 23 kDa for Bak (Figure 5.2). As can be seen, clones C and H were optimal for protein expression for RIPK3 whereas clones #2 and #4 were optimal for protein expression for BAK. Positive control lysates (X for RIPK3 and X+ for Bak) were used to determine protein detection at the predicted molecular weight. RIPK3-pSBTET plasmid labelled H and Bak-pSBTET plasmid labelled #4 would be used in subsequent transfections to make stable transgenic HaCaT cell lines.

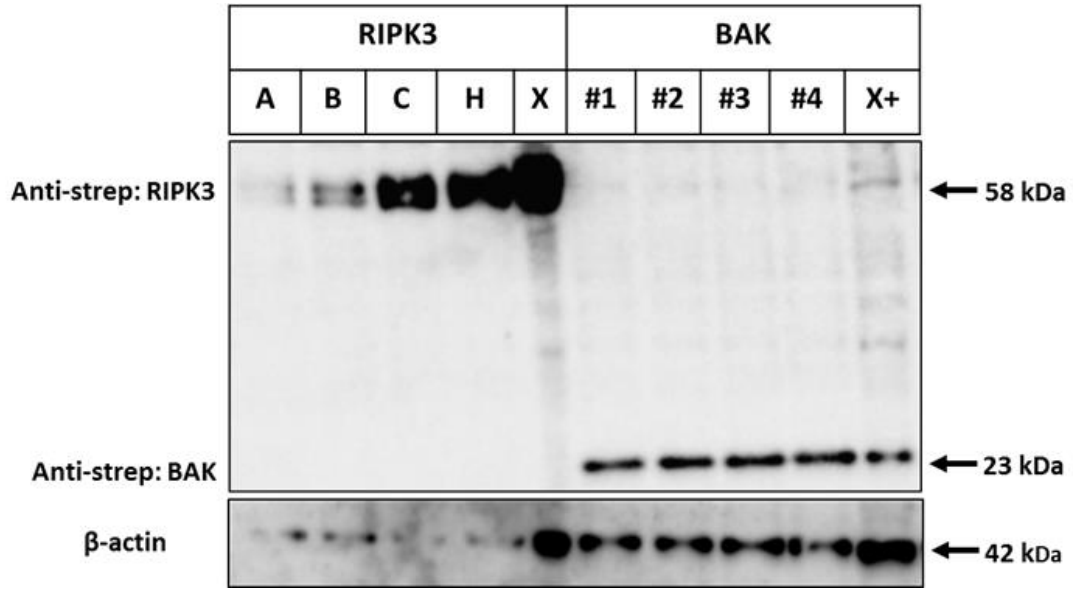

Figure 5.2: Western blotting determination of protein expression of RIPK3 and Bak pSBTET plasmids following transient transfection in HEK293T cells. Plasmid DNA (1 µg) was co-transfected with 100 ng SB100 transposase enzyme. Plasmids C and H showed protein over-expression for RIPK3. Although all four plasmids (#1 to #4) showed over-expression for Bak, only plasmids numbers #2 and #4 were eligible for subsequent studies. Positive control lysates (X for RIPK3 and X+ for Bak) were from transiently transfected pCW plasmids in HEK293T cells. Both RIPK3 and Bak proteins was detected using strep-tag II antibody. Induction of RIPK3 and Bak gene expressions was achieved using doxycycline (Dox, 5 µg/ml).

5.3.4 Assessment of MLKL protein expression in HEK293T cells transiently transfected with full length MLKL-pFRT and MLKL-pCW

To determine the protein expression of MLKL clones, both MLKL-pCW and MLKL-pFRT constructs were transiently expressed in HEK293T cells and the resulting products were analysed for protein expression by Western blotting. From the blot (Figure 5.3), it can be seen that MLKL protein expression was achieved as there were observable differences between the un-transfected and the transfected groups.

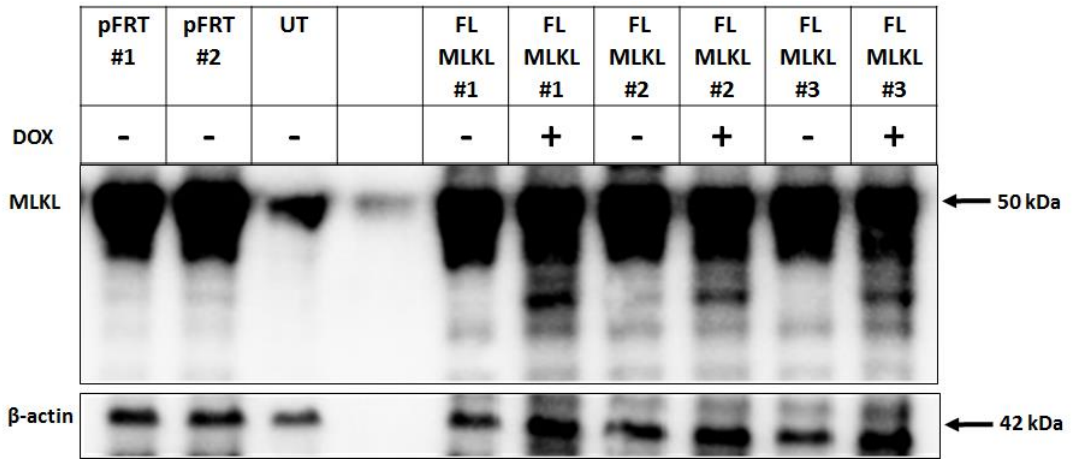

Figure 5.3: MLKL protein overexpression screening in two different plasmid constructs. MLKL-pFRT and MLKL-pCW57.1 plasmid constructs were transiently expressed in HEK293T cells in order to assess protein expression performance and determine which one was most suitable for sub-cloning purpose. Total protein lysates were extracted and full length (FL) MLKL protein was blotted for using MLKL antibody.

5.3.5 Clonal screening of MLKL-pSBTET plasmids transiently expressed in HEK293T cells.

In order to assess MLKL-pSBTET construct clonal expression performance, HEK293T cells were transfected for 24 hrs with and without Dox. An MLKL antibody that detects endogenous levels of full length human MLKL was used to recognise MLKL protein expression via Western blotting. As can be seen (Figure 5.4), MLKL expression was higher in the transfected/Dox group compared to both the un-transfected group and the transfected/DMSO group. Best expressing clone #5 was selected for expression in HaCaT cells for subsequent work.

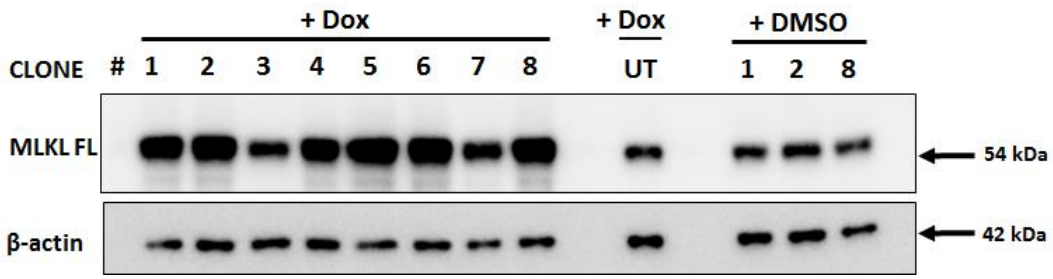

Figure 5.4: Clonal screens of MLKL-pSBTET plasmids via protein expression. MLKL-pSBTET plasmid DNA (1 µg) was co-transfected with 100 ng SB100 transposase enzyme with and without 5 µg/ml Dox. After 24 hours of incubation, protein lysates were generated and samples were subjected to Western blotting to determine best performing clones. UT denotes un-transfected which was used as a control. Detection of immobilised MLKL protein was carried using MLKL antibody.

5.3.6 Confirmation of gene integration and expression efficiency for Bak-pSBTET HaCaT using protein expression analysis

To determine the success of our stable gene expression, polyclonal Bak HaCaT post antibiotic (blasticidin) selection was harvested. Select doses of Dox (0-10,000 ng/ml) were used to induce gene expression for 24 h. Protein expression as a consequence of gene expression was determined using Western blotting. Bak was expressed by HaCaTs confirming integration (Figure 5.5). As can be seen, Dox was able to induce Bak expression even at low doses beginning from 100 ng/ml final concentration. Moreover, the protein bands were detected at the predicted molecular weight (~23 kDa) comparable to positive control (transiently expressed Bak). Interestingly, no protein band was detected in the absence of Dox (DMSO control) for Bak stable HaCaT. Similarly, no protein band was detected in the wildtype (WT) HaCaT treated with Dox as well.

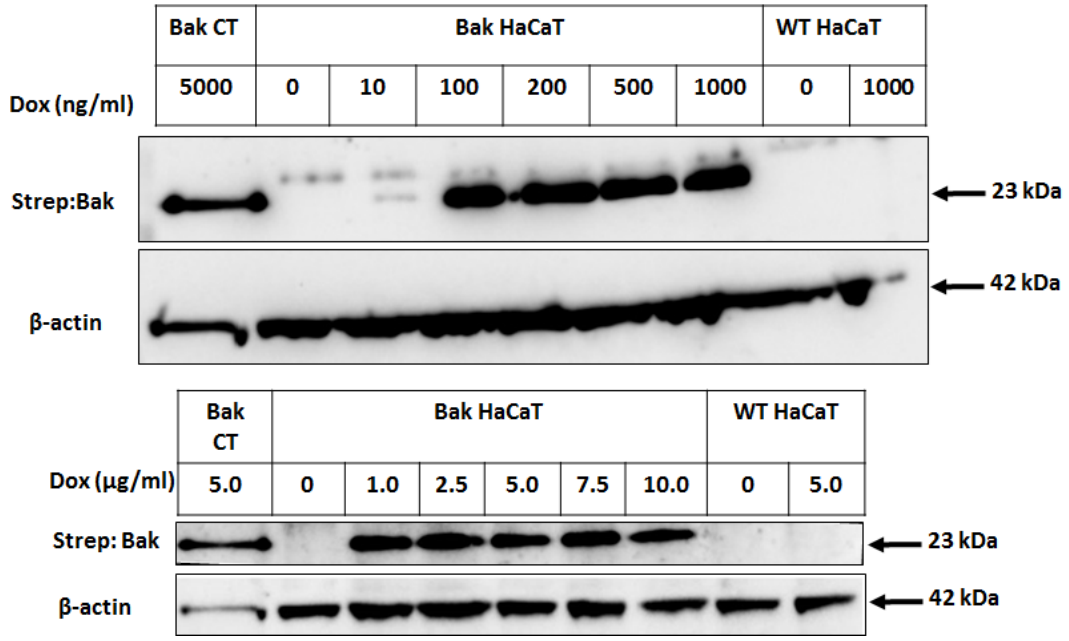

Figure 5.5: Confirmation of gene integration for Bak transgene into HaCaT cells at given doses of doxycycline via protein expression analysis. Bak polyclonal HaCaT cells seeded in 6-well plates were incubated with doxycycline (0 to 1,000 ng/ml) for 24 h. Cell lysates were harvested and protein detection was carried out using strep tag II antibody. WT denotes wildtype while CT denotes positive control.

5.3.7 Effect of time on RIPK3, Bak and MLKL protein expression in HaCaT cells post antibiotic selection

The optimal expression of all stable HaCaT expressing transgenes; RIPK3, Bak and MLKL was assessed over a time course. From the data, it was observed that RIPK3 expression occurred earlier at 3 h in a dose independent fashion (Figure 5.6A). However, this expression was not sustained for the tested time-points as RIPK3 protein degradation set in from 12 h and was completed at 18 h. For Bak, expression was also very early (3 h) reaching maximum at 12 h in a dose independent manner (Figure 5.6B). Unlike RIPK3, no degradation was seen with Bak proteins. In contrast to RIPK3 and Bak, MLKL showed delayed expression as no

protein band was seen at 3 h. Protein expression for MLKL was seen at 6 h and peaked at 12 h (Figure 5.6C). MLKL protein over-expressed in HaCaT cells was not degraded at 12 h just like Bak but in contrast to RIPK3.

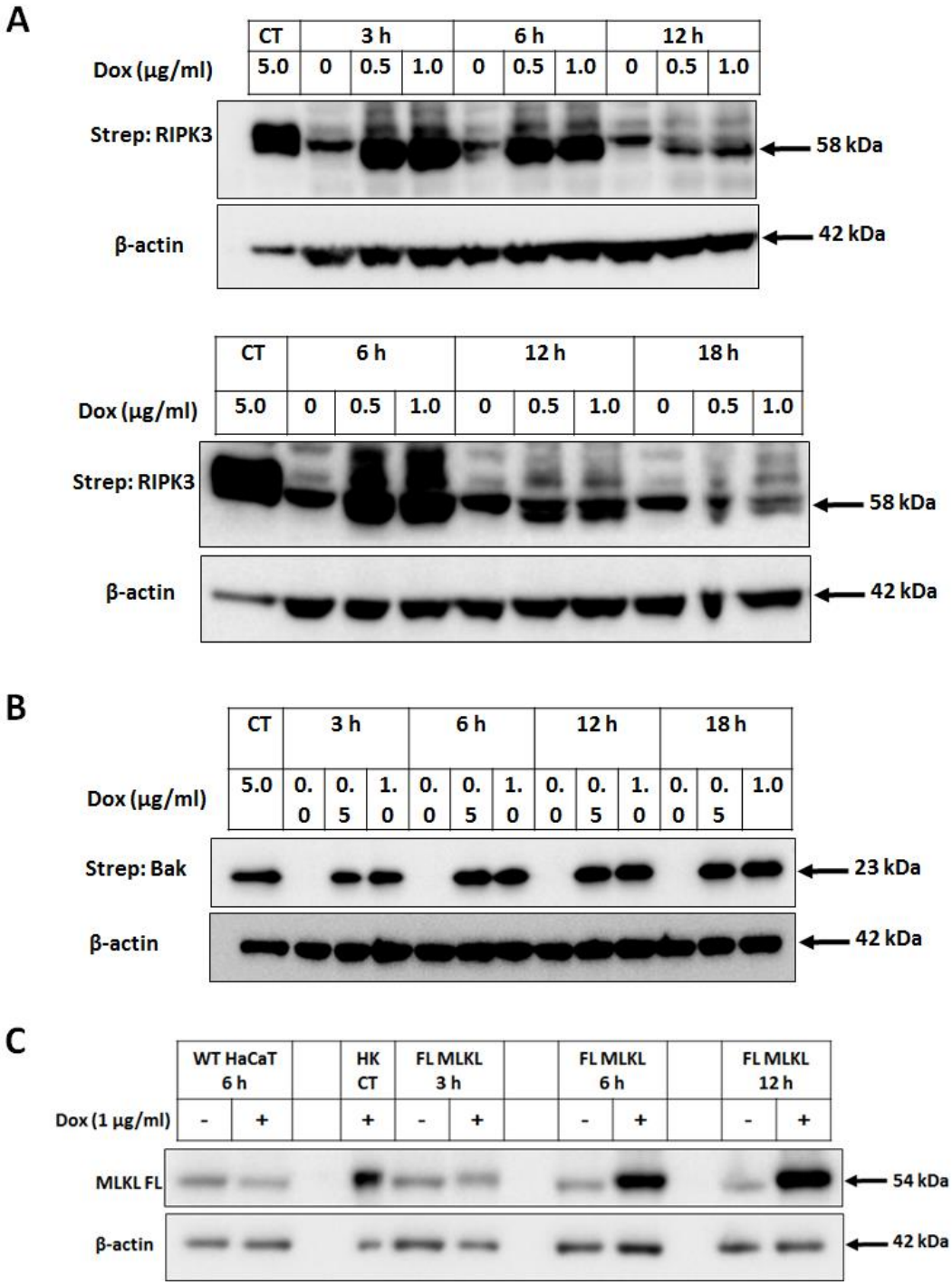

Figure 5.6: Time dependent induction of protein expression via Western blotting in HaCaT cells for (**A)** RIPK3 **(B)** Bak **(C)** MLKL**.** All samples were exposed to Dox to

induce gene expression and consequently protein elevation. RIPK3 and Bak proteins were detected using strep tag II antibody whereas MLKL protein was detected using MLKL antibody.

5.3.8 Induction of RIPK3 and Bak protein expression is sufficient to cause HaCaT cell death

The time to onset of HaCaT death mediated by RIPK3 and Bak was determined using the MTT assay. Induction of RIPK3 and Bak proteins using DOX was undertaken for 3 and 6 hrs. The viability of both wildtype HaCaT and RIPK3 stable HaCaT was unaffected 3 hours following DOX stimulation whereas Bak was affected (Figure 5.7A). The viability of Bak stable HaCaT cells was reduced by approximately 20%. By contrast, both Bak and RIPK3 caused marked HaCaT cell death at the 6 hr DOX exposure (Figure 5.7B) indicating that activation of gene expression for both proteins is sufficient to cause transgenic HaCaT cell death.

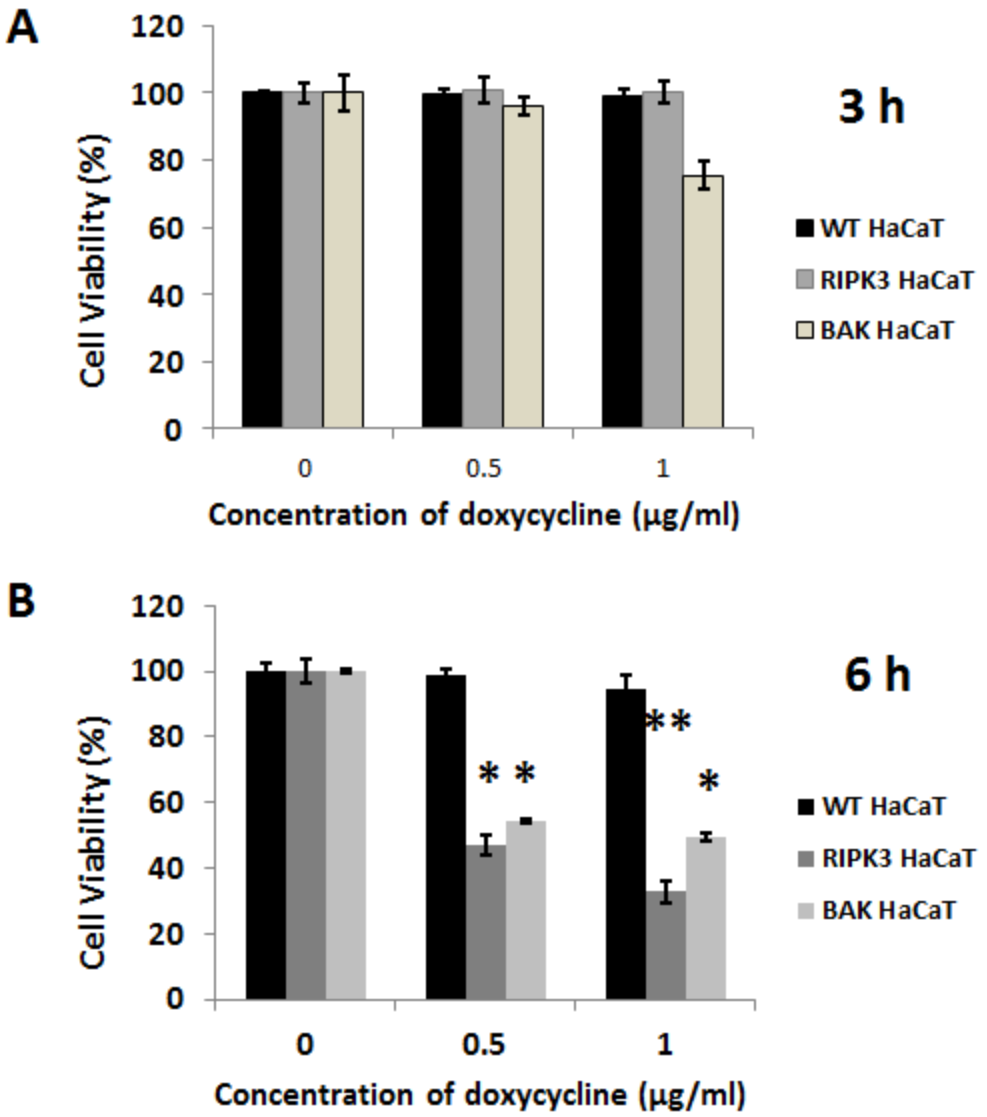

Figure 5.7: Effect of RIPK3 and Bak induction on HaCaT cell viability assessed via the MTT assay after A) 3 hours of DOX treatment B) 6 hours of DOX treatment. Data represent mean (±SEM) of 3 separate experiments conducted in triplicates normalised to untreated control. Results from wildtype (WT) HaCaT, RIPK3 and BAK stable HaCaT cells were compared. Statistical significance was determined using Student T test and values (*$p<0.05$, **$p<0.01$) indicate statistical significance.

5.3.9 Characterisation of the mechanisms of RIPK3 and BAK mediated HaCaT death

To elucidate the possible mechanisms through which RIPK3 and Bak could be mediating HaCaT death, a panel of small molecule inhibitors was utilised to block the effectors of apoptosis (caspases) and necroptosis (RIPK3 and MLKL). RIPK3 protein function was inhibited using GSK'872 (abbreviated GSK), a potent and selective inhibitor of its kinase domain (Mandal et al., 2014) while MLKL protein was inhibited using necrosulfonamide (NSA), a blocker of its adaptor function (Sun et al., 2012) (Wang et al., 2014). Apoptosis was blocked using the pan caspase inhibitor known as Z-VAD-FMK (zVAD). The effect of these various inhibitors (1 hr pre-stimulation) on HaCaT viability following induction of RIPK3 and Bak protein expressions using 1 µg/ml DOX (6 hr) was determined using the MTT assay. From the figure (Figure 5.8), both RIPK3 and Bak induction resulted in a significant decrease of HaCaT cell viability. For RIPK3 stable cells, pre-treatment with NSA and GSK individually offered marginal protection to HaCaT cells (Figure 5.8A). Surprisingly, the blockade of caspase activity using zVAD significantly rescued HaCaT cells from RIPK3-induced HaCaT death indicating the involvement of an apoptotic mechanism. Similarly, the combined inhibition of RIPK3 and MLKL using GSK and NSA respectively significantly attenuated HaCaT death resulting from RIPK3 induction (Figure 5.8C). The same protective effect was seen with the concomitant use of NSA and zVAD. For Bak stable HaCaT cells, zVAD rescued HaCaT cells from Bak-induced death (Figure 5.8B). The combined use of GSK, NSA and zVAD offered partial protection to HaCaT cells (Figure 5.8D). There was a slight increase in the

number of viable cells seen when the core effectors of necroptosis, RIPK3 and MLKL were blocked together through the combination of GSK and NSA.

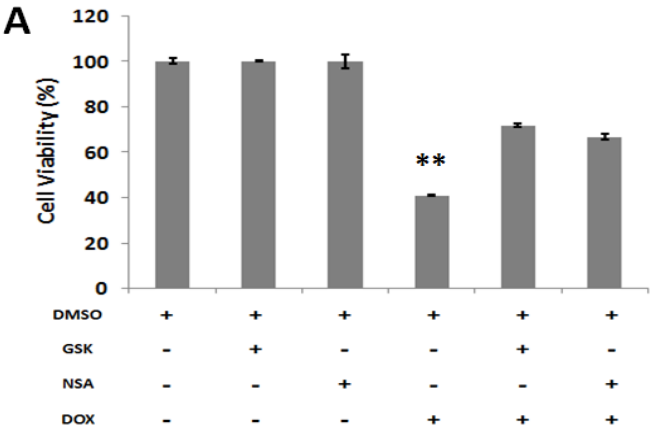

RIPK3 HaCaT

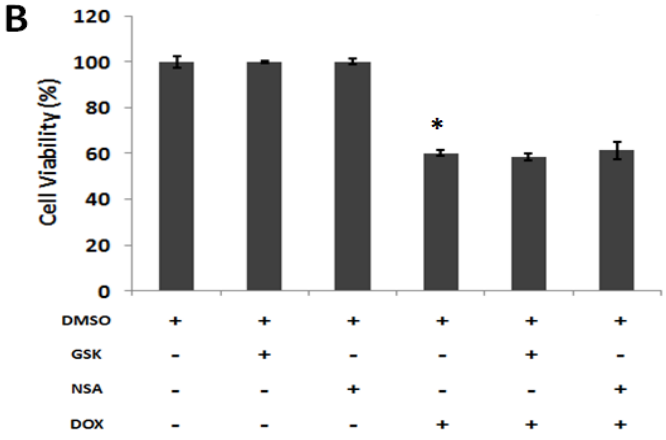

BAK HaCaT

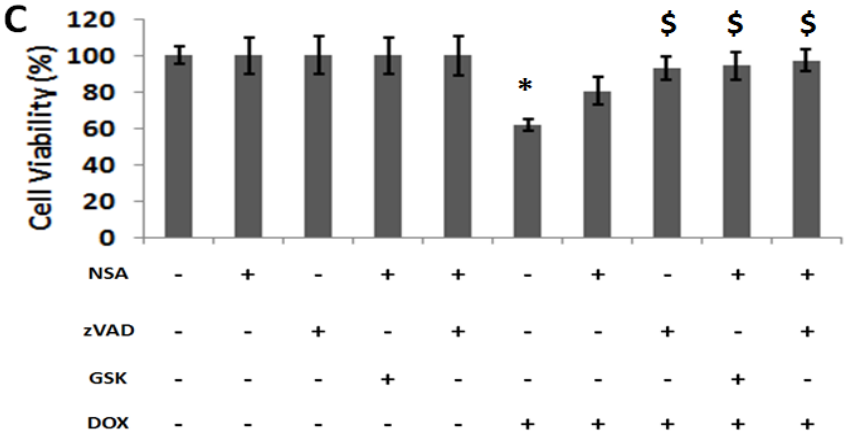

RIPK3 HaCaT

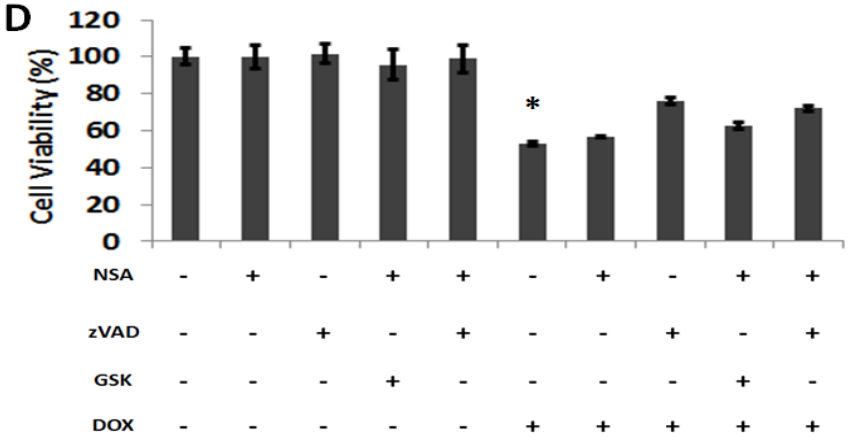

BAK HaCaT

Figure 5.8: Investigating mechanisms of HaCaT death via the MTT assay A) in RIPK3 B) Bak C) RIPK3 plus GSK/NSA treatment D) Bak GSK/NSA treatment stable HaCaT cell lines. Induction of RIPK3 and Bak expression was achieved using 1 µg/ml DOX for 6 h. Prior to this, cells were pre-treated with 5 µM NSA or 5 µM GSK or 40 µM zVAD in singles or in combinations. The final DMSO content was kept constant for all treatments at either 0.2% or 0.3% as relevant. The MTT assay was used to assess cell viability. Data presented represent mean ±SEM of three independent experiments performed in triplicate. Statistical analysis was undertaken using Mann-Whitney U test. Significance was indicated with */$ ($p<0.05$). Significant death induction was represented by * whereas significant death rescue was indicated by $.

5.3.10 PARP and caspase processing and MLKL elevation in RIPK3 and Bak mediated HaCaT death

RIPK3 and Bak stable transgenic HaCaT cells were investigated for PARP and caspase 3 processing in order to determine the involvement of apoptosis using Western blotting. The involvement of necroptosis on the other hand was probed with MLKL measurement. MLKL was elevated in the DOX stimulated RIPK3 stable HaCaT but not in the unstimulated RIPK3 group and wildtype HaCaT groups (Figure 5.9A). Surprisingly, it also appears like MLKL levels were increased in the DOX stimulated Bak stable HaCaT cells as opposed to the DOX untreated Bak HaCaT control. PARP was cleaved into the 89 kDa fragment which is typical of apoptotic processing in the both activated RIPK3 and Bak transgenic HaCaTs although maximal PARP cleavage was noticed for Bak alone. For caspase 3, significant cleavage into the p17 and p19 subunits was observed for Bak transgenic HaCaT cell line (Figure 5.9B). In addition, significant processing of caspase 3 also occurred in the activated RIPK3 transgenic HaCaT cell line as there was over 5-fold increase in cleaved caspase 3 fragments (Figure 5.9B).

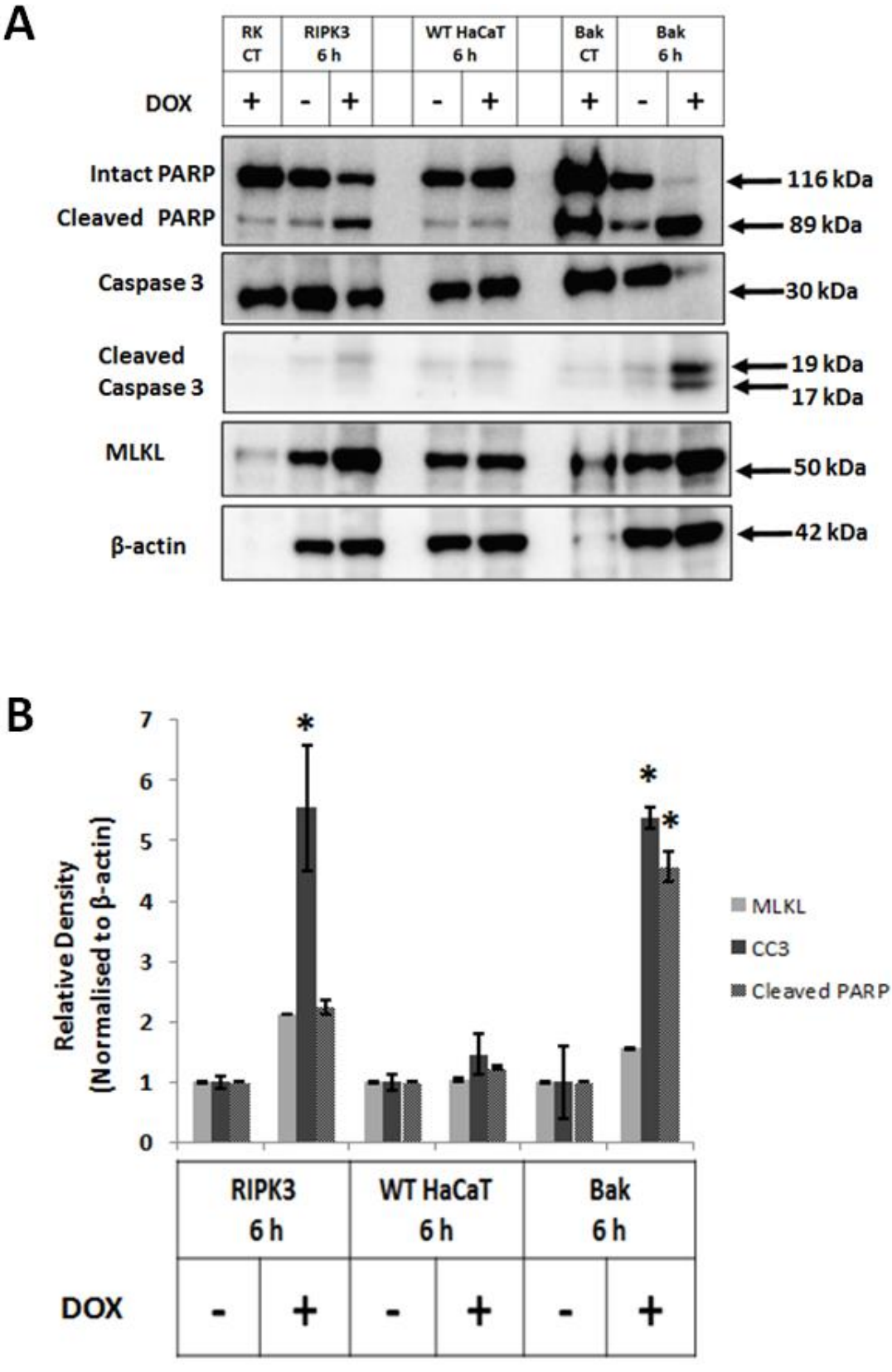
A
RK CT
RIPK3 6 h
WT HaCaT 6 h
Bak CT
Bak 6 h
DOX
+ - + - + + - + -
Intact PARP
Cleaved PARP
Caspase 3
Cleaved Caspase 3
MLKL
β-actin
116 kDa
89 kDa
30 kDa
19 kDa
17 kDa
50 kDa
42 kDa
B
Relative Density (Normalised to β-actin)
0 1 2 3 4 5 6 7
*
MLKL
CC3
Cleaved PARP
RIPK3 6 h
WT HaCaT 6 h
Bak 6 h
DOX
- + - + - +

Figure 5.9: Measurement of apoptotic and necroptotic markers in RIPK3 and Bak transgenic HaCaT cells. A) Western blotting analysis of MLKL, PARP and caspase 3 B) Densitometric measurements of presented blots probed for PARP, MLKL and cleaved caspase 3. Protein lysates were extracted from DOX (1 µg/ml) treated and untreated RIPK3 and Bak stable HaCaTs incubated for 6 h. Total lysates (20 µg) was assayed by Western blotting for PARP, caspase 3 and MLKL processing with beta actin as loading control. Quantification of relative density was achieved using ImageJ software and values were normalised against both untreated controls and β-actin loading control. Mann-Whitney U test was used to determine statistical significance of protein levels. Data indicate mean ±SEM of representative blots from n=2 repeats with consistent observation. RK and CT denote RIPK3 and control respectively. Positive control lysates (CT) were derived from either transiently expressed RIPK3 or Bak in HEK293T cells. WT represents wildtype while CC3 denotes cleaved caspase 3. Statistical significance was indicated with *p<0.05.

5.3.11 Effects of RIPK3 and Bak activation on caspase processing of PARP in the induction of apoptosis and necroptosis by RIPK3 and Bak stable expressing HaCaT cells

To verify if PARP cleavage by caspase 3/7 is involved in the downstream mechanism of RIPK3-induced HaCaT death, HaCaT cells were pre-treated with a sub-optimal dose of the pan caspase inhibitor zVAD to a final concentration of 10 µM for 1 h accompanied by stimulation with 1 µg/ml DOX for 6 h. Treated and control samples were then assayed for target protein expressions via Western blotting

Figure 5.10). The sample treated with zVAD did not show any PARP processing into the 89 kDa fragment that is used to indicate apoptosis in the RIPK3 transgenic HaCaT. However, in the Bak transgenic HaCaT, this dose of zVAD was unable to block PARP processing. Full length caspases-3 and 7 were cleaved into the p17/p19 subunits and p30/18 subunits respectively in the RIPK3 DOX stimulated group not pre-stimulated with zVAD. The same caspases 3/7 cleavage patterns were observed

even more prominently for Bak. Whilst treatment with zVAD did not seem to completely block caspases 3/7 cleavage for both RIPK3 and Bak, instead, it appeared to alter the resulting cleaved product fragment sizes. These cleaved caspase 3 fragments were seen with estimated molecular weights of 20 kDa and 22 kDa. MLKL levels in HaCaT cells were increased following activation of both RIPK3 and Bak and this increment did not appear to be altered with sub-optimal zVAD exposure.

To further discriminate between intrinsic or extrinsic apoptotic pathway, caspase 8 and caspase 9 expression and cleavage were examined. Pro-caspase 8 is known to be mainly involved in the extrinsic pathway whereas caspase 9 is widely known to play a role in mitochondrial mediated apoptotic pathway. As can be seen, caspase 8 cleaved subunits (p43/31) were detected in RIPK3 over-expressed stable HaCaT cells but absent in Bak over-expressed HaCaT cells though Bak positive control (Bak CT) derived from transiently over-expressed Bak in HEK293T cells showed caspase 8 fragments. A close examination of cleaved caspase 9 p37/35 subunits, revealed increased levels in Bak stable HaCaT but neither in wildtype nor RIPK3 stable HaCaTs indicating activation of the intrinsic apoptotic pathway. RIPK3 transgenic HaCaTs showed reduced levels of caspase 9 (p37).

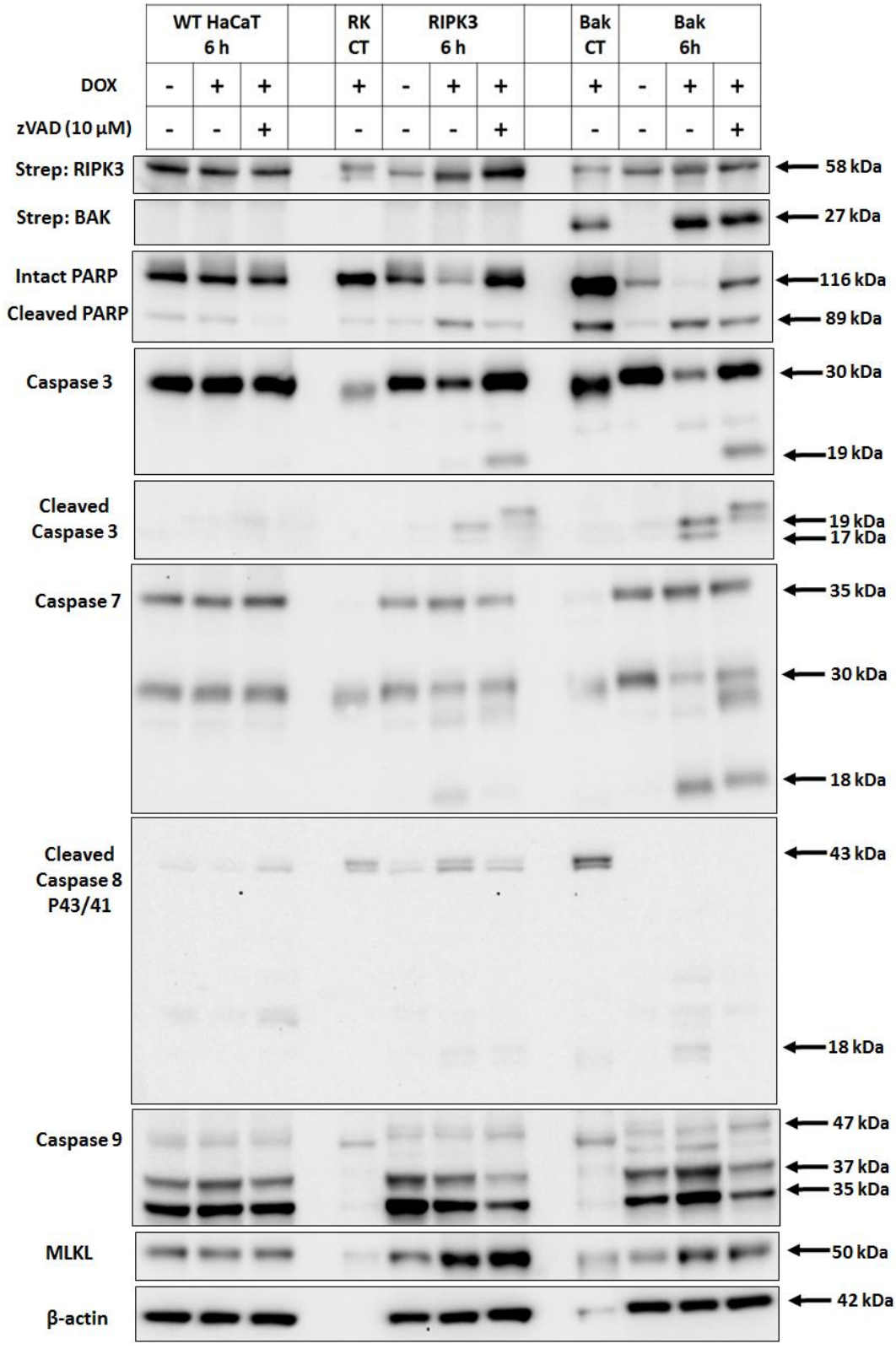

Figure 5.10: Western blotting analysis of PARP, caspases and MLKL processing in RIPK3 and Bak transgenic stables and wildtype HaCaTs. All samples with the exception of positive controls were DOX treated for 6 h in the absence or presence of 10 µM zVAD pre-treatment. Lysates were extracted from treated cells and

analysed for caspases-3, -7, -8 and -9 including MLKL and PARP processing using Western blotting. Displayed result is representative of n=2 experiments

5.3.12 Investigation of apoptotic markers in full length MLKL stable HaCaT cells

To exclude the involvement of apoptosis in the mechanism of MLKL-induced HaCaT death, PARP and caspase 3 cleavages were examined. Based on our observation, we did not detect the 89 kDa cleaved fragment of PARP in MLKL stable HaCaT though PARP was cleaved (Figure 5.11). We also did not observe any cleaved caspase 3 fragments. As expected, cleaved PARP and caspase 3 fragments were seen in the Bak activated HaCaT used as positive control for screening the presence of apoptotic markers.

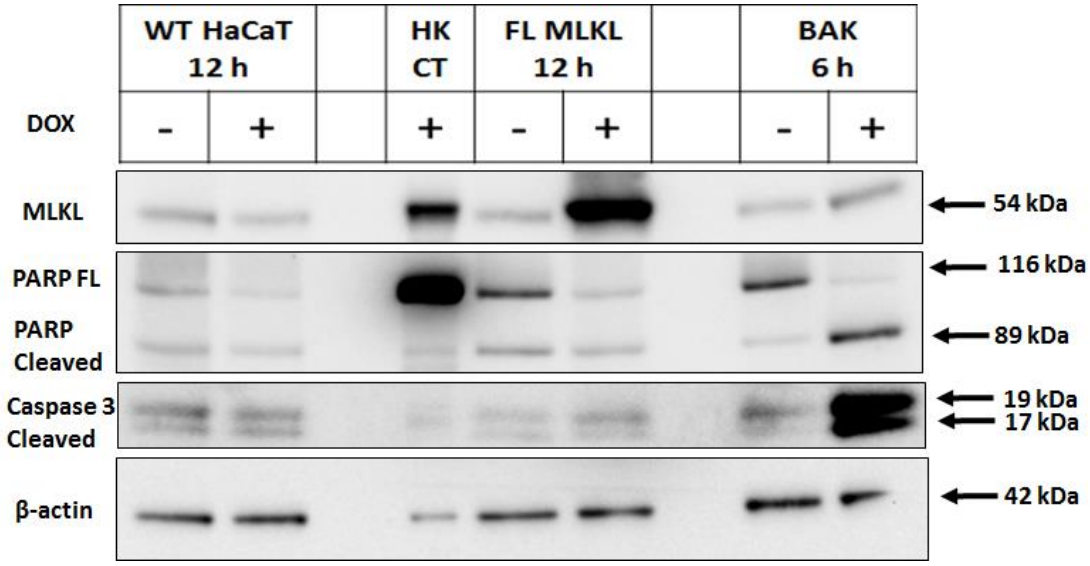

Figure 5.11: Screening for cell death markers in MLKL stable HaCaT cells via Western blotting. PARP and caspase 3 cleavages were assessed for MLKL stable HaCaT in comparison with Bak stable and parental HaCaT. HK indicates HEK293T while CT indicates control. Positive control lysate (HK CT) was derived from transiently expressed tetracycline-inducible MLKL in HEK293T cells induced with DOX (5 µg/ml). MLKL induction in MLKL transgenic stable HaCaT cells was achieved using DOX (1 µg/ml).

5.3.13 Effect of apoptotic and necroptotic death pathways on HMGB1 translocation in transgenic HaCaT cells

To understand the impact of cell death pathways triggered by the expression of cell death effectors on HMGB1 translocation in HaCaT cells, we performed immunocytochemistry on HMGB1 (green) and other cellular components like the nucleus (blue) and the cytoskeleton (red) in both stable and wildtype HaCaT cells (Figure 5.12). The nuclei of HaCaT cells that have undergone RIPK3-induced death appeared condensed and had apoptotic resemblance; nuclear to extracellular space translocated HMGB1 can be seen. Inspecting the nucleus in cells in which MLKL was the trigger for cell death revealed nucleus with less tight packing compared to un-transfected HaCaT control. HMGB1 seemed to have leaked out from MLKL-induced necroptotic nucleus through ruptured cell membrane. The nuclear morphology for Bak-induced dead HaCaT cells appeared even more tightly packed exposing its HMGB1 content to the extracellular milieu. Unlike the nuclear morphology of RIPK3 and Bak induced HaCaT demise, that of MLKL-induced HaCaT damage was more spherical likewise the pattern of HMGB1 staining. Actin cytoskeleton was disintegrated in both RIPK3 and Bak dependent HaCaT death. In MLKL-induced HaCaT necroptosis, actin cytoskeleton seemed slightly contracted (negligible) but not disintegrated like the case of RIPK3 and Bak. In contrast to Bak, RIPK3 mediated dead HaCaT cells in addition to collapsed nuclear morphology, also showed spherical nuclear morphology indicating the presence of both apoptotic and necroptotic cell death pathway.

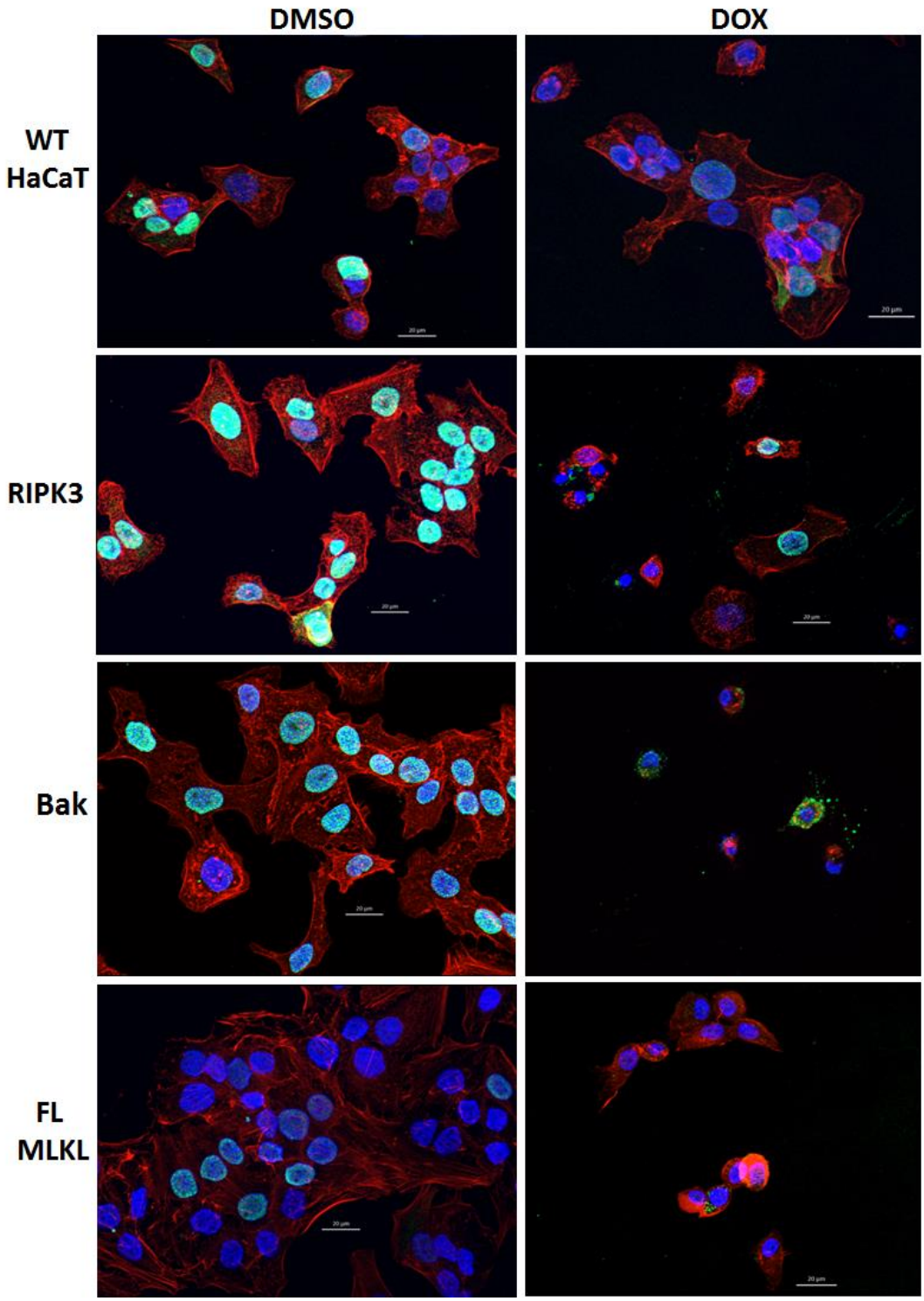

Figure 5.12: Merged immunofluorescent images of stained high mobility group box-1 (HMGB1), nucleus and actin in RIPK3, Bak, MLKL and parental HaCaT cells with and without DOX treatment. HMGB1 was stained with alexa488 (green), whereas nuclei and actin were stained with Hoechst (blue) and alexa568-Phalloidin (red) respectively. All cells were treated with 1 µg/ml DOX final concentration and images were captured under the 40X magnification objective. The diameter of cells was indicated with 20 µm scale bar. WT denotes wildtype while FL denotes full

length. Presented data was representative of findings from three independent experiments.

5.3.14 Effects of cell death pathways on HaCaT HMGB1 levels

Apoptosis and necroptosis mediating cell death effectors were examined to elucidate their effect on HMGB1 release by HaCaT cells. Supernatants from wildtype, RIPK3, full length MLKL and Bak HaCaT cells exposed to DOX or DMSO were analysed for HMGB1 profiles (Figure 5.13). Significant levels of HMGB1 (about 3 fold higher) were measured from both RIPK3 and Bak-induced HaCaT death compared to wildtype (un-transfected) HaCaT control. Even super elevated HMGB1 levels (8-fold) were measured from MLKL-induced HaCaT death when compared to wildtype HaCaT control. A further comparison of extracellularly released HMGB1 levels from all effector proteins revealed that MLKL was significantly higher giving a value about 2.3 fold higher than the amount released from both RIPK3 and Bak mediated HaCaT killing.

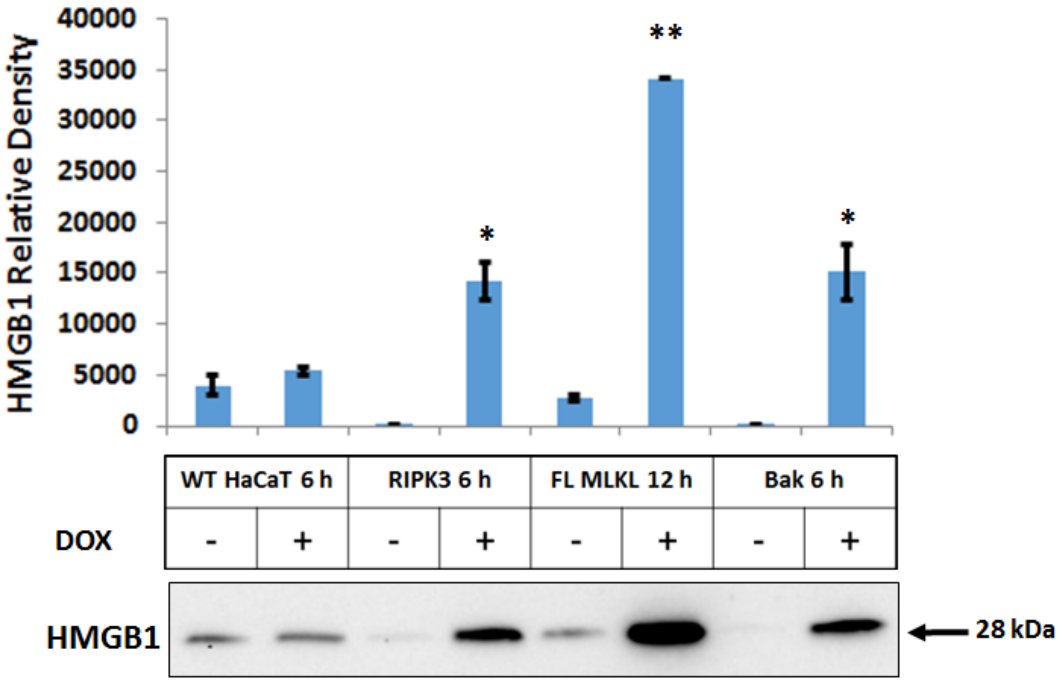

Figure 5.13: HMGB1 measurement in supernatants from RIPK3, Bak, full length (FL) MLKL transgenic and non-transgenic HaCaT cells. Data represent ±SEM of the area of three blots. Densitometric analysis was performed with ImageJ software on three separate blots and statistical analysis was undertaken using Mann-Whitney U test. Significance was indicated with *p<0.05 and **p<0.01.

5.4 Discussion

The overexpression of specific genes is one of the methods to study cell death regulation potentially devoid of mixed signals that usually accompany ligand-receptor triggered cell death signalling. We have utilised the opportunity availed to us by the Sleeping Beauty transposon (SB) system with tet-inducible promoter to achieve the stable integration of death effector transgenes; RIPK3, Bak and MLKL into HaCaT keratinocyte cell line. The problem of epigenetic silencing of integrated transgenes by epigenetic processes was successfully circumvented and expressions in HaCaT cells were confirmed. This integration is facilitated by flanking inverted

terminal repeats (ITR) specifically recognised by the transposase enzyme which makes random insertion at TA-dinucleotide sites in the host genome.

The gene expression data presented showed early degradation of RIPK3 protein in HaCaT cells (Figure 5.6). Unlike RIPK3 protein, Bak and MLKL proteins did not undergo early degradation as indicated by our data. The most likely explanation might be due to RIPK3 susceptibility to poly-ubiquitin chain attachment specifically on lysine (K) residues. Based on a review, there is evidence to prove that ubiquitin chains have different properties and that the type of ubiquitin chains added to the substrate determines the consequences thereof (Komander, 2009). The linear and K-63 ubiquitin chains provide docking sites for the activation of signalling pathways while the K-48 polyubiquitin chain on RIPK3 acts as a principal signal for the direction of RIPK3 for proteasome mediated degradation (Bertrand et al., 2011). RIPK3 and other members of the RIPK family can be directly ubiquitinated through the addition of ubiquitin chains by cIAP1 and cIAP2 including perhaps XIAP which have E3-ubiquitin ligase activity (Bertrand et al., 2008) (Bertrand et al., 2011). Our suspicion concerning ubiquitin mediated proteasome degradation of RIPK3 could be confirmed by performing an ubiquitination assay or through the use of proteasome inhibitors (examples; MG132 and bortezomib) (Moriwaki and Chan, 2016) or potentially by selectively degrading cIAP1 and cIAP2 with IAP inhibitors such as BV-6).

For the first time, our result (Figure 5.7 and Figure 5.8) showed that the inducible expression of wild-type human RIPK3 by Dox in the absence of ligand-death receptor activation was a sufficient stimulus to induce HaCaT cell death. A similar

observation was reported by a previous study which demonstrated that inducible expression of mouse RIPK3 activated by forced dimerization using coumermycin in the absence of receptor-ligand interaction was sufficient to kill mouse embryonic fibroblast (MEF) cell line (Cook et al., 2014). However, contrary to the Cook et al finding, another study argued that it was chemically enforced oligomerization but not dimerization of expressed RIPK3 that was sufficient to cause MLKL-dependent necroptotic death of NIH-3T3 cells (a cell line which lacks the ability to express endogenous RIPK3) (Orozco et al., 2014). Notably, none of these studies' observations was precisely consistent with our data as no action was taken to forcefully activate RIPK3 either via forced dimerization or oligomerization other than just induce RIPK3 gene expression. RIPK3 activation in HaCaT cells following induced overexpression appeared to be rather spontaneous. The vast majority of studies have not demonstrated RIPK3 sufficiency to bring about cell death without the involvement of ligand-receptor mediated endogenous activation (Moujalled et al., 2013), as such our data shows a possibility for spontaneous activation particularly in HaCaT cells.

NSA marginally blocked RIPK3-induced HaCaT killing suggesting an involvement of MLKL-dependent necroptosis (Figure 5.8). RIPK3 has been reported to trigger MLKL-dependent necroptosis in a number of mammalian cell lines (Mandal et al., 2014) (Pasparakis and Vandenabeele, 2015). Likewise inhibiting over-expressed RIPK3 via GSK'872 resulted in partial protection of HaCaT cells while concomitant use of GSK'872 and NSA significantly rescued HaCaT cells from RIPK3 dependent death. This strongly indicates a RIPK3/MLKL driven necroptosis. In agreement, previous

studies have reported similar results in which GSK'872 (Mandal et al., 2014) and NSA (Wang et al., 2014) blocked necroptosis induction. It is important to state here that RIPK3 induced MLKL dependent necroptosis is an already well established observation in the literature.

Caspase blockade via zVAD attenuated RIPK3-induced HaCaT demise indicating that apoptotic HaCaT death involving caspases could be activated downstream of RIPK. In a previous study, it has been reported in agreement with our data that the induction of forced dimerized murine RIPK3 mediated killing of wildtype RIPK3-expressing MEF cells was partially inhibited by a broad-spectrum caspase inhibitor called Q-VD-oph (Moujalled et al., 2014). Inconsistent with our result, RIPK3-dependent cell death was not suppressed by zVAD in two T-cell leukaemia cell lines (Jurkat and H9 cells) over-expressing wildtype murine RIPK3 (Moriwaki and Chan, 2016). Almost full suppression of cell death comparable to that seen with zVAD was observed when GSK'872 and NSA were used in combination. This suggests that both MLKL-dependent necroptosis and caspase-dependent apoptosis were present in the action of RIPK3 in causing HaCaT cells to die in a manner that appears not to be compensatory for differing cell death modes.

Bak is an important member of the Bcl-2 family of mitochondria regulated apoptosis effector that is considered to have one of the best characterised mechanisms of cell suicide (Moujalled et al., 2014). This implies that Bak provides a useful platform to study and characterise apoptotic phenotype in cells. Our MTT cell death data revealed early death of HaCaT cells from Bak-induction reaching maximum over time (Figure 5.7). The broad-spectrum caspase inhibitor zVAD partially suppressed

HaCaT cell death upon Bak induction suggesting caspase-dependent apoptosis. The inability of zVAD to completely suppress apoptosis induced by Bak was anticipated because it is a known fact that caspase inhibition alone does not fully prevent cell death that is initiated through the mitochondrial pathway as the cells can die via a different cell death modality (Feoktistova et al., 2016). Consistent with what is documented in the literature for Bak-mediated apoptosis, increased amounts of caspase 9 fragments was seen confirming the intrinsic apoptosis. In the mitochondrial apoptotic pathway, caspase 9 recruitment to the apoptosome (a high molecular weight complex) has an initiator role in activating other caspases (Wang, 2001) (Samraj et al., 2007) (Degenhardt et al., 2002). Proteolytic cleavage of caspase 8 was lacking in Bak-expressing HaCaT cells indicating a non-involvement of the extrinsic apoptotic pathway, further suggesting a favour of the intrinsic arm of the apoptosis dichotomy. Although there are divergent findings either reporting absence or presence of cleaved caspase 8 (Huang et al., 2016) in the mechanism of Bak mediated death. Differences in how different cell types activate and process caspases may perhaps be responsible for the varying observations.

As expected, our data confirmed apoptotic PARP processing, proteolytic cleavage of executional caspases-3/7 affirming Bak as a classical apoptosis effector molecule. The PARP family of enzymes have a physiological role to catalyse the transfer of ADP-ribose to target proteins in a process called poly ADP-ribosylation (D'Amours et al., 1999). PARP plays a number of important cellular functions such as modulation of chromatin structure, transcription, recombination, DNA repair and cell death (Ame et al., 2004). During apoptosis, PARP cleavage by caspases (3/7) occurs in the

bipartite nuclear localisation signal (DEVD/G) to generate a 24kDa-DNA binding fragment and an 89kDa catalytic fragment (apoptotic marker) (D'Amours et al., 1999). Accordingly, it is a general view that PARP cleavage acts to prevent apoptotic dying cells from switching to the necrotic pathway. An unusual processing of caspase 3/7 into fragments (slightly higher than conventional fragments) resulted from blocking caspases with suboptimal concentration of zVAD. This observation suggests that a cryptic second cleavage site might exist for caspases 3 and 7. A similar cleavage pattern has been reported previously for caspase 3 almost two decades ago (Boulares et al., 1999).

Intriguingly, our data showed that NSA reduced the number of dead cells by approximately 10% in Bak-expressing HaCaT cells and in addition, MLKL protein was elevated in Bak-induced HaCaT cell demise. These results suggest that MLKL-dependent necroptosis might be involved in the mechanism of Bak-induced keratinocyte demise. It was unclear if perhaps MLKL might also be recruited to the apoptosome or exactly how Bak interacts with and induces MLKL upregulation. This opens up the possibility that there could be a crosstalk between the mitochondrial mediated apoptosis and MLKL-dependent necroptosis. Furthermore, it is speculated that the unknown downstream mediator of Bak that induces the gene expression of MLKL might positively interact with an inducer of MLKL gene expression. Given that no publication has shown a link between Bak mediated mitochondrial death activation and MLKL-dependent necroptosis, this observation should be further investigated. A related phenomenon has been reported with the revelation that the mitochondrial phosphatase PGAM5, a phosphatase responsible for the de-

phosphorylation and activation of dynamin-related protein-1 (Drp1) was a component of RIPK1- and RIPK3-containing multiprotein complexes which depicted a convergent link between the mitochondrial pathway and the necroptosis effectors RIPK1/RIPK3 (Wang et al., 2012). The result of this interaction leads to the activation of Drp1 which brings about fragmentation of the mitochondria.

Interestingly, our data demonstrated novelty about cell death induction in HaCaT keratinocytes driven by full length human RIPK3 accompanied by caspase 8, PARP, caspase 3 and caspase 7 cleavages which strongly indicate activation of the extrinsic apoptotic pathway. Caspase 8 is arguably the best example of a caspase which can be activated independently of the Bcl-2 family members particularly following activation of the TNF receptor superfamily (Wang et al., 2008). The possibility of RIPK3 activating apoptotic markers has been reported by Cook et al although this investigation was carried out in a MEF cell line using mouse RIPK3 fused to a gyrase which provided a platform to forcefully dimerize induced RIPK3. It was revealed that the induction and dimerization of RIPK3 in wildtype MEFs resulted in caspase 8, caspase 3 and PARP apoptotic processing (Cook et al., 2014). Mouse and human RIPK3 are 60% identical at the gene level and 69% similar at the amino acid level. In fact, they have a conserved kinase domain that is 70% identical and 78% similar (Chen et al., 2013b). Furthermore, whilst RIPK3 ability to drive necroptosis exclusively relies on the kinase domain, it has been reported that its pro-apoptotic activity is determined by the RHIM domain (Mandal et al., 2014) (Cook et al., 2014).

Consistent with the literature, our data on wildtype human MLKL-expressing HaCaT confirmed that MLKL protein is a purely necroptotic terminal effector molecule.

MLKL oligomers induce necroptosis using its 4-helical bundle to create pores in membranes (Hildebrand et al., 2014a). Both PARP and caspase 3 analyses revealed no detectable cleaved caspase 3 or cleaved PARP 89kDa catalytic fragment. Although it appeared like PARP was cleaved but this cleavage did not generate the 89kDa apoptotic fragment. The PARP antibody used is validated to detect only full length and the 89kDa cleaved fragment of PARP. Taking a cue from a previous report, it is speculated that the cleaved PARP fragment which was not detected by our blot may be approximately 24kDa in molecular weight. PARP is thought to promote cell death through the depletion of cellular NAD and ATP whereas PARP cleavage causes its inactivation leading to breaking its ability to respond to DNA strand breaks.

Hoechst stained nucleus from both Dox-treated and untreated wildtype and stable transgenic HaCaT cells revealed remarkable differences in their nuclear morphologies. As expected for apoptosis, HaCaT cells undergoing Bak-induced cell death showed nuclear shrinkage and to a lesser degree fragmentation whereas for MLKL-driven necroptosis, the nucleus of dead cells were rounded and reduced in size with no visible evidence of shrinkage. Morphologically, they represented clearly distinct entities that conform to established hallmarks or features seen in cells undergoing either apoptosis or necroptosis (Feoktistova et al., 2016) (Galluzzi et al., 2012). Surprisingly, nuclear stain for RIPK3 expressing HaCaT cells which have undergone RIPK3-induced death showed a mixed morphology resembling that of apoptotic and necroptotic cell death but with more on the apoptotic side of the equation. This interesting observation has not been reported previously and would

require further research. Albeit, given that apoptotic markers have been seen in HaCaT cells triggered to die through RIPK3 induction, it is very possible that this observation is true and represents a novel feature that can be used to identify dead cells resulting from RIPK3-induced killing provided apoptosis-inducing agents or apoptosis-specific death receptor-ligands are excluded.

Accordingly, our HMGB1 immunofluorescence data on Dox-treated RIPK3, Bak and MLKL expressing HaCaT transgenes revealed differences in HMGB1 expression patterns and kinetics including its translocation from nucleus to cytosol and then to the extracellular milieu. RIPK3 and Bak expressing HaCaT cells showed comparable HMGB1 content that appeared to surround shrunk or collapsed apoptotic nucleus following ruptured cell membrane. HMGB1 from both Bak and RIPK3 mediated HaCaT death appeared compact. This suggests that HMGB1 might be compressed in its natural state while still bound to chromatin and they are perhaps condensed together. By contrast, nuclei of cells that have undergone MLKL-dependent necroptosis showed less HMGB1 nuclear content. A more logical explanation could be that HMGB1 falls off chromatin in necroptosis and exit from the cell through membrane pores created by MLKL. In support, a recent study demonstrated that induction of necroptosis causes a sudden and rapid disappearance of nuclear HMGB1, an event that happened after nuclear membrane rupture (Murai et al., 2018).

Further analyses showed significant HMGB1 release into the extracellular space from both RIPK and Bak driven HaCaT killing compared to wildtype HaCaT control. The difficulty of precisely discriminating between apoptotic and necroptotic

contribution to HMGB1 extracellular levels was increased by the fact that both Bak and RIPK3 drive a mixture of apoptosis and necroptosis in HaCaT cells. For this reason, it may be necessary in the future to block necroptosis in Bak and apoptosis in RIPK3 in order to accurately measure the true contribution of necroptosis and apoptosis to HMGB1 levels. It is generally believed that apoptosis rarely triggers HMGB1 release (Scaffidi et al., 2002) (Murai et al., 2018), however, in light of our finding, the extent to which this idea applies should be questioned. More importantly, our data have revealed for the first time that MLKL-driven HaCaT necroptosis contributed significantly more (2.3 fold) to HMGB1 levels compared to both RIPK3 and Bak mediated HaCaT death. Very recently, two modes of necroptotic release of HMGB1 from dying cells have been proposed namely the burst-mode and the sustained-mode (Murai et al., 2018) both of which can contribute substantially to HMGB1 extracellular levels.

There were a few limitations with our data. Firstly, batch stable transgenic HaCaT cells were used. It is known that cells from polyclonal populations of cells would have varying copies of integrated gene which may give slightly different responses. This is because with each cell division, the number of copies of transgene that is inherited by the daughter cells is halved. Secondly, HMGB1 detection was limited to total HMGB1 with no distinction between post-translationally modified isoforms. HMGB1 undergoes post-translational modifications in response to specific cell death forms that can influence its bioactivity once outside the cell. For example, the disulphide-oxidised form of HMGB1 which is said to be exclusively released by cells undergoing necroptotic cell death potently drives inflammation (Venereau et al.,

2012). Not knowing the redox and acetylation status of HMGB1 limits our interpretation of its numerous extracellular functions. Thirdly, the MTT assay might not be particularly suitable for measuring cell death orchestrated by the mitochondria, like in the case of Bak as cells may be potentially very sensitive. Compromise with mitochondrial metabolic activities is likely to occur immediately upon Bak induction as cell fate is determined by Bak which may likely affect the interpretation of the MTT cell viability assay. Flow cytometric analysis of annexin V and PI binding should be considered for future studies.

In summary, stable HaCaT cell lines over-expressing RIPK3, Bak and full length MLKL to elucidate the role and mechanism of RIPK3 in keratinocyte apoptosis and necroptosis have been successfully created. Our data have shown for the first time that induction of RIPK3 is sufficient to trigger HaCaT death and that this death encompasses both apoptotic and necroptotic mechanisms. In the same vein, our data have demonstrated novelty in the mechanism of Bak-induced HaCaT cell death with the unravelling of an MLKL-dependent necroptotic death component. These findings suggest that, at least in HaCaT cells, there might be crosstalk between dominant cell-death platforms. Since RIPK3 is upregulated in lesional TEN skin samples, and our in vitro data on RIPK3 have shown that RIPK3-killed HaCaT cells display morphological features of apoptosis, it is reasonable to speculate that RIPK3 may also possibly be able to drive keratinocyte apoptosis *in vivo* in SJS/TEN skins. This observation requires extensive investigation to confirm its applicability and relationship to SJS/TEN pathogenesis driven by RIPK3. Our data demonstrated that HMGB1 release through MLKL-dependent cell death was more than double that of

both RIPK3 and Bak mediated release. Thus this further supports chapter 4 findings that keratinocyte necroptosis is the dominant source of HMGB1 and potentially the main contributor to serum and blister fluid elevated HMGB1 levels in SJS/TEN disease described in chapter 2.

CHAPTER 6

FINAL DISCUSSION

Adverse drug reactions represent a serious burden to both clinicians and patients in terms of costs and mortality. ADRs account for 6.5% of hospital admissions in the UK alone (Pirmohamed et al., 2004). Cutaneous drug hypersensitivity is a manifestation of idiosyncratic drug reactions with immune-mediated aetiology targeting the skin. Stevens-Johnson syndrome and toxic epidermal necrolysis are life-threatening serious blistering mucocutaneous reactions characterised by epidermal and mucosal surface detachment due keratinocyte death. The pathogenesis of SJS/TEN is not fully understood. However, both keratinocyte death and inflammation are implicated as dominant factors in disease pathogenesis. The overall purpose of this study was to investigate and elucidate mechanisms and biomarkers of keratinocyte death in SJS/TEN. This study was achieved using both clinical samples and *in vitro* tools.

Following a previous report that HMGB1 protein may represent a diagnostic marker to discriminate severe cutaneous phenotypes from both DRESS and the milder phenotype MPE (Nakajima et al., 2011), we undertook a study to examine serum and blister fluid levels and skin expression of HMGB1. Interestingly, our comparison between blister-fluid and serum HMGB1 levels from the same set of patients showed for the first time a super elevation of HMGB1 in blister fluid compared to serum ($p<0.001$) (chapter 2). This result suggested that the observed levels of blister-fluid HMGB1 may be due to both i) active secretion from activated immune cells of the innate and adaptive immunity and ii) passive release from proximal dying keratinocytes. However, this study did not attempt to investigate the dominant types of immune cells present in blister-fluid from which HMGB1 concentration was quantified. Presumptively, if this was done, the cell types may

likely be the CD8+ T cells, NK and NKT cells previously reported by Chung *et al* (Chung et al., 2008).

In addition, our immunohistochemistry skin data revealed a novel observation in the skin distribution of HMGB1 as decreased epidermal expression and suprabasal retention of HMGB1 in SJS/TEN skin but not in MPE and healthy control skins was seen (chapter 2). This retention was proximal to the dermal-epidermal junction which is where the epidermis detaches from the dermis. There is a suspicion that increased serum and blister-fluid HMGB1 levels may correlate to decrease epidermal skin content, but this cannot be confirmed without matched samples. HMGB1 immunohistochemistry on SJS/TEN skin may potentially represent a diagnostic tool in SJS/TEN if further researched.

It is noteworthy to state that HMGB1 is not specific to SJS/TEN as plasma/serum levels are high in other diseases including epilepsy (Zhu et al., 2018), psoriasis vulgaris (Chen et al., 2013a) and HIV (Nowak et al., 2007). However, it is important to understand the relevance of HMGB1 in SJS/TEN disease. Research on the potential clinical utility of HMGB1 in SJS/TEN pathology is still not substantial compared to granulysin in the sense that HMGB1 secretion from PBMCs isolated from SJS/TEN has not been reported. It will be interesting to see how PBMC derived HMGB1 interacts with immune cells and perhaps if there is any cytotoxic action on keratinocytes *in vitro* similar to granulysin action as demonstrated by Chung et al (Chung et al., 2008).

Nitric oxide (NO) is implicated in the damage of the epidermis and there is a prominent epidermal expression of iNOS in SJS/TEN skin biopsy samples (Lerner et

al., 2000). To understand the implications of NO on keratinocyte death, keratinocytes were treated with NOC-18 *in vitro*. Our results demonstrated that NO killed keratinocytes by both apoptosis and necrosis and promoted the translocation of HMGB1 from nucleus from cytosol and to extracellular space in a dose-dependent fashion (chapter 3). This implies that NO expression and production in the epidermis in SJS/TEN may be contributing to HMGB1 exit from the nucleus. Furthermore, our data also revealed a dose-dependent release of HMGB1 into supernatants. The understanding of nitric oxide in SJS/TEN pathogenesis has been advanced by the revelation that NO may also be triggering keratinocyte necrosis and consequently inflammation due to HMGB1 release (Figure 6.1). Although it appears likely that MLKL driven necroptosis may also have a role in NO action but this would require further investigation.

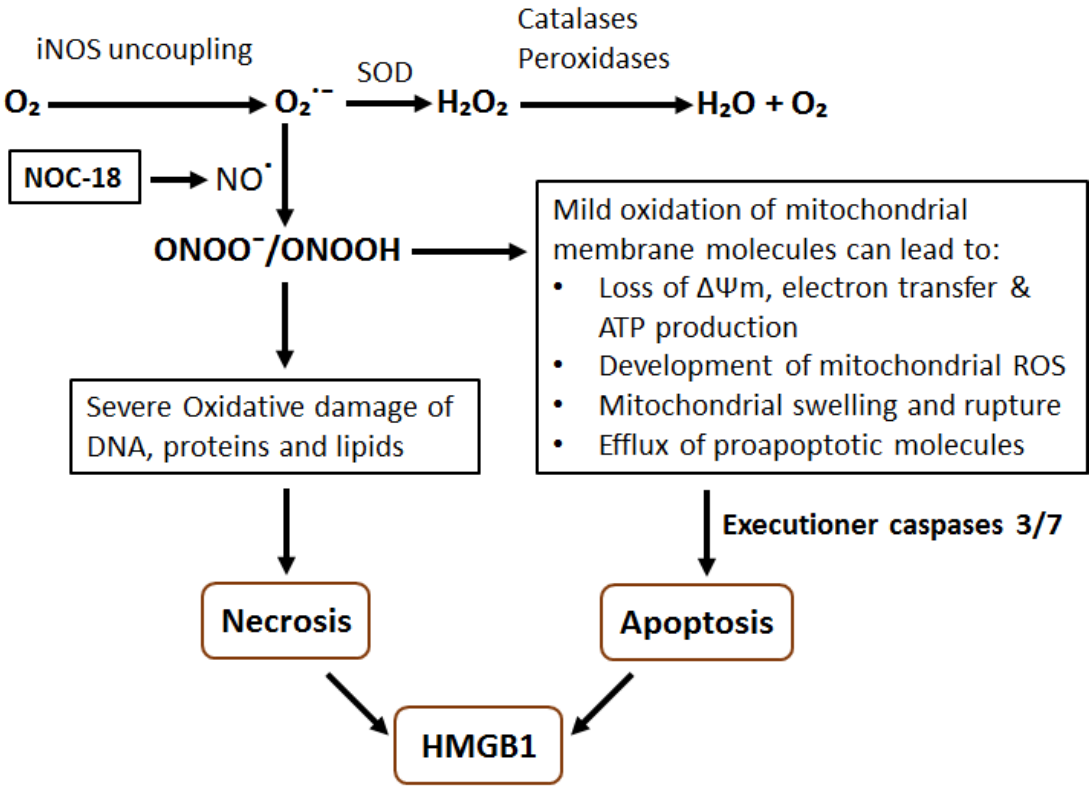

Figure 6.1: Reactive nitrogen species (RNS) generated via nitric oxide and resulting downstream signalling. NOC-18 derived NO caused keratinocyte apoptosis and necrosis both of which contributed to HMGB1 release.

Significant advances have been made in tumour necrosis factor alpha (TNF-α) biology and signalling. TNF-α is thought to play a key role in SJS/TEN pathology as levels are high in both serum and blister-fluid samples taken from SJS/TEN patients (Wang et al., 2018c) (Correia et al., 2002a). Our TNF-α data demonstrated for the first time that TNF-α induced necroptosis contributed significantly more to HMGB1 supernatant levels compared to TNF-α mediated apoptosis in keratinocytes (chapter 4) (Figure 6.2). This finding has an important implication. It shows that inhibition of TNF-α may not only prevent keratinocyte death by apoptosis and necroptosis but also prevent HMGB1 release and the further inflammation that this may potentially cause. The chapter findings collectively suggest that TNF-α is an

important player both in the mechanisms of keratinocyte apoptosis and necroptosis and potentially in inflammation through necroptosis mediated HMGB1 release. Thus further highlighting TNF-α as a possible cause of the elevated serum HMGB1 observed in chapter 2.

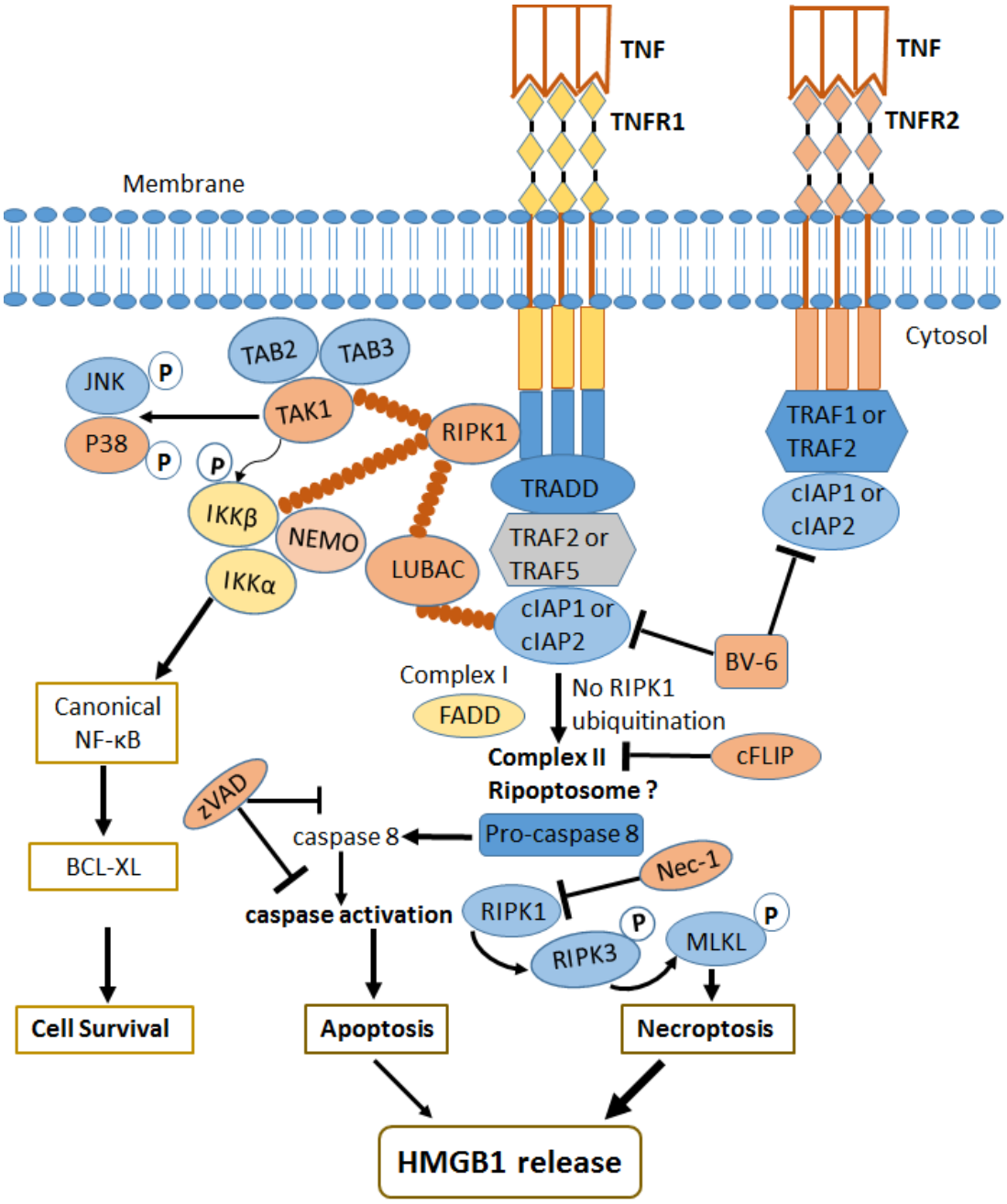

Figure 6.2: Activation of TNF-α leads to apoptosis and necroptosis in keratinocytes and keratinocyte necroptosis drives substantially higher HMGB1 release. In keratinocytes, treatment with TNF-α triggered both caspase dependent apoptosis and RIPK1-dependent necroptosis. TNF-α induced Keratinocyte necroptosis contributed substantially more to HMGB1 supernatant levels.

Chapter four has shown the importance of necroptosis driven by TNF-α on keratinocyte killing and HMGB1 release. Necroptosis has been reported to play a

vital role in SJS/TEN pathology (Panayotova-Dimitrova et al., 2015) (Kim et al., 2015b). Necroptosis is a form of regulated necrosis that has received much attention in recent times. The key regulators of necroptosis are RIPK1, RIPK3 and the terminal MLKL (Vandenabeele et al., 2010a) (Vandenabeele et al., 2010b) (Petrie et al., 2018). Taking advantage of molecular cloning tools, human RIPK3, MLKL and Bak tet-inducible constructs were made and stably expressed in the HaCaT cell line. Interestingly, human RIPK3 was shown for the first time to undergo spontaneous activation and that spontaneously activated RIPK3 resulted in keratinocyte death (Chapter 5). Our data also revealed convincingly for the first time that RIPK3 induction produced both caspase-dependent apoptosis and MLKL-dependent necroptosis (Figure 6.3).

Evidence from PARP cleavage, caspases 3 and 7 analyses including zVAD rescue of RIPK3 induced HaCaT death were used to substantiate the involvement of caspase in the mechanisms of RIPK3 mediated keratinocyte death. This is a highly significant finding. It challenges the long-held believe that necroptosis is caspase-independent; as such the mechanisms associated with human RIPK3 death pathway signalling should be investigated in other cell lines. Our data might imply that RIPK3 SJS/TEN lesional skin upregulation demonstrated in previous reports (Panayotova-Dimitrova et al., 2015) (Kim et al., 2015b) could play an important role in SJS/TEN pathogenesis through the dual function of activating both necroptotic and apoptotic epidermal keratinocyte death.

MLKL is an established substrate of RIPK3 (Hildebrand et al., 2014b). It appears to be important in the necroptotic death of keratinocytes in SJS/TEN as increased

phosphorylated levels were observed indicating death signalling competent MLKL (Kim et al., 2015b). MLKL is an end-point effector of necroptosis and as expected, its induction was exclusively necroptotic in nature without a mixed death pathway signalling (Figure 6.3).

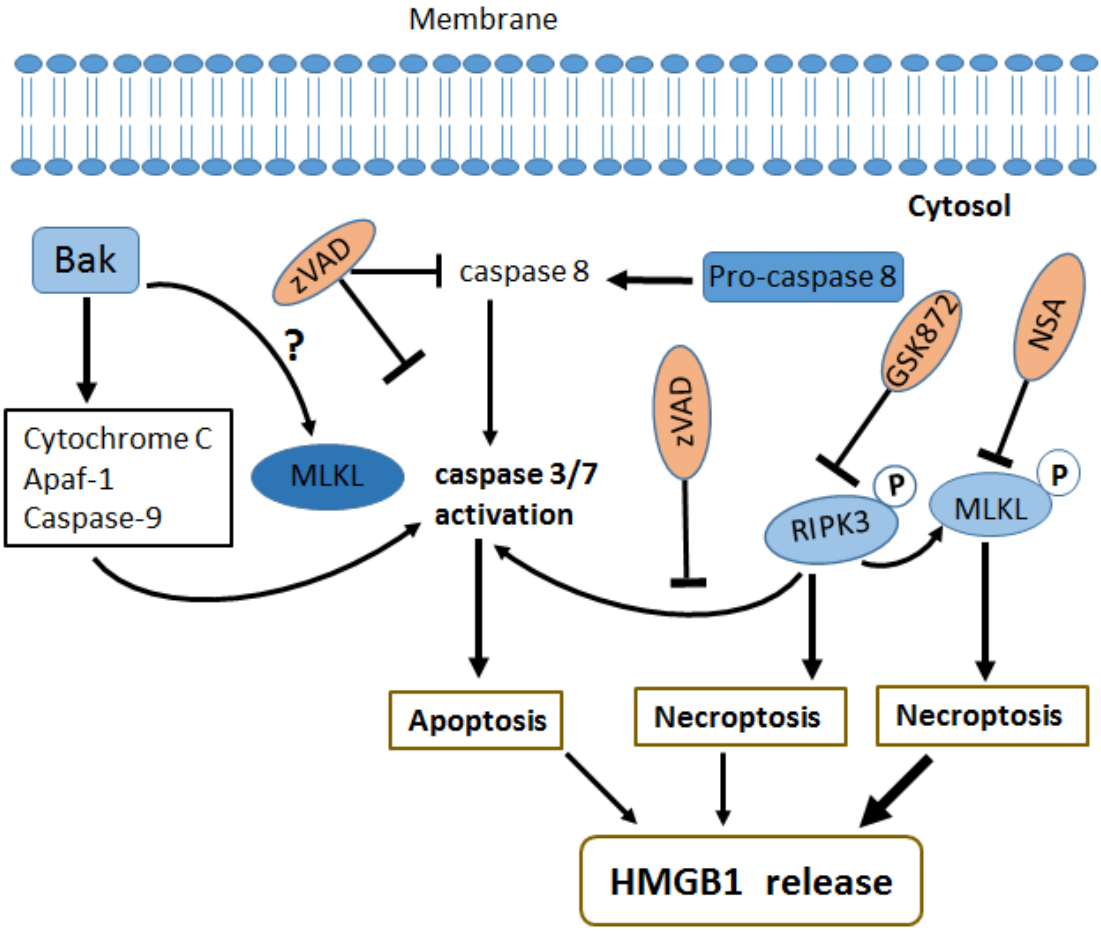

Figure 6.3: Characterisation of cell death effectors highlighting novel mechanisms in keratinocyte death pathways. Expression of Bak causes permeabilization of the mitochondrial membrane leading to formation of the apoptosome (a molecular complex containing cytochrome C and Apaf-1). The apoptosome activates caspase-9 leading to the activation of downstream pathways. RIPK3 induction triggered both caspase-dependent apoptosis and MLKL-dependent necroptosis. MLKL expression induced keratinocyte death in a purely caspase-independent manner as already established. Both Bak and RIPK3 induced keratinocyte killing resulted in a significant HMGB1 release. However, MLKL-induced keratinocyte necroptosis promoted twice as much HMGB1 release compared to both Bak and RIPK3 induced HaCaT death. Bak activation seemed to result in MLKL upregulation and blockade of MLKL using necrosulfonamide (NSA) tended to increase HaCaT viability in Bak expressing HaCaT cells.

Bak is a well characterised pro-apoptotic molecule in the mitochondrial apoptotic pathway. Indeed, it has been characterised for its apoptotic activity in several cell lines (Wang, 2001) (Elmore, 2007) (Adams and Cory, 2007). Surprisingly, our results appeared to suggest that Bak may also promote MLKL-dependent necroptosis to a lower degree (Figure 6.3). This warrants further investigations to determine and comprehend the proper connection if at all potentially existing between Bak and MLKL. Dondelinger *et al* reported that MLKL induces plasma membrane leakage as potently as Bax (Dondelinger et al., 2014). It is therefore logical to speculate an interaction of some sort might exist between Bak and MLKL. In addition, our data demonstrated that activation of MLKL-dependent necroptosis was responsible for significantly higher (over 2 fold in magnitude) HMGB1 release by keratinocytes compared both RIPK3 and Bak dependent keratinocyte death (Chapter 5) (Figure 6.3). Chapter 5 in conjunction with chapter 4 strongly suggest that necroptosis contributes more to extracellular HMGB1 levels than apoptosis.

Our findings discussed in chapter 5 can provide a useful platform to be built upon by future studies. There is need to identify potential unknown substrates for RIPK3 other than the already known MLKL. The most probable unknown downstream substrate for RIPK3 implicated by our results may likely be a molecule containing a CARD domain since CARD motif is required for the recruitment and activation of caspases. To do this, a gene-editing tool known as clustered regularly interspaced short palindromic repeats/CRISPR-associated endonuclease protein (CRISPR/Cas9) will be required to delete MLKL gene (exons) in HaCaT cells stably expressing human RIPK3 followed by a pull down assay to determine potential RIPK3 downstream binding partners (substrates).

The development of an assay to analyse post-translational modifications of HMGB1 will be very useful. This will allow us to determine the acetylation and redox status of both serum and supernatant derived extracellular HMGB1. HMGB1 sits at the junction between innate immunity and sterile inflammation (Andersson and Tracey, 2011) (Harris et al., 2012), and as such it is suitable for HMGB1 to be assessed for post-translational modifications in order to fully understand its full potential in SJS/TEN. It will be interesting to know if there are any differences in the post-translational modifications of necroptotic and apoptotic exited extracellular HMGB1. It has already been reported that apoptosis produces acetylated HMGB1 (Bell et al., 2006a) but no report on necroptosis. Given that HMGB1 can act as both a cytokine and a pro-inflammatory activator, we speculate that extracellular HMGB1 is a putative mediator and marker of keratinocyte damage in SJS/TEN (Figure 6.4). Thus, HMGB1 may represent a promising potential therapeutic target in SJS/TEN.

At the moment, there is no targeted treatment for SJS/TEN disease. Future development of targeted therapy for SJS/TEN will improve disease prognosis. Collectively, the findings of this thesis have advanced knowledge and understanding of keratinocyte cell death mechanisms and putative biomarkers of SJS/TEN which have provided insight into the development of therapeutic strategies relevant to SJS/TEN disease mechanisms.

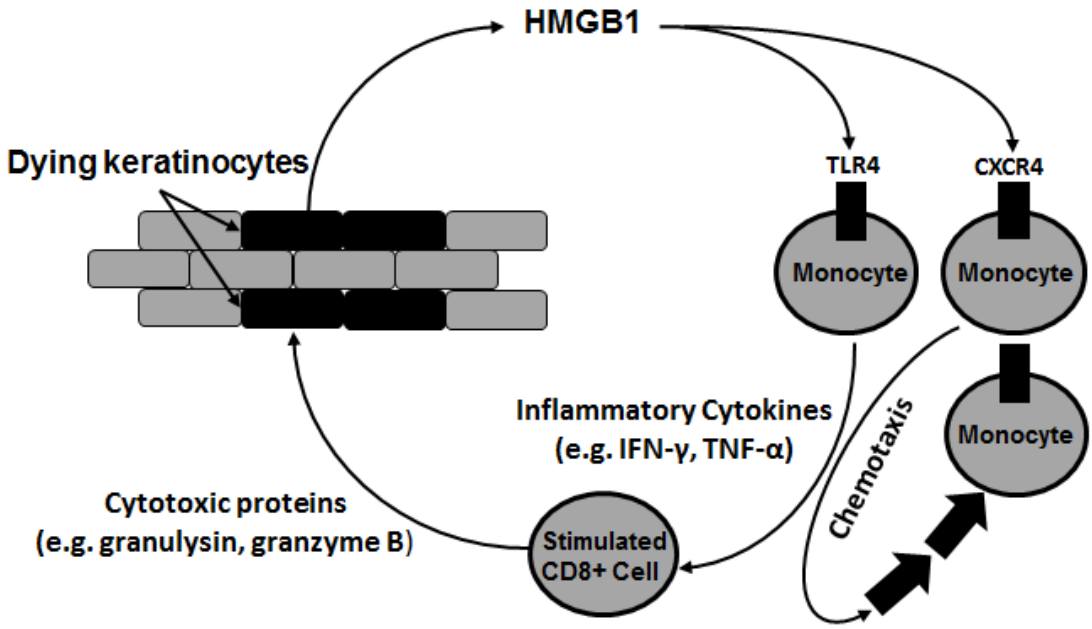

Figure 6.4: Extracellular HMGB1 mediates exacerbation of SJS/TEN pathogenesis as well as serving as a marker of keratinocyte injury. Initial death stimuli cause damage to keratinocytes leading to the release of HMGB1 to the extracellular space. Extracellular HMGB1 through its pro-inflammatory function can bind to TLR4 on monocytes promoting cytokine induction. Activated monocytes secrete pro-inflammatory cytokines such as IFN-γ and TNF-α. Secreted pro-inflammatory cytokines can stimulate CD8+ cells to produce cytotoxic proteins particularly granulysin and granzyme B to kill target keratinocytes by cell lysis (granulysin) and caspase-dependent killing (granzyme B) further exacerbating keratinocyte damage and as a result releasing more HMGB1 into the extracellular milieu. HMGB1 can also chemo-attractant through its binding to CXCR4 receptors on monocytes inducing chemotaxis and recruitment of more monocytes.

REFERENCES AND BIBLIOGRAPHY

ABE, R. 2015. Immunological response in Stevens-Johnson syndrome and toxic epidermal necrolysis. *J Dermatol,* 42**,** 42-8.

ABE, R., SHIMIZU, T., SHIBAKI, A., NAKAMURA, H., WATANABE, H. & SHIMIZU, H. 2003. Toxic epidermal necrolysis and Stevens-Johnson syndrome are induced by soluble Fas ligand. *Am J Pathol,* 162**,** 1515-20.

ADAM, J., PICHLER, W. J. & YERLY, D. 2011. Delayed drug hypersensitivity: models of T-cell stimulation. *Br J Clin Pharmacol,* 71**,** 701-7.

ADAMS, J. M. & CORY, S. 2007. The Bcl-2-regulated apoptosis switch: mechanism and therapeutic potential. *Current opinion in immunology,* 19**,** 488-496.

AGRESTI, A. & BIANCHI, M. E. 2003. HMGB proteins and gene expression. *Curr Opin Genet Dev,* 13**,** 170-8.

ALFIREVIC, A., JORGENSEN, A. L., WILLIAMSON, P. R., CHADWICK, D. W., PARK, B. K. & PIRMOHAMED, M. 2006. HLA-B locus in Caucasian patients with carbamazepine hypersensitivity. *Pharmacogenomics,* 7**,** 813-8.

ALOMAR, M. J. 2014. Factors affecting the development of adverse drug reactions (Review article). *Saudi Pharm J,* 22**,** 83-94.

ALTURKI, N. A., MCCOMB, S., ARIANA, A., RIJAL, D., KORNELUK, R. G., SUN, S.-C., ALNEMRI, E. & SAD, S. 2018. Triad3a induces the degradation of early necrosome to limit RipK1-dependent cytokine production and necroptosis. *Cell Death & Disease,* 9**,** 592.

AME, J. C., SPENLEHAUER, C. & DE MURCIA, G. 2004. The PARP superfamily. *Bioessays,* 26**,** 882-93.

AMSTUTZ, U., SHEAR, N. H., RIEDER, M. J., HWANG, S., FUNG, V., NAKAMURA, H., CONNOLLY, M. B., ITO, S. & CARLETON, B. C. 2014. Recommendations for HLA-B*15:02 and HLA-A*31:01 genetic testing to reduce the risk of carbamazepine-induced hypersensitivity reactions. *Epilepsia,* 55**,** 496-506.

ANDERSSON, U., ANTOINE, D. J. & TRACEY, K. J. 2014. The functions of HMGB1 depend on molecular localization and post-translational modifications. *Journal of Internal Medicine,* 276**,** 420-424.

ANDERSSON, U. & TRACEY, K. J. 2011. HMGB1 is a therapeutic target for sterile inflammation and infection. *Annu Rev Immunol,* 29**,** 139-62.

ANDERSSON, U., WANG, H., PALMBLAD, K., AVEBERGER, A. C., BLOOM, O., ERLANDSSON-HARRIS, H., JANSON, A., KOKKOLA, R., ZHANG, M., YANG, H. & TRACEY, K. J. 2000. High mobility group 1 protein (HMG-1) stimulates proinflammatory cytokine synthesis in human monocytes. *J Exp Med,* 192**,** 565-70.

ANDERSSON, U., YANG, H. & HARRIS, H. 2018. High-mobility group box 1 protein (HMGB1) operates as an alarmin outside as well as inside cells. *Semin Immunol,* 38**,** 40-48.

ARONSON, J. K. & FERNER, R. E. 2003. Joining the DoTS: new approach to classifying adverse drug reactions. *Bmj,* 327**,** 1222-5.

AUQUIER-DUNANT, A., MOCKENHAUPT, M., NALDI, L., CORREIA, O., SCHRODER, W. & ROUJEAU, J. C. 2002. Correlations between clinical patterns and causes of erythema multiforme majus, Stevens-Johnson syndrome, and toxic epidermal necrolysis: results of an international prospective study. *Arch Dermatol,* 138**,** 1019-24.

BAL-PRICE, A., BORUTAITE, V. & BROWN, G. C. 1999. Mitochondria mediate nitric oxide-induced cell death. *Ann N Y Acad Sci,* 893**,** 376-8.

BAL-PRICE, A. & BROWN, G. C. 2000. Nitric-oxide-induced necrosis and apoptosis in PC12 cells mediated by mitochondria. *J Neurochem,* 75**,** 1455-64.

BARKER, J. N., MITRA, R. S., GRIFFITHS, C. E., DIXIT, V. M. & NICKOLOFF, B. J. 1991. Keratinocytes as initiators of inflammation. *Lancet,* 337**,** 211-4.

BASTUJI-GARIN, S., FOUCHARD, N., BERTOCCHI, M., ROUJEAU, J. C., REVUZ, J. & WOLKENSTEIN, P. 2000. SCORTEN: a severity-of-illness score for toxic epidermal necrolysis. *J Invest Dermatol,* 115**,** 149-53.

BASTUJI-GARIN, S., RZANY, B., STERN, R. S., SHEAR, N. H., NALDI, L. & ROUJEAU, J. C. 1993. Clinical classification of cases of toxic epidermal necrolysis, Stevens-Johnson syndrome, and erythema multiforme. *Arch Dermatol,* 129**,** 92-6.

BECQUEMONT, L. 2009. Pharmacogenomics of adverse drug reactions: practical applications and perspectives. *Pharmacogenomics,* 10**,** 961-9.

BEDOUI, S., HEATH, W. R. & MUELLER, S. N. 2016. CD4(+) T-cell help amplifies innate signals for primary CD8(+) T-cell immunity. *Immunol Rev,* 272**,** 52-64.

BEELER, A., ZACCARIA, L., KAWABATA, T., GERBER, B. O. & PICHLER, W. J. 2008. CD69 upregulation on T cells as an in vitro marker for delayed-type drug hypersensitivity. *Allergy,* 63**,** 181-8.

BELL, C. C., FAULKNER, L., MARTINSSON, K., FARRELL, J., ALFIREVIC, A., TUGWOOD, J., PIRMOHAMED, M., NAISBITT, D. J. & PARK, B. K. 2013. T-cells from HLA-B*57:01+ human subjects are activated with abacavir through two independent pathways and induce cell death by multiple mechanisms. *Chem Res Toxicol,* 26**,** 759-66.

BELL, C. W., JIANG, W., CHARLES F. REICH, I. & PISETSKY, D. S. 2006a. The extracellular release of HMGB1 during apoptotic cell death. *American Journal of Physiology-Cell Physiology,* 291**,** C1318-C1325.

BELL, C. W., JIANG, W., REICH, C. F., 3RD & PISETSKY, D. S. 2006b. The extracellular release of HMGB1 during apoptotic cell death. *Am J Physiol Cell Physiol,* 291**,** C1318-25.

BELMOKHTAR, C. A., HILLION, J. & SÉGAL-BENDIRDJIAN, E. 2001. Staurosporine induces apoptosis through both caspase-dependent and caspase-independent mechanisms. *Oncogene,* 20**,** 3354.

BERGAMASCHI, D., VOSSENKAMPER, A., LEE, W. Y. J., WANG, P., BOCHUKOVA, E. & WARNES, G. 2019. Simultaneous polychromatic flow cytometric detection of multiple forms of regulated cell death. *Apoptosis*.

BERTRAND, M. J., LIPPENS, S., STAES, A., GILBERT, B., ROELANDT, R., DE MEDTS, J., GEVAERT, K., DECLERCQ, W. & VANDENABEELE, P. 2011. cIAP1/2 are direct E3 ligases conjugating diverse types of ubiquitin chains to receptor interacting proteins kinases 1 to 4 (RIP1-4). *PLoS One,* 6**,** e22356.

BERTRAND, M. J., MILUTINOVIC, S., DICKSON, K. M., HO, W. C., BOUDREAULT, A., DURKIN, J., GILLARD, J. W., JAQUITH, J. B., MORRIS, S. J. & BARKER, P. A. 2008. cIAP1 and cIAP2 facilitate cancer cell survival by functioning as E3 ligases that promote RIP1 ubiquitination. *Mol Cell,* 30**,** 689-700.

BHARADWAJ, M., ILLING, P., THEODOSSIS, A., PURCELL, A. W., ROSSJOHN, J. & MCCLUSKEY, J. 2012. Drug hypersensitivity and human leukocyte antigens of the major histocompatibility complex. *Annu Rev Pharmacol Toxicol,* 52**,** 401-31.

BIANCHI, M. E. & MANFREDI, A. A. 2007. High-mobility group box 1 (HMGB1) protein at the crossroads between innate and adaptive immunity. *Immunol Rev,* 220**,** 35-46.

BIRNBAUM, M. E., MENDOZA, J. L., SETHI, D. K., DONG, S., GLANVILLE, J., DOBBINS, J., OZKAN, E., DAVIS, M. M., WUCHERPFENNIG, K. W. & GARCIA, K. C. 2014. Deconstructing the peptide-MHC specificity of T cell recognition. *Cell,* 157**,** 1073-87.

BLUM, J. S., WEARSCH, P. A. & CRESSWELL, P. 2013. Pathways of antigen processing. *Annu Rev Immunol,* 31**,** 443-73.

BÖHM, R. & CASCORBI, I. 2016. Pharmacogenetics and Predictive Testing of Drug Hypersensitivity Reactions. *Frontiers in pharmacology,* 7**,** 396-396.

BONALDI, T., TALAMO, F., SCAFFIDI, P., FERRERA, D., PORTO, A., BACHI, A., RUBARTELLI, A., AGRESTI, A. & BIANCHI, M. E. 2003. Monocytic cells hyperacetylate chromatin protein HMGB1 to redirect it towards secretion. *Embo j,* 22**,** 5551-60.

BOS, J. D. & KAPSENBERG, M. L. 1993. The skin immune system: progress in cutaneous biology. *Immunol Today,* 14**,** 75-8.

BOSCA, L. & HORTELANO, S. 1999. Mechanisms of nitric oxide-dependent apoptosis: involvement of mitochondrial mediators. *Cell Signal,* 11**,** 239-44.

BOULARES, A. H., YAKOVLEV, A. G., IVANOVA, V., STOICA, B. A., WANG, G., IYER, S. & SMULSON, M. 1999. Role of Poly(ADP-ribose) Polymerase (PARP) Cleavage in Apoptosis: CASPASE 3-RESISTANT PARP MUTANT INCREASES RATES OF APOPTOSIS IN TRANSFECTED CELLS. *Journal of Biological Chemistry,* 274**,** 22932-22940.

BROCKHAUS, F. & BRUNE, B. 1998. U937 apoptotic cell death by nitric oxide: Bcl-2 downregulation and caspase activation. *Exp Cell Res,* 238**,** 33-41.

BROOKES, P. S., YOON, Y., ROBOTHAM, J. L., ANDERS, M. W. & SHEU, S. S. 2004. Calcium, ATP, and ROS: a mitochondrial love-hate triangle. *Am J Physiol Cell Physiol,* 287**,** C817-33.

BROWN, G. C. & BORUTAITE, V. 2001. Nitric oxide, mitochondria, and cell death. *IUBMB Life,* 52**,** 189-95.

BRÜNE, B., VON KNETHEN, A. & SANDAU, K. B. 1998. Nitric oxide and its role in apoptosis. *European Journal of Pharmacology,* 351**,** 261-272.

BRUNELLE, J. K. & LETAI, A. 2009. Control of mitochondrial apoptosis by the Bcl-2 family. *J Cell Sci,* 122**,** 437-41.

CARR, D. F., CHAPONDA, M., JORGENSEN, A. L., CASTRO, E. C., VAN OOSTERHOUT, J. J., KHOO, S. H., LALLOO, D. G., HEYDERMAN, R. S., ALFIREVIC, A. & PIRMOHAMED, M. 2013. Association of

human leukocyte antigen alleles and nevirapine hypersensitivity in a Malawian HIV-infected population. *Clin Infect Dis,* 56**,** 1330-9.

CASTREJON, J. L., LAVERGNE, S. N., EL-SHEIKH, A., FARRELL, J., MAGGS, J. L., SABBANI, S., O'NEILL, P. M., PARK, B. K. & NAISBITT, D. J. 2010. Metabolic and chemical origins of cross-reactive immunological reactions to arylamine benzenesulfonamides: T-cell responses to hydroxylamine and nitroso derivatives. *Chem Res Toxicol,* 23**,** 184-92.

CHARLI-JOSEPH, Y., LIMA, G., RAMOS-BELLO, D., AGUILAR, D., OROZCO-TOPETE, R. & LLORENTE, L. 2013. Genetic association of IFN-gamma +874T/A polymorphism in Mexican patients with drug-induced Stevens-Johnson syndrome/toxic epidermal necrolysis. *Arch Dermatol Res,* 305**,** 353-7.

CHEN, L. & FLIES, D. B. 2013. Molecular mechanisms of T cell co-stimulation and co-inhibition. *Nat Rev Immunol,* 13**,** 227-42.

CHEN, T., GUO, Z. P., LI, L., WANG, L., JIA, R. Z., CAO, N., QIN, S. & LI, M. M. 2013a. Increased HMGB1 serum levels and altered HMGB1 expression in patients with psoriasis vulgaris. *Arch Dermatol Res,* 305**,** 263-7.

CHEN, W., ZHOU, Z., LI, L., ZHONG, C.-Q., ZHENG, X., WU, X., ZHANG, Y., MA, H., HUANG, D., LI, W., XIA, Z. & HAN, J. 2013b. Diverse sequence determinants control human and mouse receptor interacting protein 3 (RIP3) and mixed lineage kinase domain-like (MLKL) interaction in necroptotic signaling. *The Journal of biological chemistry,* 288**,** 16247-16261.

CHEN, X., LI, W., REN, J., HUANG, D., HE, W.-T., SONG, Y., YANG, C., LI, W., ZHENG, X., CHEN, P. & HAN, J. 2014. Translocation of mixed lineage kinase domain-like protein to plasma membrane leads to necrotic cell death. *Cell Res,* 24**,** 105-121.

CHENG, Y., WANG, D., WANG, B., LI, H., XIONG, J., XU, S., CHEN, Q., TAO, K., YANG, X., ZHU, Y. & HE, S. 2017. HMGB1 translocation and release mediate cigarette smoke-induced pulmonary inflammation in mice through a TLR4/MyD88-dependent signaling pathway. *Mol Biol Cell,* 28**,** 201-209.

CHESSMAN, D., KOSTENKO, L., LETHBORG, T., PURCELL, A. W., WILLIAMSON, N. A., CHEN, Z., KJER-NIELSEN, L., MIFSUD, N. A., TAIT, B. D., HOLDSWORTH, R., ALMEIDA, C. A., NOLAN, D., MACDONALD, W. A., ARCHBOLD, J. K., KELLERHER, A. D., MARRIOTT, D., MALLAL, S., BHARADWAJ, M., ROSSJOHN, J. & MCCLUSKEY, J. 2008. Human leukocyte antigen class I-restricted

activation of CD8+ T cells provides the immunogenetic basis of a systemic drug hypersensitivity. *Immunity,* 28**,** 822-32.

CHIKH, A., SANZÀ, P., RAIMONDI, C., AKINDURO, O., WARNES, G., CHIORINO, G., BYRNE, C., HARWOOD, C. A. & BERGAMASCHI, D. 2014. iASPP is a novel autophagy inhibitor in keratinocytes. *Journal of Cell Science,* 127**,** 3079.

CHRISTOFFERSON, D. E., LI, Y., HITOMI, J., ZHOU, W., UPPERMAN, C., ZHU, H., GERBER, S. A., GYGI, S. & YUAN, J. 2012. A novel role for RIP1 kinase in mediating TNFalpha production. *Cell Death Dis,* 3**,** e320.

CHUNG, W. H., HUNG, S. I., HONG, H. S., HSIH, M. S., YANG, L. C., HO, H. C., WU, J. Y. & CHEN, Y. T. 2004. A marker for Stevens-Johnson syndrome. *Nature,* 428**,** 486.

CHUNG, W. H., HUNG, S. I., YANG, J. Y., SU, S. C., HUANG, S. P., WEI, C. Y., CHIN, S. W., CHIOU, C. C., CHU, S. C., HO, H. C., YANG, C. H., LU, C. F., WU, J. Y., LIAO, Y. D. & CHEN, Y. T. 2008. Granulysin is a key mediator for disseminated keratinocyte death in Stevens-Johnson syndrome and toxic epidermal necrolysis. *Nat Med,* 14**,** 1343-50.

COHEN, N. R., GARG, S. & BRENNER, M. B. 2009. Antigen Presentation by CD1 Lipids, T Cells, and NKT Cells in Microbial Immunity. *Adv Immunol,* 102**,** 1-94.

COLOMBO, I., SANGIOVANNI, E., MAGGIO, R., MATTOZZI, C., ZAVA, S., CORBETT, Y., FUMAGALLI, M., CARLINO, C., CORSETTO, P. A., SCACCABAROZZI, D., CALVIERI, S., GISMONDI, A., TARAMELLI, D. & DELL'AGLI, M. 2017. HaCaT Cells as a Reliable In Vitro Differentiation Model to Dissect the Inflammatory/Repair Response of Human Keratinocytes. *Mediators of inflammation,* 2017**,** 7435621-7435621.

COOK, W. D., MOUJALLED, D. M., RALPH, T. J., LOCK, P., YOUNG, S. N., MURPHY, J. M. & VAUX, D. L. 2014. RIPK1- and RIPK3-induced cell death mode is determined by target availability. *Cell Death Differ,* 21**,** 1600-12.

COOMBS, R. & GELL, P. 1976. Classification of allergic reactions responsible for clinical hypersensitivity and disease. *clinical Aspects of Immunology.* New York: Oxford University Press.

CORREIA, O., DELGADO, L., BARBOSA, I. L., CAMPILHO, F. & FLEMING-TORRINHA, J. 2002a. Increased interleukin 10, tumor necrosis factor alpha, and interleukin 6 levels in blister fluid of toxic epidermal necrolysis. *J Am Acad Dermatol,* 47**,** 58-62.

CORREIA, O., DELGADO, L., RAMOS, J. P., RESENDE, C. & TORRINHA, J. A. 1993. Cutaneous T-cell recruitment in toxic epidermal necrolysis. Further evidence of CD8+ lymphocyte involvement. *Arch Dermatol,* 129**,** 466-8.

CORREIA, O., DELGADO, L., ROUJEAU, J. C., LE CLEACH, L. & FLEMING-TORRINHA, J. A. 2002b. Soluble interleukin 2 receptor and interleukin 1alpha in toxic epidermal necrolysis: a comparative analysis of serum and blister fluid samples. *Arch Dermatol,* 138**,** 29-32.

CREAMER, D., WALSH, S. A., DZIEWULSKI, P., EXTON, L. S., LEE, H. Y., DART, J. K., SETTERFIELD, J., BUNKER, C. B., ARDERN-JONES, M. R., WATSON, K. M., WONG, G. A., PHILIPPIDOU, M., VERCUEIL, A., MARTIN, R. V., WILLIAMS, G., SHAH, M., BROWN, D., WILLIAMS, P., MOHD MUSTAPA, M. F. & SMITH, C. H. 2016. U.K. guidelines for the management of Stevens-Johnson syndrome/toxic epidermal necrolysis in adults 2016. *Br J Dermatol,* 174**,** 1194-227.

D'AMOURS, D., DESNOYERS, S., D'SILVA, I. & POIRIER, G. G. 1999. Poly(ADP-ribosyl)ation reactions in the regulation of nuclear functions. *Biochem J,* 342 (Pt 2)**,** 249-68.

DANIAL, N. N. & KORSMEYER, S. J. 2004. Cell Death: Critical Control Points. *Cell,* 116**,** 205-219.

DANIELA, B.-G., THOMAS, R. & KOLB-BACHOFEN, V. 1998. Nitric Oxide in Human Skin: Current Status and Future Prospects. *Journal of Investigative Dermatology,* 110**,** 1-7.

DAVIDOVICH, P., KEARNEY, C. J. & MARTIN, S. J. 2014. Inflammatory outcomes of apoptosis, necrosis and necroptosis. *Biol Chem,* 395**,** 1163-71.

DEGENHARDT, K., SUNDARARAJAN, R., LINDSTEN, T., THOMPSON, C. & WHITE, E. 2002. Bax and Bak independently promote cytochrome C release from mitochondria. *J Biol Chem,* 277**,** 14127-34.

DENG, A., CHEN, S., LI, Q., LYU, S. C., CLAYBERGER, C. & KRENSKY, A. M. 2005. Granulysin, a cytolytic molecule, is also a chemoattractant and proinflammatory activator. *J Immunol,* 174**,** 5243-8.

DILLON, CHRISTOPHER P., WEINLICH, R., RODRIGUEZ, DIEGO A., CRIPPS, JAMES G., QUARATO, G., GURUNG, P., VERBIST, KATHERINE C., BREWER, TAYLOR L., LLAMBI, F., GONG, Y.-N., JANKE, LAURA J., KELLIHER, MICHELLE A., KANNEGANTI, T.-D. & GREEN, DOUGLAS R. 2014. RIPK1 Blocks Early Postnatal Lethality Mediated by Caspase-8 and RIPK3. *Cell,* 157**,** 1189-1202.

DONDELINGER, Y., DECLERCQ, W., MONTESSUIT, S., ROELANDT, R., GONCALVES, A., BRUGGEMAN, I., HULPIAU, P., WEBER, K., SEHON, CLARK A., MARQUIS, ROBERT W., BERTIN, J., GOUGH, PETER J., SAVVIDES, S., MARTINOU, J.-C., BERTRAND, MATHIEU J. M. & VANDENABEELE, P. 2014. MLKL Compromises Plasma Membrane Integrity by Binding to Phosphatidylinositol Phosphates. *Cell Reports,* 7**,** 971-981.

DUEBER, E. C., SCHOEFFLER, A. J., LINGEL, A., ELLIOTT, J. M., FEDOROVA, A. V., GIANNETTI, A. M., ZOBEL, K., MAURER, B., VARFOLOMEEV, E., WU, P., WALLWEBER, H. J. A., HYMOWITZ, S. G., DESHAYES, K., VUCIC, D. & FAIRBROTHER, W. J. 2011. Antagonists Induce a Conformational Change in cIAP1 That Promotes Autoubiquitination. *Science,* 334**,** 376-380.

DURAN-FIGUEROA, N., BADILLO-CORONA, J. A., NAISBITT, D. J. & CASTREJON-FLORES, J. L. 2015. Towards the development of mechanism-based biomarkers to diagnose drug hypersensitivity. *Toxicology Research,* 4**,** 777-795.

EDINGER, A. L. & THOMPSON, C. B. 2004. Death by design: apoptosis, necrosis and autophagy. *Curr Opin Cell Biol,* 16**,** 663-9.

EDWARDS, I. R. & ARONSON, J. K. 2000. Adverse drug reactions: definitions, diagnosis, and management. *Lancet,* 356**,** 1255-9.

EL-MESERY, M., SHAKER, M. E. & ELGAML, A. 2016. The SMAC mimetic BV6 induces cell death and sensitizes different cell lines to TNF-α and TRAIL-induced apoptosis. *Experimental Biology and Medicine,* 241**,** 2015-2022.

EL DARZI, E., BAZZI, S., DAOUD, S., ECHTAY, K. S. & BAHR, G. M. 2017. Differential regulation of surface receptor expression, proliferation, and apoptosis in HaCaT cells stimulated with interferon-γ, interleukin-4, tumor necrosis factor-α, or muramyl dipeptide. *International Journal of Immunopathology and Pharmacology,* 30**,** 130-145.

ELMORE, S. 2007. Apoptosis: a review of programmed cell death. *Toxicol Pathol,* 35**,** 495-516.

ELSHEIKH, A., LAVERGNE, S. N., CASTREJON, J. L., FARRELL, J., WANG, H., SATHISH, J., PICHLER, W. J., PARK, B. K. & NAISBITT, D. J. 2010. Drug antigenicity, immunogenicity, and costimulatory signaling: evidence for formation of a functional antigen through immune cell metabolism. *Journal of immunology (Baltimore, Md. : 1950),* 185**,** 6448-6460.

EU 2010. Directive 2010/84/EU of the Europian Parliament and of the Council. *In:* UNION, E. (ed.). Strasbourg: In: UNION, E.P.A.T.C.O.T.E (ed.).

FEHNIGER, T. A. & CALIGIURI, M. A. 2001. Interleukin 15: biology and relevance to human disease. *Blood,* 97**,** 14-32.

FELTHAM, R., BETTJEMAN, B., BUDHIDARMO, R., MACE, P. D., SHIRLEY, S., CONDON, S. M., CHUNDURU, S. K., MCKINLAY, M. A., VAUX, D. L., SILKE, J. & DAY, C. L. 2011. Smac Mimetics Activate the E3 Ligase Activity of cIAP1 Protein by Promoting RING Domain Dimerization. *The Journal of Biological Chemistry,* 286**,** 17015-17028.

FEOKTISTOVA, M., GESERICK, P., KELLERT, B., DIMITROVA, DIANA P., LANGLAIS, C., HUPE, M., CAIN, K., MACFARLANE, M., HÄCKER, G. & LEVERKUS, M. 2011. cIAPs Block Ripoptosome Formation, a RIP1/Caspase-8 Containing Intracellular Cell Death Complex Differentially Regulated by cFLIP Isoforms. *Molecular Cell,* 43**,** 449-463.

FEOKTISTOVA, M., WALLBERG, F., TENEV, T., GESERICK, P., LEVERKUS, M. & MEIER, P. 2016. Techniques to Distinguish Apoptosis from Necroptosis. *Cold Spring Harb Protoc,* 2016**,** pdb.top070375.

FERRARI, S., FINELLI, P., ROCCHI, M. & BIANCHI, M. E. 1996. The active gene that encodes human high mobility group 1 protein (HMG1) contains introns and maps to chromosome 13. *Genomics,* 35**,** 367-71.

FERRELL, P. B., JR. & MCLEOD, H. L. 2008. Carbamazepine, HLA-B*1502 and risk of Stevens-Johnson syndrome and toxic epidermal necrolysis: US FDA recommendations. *Pharmacogenomics,* 9**,** 1543-6.

FÖRSTERMANN, U. & SESSA, W. C. 2012. Nitric oxide synthases: regulation and function. *European heart journal,* 33**,** 829-837d.

FRENCH, L. E. 2006. Toxic epidermal necrolysis and Stevens Johnson syndrome: our current understanding. *Allergol Int,* 55**,** 9-16.

FREY, N., JOSSI, J., BODMER, M., BIRCHER, A., JICK, S. S., MEIER, C. R. & SPOENDLIN, J. 2017. The Epidemiology of Stevens-Johnson Syndrome and Toxic Epidermal Necrolysis in the UK. *Journal of Investigative Dermatology,* 137**,** 1240-1247.

FUJITA, H., MATSUKURA, S., WATANABE, T., KOMITSU, N., WATANABE, Y., TAKAHASHI, Y., KAMBARA, T., IKEZAWA, Z. & AIHARA, M. 2014. The serum level of HMGB1 (high mobility group box 1 protein) is preferentially high in drug-induced hypersensitivity

syndrome/drug reaction with eosinophilia and systemic symptoms. *British Journal of Dermatology,* 171**,** 1585-1588.

FUKUO, K., HATA, S., SUHARA, T., NAKAHASHI, T., SHINTO, Y., TSUJIMOTO, Y., MORIMOTO, S. & OGIHARA, T. 1996. Nitric oxide induces upregulation of Fas and apoptosis in vascular smooth muscle. *Hypertension,* 27**,** 823-6.

GALLUZZI, L., VITALE, I., ABRAMS, J. M., ALNEMRI, E. S., BAEHRECKE, E. H., BLAGOSKLONNY, M. V., DAWSON, T. M., DAWSON, V. L., EL-DEIRY, W. S., FULDA, S., GOTTLIEB, E., GREEN, D. R., HENGARTNER, M. O., KEPP, O., KNIGHT, R. A., KUMAR, S., LIPTON, S. A., LU, X., MADEO, F., MALORNI, W., MEHLEN, P., NUNEZ, G., PETER, M. E., PIACENTINI, M., RUBINSZTEIN, D. C., SHI, Y., SIMON, H. U., VANDENABEELE, P., WHITE, E., YUAN, J., ZHIVOTOVSKY, B., MELINO, G. & KROEMER, G. 2012. Molecular definitions of cell death subroutines: recommendations of the Nomenclature Committee on Cell Death 2012. *Cell Death Differ,* 19**,** 107-120.

GARDELLA, S., ANDREI, C., FERRERA, D., LOTTI, L. V., TORRISI, M. R., BIANCHI, M. E. & RUBARTELLI, A. 2002. The nuclear protein HMGB1 is secreted by monocytes via a non-classical, vesicle-mediated secretory pathway. *EMBO reports,* 3**,** 995-1001.

GAVIGAN, G. M., KANIGSBERG, N. D. & RAMIEN, M. L. 2018. Pediatric Stevens-Johnson Syndrome/Toxic Epidermal Necrolysis Halted by Etanercept. *J Cutan Med Surg,* 22**,** 514-515.

GENIN, E., CHEN, D. P., HUNG, S. I., SEKULA, P., SCHUMACHER, M., CHANG, P. Y., TSAI, S. H., WU, T. L., BELLON, T., TAMOUZA, R., FORTIER, C., TOUBERT, A., CHARRON, D., HOVNANIAN, A., WOLKENSTEIN, P., CHUNG, W. H., MOCKENHAUPT, M. & ROUJEAU, J. C. 2014. HLA-A*31:01 and different types of carbamazepine-induced severe cutaneous adverse reactions: an international study and meta-analysis. *Pharmacogenomics J,* 14**,** 281-8.

GENIN, E., SCHUMACHER, M., ROUJEAU, J. C., NALDI, L., LISS, Y., KAZMA, R., SEKULA, P., HOVNANIAN, A. & MOCKENHAUPT, M. 2011. Genome-wide association study of Stevens-Johnson Syndrome and Toxic Epidermal Necrolysis in Europe. *Orphanet J Rare Dis,* 6**,** 52.

GHOSH, R., GILDA, J. E. & GOMES, A. V. 2014. The necessity of and strategies for improving confidence in the accuracy of western blots. *Expert review of proteomics,* 11**,** 549-560.

GOLSTEIN, P. & KROEMER, G. 2007. Cell death by necrosis: towards a molecular definition. *Trends in Biochemical Sciences,* 32**,** 37-43.

GONG, H., ZULIANI, P., KOMURAVELLI, A., FAEDER, J. R. & CLARKE, E. M. 2010. Analysis and verification of the HMGB1 signaling pathway. *BMC Bioinformatics,* 11**,** S10.

GONZÁLEZ-HERRADA, C., RODRÍGUEZ-MARTÍN, S., CACHAFEIRO, L., LERMA, V., GONZÁLEZ, O., LORENTE, J. A., RODRÍGUEZ-MIGUEL, A., GONZÁLEZ-RAMOS, J., ROUSTAN, G., RAMÍREZ, E., BELLÓN, T., DE ABAJO, F. J., BELLÓN, T., CABAÑAS, R., CACHAFEIRO, L., GARCÍA DE LORENZO, A., GONZÁLEZ-RAMOS, J., HERNÁNDEZ, O., HERRANZ, P., RAMÍREZ, E., BRAVO, E. R., ALONSO, Y., ARAMBURU, J. A., CÁMARA, N., GONZÁLEZ, O., GONZÁLEZ-HERRADA, C., LAOSA, O., LORENTE, J. A., MOSCOSO, A., PAYARES, C., ROUSTAN, G., DE ABAJO, F. J., QUESADA, A., LERMA, V. & RODRÍGUEZ-MARTÍN, S. 2017. Cyclosporine Use in Epidermal Necrolysis Is Associated with an Important Mortality Reduction: Evidence from Three Different Approaches. *Journal of Investigative Dermatology,* 137**,** 2092-2100.

GOODWIN, G. H., SANDERS, C. & JOHNS, E. W. 1973. A new group of chromatin-associated proteins with a high content of acidic and basic amino acids. *Eur J Biochem,* 38**,** 14-9.

GUILLAUME, J. C., ROUJEAU, J. C., REVUZ, J., PENSO, D. & TOURAINE, R. 1987. The culprit drugs in 87 cases of toxic epidermal necrolysis (Lyell's syndrome). *Arch Dermatol,* 123**,** 1166-70.

HAO, Z. & MAK, T. W. 2010. Type I and Type II Pathways of Fas-mediated Apoptosis Are Differentially Controlled by XIAP. *Journal of Molecular Cell Biology,* 2**,** 63-64.

HARR, T. & FRENCH, L. E. 2010. Toxic epidermal necrolysis and Stevens-Johnson syndrome. *Orphanet Journal of Rare Diseases,* 5**,** 39-39.

HARRIS, H. E., ANDERSSON, U. & PISETSKY, D. S. 2012. HMGB1: a multifunctional alarmin driving autoimmune and inflammatory disease. *Nat Rev Rheumatol,* 8**,** 195-202.

HARRIS, V., JACKSON, C. & COOPER, A. 2016. Review of Toxic Epidermal Necrolysis. *International journal of molecular sciences,* 17**,** 2135.

HATA, A. N., ENGELMAN, J. A. & FABER, A. C. 2015. The BCL2 Family: Key Mediators of the Apoptotic Response to Targeted Anticancer Therapeutics. *Cancer discovery,* 5**,** 475-487.

HATHCOCK, K. S., LASZLO, G., PUCILLO, C., LINSLEY, P. & HODES, R. J. 1994. Comparative analysis of B7-1 and B7-2 costimulatory ligands: expression and function. *J Exp Med,* 180**,** 631-40.

HEIL, M. & LAND, W. G. 2014. Danger signals - damaged-self recognition across the tree of life. *Frontiers in plant science,* 5**,** 578-578.

HENNECKE, J. & WILEY, D. C. 2001. T Cell Receptor–MHC Interactions up Close. *Cell,* 104**,** 1-4.

HILDEBRAND, J. M., TANZER, M. C., LUCET, I. S., YOUNG, S. N., SPALL, S. K., SHARMA, P., PIEROTTI, C., GARNIER, J.-M., DOBSON, R. C. J., WEBB, A. I., TRIPAYDONIS, A., BABON, J. J., MULCAIR, M. D., SCANLON, M. J., ALEXANDER, W. S., WILKS, A. F., CZABOTAR, P. E., LESSENE, G., MURPHY, J. M. & SILKE, J. 2014a. Activation of the pseudokinase MLKL unleashes the four-helix bundle domain to induce membrane localization and necroptotic cell death. *Proceedings of the National Academy of Sciences,* 111**,** 15072-15077.

HILDEBRAND, J. M., TANZER, M. C., LUCET, I. S., YOUNG, S. N., SPALL, S. K., SHARMA, P., PIEROTTI, C., GARNIER, J. M., DOBSON, R. C., WEBB, A. I., TRIPAYDONIS, A., BABON, J. J., MULCAIR, M. D., SCANLON, M. J., ALEXANDER, W. S., WILKS, A. F., CZABOTAR, P. E., LESSENE, G., MURPHY, J. M. & SILKE, J. 2014b. Activation of the pseudokinase MLKL unleashes the four-helix bundle domain to induce membrane localization and necroptotic cell death. *Proc Natl Acad Sci U S A,* 111**,** 15072-7.

HOPPE, G., TALCOTT, K. E., BHATTACHARYA, S. K., CRABB, J. W. & SEARS, J. E. 2006. Molecular basis for the redox control of nuclear transport of the structural chromatin protein Hmgb1. *Exp Cell Res,* 312**,** 3526-38.

HOTZ, M. A., GONG, J., TRAGANOS, F. & DARZYNKIEWICZ, Z. 1994. Flow cytometric detection of apoptosis: comparison of the assays of in situ DNA degradation and chromatin changes. *Cytometry,* 15**,** 237-44.

HSU, H., SHU, H.-B., PAN, M.-G. & GOEDDEL, D. V. 1996. TRADD–TRAF2 and TRADD–FADD Interactions Define Two Distinct TNF Receptor 1 Signal Transduction Pathways. *Cell,* 84**,** 299-308.

HSU, H., XIONG, J. & GOEDDEL, D. V. 1995. The TNF receptor 1-associated protein TRADD signals cell death and NF-κB activation. *Cell,* 81**,** 495-504.

HU, C.-H., CHANG, N.-J., CHUANG, S.-S., YANG, J.-Y. & CHUNG, W.-H. 2015. Toxic epidermal necrolysis secondary to Mycoplasma pneumoniae and herpes simplex virus infection. *Formosan Journal of Surgery,* 48**,** 37-43.

HUANG, K., ZHANG, J., O'NEILL, K. L., GURUMURTHY, C. B., QUADROS, R. M., TU, Y. & LUO, X. 2016. Cleavage by Caspase 8 and Mitochondrial Membrane Association Activate the BH3-only Protein Bid during TRAIL-induced Apoptosis. *J Biol Chem,* 291**,** 11843-51.

HUNG, S. I., CHUNG, W. H., JEE, S. H., CHEN, W. C., CHANG, Y. T., LEE, W. R., HU, S. L., WU, M. T., CHEN, G. S., WONG, T. W., HSIAO, P. F., CHEN, W. H., SHIH, H. Y., FANG, W. H., WEI, C. Y., LOU, Y. H., HUANG, Y. L., LIN, J. J. & CHEN, Y. T. 2006. Genetic susceptibility to carbamazepine-induced cutaneous adverse drug reactions. *Pharmacogenetics and Genomics,* 16**,** 297-306.

HUNG, S. I., CHUNG, W. H., LIU, Z. S., CHEN, C. H., HSIH, M. S., HUI, R. C. Y., CHU, C. Y. & CHEN, Y. T. 2010. Common risk allele in aromatic antiepileptic-drug induced Stevens-Johnson syndrome and toxic epidermal necrolysis in Han Chinese. *Pharmacogenomics,* 11**,** 349-356.

HUNG, S. L., CHUNG, W. H., LIOU, L. B., CHU, C. C., LIN, M., HUANG, H. P., LIN, Y. L., LAN, J. L., YANG, L. C., HONG, H. S., CHEN, M. J., LAI, P. C., WU, M. S., CHU, C. Y., WANG, K. H., CHEN, C. H., FANN, C. S. J., WU, J. Y. & CHEN, Y. T. 2005. HLA-B*5801 allele as a genetic marker for severe cutaneous adverse reactions caused by allopurinol. *Proceedings of the National Academy of Sciences of the United States of America,* 102**,** 4134-4139.

HUR, J., ZHAO, C. & BAI, J. P. F. 2015. Systems Pharmacological Analysis of Drugs Inducing Stevens–Johnson Syndrome and Toxic Epidermal Necrolysis. *Chemical Research in Toxicology,* 28**,** 927-934.

ICHIHARA, A., WANG, Z., JINNIN, M., IZUNO, Y., SHIMOZONO, N., YAMANE, K., FUJISAWA, A., MORIYA, C., FUKUSHIMA, S., INOUE, Y. & IHN, H. 2014. Upregulation of miR-18a-5p contributes to epidermal necrolysis in severe drug eruptions. *J Allergy Clin Immunol,* 133**,** 1065-74.

IKEDA, H., TAKAHASHI, Y., YAMAZAKI, E., FUJIWARA, T., KANIWA, N., SAITO, Y., AIHARA, M., KASHIWAGI, M. & MURAMATSU, M. 2010. HLA class I markers in Japanese patients with carbamazepine-induced cutaneous adverse reactions. *Epilepsia,* 51**,** 297-300.

ILLING, P. T., VIVIAN, J. P., DUDEK, N. L., KOSTENKO, L., CHEN, Z., BHARADWAJ, M., MILES, J. J., KJER-NIELSEN, L., GRAS, S., WILLIAMSON, N. A., BURROWS, S. R., PURCELL, A. W., ROSSJOHN,

J. & MCCLUSKEY, J. 2012. Immune self-reactivity triggered by drug-modified HLA-peptide repertoire. *Nature,* 486**,** 554.

INACHI, S., MIZUTANI, H. & SHIMIZU, M. 1997. Epidermal apoptotic cell death in erythema multiforme and Stevens-Johnson syndrome. Contribution of perforin-positive cell infiltration. *Arch Dermatol,* 133**,** 845-9.

JANEWAY, C. A., TRAVERS, P. & WALPORT, M. 2001. *The major histocompatibility complex and its functions,* New York, Garland Science.

JANKO, C., FILIPOVIC, M., MUNOZ, L. E., SCHORN, C., SCHETT, G., IVANOVIC-BURMAZOVIC, I. & HERRMANN, M. 2014. Redox modulation of HMGB1-related signaling. *Antioxid Redox Signal,* 20**,** 1075-85.

JIANG, W., BELL, C. W. & PISETSKY, D. S. 2007. The Relationship between Apoptosis and High-Mobility Group Protein 1 Release from Murine Macrophages Stimulated with Lipopolysaccharide or Polyinosinic-Polycytidylic Acid. *The Journal of Immunology,* 178**,** 6495-6503.

JIANG, W. & PISETSKY, D. S. 2006. The role of IFN-alpha and nitric oxide in the release of HMGB1 by RAW 264.7 cells stimulated with polyinosinic-polycytidylic acid or lipopolysaccharide. *J Immunol,* 177**,** 3337-43.

JIANG, W. & PISETSKY, D. S. 2008. The Induction of HMGB1 Release from RAW 264.7 Cells by Transfected DNA. *Molecular immunology,* 45**,** 2038-2044.

JIN, Z. & EL-DEIRY, W. S. 2005. Overview of cell death signaling pathways. *Cancer Biology & Therapy,* 4**,** 147-171.

JOFFRE, O. P., SEGURA, E., SAVINA, A. & AMIGORENA, S. 2012. Cross-presentation by dendritic cells. *Nature Reviews Immunology,* 12**,** 557.

KACZMAREK, A., VANDENABEELE, P. & KRYSKO, DMITRI V. 2013. Necroptosis: The Release of Damage-Associated Molecular Patterns and Its Physiological Relevance. *Immunity,* 38**,** 209-223.

KAGAN, R. J., EDELMAN, L., SOLEM, L., SAFFLE, J. R. & GAMELLI, R. 2007. DRG 272: Does it Provide Adequate Burn Center Reimbursement for the Care of Patients With Stevens–Johnson Syndrome and Toxic Epidermal Necrolysis? *Journal of Burn Care & Research,* 28**,** 669-674.

KAISER, W. J., DALEY-BAUER, L. P., THAPA, R. J., MANDAL, P., BERGER, S. B., HUANG, C., SUNDARARAJAN, A., GUO, H., ROBACK, L., SPECK,

S. H., BERTIN, J., GOUGH, P. J., BALACHANDRAN, S. & MOCARSKI, E. S. 2014. RIP1 suppresses innate immune necrotic as well as apoptotic cell death during mammalian parturition. *Proceedings of the National Academy of Sciences,* 111**,** 7753-7758.

KAM, P. C. A. & FERCH, N. I. 2000. Apoptosis: mechanisms and clinical implications. *Anaesthesia,* 55**,** 1081-1093.

KANIWA, N., SAITO, Y., AIHARA, M., MATSUNAGA, K., TOHKIN, M., KUROSE, K., FURUYA, H., TAKAHASHI, Y., MURAMATSU, M., KINOSHITA, S., ABE, M., IKEDA, H., KASHIWAGI, M., SONG, Y., UETA, M., SOTOZONO, C., IKEZAWA, Z. & HASEGAWA, R. 2010. HLA-B*1511 is a risk factor for carbamazepine-induced Stevens-Johnson syndrome and toxic epidermal necrolysis in Japanese patients. *Epilepsia,* 51**,** 2461-2465.

KANIWA, N., SAITO, Y., AIHARA, M., MATSUNAGA, K., TOHKIN, M., KUROSE, K., SAWADA, J., FURUYA, H., TAKAHASHI, Y., MURAMATSU, M., KINOSHITA, S., ABE, M., IKEDA, H., KASHIWAGI, M., SONG, Y., UETA, M., SOTOZONO, C., IKEZAWA, Z. & HASEGAWA, R. 2008. HLA-B locus in Japanese patients with anti-epileptics and allopurinol-related Stevens-Johnson syndrome and toxic epidermal necrolysis. *Pharmacogenomics,* 9**,** 1617-22.

KANO, Y., HIRAHARA, K., MITSUYAMA, Y., TAKAHASHI, R. & SHIOHARA, T. 2007. Utility of the lymphocyte transformation test in the diagnosis of drug sensitivity: dependence on its timing and the type of drug eruption. *Allergy,* 62**,** 1439-44.

KAPOOR, S. 2013. Emerging new markers of toxic epidermal necrolysis. *J Intensive Care Med,* 28**,** 72.

KAZAMA, H., RICCI, J. E., HERNDON, J. M., HOPPE, G., GREEN, D. R. & FERGUSON, T. A. 2008. Induction of immunological tolerance by apoptotic cells requires caspase-dependent oxidation of high-mobility group box-1 protein. *Immunity,* 29**,** 21-32.

KAZEEM, G. R., COX, C., APONTE, J., MESSENHEIMER, J., BRAZELL, C., NELSEN, A. C., NELSON, M. R. & FOOT, E. 2009. High-resolution HLA genotyping and severe cutaneous adverse reactions in lamotrigine-treated patients. *Pharmacogenetics and Genomics,* 19**,** 661-665.

KERR, J. F., WYLLIE, A. H. & CURRIE, A. R. 1972. Apoptosis: a basic biological phenomenon with wide-ranging implications in tissue kinetics. *Br J Cancer,* 26**,** 239-57.

KIM, J. S., HE, L. & LEMASTERS, J. J. 2003. Mitochondrial permeability transition: a common pathway to necrosis and apoptosis. *Biochem Biophys Res Commun,* 304**,** 463-70.

KIM, M. Y., LIM, Y. Y., KIM, H. M., PARK, Y. M., KANG, H. & KIM, B. J. 2015a. Synergistic Inhibition of Tumor Necrosis Factor-Alpha-Stimulated Pro-Inflammatory Cytokine Expression in HaCaT Cells by a Combination of Rapamycin and Mycophenolic Acid. *Ann Dermatol,* 27**,** 32-9.

KIM, S. H., KIM, M., LEE, K. W., KIM, S. H., KANG, H. R., PARK, H. W. & JEE, Y. K. 2010. HLA-B*5901 is strongly associated with methazolamide-induced Stevens-Johnson syndrome/toxic epidermal necrolysis. *Pharmacogenomics,* 11**,** 879-884.

KIM, S. K., KIM, W. J., YOON, J. H., JI, J. H., MORGAN, M. J., CHO, H., KIM, Y. C. & KIM, Y. S. 2015b. Upregulated RIP3 Expression Potentiates MLKL Phosphorylation-Mediated Programmed Necrosis in Toxic Epidermal Necrolysis. *J Invest Dermatol,* 135**,** 2021-30.

KIRKHAM, N., PEACOCK, S. J. & JONES, D. B. 1990. Monoclonal antibody MAC 387 recognizes a myelomonocytic antigen shared by epithelial cells in inflammatory skin diseases. *Br J Dermatol,* 122**,** 61-9.

KO, T.-M., CHUNG, W.-H., WEI, C.-Y., SHIH, H.-Y., CHEN, J.-K., LIN, C.-H., CHEN, Y.-T. & HUNG, S.-I. 2011. Shared and restricted T-cell receptor use is crucial for carbamazepine-induced Stevens-Johnson syndrome. *Journal of Allergy and Clinical Immunology,* 128**,** 1266-1276.e11.

KOHANIM, S., PALIOURA, S., SAEED, H. N., AKPEK, E. K., AMESCUA, G., BASU, S., BLOMQUIST, P. H., BOUCHARD, C. S., DART, J. K., GAI, X., GOMES, J. A., GREGORY, D. G., IYER, G., JACOBS, D. S., JOHNSON, A. J., KINOSHITA, S., MANTAGOS, I. S., MEHTA, J. S., PEREZ, V. L., PFLUGFELDER, S. C., SANGWAN, V. S., SIPPEL, K. C., SOTOZONO, C., SRINIVASAN, B., TAN, D. T., TANDON, R., TSENG, S. C., UETA, M. & CHODOSH, J. 2016. Stevens-Johnson Syndrome/Toxic Epidermal Necrolysis--A Comprehensive Review and Guide to Therapy. I. Systemic Disease. *Ocul Surf,* 14**,** 2-19.

KOMANDER, D. 2009. The emerging complexity of protein ubiquitination. *Biochem Soc Trans,* 37**,** 937-53.

KROEMER, G., EL-DEIRY, W. S., GOLSTEIN, P., PETER, M. E., VAUX, D., VANDENABEELE, P., ZHIVOTOVSKY, B., BLAGOSKLONNY, M. V., MALORNI, W., KNIGHT, R. A., PIACENTINI, M., NAGATA, S. &

MELINO, G. 2005. Classification of cell death: recommendations of the Nomenclature Committee on Cell Death. *Cell Death And Differentiation,* 12**,** 1463.

LABBÉ, K., MCINTIRE, CHRISTIAN R., DOIRON, K., LEBLANC, PHILIPPE M. & SALEH, M. 2011. Cellular Inhibitors of Apoptosis Proteins cIAP1 and cIAP2 Are Required for Efficient Caspase-1 Activation by the Inflammasome. *Immunity,* 35**,** 897-907.

LANDSTEINER, K. & JACOBS, J. 1935. STUDIES ON THE SENSITIZATION OF ANIMALS WITH SIMPLE CHEMICAL COMPOUNDS. *The Journal of experimental medicine,* 61**,** 643-656.

LAVOIE, J. N., NGUYEN, M., MARCELLUS, R. C., BRANTON, P. E. & SHORE, G. C. 1998. E4orf4, a Novel Adenovirus Death Factor That Induces p53-independent Apoptosis by a Pathway That Is Not Inhibited by zVAD-fmk. *The Journal of Cell Biology,* 140**,** 637-645.

LAZEBNIK, Y. A., KAUFMANN, S. H., DESNOYERS, S., POIRIER, G. G. & EARNSHAW, W. C. 1994. Cleavage of poly(ADP-ribose) polymerase by a proteinase with properties like ICE. *Nature,* 371**,** 346-7.

LE CLEACH, L., DELAIRE, S., BOUMSELL, L., BAGOT, M., BOURGAULT-VILLADA, I., BENSUSSAN, A. & ROUJEAU, J. C. 2000. Blister fluid T lymphocytes during toxic epidermal necrolysis are functional cytotoxic cells which express human natural killer (NK) inhibitory receptors. *Clin Exp Immunol,* 119**,** 225-30.

LEE, Y.-Y., KO, J.-H., WEI, C.-H. & CHUNG, W.-H. 2013. Use of etanercept to treat toxic epidermal necrolysis in a human immunodeficiency virus-positive patient. *Dermatologica Sinica,* 31**,** 78-81.

LERNER, L. H., QURESHI, A. A., REDDY, B. V. & LERNER, E. A. 2000. Nitric oxide synthase in toxic epidermal necrolysis and Stevens-Johnson syndrome. *J Invest Dermatol,* 114**,** 196-9.

LETKO, E., BHOL, K., FOSTER, C. S. & AHMED, A. R. 2011. Possible in vitro model of toxic epidermal necrolysis. *Arch Ophthalmol,* 129**,** 666-7.

LEVENTIS, P. A. & GRINSTEIN, S. 2010. The Distribution and Function of Phosphatidylserine in Cellular Membranes. *Annual Review of Biophysics,* 39**,** 407-427.

LEYVA, L., TORRES, M. J., POSADAS, S., BLANCA, M., BESSO, G., O'VALLE, F., DEL MORAL, R. G., SANTAMARÍA, L. F. & JUÁREZ, C. 2000. Anticonvulsant-induced toxic epidermal necrolysis: Monitoring the immunologic response. *Journal of Allergy and Clinical Immunology,* 105**,** 157-165.

LI, J., MCQUADE, T., SIEMER, A. B., NAPETSCHNIG, J., MORIWAKI, K., HSIAO, Y.-S., DAMKO, E., MOQUIN, D., WALZ, T., MCDERMOTT, A., CHAN, F. K.-M. & WU, H. 2012. The RIP1/RIP3 necrosome forms a functional amyloid signaling complex required for programmed necrosis. *Cell,* 150**,** 339-350.

LI, J. & UETRECHT, J. P. 2010. The danger hypothesis applied to idiosyncratic drug reactions. *Handb Exp Pharmacol***,** 493-509.

LOCHARERNKUL, C., LOPLUMLERT, J., LIMOTAI, C., KORKIJ, W., DESUDCHIT, T., TONGKOBPETCH, S., KANGWANSHIRATADA, O., HIRANKARN, N., SUPHAPEETIPORN, K. & SHOTELERSUK, V. 2008. Carbamazepine and phenytoin induced Stevens-Johnson syndrome is associated with HLA-B*1502 allele in Thai population. *Epilepsia,* 49**,** 2087-2091.

LOCKSLEY, R. M., KILLEEN, N. & LENARDO, M. J. 2001. The TNF and TNF receptor superfamilies: integrating mammalian biology. *Cell,* 104**,** 487-501.

LONJOU, C., BOROT, N., SEKULA, P., LEDGER, N., THOMAS, L., HALEVY, S., NALDI, L., BOUWES-BAVINCK, J. N., SIDOROFF, A., DE TOMA, C., SCHUMACHER, M., ROUJEAU, J. C., HOVNANIAN, A. & MOCKENHAUPT, M. 2008. A European study of HLA-B in Stevens-Johnson syndrome and toxic epidermal necrolysis related to five high-risk drugs. *Pharmacogenetics and Genomics,* 18**,** 99-107.

LOTFI, R., HERZOG, G. I., DEMARCO, R. A., BEER-STOLZ, D., LEE, J. J., RUBARTELLI, A., SCHREZENMEIER, H. & LOTZE, M. T. 2009. Eosinophils oxidize damage-associated molecular pattern molecules derived from stressed cells. *J Immunol,* 183**,** 5023-31.

LOTZE, M. T. & TRACEY, K. J. 2005. High-mobility group box 1 protein (HMGB1): nuclear weapon in the immune arsenal. *Nat Rev Immunol,* 5**,** 331-42.

MA, J. D., LEE, K. C. & KUO, G. M. 2010. HLA-B*5701 testing to predict abacavir hypersensitivity. *PLoS currents,* 2**,** RRN1203-RRN1203.

MAEDA, A. & FADEEL, B. 2014. Mitochondria released by cells undergoing TNF-α-induced necroptosis act as danger signals. *Cell Death &Amp; Disease,* 5**,** e1312.

MAGNA, M. & PISETSKY, D. S. 2014. The role of HMGB1 in the pathogenesis of inflammatory and autoimmune diseases. *Mol Med,* 20**,** 138-46.

MAHMOOD, T. & YANG, P.-C. 2012. Western Blot: Technique, Theory, and Trouble Shooting. *North American Journal of Medical Sciences,* 4**,** 429-434.

MALLAL, S., NOLAN, D., WITT, C., MASEL, G., MARTIN, A. M., MOORE, C., SAYER, D., CASTLEY, A., MAMOTTE, C., MAXWELL, D., JAMES, I. & CHRISTIANSEN, F. T. 2002. Association between presence of HLA-B*5701, HLA-DR7, and HLA-DQ3 and hypersensitivity to HIV-1 reverse-transcriptase inhibitor abacavir. *Lancet,* 359**,** 727-32.

MANDAL, P., BERGER, S. B., PILLAY, S., MORIWAKI, K., HUANG, C., GUO, H., LICH, J. D., FINGER, J., KASPARCOVA, V., VOTTA, B., OUELLETTE, M., KING, B. W., WISNOSKI, D., LAKDAWALA, A. S., DEMARTINO, M. P., CASILLAS, L. N., HAILE, P. A., SEHON, C. A., MARQUIS, R. W., UPTON, J., DALEY-BAUER, L. P., ROBACK, L., RAMIA, N., DOVEY, C. M., CARETTE, J. E., CHAN, F. K.-M., BERTIN, J., GOUGH, P. J., MOCARSKI, E. S. & KAISER, W. J. 2014. RIP3 induces apoptosis independent of pronecrotic kinase activity. *Molecular cell,* 56**,** 481-495.

MARTINOTTI, S., PATRONE, M. & RANZATO, E. 2015. Emerging roles for HMGB1 protein in immunity, inflammation, and cancer. *Immunotargets and Therapy,* 4**,** 101-109.

MARTINS, L. M., KOTTKE, T., MESNER, P. W., BASI, G. S., SINHA, S., FRIGON, N., TATAR, E., TUNG, J. S., BRYANT, K., TAKAHASHI, A., SVINGEN, P. A., MADDEN, B. J., MCCORMICK, D. J., EARNSHAW, W. C. & KAUFMANN, S. H. 1997. Activation of Multiple Interleukin-1β Converting Enzyme Homologues in Cytosol and Nuclei of HL-60 Cells during Etoposide-induced Apoptosis. *Journal of Biological Chemistry,* 272**,** 7421-7430.

MARZANO, A. V., FREZZOLINI, A., CAPRONI, M., PARODI, A., FANONI, D., QUAGLINO, P., GIRGENTI, V., LA PLACA, M., FABBRI, P., CAPUTO, R. & BERTI, E. 2007. Immunohistochemical expression of apoptotic markers in drug-induced erythema multiforme, Stevens-Johnson syndrome and toxic epidermal necrolysis. *Int J Immunopathol Pharmacol,* 20**,** 557-66.

MATSUE, H., KOBAYASHI, H., HOSOKAWA, T., AKITAYA, T. & OHKAWARA, A. 1995. Keratinocytes constitutively express the Fas antigen that mediates apoptosis in IFN gamma-treated cultured keratinocytes. *Arch Dermatol Res,* 287**,** 315-20.

MATZINGER, P. 1994. Tolerance, danger, and the extended family. *Annu Rev Immunol,* 12**,** 991-1045.

MCCORMACK, M., ALFIREVIC, A., BOURGEOIS, S., FARRELL, J. J., KASPERAVIČIUTE, D., CARRINGTON, M., SILLS, G. J., MARSON, T., JIA, X., DE BAKKER, P. I. W., CHINTHAPALLI, K., MOLOKHIA, M., JOHNSON, M. R., O'CONNOR, G. D., CHAILA, E., ALHUSAINI, S.,

SHIANNA, K. V., RADTKE, R. A., HEINZEN, E. L., WALLEY, N., PANDOLFO, M., PICHLER, W., PARK, B. K., DEPONDT, C., SISODIYA, S. M., GOLDSTEIN, D. B., DELOUKAS, P., DELANTY, N., CAVALLERI, G. L. & PIRMOHAMED, M. 2011. HLA-A*3101 and carbamazepine-induced hypersensitivity reactions in Europeans. *New England Journal of Medicine,* 364**,** 1134-1143.

MEHTA, T. Y., PRAJAPATI, L. M., MITTAL, B., JOSHI, C. G., SHETH, J. J., PATEL, D. B., DAVE, D. M. & GOYAL, R. K. 2009. Association of HLA-BFNx011502 allele and carbamazepine-induced Stevens-Johnson syndrome among Indians. *Indian Journal of Dermatology, Venereology and Leprology,* 75**,** 579-582.

MENG, X., YERLY, D. & NAISBITT, D. J. 2018. Mechanisms leading to T-cell activation in drug hypersensitivity. *Current Opinion in Allergy and Clinical Immunology,* 18**,** 317-324.

MESSMER, U. K., ANKARCRONA, M., NICOTERA, P. & BRUNE, B. 1994. p53 expression in nitric oxide-induced apoptosis. *FEBS Lett,* 355**,** 23-6.

MICHEAU, O. & TSCHOPP, J. 2003. Induction of TNF Receptor I-Mediated Apoptosis via Two Sequential Signaling Complexes. *Cell,* 114**,** 181-190.

MILLER, T. M., MOULDER, K. L., KNUDSON, C. M., CREEDON, D. J., DESHMUKH, M., KORSMEYER, S. J. & JOHNSON, E. M. 1997. Bax Deletion Further Orders the Cell Death Pathway in Cerebellar Granule Cells and Suggests a Caspase-independent Pathway to Cell Death. *The Journal of Cell Biology,* 139**,** 205-217.

MITROVIC, B., IGNARRO, L. J., VINTERS, H. V., AKERS, M. A., SCHMID, I., UITTENBOGAART, C. & MERRILL, J. E. 1995. Nitric oxide induces necrotic but not apoptotic cell death in oligodendrocytes. *Neuroscience,* 65**,** 531-9.

MOCKENHAUPT, M. 2011. The current understanding of Stevens–Johnson syndrome and toxic epidermal necrolysis. *Expert Review of Clinical Immunology,* 7**,** 803-815.

MOLLER, M. N., RIOS, N., TRUJILLO, M., RADI, R., DENICOLA, A. & ALVAREZ, B. 2019. Detection and quantification of nitric oxide-derived oxidants in biological systems. *J Biol Chem*.

MOREL, E., ALVAREZ, L., CABANAS, R., FIANDOR, A., DIAZ, R., ESCAMOCHERO, S., PRIOR, N., BLANCA, M. & BELLON, T. 2011. Expression of alpha-defensin 1-3 in T cells from severe cutaneous drug-induced hypersensitivity reactions. *Allergy,* 66**,** 360-7.

MORIWAKI, K. & CHAN, F. K. 2016. Regulation of RIPK3- and RHIM-dependent Necroptosis by the Proteasome. *J Biol Chem,* 291**,** 5948-59.

MORSY, H., TAHA, E. A., NIGM, D. A., SHAHIN, R. & YOUSSEF, E. M. K. 2017. Serum IL-17 in patients with erythema multiforme or Stevens-Johnson syndrome/toxic epidermal necrolysis drug reaction, and correlation with disease severity. *Clin Exp Dermatol,* 42**,** 868-873.

MOSMANN, T. 1983. Rapid colorimetric assay for cellular growth and survival: application to proliferation and cytotoxicity assays. *J Immunol Methods,* 65**,** 55-63.

MOUJALLED, D. M., COOK, W. D., MURPHY, J. M. & VAUX, D. L. 2014. Necroptosis induced by RIPK3 requires MLKL but not Drp1. *Cell death & disease,* 5**,** e1086-e1086.

MOUJALLED, D. M., COOK, W. D., OKAMOTO, T., MURPHY, J., LAWLOR, K. E., VINCE, J. E. & VAUX, D. L. 2013. TNF can activate RIPK3 and cause programmed necrosis in the absence of RIPK1. *Cell Death Dis,* 4**,** e465.

MUNZ, C. 2012. Antigen Processing for MHC Class II Presentation via Autophagy. *Front Immunol,* 3**,** 9.

MURAI, S., YAMAGUCHI, Y., SHIRASAKI, Y., YAMAGISHI, M., SHINDO, R., HILDEBRAND, J. M., MIURA, R., NAKABAYASHI, O., TOTSUKA, M., TOMIDA, T., ADACHI-AKAHANE, S., UEMURA, S., SILKE, J., YAGITA, H., MIURA, M. & NAKANO, H. 2018. A FRET biosensor for necroptosis uncovers two different modes of the release of DAMPs. *Nat Commun,* 9**,** 4457.

MURPHY, J. M., CZABOTAR, P. E., HILDEBRAND, J. M., LUCET, I. S., ZHANG, J. G., ALVAREZ-DIAZ, S., LEWIS, R., LALAOUI, N., METCALF, D., WEBB, A. I., YOUNG, S. N., VARGHESE, L. N., TANNAHILL, G. M., HATCHELL, E. C., MAJEWSKI, I. J., OKAMOTO, T., DOBSON, R. C., HILTON, D. J., BABON, J. J., NICOLA, N. A., STRASSER, A., SILKE, J. & ALEXANDER, W. S. 2013. The pseudokinase MLKL mediates necroptosis via a molecular switch mechanism. *Immunity,* 39**,** 443-53.

MURPHY, M. P. 1999. Nitric oxide and cell death. *Biochim Biophys Acta,* 1411**,** 401-14.

NAGATA, S. 1997. Apoptosis by Death Factor. *Cell,* 88**,** 355-365.

NAISBITT, D. J., GORDON, S. F., PIRMOHAMED, M. & PARK, B. K. 2000. Immunological principles of adverse drug reactions: the initiation

and propagation of immune responses elicited by drug treatment. *Drug Saf,* 23**,** 483-507.

NAKAJIMA, S., WATANABE, H., TOHYAMA, M., SUGITA, K., IIJIMA, M., HASHIMOTO, K., TOKURA, Y., NISHIMURA, Y., DOI, H., TANIOKA, M., MIYACHI, Y. & KABASHIMA, K. 2011. High-mobility group box 1 protein (HMGB1) as a novel diagnostic tool for toxic epidermal necrolysis and Stevens-Johnson syndrome. *Arch Dermatol,* 147**,** 1110-2.

NASSIF, A., BENSUSSAN, A., BOUMSELL, L., DENIAUD, A., MOSLEHI, H., WOLKENSTEIN, P., BAGOT, M. & ROUJEAU, J. C. 2004a. Toxic epidermal necrolysis: effector cells are drug-specific cytotoxic T cells. *J Allergy Clin Immunol,* 114**,** 1209-15.

NASSIF, A., BENSUSSAN, A., DOROTHEE, G., MAMI-CHOUAIB, F., BACHOT, N., BAGOT, M., BOUMSELL, L. & ROUJEAU, J. C. 2002. Drug specific cytotoxic T-cells in the skin lesions of a patient with toxic epidermal necrolysis. *J Invest Dermatol,* 118**,** 728-33.

NASSIF, A., MOSLEHI, H., LE GOUVELLO, S., BAGOT, M., LYONNET, L., MICHEL, L., BOUMSELL, L., BENSUSSAN, A. & ROUJEAU, J. C. 2004b. Evaluation of the potential role of cytokines in toxic epidermal necrolysis. *J Invest Dermatol,* 123**,** 850-5.

NICKOLOFF, B. J. 2008. Saving the skin from drug-induced detachment. *Nature Medicine,* 14**,** 1311.

NOMURA, Y., AIHARA, M., MATSUKURA, S., IKEZAWA, Y., KAMBARA, T., AIHARA, Y., TAKAHASHI, Y. & IKEZAWA, Z. 2011. Evaluation of serum cytokine levels in toxic epidermal necrolysis and Stevens–Johnson syndrome compared with other delayed-type adverse drug reactions. *The Journal of Dermatology,* 38**,** 1076-1079.

NORCROSS, M. A., LUO, S., LU, L., BOYNE, M. T., GOMARTELI, M., RENNELS, A. D., WOODCOCK, J., MARGULIES, D. H., MCMURTREY, C., VERNON, S., HILDEBRAND, W. H. & BUCHLI, R. 2012. Abacavir induces loading of novel self-peptides into HLA-B*57: 01: an autoimmune model for HLA-associated drug hypersensitivity. *Aids,* 26**,** F21-9.

NOWAK, P., ABDURAHMAN, S., LINDKVIST, A., TROSEID, M. & SÖNNERBORG, A. 2012. Impact of HMGB1/TLR Ligand Complexes on HIV-1 Replication: Possible Role for Flagellin during HIV-1 Infection. *International journal of microbiology,* 2012**,** 263836-263836.

NOWAK, P., BARQASHO, B. & SONNERBORG, A. 2007. Elevated plasma levels of high mobility group box protein 1 in patients with HIV-1 infection. *Aids,* 21**,** 869-71.

O'DONNELL, M. A., PEREZ-JIMENEZ, E., OBERST, A., NG, A., MASSOUMI, R., XAVIER, R., GREEN, D. R. & TING, A. T. 2011. CASPASE 8 inhibits programmed necrosis by processing CYLD. *Nature cell biology,* 13**,** 1437-1442.

OROZCO, S., YATIM, N., WERNER, M. R., TRAN, H., GUNJA, S. Y., TAIT, S. W. G., ALBERT, M. L., GREEN, D. R. & OBERST, A. 2014. RIPK1 both positively and negatively regulates RIPK3 oligomerization and necroptosis. *Cell death and differentiation,* 21**,** 1511-1521.

OSTROV, D. A., GRANT, B. J., POMPEU, Y. A., SIDNEY, J., HARNDAHL, M., SOUTHWOOD, S., OSEROFF, C., LU, S., JAKONCIC, J., DE OLIVEIRA, C. A., YANG, L., MEI, H., SHI, L., SHABANOWITZ, J., ENGLISH, A. M., WRISTON, A., LUCAS, A., PHILLIPS, E., MALLAL, S., GREY, H. M., SETTE, A., HUNT, D. F., BUUS, S. & PETERS, B. 2012. Drug hypersensitivity caused by alteration of the MHC-presented self-peptide repertoire. *Proc Natl Acad Sci U S A,* 109**,** 9959-64.

OUYANG, L., SHI, Z., ZHAO, S., WANG, F.-T., ZHOU, T.-T., LIU, B. & BAO, J.-K. 2012. Programmed cell death pathways in cancer: a review of apoptosis, autophagy and programmed necrosis. *Cell Proliferation,* 45**,** 487-498.

PALLIER, C., SCAFFIDI, P., CHOPINEAU-PROUST, S., AGRESTI, A., NORDMANN, P., BIANCHI, M. E. & MARECHAL, V. 2003. Association of chromatin proteins high mobility group box (HMGB) 1 and HMGB2 with mitotic chromosomes. *Molecular biology of the cell,* 14**,** 3414-3426.

PANAYOTOVA-DIMITROVA, D., FEOKTISTOVA, M. & LEVERKUS, M. 2015. RIPping the Skin Apart: Necroptosis Signaling in Toxic Epidermal Necrolysis. *J Invest Dermatol,* 135**,** 1940-3.

PAQUET, P., NIKKELS, A., ARRESE, J. E., VANDERKELEN, A. & PIÉRARD, G. E. 1994. Macrophages and Tumor Necrosis Factor α in Toxic Epidermal Necrolysis. *Archives of Dermatology,* 130**,** 605-608.

PAQUET, P., PAQUET, F., AL SALEH, W., REPER, P., VANDERKELEN, A. & PIERARD, G. E. 2000. Immunoregulatory effector cells in drug-induced toxic epidermal necrolysis. *Am J Dermatopathol,* 22**,** 413-7.

PAQUET, P., QUATRESOOZ, P. & PIERARD, G. E. 2003. Factor-XIIIa-positive dendrocytes in drug-induced toxic epidermal necrolysis

(Lyell's syndrome): paradoxical activation in skin and rarefaction in lymph nodes. *Dermatology,* 206**,** 374-8.

PARADISI, A., ABENI, D., BERGAMO, F., RICCI, F., DIDONA, D. & DIDONA, B. 2014. Etanercept therapy for toxic epidermal necrolysis. *Journal of the American Academy of Dermatology,* 71**,** 278-283.

PARKER, T. M., NGUYEN, A. H., RABANG, J. R., PATIL, A.-A. & AGRAWAL, D. K. 2017. The danger zone: Systematic review of the role of HMGB1 danger signalling in traumatic brain injury. *Brain injury,* 31**,** 2-8.

PASPARAKIS, M. & VANDENABEELE, P. 2015. Necroptosis and its role in inflammation. *Nature,* 517**,** 311-20.

PAUDEL, Y. N., SHAIKH, M. F., CHAKRABORTI, A., KUMARI, Y., ALEDO-SERRANO, Á., ALEKSOVSKA, K., ALVIM, M. K. M. & OTHMAN, I. 2018. HMGB1: A Common Biomarker and Potential Target for TBI, Neuroinflammation, Epilepsy, and Cognitive Dysfunction. *Frontiers in neuroscience,* 12**,** 628-628.

PAUL, C., WOLKENSTEIN, P., ADLE, H., WECHSLER, J., GARCHON, H. J., REVUZ, J. & ROUJEAU, J. C. 1996. Apoptosis as a mechanism of keratinocyte death in toxic epidermal necrolysis. *Br J Dermatol,* 134**,** 710-4.

PEREIRA, F. A., MUDGIL, A. V. & ROSMARIN, D. M. 2007. Toxic epidermal necrolysis. *J Am Acad Dermatol,* 56**,** 181-200.

PETRIE, E. J., SANDOW, J. J., JACOBSEN, A. V., SMITH, B. J., GRIFFIN, M. D. W., LUCET, I. S., DAI, W., YOUNG, S. N., TANZER, M. C., WARDAK, A., LIANG, L.-Y., COWAN, A. D., HILDEBRAND, J. M., KERSTEN, W. J. A., LESSENE, G., SILKE, J., CZABOTAR, P. E., WEBB, A. I. & MURPHY, J. M. 2018. Conformational switching of the pseudokinase domain promotes human MLKL tetramerization and cell death by necroptosis. *Nature Communications,* 9**,** 2422.

PHAM-HUY, L. A., HE, H. & PHAM-HUY, C. 2008. Free Radicals, Antioxidants in Disease and Health. *International Journal of Biomedical Science : IJBS,* 4**,** 89-96.

PICHLER, W. J. 2002. Pharmacological interaction of drugs with antigen-specific immune receptors: the p-i concept. *Curr Opin Allergy Clin Immunol,* 2**,** 301-5.

PICHLER, W. J. 2003. Delayed drug hypersensitivity reactions. *Ann Intern Med,* 139**,** 683-93.

PICHLER, W. J. 2008. The p-i Concept: Pharmacological Interaction of Drugs With Immune Receptors. *World Allergy Organ J,* 1**,** 96-102.

PICHLER, W. J. 2019. *Drug hypersensitivity: Classification and clinical features* [Online]. Available: https://www.uptodate.com/contents/drug-hypersensitivity-classification-and-clinical-features [Accessed 15th March 2019].

PICHLER, W. J., ADAM, J., DAUBNER, B., GENTINETTA, T., KELLER, M. & YERLY, D. 2010. Drug hypersensitivity reactions: pathomechanism and clinical symptoms. *Med Clin North Am,* 94**,** 645-64, xv.

PICHLER, W. J., ADAM, J., WATKINS, S., WUILLEMIN, N., YUN, J. & YERLY, D. 2015. Drug Hypersensitivity: How Drugs Stimulate T Cells via Pharmacological Interaction with Immune Receptors. *Int Arch Allergy Immunol,* 168**,** 13-24.

PICHLER, W. J., BEELER, A., KELLER, M., LERCH, M., POSADAS, S., SCHMID, D., SPANOU, Z., ZAWODNIAK, A. & GERBER, B. 2006. Pharmacological interaction of drugs with immune receptors: the p-i concept. *Allergol Int,* 55**,** 17-25.

PICHLER, W. J. & HAUSMANN, O. 2016. Classification of Drug Hypersensitivity into Allergic, p-i, and Pseudo-Allergic Forms. *International Archives of Allergy and Immunology,* 171**,** 166-179.

PIRMOHAMED, M., BRECKENRIDGE, A. M., KITTERINGHAM, N. R. & PARK, B. K. 1998. Adverse drug reactions. *BMJ (Clinical research ed.),* 316**,** 1295-1298.

PIRMOHAMED, M., JAMES, S., MEAKIN, S., GREEN, C., SCOTT, A. K., WALLEY, T. J., FARRAR, K., PARK, B. K. & BRECKENRIDGE, A. M. 2004. Adverse drug reactions as cause of admission to hospital: prospective analysis of 18 820 patients. *BMJ,* 329**,** 15-19.

PIRMOHAMED, M., NAISBITT, D. J., GORDON, F. & PARK, B. K. 2002. The danger hypothesis--potential role in idiosyncratic drug reactions. *Toxicology,* 181-182**,** 55-63.

PIRMOHAMED, M., OSTROV, D. A. & PARK, B. K. 2015. New genetic findings lead the way to a better understanding of fundamental mechanisms of drug hypersensitivity. *J Allergy Clin Immunol,* 136**,** 236-44.

PIRMOHAMED, M. & PARK, B. K. 2001. Genetic susceptibility to adverse drug reactions. *Trends in Pharmacological Sciences,* 22**,** 298-305.

POREBSKI, G. 2017. In Vitro Assays in Severe Cutaneous Adverse Drug Reactions: Are They Still Research Tools or Diagnostic Tests Already? *International journal of molecular sciences,* 18**,** 1737.

POREBSKI, G., PECARIC-PETKOVIC, T., GROUX-KELLER, M., BOSAK, M., KAWABATA, T. T. & PICHLER, W. J. 2013. In vitro drug causality

assessment in Stevens-Johnson syndrome - alternatives for lymphocyte transformation test. *Clin Exp Allergy,* 43**,** 1027-37.

POSADAS, S. J., PADIAL, A., TORRES, M. J., MAYORGA, C., LEYVA, L., SANCHEZ, E., ALVAREZ, J., ROMANO, A., JUAREZ, C. & BLANCA, M. 2002. Delayed reactions to drugs show levels of perforin, granzyme B, and Fas-L to be related to disease severity. *J Allergy Clin Immunol,* 109**,** 155-61.

POSADAS, S. J. & PICHLER, W. J. 2007. Delayed drug hypersensitivity reactions - new concepts. *Clin Exp Allergy,* 37**,** 989-99.

POWER, W. J., SAIDMAN, S. L., ZHANG, D. S., VAMVAKAS, E. C., MERAYO-LLOVES, J. M., KAUFMAN, A. H. & FOSTER, C. S. 1996. HLA typing in patients with ocular manifestations of Stevens-Johnson syndrome. *Ophthalmology,* 103**,** 1406-9.

PRADEU, T. & COOPER, E. L. 2012. The danger theory: 20 years later. *Frontiers in immunology,* 3**,** 287-287.

QURESHI, A. A., LERNER, L. H. & LERNER, E. A. 1996. From bedside to the bench and back: Nitric oxide and the cutis. *Archives of Dermatology,* 132**,** 889-893.

RAUVALA, H. & ROUHIAINEN, A. 2007. RAGE as a receptor of HMGB1 (Amphoterin): roles in health and disease. *Curr Mol Med,* 7**,** 725-34.

RAWLINGS, M. D. & THOMPSON, J. W. 1977. *Pathogenesis of adverse drug reactions* New York, Oxford University Press.

REVUZ, J., PENSO, D., ROUJEAU, J. C., GUILLAUME, J. C., PAYNE, C. R., WECHSLER, J. & TOURAINE, R. 1987. Toxic epidermal necrolysis. Clinical findings and prognosis factors in 87 patients. *Arch Dermatol,* 123**,** 1160-5.

RICHARD, S. A., JIANG, Y., XIANG, L. H., ZHOU, S., WANG, J., SU, Z. & XU, H. 2017. Post-translational modifications of high mobility group box 1 and cancer. *American journal of translational research,* 9**,** 5181-5196.

ROSIN, D. L. & OKUSA, M. D. 2011. Dangers Within: DAMP Responses to Damage and Cell Death in Kidney Disease. *Journal of the American Society of Nephrology,* 22**,** 416-425.

ROTHE, M., PAN, M.-G., HENZEL, W. J., AYRES, T. M. & V. GOEDDEL, D. 1995. The TNFR2-TRAF signaling complex contains two novel proteins related to baculoviral inhibitor of apoptosis proteins. *Cell,* 83**,** 1243-1252.

ROUJEAU, J. C. 2005. Clinical heterogeneity of drug hypersensitivity. *Toxicology,* 209**,** 123-9.

ROUJEAU, J. C., HUYNH, T. N., BRACQ, C., GUILLAUME, J. C., REVUZ, J. & TOURAINE, R. 1987. Genetic susceptibility to toxic epidermal necrolysis. *Arch Dermatol,* 123**,** 1171-3.

ROUJEAU, J. C., KELLY, J. P., NALDI, L., RZANY, B., STERN, R. S., ANDERSON, T., AUQUIER, A., BASTUJI-GARIN, S., CORREIA, O., LOCATI, F. & ET AL. 1995. Medication use and the risk of Stevens-Johnson syndrome or toxic epidermal necrolysis. *N Engl J Med,* 333**,** 1600-7.

RZANY, B., HERING, O., MOCKENHAUPT, M., SCHRODER, W., GOERTTLER, E., RING, J. & SCHOPF, E. 1996. Histopathological and epidemiological characteristics of patients with erythema exudativum multiforme major, Stevens-Johnson syndrome and toxic epidermal necrolysis. *Br J Dermatol,* 135**,** 6-11.

SAITO, N., QIAO, H., YANAGI, T., SHINKUMA, S., NISHIMURA, K., SUTO, A., FUJITA, Y., SUZUKI, S., NOMURA, T., NAKAMURA, H., NAGAO, K., OBUSE, C., SHIMIZU, H. & ABE, R. 2014. An annexin A1-FPR1 interaction contributes to necroptosis of keratinocytes in severe cutaneous adverse drug reactions. *Sci Transl Med,* 6**,** 245ra95.

SAMRAJ, A. K., SOHN, D., SCHULZE-OSTHOFF, K. & SCHMITZ, I. 2007. Loss of caspase-9 reveals its essential role for caspase-2 activation and mitochondrial membrane depolarization. *Mol Biol Cell,* 18**,** 84-93.

SASSOLAS, B., HADDAD, C., MOCKENHAUPT, M., DUNANT, A., LISS, Y., BORK, K., HAUSTEIN, U. F., VIELUF, D., ROUJEAU, J. C. & LE LOUET, H. 2010. ALDEN, an algorithm for assessment of drug causality in Stevens-Johnson Syndrome and toxic epidermal necrolysis: comparison with case-control analysis. *Clin Pharmacol Ther,* 88**,** 60-8.

SCAFFIDI, P., MISTELI, T. & BIANCHI, M. E. 2002. Release of chromatin protein HMGB1 by necrotic cells triggers inflammation. *Nature,* 418**,** 191-5.

SCHILLING, R., GESERICK, P. & LEVERKUS, M. 2014. Characterization of the ripoptosome and its components: implications for anti-inflammatory and cancer therapy. *Methods Enzymol,* 545**,** 83-102.

SCHOOP, V. M., FUSENIG, N. E. & MIRANCEA, N. 1999. Epidermal Organization and Differentiation of HaCaT Keratinocytes in Organotypic Coculture with Human Dermal Fibroblasts. *Journal of Investigative Dermatology,* 112**,** 343-353.

SCHÜRER, N., KÖHNE, A., SCHLIEP, V., BARLAG, K. & GOERZ, G. 1993. Lipid composition and synthesis of HaCaT cells, an immortalized human keratinocyte line, in comparison with normal human adult keratinocytes. *Experimental Dermatology,* 2**,** 179-185.

SCHWARTZ, R. A., MCDONOUGH, P. H. & LEE, B. W. 2013a. Toxic epidermal necrolysis: Part I. Introduction, history, classification, clinical features, systemic manifestations, etiology, and immunopathogenesis. *Journal of the American Academy of Dermatology,* 69**,** 173.e1-173.e13.

SCHWARTZ, R. A., MCDONOUGH, P. H. & LEE, B. W. 2013b. Toxic epidermal necrolysis: Part I. Introduction, history, classification, clinical features, systemic manifestations, etiology, and immunopathogenesis. *J Am Acad Dermatol,* 69**,** 173.e1-13; quiz 185-6.

SCHWARTZ, R. A., MCDONOUGH, P. H. & LEE, B. W. 2013c. Toxic epidermal necrolysis: Part II. Prognosis, sequelae, diagnosis, differential diagnosis, prevention, and treatment. *Journal of the American Academy of Dermatology,* 69**,** 187.e1-187.e16.

SHAH, A., ROBERTS, E., ENGELINA, S. & CARRAS, E. 2018. The Nikolsky sign. *Br J Hosp Med (Lond),* 79**,** C142-c144.

SHAMAS-DIN, A., KALE, J., LEBER, B. & ANDREWS, D. W. 2013. Mechanisms of action of Bcl-2 family proteins. *Cold Spring Harbor perspectives in biology,* 5**,** a008714-a008714.

SHIMAOKA, M., IIDA, T., OHARA, A., TAENAKA, N., MASHIMO, T., HONDA, T. & YOSHIYA, I. 1995. NOC, A Nitric-Oxide-Releasing Compound, Induces Dose-Dependent Apoptosis in Macrophages. *Biochemical and Biophysical Research Communications,* 209**,** 519-526.

SHU, H. D., TAKEUCHI, M. & GOEDDEL, D. V. 1996. The tumor necrosis factor receptor 2 signal transducers TRAF2 and c-IAP1 are components of the tumor necrosis factor receptor 1 signaling complex. *Proceedings of the National Academy of Sciences of the United States of America,* 93**,** 13973-13978.

SIMS, G. P., ROWE, D. C., RIETDIJK, S. T., HERBST, R. & COYLE, A. J. 2010. HMGB1 and RAGE in inflammation and cancer. *Annu Rev Immunol,* 28**,** 367-88.

SNYDER, C. M., SHROFF, E. H., LIU, J. & CHANDEL, N. S. 2009. Nitric oxide induces cell death by regulating anti-apoptotic BCL-2 family members. *PLoS One,* 4**,** e7059.

SPRENGER, A., WEBER, S., ZARAI, M., ENGELKE, R., NASCIMENTO, J. M., GRETZMEIER, C., HILPERT, M., BOERRIES, M., HAS, C., BUSCH, H., BRUCKNER-TUDERMAN, L. & DENGJEL, J. 2013. Consistency of the Proteome in Primary Human Keratinocytes With Respect to Gender, Age, and Skin Localization. *Molecular & Cellular Proteomics : MCP,* 12**,** 2509-2521.

STASSI, G., DE MARIA, R., TRUCCO, G., RUDERT, W., TESTI, R., GALLUZZO, A., GIORDANO, C. & TRUCCO, M. 1997. Nitric oxide primes pancreatic beta cells for Fas-mediated destruction in insulin-dependent diabetes mellitus. *The Journal of experimental medicine,* 186**,** 1193-1200.

STERN, R. S. & DIVITO, S. J. 2017. Stevens-Johnson Syndrome and Toxic Epidermal Necrolysis: Associations, Outcomes, and Pathobiology-Thirty Years of Progress but Still Much to Be Done. *The Journal of investigative dermatology,* 137**,** 1004-1008.

STRASSER, A., JOST, P. J. & NAGATA, S. 2009. The many roles of FAS receptor signaling in the immune system. *Immunity,* 30**,** 180-192.

STUMBO, A. C., CORTEZ, E., RODRIGUES, C. A., HENRIQUES, M., PORTO, L. C., BARBOSA, H. S. & CARVALHO, L. 2008. Mitochondrial localization of non-histone protein HMGB1 during human endothelial cell-Toxoplasma gondii infection. *Cell Biol Int,* 32**,** 235-8.

SU, S.-C. & CHUNG, W.-H. 2013. Update on pathobiology in Stevens-Johnson syndrome and toxic epidermal necrolysis. *Dermatologica Sinica,* 31**,** 175-180.

SU, S.-C. & CHUNG, W.-H. 2014. Cytotoxic proteins and therapeutic targets in severe cutaneous adverse reactions. *Toxins,* 6**,** 194-210.

SU, S. C., MOCKENHAUPT, M., WOLKENSTEIN, P., DUNANT, A., LE GOUVELLO, S., CHEN, C. B., CHOSIDOW, O., VALEYRIE-ALLANORE, L., BELLON, T., SEKULA, P., WANG, C. W., SCHUMACHER, M., KARDAUN, S. H., HUNG, S. I., ROUJEAU, J. C. & CHUNG, W. H. 2017. Interleukin-15 Is Associated with Severity and Mortality in Stevens-Johnson Syndrome/Toxic Epidermal Necrolysis. *J Invest Dermatol,* 137**,** 1065-1073.

SUN, L., WANG, H., WANG, Z., HE, S., CHEN, S., LIAO, D., WANG, L., YAN, J., LIU, W., LEI, X. & WANG, X. 2012. Mixed lineage kinase domain-like protein mediates necrosis signaling downstream of RIP3 kinase. *Cell,* 148**,** 213-227.

SUN, X., LEE, J., NAVAS, T., BALDWIN, D. T., STEWART, T. A. & DIXIT, V. M. 1999. RIP3, a Novel Apoptosis-inducing Kinase. *Journal of Biological Chemistry,* 274**,** 16871-16875.

TANG, D., BILLIAR, T. R. & LOTZE, M. T. 2012a. A Janus tale of two active high mobility group box 1 (HMGB1) redox states. *Mol Med,* 18**,** 1360-2.

TANG, D., KANG, R., CHEH, C.-W., LIVESEY, K. M., LIANG, X., SCHAPIRO, N. E., BENSCHOP, R., SPARVERO, L. J., AMOSCATO, A. A., TRACEY, K. J., ZEH, H. J. & LOTZE, M. T. 2010. HMGB1 Release and Redox Regulates Autophagy and Apoptosis in Cancer Cells. *Oncogene,* 29**,** 5299-5310.

TANG, D., KANG, R., COYNE, C. B., ZEH, H. J. & LOTZE, M. T. 2012b. PAMPs and DAMPs: Signal 0s that Spur Autophagy and Immunity. *Immunological reviews,* 249**,** 158-175.

TANIUCHI, I. 2018. CD4 Helper and CD8 Cytotoxic T Cell Differentiation. *Annu Rev Immunol,* 36**,** 579-601.

TANZER, M. C., MATTI, I., HILDEBRAND, J. M., YOUNG, S. N., WARDAK, A., TRIPAYDONIS, A., PETRIE, E. J., MILDENHALL, A. L., VAUX, D. L., VINCE, J. E., CZABOTAR, P. E., SILKE, J. & MURPHY, J. M. 2016. Evolutionary divergence of the necroptosis effector MLKL. *Cell Death Differ,* 23**,** 1185-97.

TASSANEEYAKUL, W., JANTARAROUNGTONG, T., CHEN, P., LIN, P. Y., TIAMKAO, S., KHUNARKORNSIRI, U., CHUCHERD, P., KONYOUNG, P., VANNAPRASAHT, S., CHOONHAKARN, C., PISUTTIMARN, P., SANGVIROON, A. & TASSANEEYAKUL, W. 2009. Strong association between HLA-B*5801 and allopurinol-induced Stevens-Johnson syndrome and toxic epidermal necrolysis in a Thai population. *Pharmacogenetics and Genomics,* 19**,** 704-709.

TAY, Y. K., HUFF, J. C. & WESTON, W. L. 1996. Mycoplasma pneumoniae infection is associated with Stevens-Johnson syndrome, not erythema multiforme (von Hebra). *J Am Acad Dermatol,* 35**,** 757-60.

TAYLOR, S. C., BERKELMAN, T., YADAV, G. & HAMMOND, M. 2013. A Defined Methodology for Reliable Quantification of Western Blot Data. *Molecular Biotechnology,* 55**,** 217-226.

TENEV, T., BIANCHI, K., DARDING, M., BROEMER, M., LANGLAIS, C., WALLBERG, F., ZACHARIOU, A., LOPEZ, J., MACFARLANE, M., CAIN, K. & MEIER, P. 2011. The Ripoptosome, a signaling platform that assembles in response to genotoxic stress and loss of IAPs. *Mol Cell,* 43**,** 432-48.

THIEN, F. C. K. 2006. 3. Drug hypersensitivity. *Medical Journal of Australia,* 185**,** 333-338.

TRENT, J. T., KIRSNER, R. S., ROMANELLI, P. & KERDEL, F. A. 2004. Use of SCORTEN to accurately predict mortality in patients with toxic epidermal necrolysis in the United States. *Arch Dermatol,* 140**,** 890-2.

TRINH, Q. D., PHAM, N. T., FUWA, K., TAKADA, K., KOMINE-AIZAWA, S., HONDA, M., USHIJIMA, H. & HAYAKAWA, S. 2016. High Mobility Group Box 1 Protein Enhances HIV Replication in Newly Infected Primary T Cells. *Clin Lab,* 62**,** 2305-2311.

TROSEID, M., NOWAK, P., NYSTROM, J., LINDKVIST, A., ABDURAHMAN, S. & SONNERBORG, A. 2010. Elevated plasma levels of lipopolysaccharide and high mobility group box-1 protein are associated with high viral load in HIV-1 infection: reduction by 2-year antiretroviral therapy. *Aids,* 24**,** 1733-7.

TSUDA, K., KIKUCHI, M., MORI, K., WAGA, S. & YOSHIDA, M. 1988. Primary structure of non-histone protein HMG1 revealed by the nucleotide sequence. *Biochemistry,* 27**,** 6159-63.

UEHARA, T., KIKUCHI, Y. & NOMURA, Y. 1999. Caspase activation accompanying cytochrome c release from mitochondria is possibly involved in nitric oxide-induced neuronal apoptosis in SH-SY5Y cells. *J Neurochem,* 72**,** 196-205.

UETA, M., SAWAI, H., SHINGAKI, R., KAWAI, Y., SOTOZONO, C., KOJIMA, K., YOON, K.-C., KIM, M. K., SEO, K. Y., JOO, C.-K., NAGASAKI, M., KINOSHITA, S. & TOKUNAGA, K. 2017. Genome-wide association study using the ethnicity-specific Japonica array: identification of new susceptibility loci for cold medicine-related Stevens–Johnson syndrome with severe ocular complications. *Journal Of Human Genetics,* 62**,** 485.

UETA, M., SOTOZONO, C., INATOMI, T., KOJIMA, K., TASHIRO, K., HAMURO, J. & KINOSHITA, S. 2007. Toll-like receptor 3 gene polymorphisms in Japanese patients with Stevens-Johnson syndrome. *Br J Ophthalmol,* 91**,** 962-5.

UETRECHT, J. 2007. Idiosyncratic drug reactions: current understanding. *Annu Rev Pharmacol Toxicol,* 47**,** 513-39.

UETRECHT, J. & NAISBITT, D. J. 2013. Idiosyncratic adverse drug reactions: current concepts. *Pharmacol Rev,* 65**,** 779-808.

USUI, T. & NAISBITT, D. J. 2017. Human leukocyte antigen and idiosyncratic adverse drug reactions. *Drug Metab Pharmacokinet,* 32**,** 21-30.

VANDENABEELE, P., DECLERCQ, W., BEYAERT, R. & FIERS, W. 1995. Two tumour necrosis factor receptors: structure and function. *Trends in Cell Biology,* 5**,** 392-399.

VANDENABEELE, P., DECLERCQ, W., VAN HERREWEGHE, F. & VANDEN BERGHE, T. 2010a. The Role of the Kinases RIP1 and RIP3 in TNF-Induced Necrosis. *Science Signaling,* 3**,** re4-re4.

VANDENABEELE, P., GALLUZZI, L., VANDEN BERGHE, T. & KROEMER, G. 2010b. Molecular mechanisms of necroptosis: an ordered cellular explosion. *Nat Rev Mol Cell Biol,* 11**,** 700-714.

VANLANGENAKKER, N., BERTRAND, M. J. M., BOGAERT, P., VANDENABEELE, P. & VANDEN BERGHE, T. 2011. TNF-induced necroptosis in L929 cells is tightly regulated by multiple TNFR1 complex I and II members. *Cell Death & Disease,* 2**,** e230.

VENEREAU, E., CASALGRANDI, M., SCHIRALDI, M., ANTOINE, D. J., CATTANEO, A., DE MARCHIS, F., LIU, J., ANTONELLI, A., PRETI, A., RAELI, L., SHAMS, S. S., YANG, H., VARANI, L., ANDERSSON, U., TRACEY, K. J., BACHI, A., UGUCCIONI, M. & BIANCHI, M. E. 2012. Mutually exclusive redox forms of HMGB1 promote cell recruitment or proinflammatory cytokine release. *The Journal of Experimental Medicine,* 209**,** 1519-1528.

VERCAMMEN, D., VANDENABEELE, P., BEYAERT, R., DECLERCQ, W. & FIERS, W. 1997. Tumour necrosis factor-induced necrosis versus anti-Fas-induced apoptosis in L929 cells. *Cytokine,* 9**,** 801-8.

VEUGELERS, K., MOTYKA, B., GOPING, I. S., SHOSTAK, I., SAWCHUK, T. & BLEACKLEY, R. C. 2006. Granule-mediated killing by granzyme B and perforin requires a mannose 6-phosphate receptor and is augmented by cell surface heparan sulfate. *Mol Biol Cell,* 17**,** 623-33.

VIARD-LEVEUGLE, I., BULLANI, R. R., MEDA, P., MICHEAU, O., LIMAT, A., SAURAT, J.-H., TSCHOPP, J. & FRENCH, L. E. 2003. Intracellular Localization of Keratinocyte Fas Ligand Explains Lack of Cytolytic Activity under Physiological Conditions. *Journal of Biological Chemistry,* 278**,** 16183-16188.

VIARD-LEVEUGLE, I., GAIDE, O., JANKOVIC, D., FELDMEYER, L., KERL, K., PICKARD, C., ROQUES, S., FRIEDMANN, P. S., CONTASSOT, E. & FRENCH, L. E. 2013. TNF-alpha and IFN-gamma are potential inducers of Fas-mediated keratinocyte apoptosis through activation of inducible nitric oxide synthase in toxic epidermal necrolysis. *J Invest Dermatol,* 133**,** 489-98.

VIARD, I., WEHRLI, P., BULLANI, R., SCHNEIDER, P., HOLLER, N., SALOMON, D., HUNZIKER, T., SAURAT, J. H., TSCHOPP, J. & FRENCH, L. E. 1998. Inhibition of toxic epidermal necrolysis by blockade of CD95 with human intravenous immunoglobulin. *Science,* 282**,** 490-3.

VILLADA, G., ROUJEAU, J. C., CLERICI, T., BOURGAULT, I. & REVUZ, J. 1992. Immunopathology of toxic epidermal necrolysis. Keratinocytes, HLA-DR expression, Langerhans cells, and mononuclear cells: an immunopathologic study of five cases. *Arch Dermatol,* 128**,** 50-3.

WAJANT, H., PFIZENMAIER, K. & SCHEURICH, P. 2003. Tumor necrosis factor signaling. *Cell Death Differ,* 10**,** 45-65.

WANG, C.-W., YANG, L.-Y., CHEN, C.-B., HO, H.-C., HUNG, S.-I., YANG, C.-H., CHANG, C.-J., SU, S.-C., HUI, R. C.-Y., CHIN, S.-W., HUANG, L.-F., LIN, Y. Y.-W., CHANG, W.-Y., FAN, W.-L., YANG, C.-Y., HO, J.-C., CHANG, Y.-C., LU, C.-W. & CHUNG, W.-H. 2018a. Randomized, controlled trial of TNF-α antagonist in CTL-mediated severe cutaneous adverse reactions. *The Journal of Clinical Investigation,* 128**,** 985-996.

WANG, C. & YOULE, R. J. 2009. The role of mitochondria in apoptosis*. *Annual review of genetics,* 43**,** 95-118.

WANG, F., YE, Y., LUO, Z.-Y., GAO, Q., LUO, D.-Q. & ZHANG, X. 2018b. Diverse expression of TNF-α and CCL27 in serum and blister of Stevens-Johnson syndrome/toxic epidermal necrolysis. *Clinical and translational allergy,* 8**,** 12-12.

WANG, F., YE, Y., LUO, Z.-Y., GAO, Q., LUO, D.-Q. & ZHANG, X. 2018c. Diverse expression of TNF-α and CCL27 in serum and blister of Stevens–Johnson syndrome/toxic epidermal necrolysis. *Clinical and Translational Allergy,* 8**,** 12.

WANG, H., SUN, L., SU, L., RIZO, J., LIU, L., WANG, L. F., WANG, F. S. & WANG, X. 2014. Mixed lineage kinase domain-like protein MLKL causes necrotic membrane disruption upon phosphorylation by RIP3. *Mol Cell,* 54**,** 133-146.

WANG, H. L., TSAO, S. M., YEH, C. B., CHOU, Y. E. & YANG, S. F. 2017. Circulating level of high mobility group box1 predicts the severity of communityacquired pneumonia: Regulation of inflammatory responses via the cJun Nterminal signaling pathway in macrophages. *Mol Med Rep,* 16**,** 2361-2366.

WANG, L., DU, F. & WANG, X. 2008. TNF-alpha induces two distinct caspase-8 activation pathways. *Cell,* 133**,** 693-703.

WANG, X. 2001. The expanding role of mitochondria in apoptosis. *Genes Dev,* 15**,** 2922-33.

WANG, Z., JIANG, H., CHEN, S., DU, F. & WANG, X. 2012. The mitochondrial phosphatase PGAM5 functions at the convergence point of multiple necrotic death pathways. *Cell,* 148**,** 228-43.

WARING, M. J. 1965. Complex formation between ethidium bromide and nucleic acids. *J Mol Biol,* 13**,** 269-82.

WARING, M. J., ARROWSMITH, J., LEACH, A. R., LEESON, P. D., MANDRELL, S., OWEN, R. M., PAIRAUDEAU, G., PENNIE, W. D., PICKETT, S. D., WANG, J., WALLACE, O. & WEIR, A. 2015. An analysis of the attrition of drug candidates from four major pharmaceutical companies. *Nat Rev Drug Discov,* 14**,** 475-86.

WEHRLI, P., VIARD, I., BULLANI, R., TSCHOPP, J. & FRENCH, L. E. 2000. Death receptors in cutaneous biology and disease. *J Invest Dermatol,* 115**,** 141-8.

WELLER, R. 1997. Nitric oxide - A newly discovered chemical transmitter in human skin. *British Journal of Dermatology,* 137**,** 665-672.

WELSH, K., MILUTINOVIC, S., ARDECKY, R. J., GONZALEZ-LOPEZ, M., GANJI, S. R., TERIETE, P., FINLAY, D., RIEDL, S., MATSUZAWA, S.-I., PINILLA, C., HOUGHTEN, R., VUORI, K., REED, J. C. & COSFORD, N. D. P. 2016. Characterization of Potent SMAC Mimetics that Sensitize Cancer Cells to TNF Family-Induced Apoptosis. *PLOS ONE,* 11**,** e0161952.

WENTZELL, L. M., NOBBS, T. J. & HALFORD, S. E. 1995. The SfiI restriction endonuclease makes a four-strand DNA break at two copies of its recognition sequence. *J Mol Biol,* 248**,** 581-95.

WHITAKER, P., MENG, X., LAVERGNE, S. N., EL-GHAIESH, S., MONSHI, M., EARNSHAW, C., PECKHAM, D., GOOI, J., CONWAY, S., PIRMOHAMED, M., JENKINS, R. E., NAISBITT, D. J. & PARK, B. K. 2011. Mass spectrometric characterization of circulating and functional antigens derived from piperacillin in patients with cystic fibrosis. *J Immunol,* 187**,** 200-11.

WHITE, K. D., CHUNG, W. H., HUNG, S. I., MALLAL, S. & PHILLIPS, E. J. 2015. Evolving models of the immunopathogenesis of T cell-mediated drug allergy: The role of host, pathogens, and drug response. *J Allergy Clin Immunol,* 136**,** 219-34; quiz 235.

WHO. International Drug Monitoring: the role of national centres., 1972 Geneva. Technical Report Series.

WIECZOREK, M., ABUALROUS, E. T., STICHT, J., ÁLVARO-BENITO, M., STOLZENBERG, S., NOÉ, F. & FREUND, C. 2017. Major

Histocompatibility Complex (MHC) Class I and MHC Class II Proteins: Conformational Plasticity in Antigen Presentation. *Frontiers in Immunology,* 8.

WIEGMANN, K., SCHÜTZE, S., KAMPEN, E., HIMMLER, A., MACHLEIDT, T. & KRÖNKE, M. 1992. Human 55-kDa receptor for tumor necrosis factor coupled to signal transduction cascades. *Journal of Biological Chemistry,* 267**,** 17997-18001.

WILLIAMS, S. A. & HALFORD, S. E. 2001. SfiI endonuclease activity is strongly influenced by the non-specific sequence in the middle of its recognition site. *Nucleic acids research,* 29**,** 1476-1483.

WLODKOWIC, D., SKOMMER, J. & DARZYNKIEWICZ, Z. 2009. Flow cytometry-based apoptosis detection. *Methods in molecular biology (Clifton, N.J.),* 559**,** 19-32.

WOLFFE, A. 1994. Architectural transcription factors. *Science,* 264**,** 1100-1101.

WOLKENSTEIN, P., CHOSIDOW, O., FLECHET, M. L., ROBBIOLA, O., PAUL, M., DUME, L., REVUZ, J. & ROUJEAU, J. C. 1996. Patch testing in severe cutaneous adverse drug reactions, including Stevens-Johnson syndrome and toxic epidermal necrolysis. *Contact Dermatitis,* 35**,** 234-6.

WOO, M., HAKEM, R., SOENGAS, M. S., DUNCAN, G. S., SHAHINIAN, A., KÄGI, D., HAKEM, A., MCCURRACH, M., KHOO, W., KAUFMAN, S. A., SENALDI, G., HOWARD, T., LOWE, S. W. & MAK, T. W. 1998. Essential contribution of caspase 3/CPP32 to apoptosis and its associated nuclear changes. *Genes & Development,* 12**,** 806-819.

WU, X., MI, Y., YANG, H., HU, A., ZHANG, Q. & SHANG, C. 2013. The activation of HMGB1 as a progression factor on inflammation response in normal human bronchial epithelial cells through RAGE/JNK/NF-kappaB pathway. *Mol Cell Biochem,* 380**,** 249-57.

XIANG, J., CHAO, D. T. & KORSMEYER, S. J. 1996. BAX-induced cell death may not require interleukin 1 beta-converting enzyme-like proteases. *Proc Natl Acad Sci U S A,* 93**,** 14559-63.

YABUKI, M., A, S., INNI, Y., HAMAZAKI, K., YOSHIOKA, T., YASUDA, T., HORTON, A. A. & UTSUMI, K. 1997. Molecular Mechanisms of Apoptosis in HL-60 Cells Induced by a Nitric Oxide-Releasing Compound. *Free Radical Research,* 27**,** 325-335.

YANG, F., XUAN, J., CHEN, J., ZHONG, H., LUO, H., ZHOU, P., SUN, X., HE, L., CHEN, S., CAO, Z., LUO, X. & XING, Q. 2016. HLA-B∗59:01: A marker for Stevens-Johnson syndrome/toxic epidermal necrolysis

caused by methazolamide in Han Chinese. *Pharmacogenomics Journal,* 16**,** 83-87.

YANG, H., HREGGVIDSDOTTIR, H. S., PALMBLAD, K., WANG, H., OCHANI, M., LI, J., LU, B., CHAVAN, S., ROSAS-BALLINA, M., AL-ABED, Y., AKIRA, S., BIERHAUS, A., ERLANDSSON-HARRIS, H., ANDERSSON, U. & TRACEY, K. J. 2010. A critical cysteine is required for HMGB1 binding to Toll-like receptor 4 and activation of macrophage cytokine release. *Proc Natl Acad Sci U S A,* 107**,** 11942-7.

YANG, H., OCHANI, M., LI, J., QIANG, X., TANOVIC, M., HARRIS, H. E., SUSARLA, S. M., ULLOA, L., WANG, H., DIRAIMO, R., CZURA, C. J., WANG, H., ROTH, J., WARREN, H. S., FINK, M. P., FENTON, M. J., ANDERSSON, U. & TRACEY, K. J. 2004. Reversing established sepsis with antagonists of endogenous high-mobility group box 1. *Proc Natl Acad Sci U S A,* 101**,** 296-301.

YANG, Y., JIANG, G., ZHANG, P. & FAN, J. 2015. Programmed cell death and its role in inflammation. *Military Medical Research,* 2**,** 12.

YIP, V. L., MARSON, A. G., JORGENSEN, A. L., PIRMOHAMED, M. & ALFIREVIC, A. 2012. HLA genotype and carbamazepine-induced cutaneous adverse drug reactions: a systematic review. *Clin Pharmacol Ther,* 92**,** 757-65.

YOON, S., BOGDANOV, K., KOVALENKO, A. & WALLACH, D. 2016. Necroptosis is preceded by nuclear translocation of the signaling proteins that induce it. *Cell Death Differ,* 23**,** 253-260.

YUN, J., CAI, F., LEE, F. J. & PICHLER, W. J. 2016. T-cell-mediated drug hypersensitivity: immune mechanisms and their clinical relevance. *Asia Pacific allergy,* 6**,** 77-89.

ZHANG, G., GURTU, V., KAIN, S. R. & YAN, G. 1997. Early Detection of Apoptosis Using a Fluorescent Conjugate of Annexin V. *BioTechniques,* 23**,** 525-531.

ZHANG, S., TANG, S., LI, S., PAN, Y. & DING, Y. 2019. Biologic TNF-alpha inhibitors in the treatment of Stevens-Johnson syndrome and toxic epidermal necrolysis: a systemic review. *J Dermatolog Treat***,** 1-8.

ZHANG, X., LIU, F., CHEN, X., ZHU, X. & UETRECHT, J. 2011. Involvement of the immune system in idiosyncratic drug reactions. *Drug Metab Pharmacokinet,* 26**,** 47-59.

ZHU, M., CHEN, J., GUO, H., DING, L., ZHANG, Y. & XU, Y. 2018. High Mobility Group Protein B1 (HMGB1) and Interleukin-1beta as Prognostic Biomarkers of Epilepsy in Children. *J Child Neurol,* 33**,** 909-917.

ZITVOGEL, L., KEPP, O. & KROEMER, G. 2010. Decoding Cell Death Signals in Inflammation and Immunity. *Cell,* 140**,** 798-804.